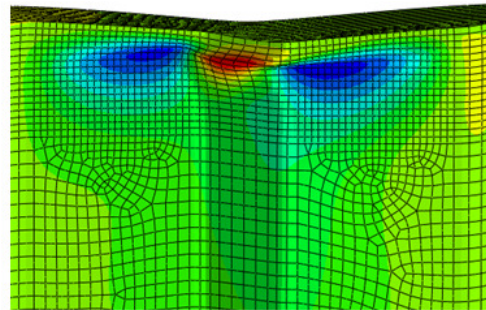


CHALMERS



Girders with Trapezoidally Corrugated Webs under Patch Loading

Master of Science Thesis in the Master's Programme Structural Engineering and Building Performance Design

NIKOLAUS LJUNGSTRÖM
OLOF KARLBERG

Department of Civil and Environmental Engineering
Division of Structural Engineering
Steel and Timber Structures
CHALMERS UNIVERSITY OF TECHNOLOGY
Göteborg, Sweden 2010
Master's Thesis 2010:146

MASTER'S THESIS 2010:146

Girders with Trapezoidally Corrugated Webs under Patch Loading

Master of Science Thesis in the Master's Programme Structural Engineering and Building Performance Design

NIKOLAUS LJUNGSTRÖM

OLOF KARLBERG

Department of Civil and Environmental Engineering
Division of Structural Engineering
Steel and Timber Structures
CHALMERS UNIVERSITY OF TECHNOLOGY
Göteborg, Sweden 2010

Girders with Trapezoidally Corrugated Webs under Patch Loading
Master of Science Thesis in the Master's Programme Structural Engineering and
Building Performance Design
NIKOLAUS LJUNGSTRÖM
OLOF KARLBERG

© NIKOLAUS LJUNGSTRÖM & OLOF KARLBERG, 2010

Examensarbete/Institutionen för bygg- och miljöteknik,
Chalmers tekniska högskola 2010:146

Department of Civil and Environmental Engineering
Division of Structural Engineering
Steel and Timber Structures
Chalmers University of Technology
SE-412 96 Göteborg
Sweden
Telephone: + 46 (0)31-772 1000

Cover:

Comparison of buckle distribution obtained from experimental test and obtained from FE-analysis. Blue colour represents outward deformations while red colour represents inward deformations (away from the reader).

Chalmers Repro Service / Department of Civil and Environmental Engineering
Göteborg, Sweden 2010

Girders with Trapezoidally Corrugated Webs under Patch Loading

Master of Science Thesis in the Master's Programme Structural Engineering and Building Performance Design

NIKOLAUS LJUNGSTRÖM
OLOF KARLBERG

Department of Civil and Environmental Engineering
Division of Structural Engineering
Steel and Timber Structures
Chalmers University of Technology

ABSTRACT

Since the 1960s, there has been ongoing research of using steel girders with trapezoidally corrugated webs instead of flat webs. As this has mainly been focused on the shear resistance, the research on the patch loading behaviour of such girders has been limited and no official design model concerning this case has been developed. Nevertheless, girders with trapezoidally corrugated webs have been used in some extent.

Today, the Swedish company Borga Plåt AB manufactures steel frame structures using girders with corrugated webs. The carrying girders of the roof structure are subjected to concentrated loads as they support the purlins carrying the actual roof. Hence, for thin webs, vertical stiffeners at the positions of each purlin have been necessary. Borga Plåt AB wants to eliminate the need of vertical stiffeners at each purlin in order to optimize the production. To do so, however, a more thorough analysis on the patch load behaviour of girders with trapezoidally corrugated webs is needed.

This master's thesis includes a presentation of previous studies on the subject of patch load capacity of girders with trapezoidally corrugated webs. The design models which result from these studies are compared to each other in a parametric study and validated through results from experimental tests. Further, six additional experimental tests have been performed at the *Division of Structural Engineering*, Chalmers University of Technology, on a girder supplied by Borga Plåt AB. A FE-model of this girder is then developed using the software ABAQUS CAE and the behaviour of the girder is validated through comparisons with the girder used in the tests. Finally, a parametric study is performed using the FE-model where the influence of certain parameters on the ultimate load and buckling behaviour is investigated. The results from this parametric study are compared and evaluated together with a few design models chosen to be most suitable.

Key words: Corrugated web, steel girders, patch loading, thin steel plate girder, trapezoidally corrugated, concentrated load

Bärförmåga hos stålbalkar med trapetsprofilerat liv utsatta för koncentrerad last

Examensarbete inom Mastersprogrammet *Structural Engineering and Building Performance Design*

NIKOLAUS LJUNGSTRÖM
OLOF KARLBERG

Institutionen för bygg- och miljöteknik
Avdelningen för konstruktionsteknik
Stål- och träbyggnad
Chalmers tekniska högskola

SAMMANFATTNING

Sedan 1960-talet har forskning rörande stålbalkar med trapetsprofilerat liv pågått. Då denna huvudsakligen har fokuserat på tvärkraftskapacitet är kunskapen om beteendet hos dessa balkar utsatta för koncentrerade laster begränsad och ingen officiell beräkningsmodell finns i dagsläget. Dock används balkar av denna typ i viss utsträckning i nuläget.

Idag tillverkar Borga Plåt AB stålramar med trapetsprofilerade liv. Dessa ramar blir utsatta för koncentrerade laster där de är upplag åt takåsarna. Detta kan ge ett behov av vertikala avstyvare vid varje stöd. För att effektivisera produktionen vill Borga Plåt AB eliminera behovet av avstyvare vid varje takås. För att möjliggöra detta krävs mer noggrann analys av stålbalkar med trapetsprofilerade liv utsatta för koncentrerade laster.

Detta examensarbete presenterar först tidigare analyser av beteendet hos stålbalkar med trapetsprofilerade liv utsatta för koncentrerade laster. De beräkningsmodeller som dessa har resulterat i jämförs med varandra i en parameterstudie samt utvärderas med hjälp av tidigare experimentella tester. Ytterligare sex tester genomförda på en balk tillhandahållen av Borga Plåt AB har utförts på laboratoriet vid *Avdelningen för Konstruktionsteknik* på Chalmers Tekniska Högskola. En FE-modell av balken har sedan konstruerats med ABAQUS CAE och dess beteende verifierat mot de sex testerna. Slutligen genomförs en ny parameterstudie med FE-modellen där inverkan av valda parametrar på brottlasten och bucklingsbeteende är analyserad. Resultaten av denna parameterstudie har jämförts och utvärderats mot utvalda beräkningsmodeller som ansetts vara mest passande.

Nyckelord: Korrugerat liv, stålbalk, trapetsprofilerat liv, koncentrerad last

CONTENTS

| | |
|--|-----|
| ABSTRACT | I |
| SAMMANFATTNING | II |
| CONTENTS | III |
| PREFACE | VI |
| NOTATIONS | VII |
| 1 INTRODUCTION | 1 |
| 1.1 Background | 1 |
| 1.2 Objectives | 1 |
| 1.3 Method | 1 |
| 1.4 Limitations | 2 |
| 1.5 Outline and content | 2 |
| 2 LITERATURE STUDY | 3 |
| 2.1 Rectangular thin plates under compression | 3 |
| 2.1.1 Plates under uniformly distributed load | 3 |
| 2.1.2 Plates with partial edge load (patch load) | 5 |
| 2.2 Overview of research on girders with corrugated webs | 7 |
| 2.2.1 Shear capacity | 8 |
| 2.2.2 Bending capacity | 10 |
| 2.2.3 Overview of experimental tests on girders subjected to patch loading | 11 |
| 2.2.4 FE-analyses performed to study girders subjected to patch loading | 14 |
| 2.2.5 Summary of previous studies on patch loaded girders | 18 |
| 2.3 Parametric study based on presented models | 21 |
| 2.3.1 Web thickness | 21 |
| 2.3.2 Corrugation angle and depth | 22 |
| 2.3.3 Web depth | 23 |
| 2.3.4 Flange thickness | 23 |
| 2.3.5 Flange width | 24 |
| 2.3.6 Length of longitudinal folds | 24 |
| 2.3.7 Load length | 25 |
| 2.3.8 Loading position | 26 |
| 2.3.9 Validity of the presented models | 27 |

| | | |
|-------|--|----|
| 2.4 | Comparison between flat plate girders and girders with corrugated webs | 28 |
| 3 | EXPERIMENTAL TESTS | 30 |
| 3.1 | Test setup and execution | 30 |
| 3.2 | Load case A1 and B3: Position over an inclined fold | 32 |
| 3.3 | Load case A2 and B2: Position over a junction between two folds | 32 |
| 3.4 | Load case A3 and B1: Position over the centre of a longitudinal fold | 33 |
| 3.5 | Summary of test results | 33 |
| 4 | FINITE ELEMENT ANALYSIS | 34 |
| 4.1 | Modelling | 34 |
| 4.1.1 | Linear buckling analysis | 36 |
| 4.1.2 | Non-linear buckling analysis | 37 |
| 4.2 | Verification of the model | 38 |
| 4.2.1 | Beam theory – vertical deflection | 38 |
| 4.2.2 | Load-displacement curves and ultimate load | 39 |
| 4.2.3 | Buckling behaviour | 42 |
| 4.3 | Approximations and limitations | 46 |
| 4.4 | Parametric study | 47 |
| 5 | RESULTS | 48 |
| 5.1 | Influence of web thickness | 48 |
| 5.1.1 | Ultimate load | 48 |
| 5.1.2 | Load-deformation relationship | 49 |
| 5.1.3 | Postbuckling behaviour | 50 |
| 5.2 | Influence of flange thickness | 52 |
| 5.2.1 | Ultimate load | 52 |
| 5.2.2 | Load-deformation relationship | 53 |
| 5.2.3 | Postbuckling behaviour | 54 |
| 5.3 | Influence of local initial imperfections | 56 |
| 5.3.1 | Ultimate load | 56 |
| 5.3.2 | Load-deformation relationship | 57 |
| 5.3.3 | Postbuckling behaviour | 59 |
| 5.4 | Influence of load position | 61 |
| 5.4.1 | Ultimate load | 61 |
| 6 | CONCLUSIONS | 63 |

| | | |
|-----|--|----|
| 6.1 | On design models and comparison with FE-simulation results | 63 |
| 6.2 | Influence of increasing plate thickness | 63 |
| 6.3 | Influence of the load position | 63 |
| 6.4 | Influence of initial imperfections | 64 |
| 6.5 | Load-deformation behaviour | 64 |
| 7 | SUGGESTIONS FOR FURTHER RESEARCH | 65 |
| 8 | REFERENCES | 66 |

Appendix A: Comparison of earlier models (Mathcad)

Appendix B: Material properties

Appendix C: Test results

Appendix D: Result obtained using ABAQUS CAE

PREFACE

This master's thesis was carried out at the Division of Structural Engineering, department of Civil and Environmental Engineering at Chalmers University of Technology, Sweden, from January 2010 to September 2010.

First of all, we would like to thank our supervisor Professor emeritus Bo Edlund, for his valuable engagement and expertise during this thesis work. We would also like to thank our examiner Associate Professor (Docent) Mohammad Al-Emrani for his guidance and dedication.

We would also like to thank Ulf Mårtensson and Stefan Fogelström together with Borga Plåt AB for proposing the subject of the thesis and supplying the girder for experimental testing and Mathias Flansbjer at SP for his help during the experimental tests by providing measuring assistance. Additionally, we would like to thank Lars Wahlström for invaluable help during the preparation and performance of the experimental tests.

Further, we would like to express our gratitude towards our opponent group consisting of Anders Bohlin and Karin Olofsson for their interest and comments on the thesis.

Finally, our roommates during this semester, Robert Bengtsson and Mikael Widén, deserve some acknowledgements for their help and contributing to the positive atmosphere in the office.

Nikolaus Ljungström

Olof Karlberg

NOTATIONS

Roman upper case letters

| | | |
|----------|---|-------------------|
| D_x | flexural stiffness per unit-corrugation about the x-axis | [Pa] |
| D_y | flexural stiffness per unit-corrugation about the y-axis | [Pa] |
| E | Young's modulus of elasticity | [Pa] |
| E_w | Young's modulus of elasticity in the web | [N] |
| E_f | flange Young's modulus of elasticity in the flange | [N] |
| F_{cr} | elastic critical buckling load | [N] |
| F_R | ultimate load | [N] |
| F_y | yield resistance | [N] |
| I | moment of inertia | [m ⁴] |
| L | span length | [m] |
| M_{pf} | flange plastic moment capacity | [N] |
| P | load | [N] |
| P_b | buckling load | [N] |
| P_c | web crippling load | [N] |
| P_e | ultimate load obtained from tests | [N] |
| P_{fl} | flange capacity calculated from mechanism | [Nm] |
| P_u | ultimate load | [N] |
| P_w | web capacity calculated from mechanism, see Equation (2.27) | [N] |
| V | shear force | [N] |
| V_u | ultimate shear force | [N] |

Roman lower case letters

| | | |
|-----|--|-----|
| a | plate length (for flat steel plates) | [m] |
| a | width of an inclined fold of the corrugation | [m] |
| a | coefficient | [-] |
| b | coefficient | [-] |

| | | |
|--------------|--|------|
| b | plate length (for flat steel plates) | [m] |
| b | width of a longitudinal fold of the corrugation | [m] |
| b_a | coefficient | [-] |
| b_{eff} | effective width | [m] |
| b_f | flange width | [m] |
| c | longitudinal length of one corrugation, see Figure 2.5 | [m] |
| s_s | load length | [m] |
| d | longitudinal projection of an inclined fold of the corrugation | [m] |
| e_o | initial imperfection amplitude | [m] |
| f_{uf} | flange ultimate stress | [Pa] |
| f_{uw} | web ultimate stress | [Pa] |
| f_y | yield stress | [Pa] |
| f_{yf} | flange yield stress | [Pa] |
| f_{yw} | web yield stress | [Pa] |
| h | corrugation depth | [m] |
| h | plate height | [m] |
| h_w | web height | [m] |
| k | coefficient | [-] |
| $k_{cr,G}^e$ | coefficient for elastic critical global shear buckling | [-] |
| $k_{cr,I}^e$ | coefficient for elastic critical interactive shear buckling | [-] |
| k_F | buckling coefficient | [-] |
| k_G | global buckling coefficient | [-] |
| k_L | local buckling coefficient | [-] |
| k_σ | buckling coefficient | [-] |
| l | length of a fold | [m] |
| m | coefficient | [-] |
| p_{bt} | vertical deflection calculated with beam theory | [m] |
| p_{FEM} | deflections calculated with a FE-analysis | [m] |

| | | |
|-------------|---|-----|
| p_{test} | deflections obtained from test | [m] |
| p_{s1} | displacement obtained with a sensor | [m] |
| p_{s2} | displacement obtained with a sensor | [m] |
| p_{s3} | weighted displacement obtained with sensors | [m] |
| s | unfolded length of one corrugation | [m] |
| a_{yield} | distance between plastic hinges | [m] |
| t | plate thickness | [m] |
| t_f | flange thickness | [m] |
| t_w | web thickness | [m] |
| w | maximum fold width | [m] |

Greek lower case letters

| | | |
|-----------------|---|------|
| α | angle of corrugation | [°] |
| γ | coefficient | [-] |
| γ_s | coefficient in Equation (2.23) | [-] |
| γ_α | coefficient in Equation (2.23) | [-] |
| η | correction coefficient | [m] |
| λ | slenderness ratio | [-] |
| λ_s | shear buckling parameter | [-] |
| ν | Poisson's ratio | [-] |
| $\bar{\sigma}$ | mean stress in plate | [Pa] |
| σ_{cr} | elastic critical stress | [Pa] |
| σ_{min} | minimum stress in plate | [Pa] |
| σ_{max} | maximum stress in plate | [Pa] |
| σ_w | average failure stress of the web | [Pa] |
| τ | shear stress | [Pa] |
| $\tau_{cr,G}$ | critical shear stress for global buckling | [Pa] |
| $\tau_{cr,G}^e$ | critical shear stress for elastic global buckling | [Pa] |

| | | |
|-------------------|---|------|
| $\tau_{cr,I}^e$ | critical shear stress for elastic interactive buckling | [Pa] |
| $\tau_{cr,L}$ | critical shear stress for local buckling | [Pa] |
| $\tau_{cr,L}^e$ | critical shear stress for elastic local buckling | [Pa] |
| τ_y | shear yielding stress | [Pa] |
| χ | reduction coefficient | [-] |
| <i>Girder 10X</i> | Girder with load over inclined fold, see Appendix D for details | |
| <i>Girder 20X</i> | Girder with load over junction, see Appendix D for details | |
| <i>Girder 30X</i> | Girder with load over long. fold, see Appendix D for details | |

1 INTRODUCTION

1.1 Background

Since the 1960s, there has been an ongoing research of using thin-walled corrugated webs instead of flat webs in steel girders. This research has mainly been focused on the shear resistance of corrugated webs. However, the research on the patch load capacity of girders with corrugated webs has been limited.

Borga Plåt AB is a company which has manufactured and sold prefabricated building systems using thin-walled steel elements since the mid 1980s. Today, Borga Plåt AB offers steel frame structures using girders with corrugated webs. The purlins supported by these girders act as concentrated loads on the top flange. Hence, vertical stiffeners have been necessary to arrange at the load positions. In order to optimize the production, Borga Plåt AB wants to eliminate the need for vertical stiffeners but because of the lack of codes with design models considering patch loading on girders with corrugated webs, a more thorough analysis on the topic is needed.

1.2 Objectives

The purpose of this master's thesis is to investigate existing design models for steel girders with corrugated webs subjected to patch loading. Further, the aim is to – through a FE-analysis – study how the patch load capacity of a girder with a corrugated web is affected by changes in the dimensional properties of the girder.

1.3 Method

In order to reach the pronounced aim, the project is divided into four stages:

Initially, a literature study is performed to achieve deeper knowledge of the subject and to locate the existing design models regarding patch load capacity of girders with corrugated webs. Included in this stage is a parametric study in which the objective is to investigate how each model responds to changes in certain parameters.

In the next stage, experimental tests are performed on a girder provided by Borga Plåt AB. This to increase the amount and variation of the experimental tests performed to investigate the patch load capacity of the type of girders concerned.

Based on the girder used in the experimental tests, a FE-model is developed in ABAQUS CAE. Additionally, the results from the experimental tests are used in the verification process of the FE-model.

Finally, a parametric study is carried out using the FE-model developed in the earlier stage. In this study, certain parameters are selected based on information gathered from the initial stage and discussions with Borga Plåt AB. The results from the parametric study are then analysed in the final chapter along with conclusions.

1.4 Limitations

The scope of this master's thesis is limited as follows:

- Girders with webs of constant depth will be analysed.
- Patch loading on top flange and at positions within positive moment.
- Same material properties in flanges and web.
- The corrugation profiles regarded in this thesis will be of trapezoidal shape.
- Though the final parametric study includes results on the buckling behaviour and load-deformation relationship, the main focus will be on results concerning the ultimate load.

1.5 Outline and content

In chapter 2, a literature study is presented involving a presentation of the behaviour of rectangular thin plates under compression and an overview of research on girders with corrugated webs. Here, existing design models regarding patch load capacity of girders with corrugated webs are presented. Finally, this chapter includes a parametric study which is performed to investigate how changes in certain parameters affect the results using the presented design models.

In chapter 3, the setup and execution of the experimental tests are presented along with results divided into sections for each load case.

In chapter 4, the FE-modelling process and analysis are presented. The chapter is divided into four sections. Initially, the details of the model regarding: dimensions, material properties, element types, mesh, boundary conditions and load types are presented. Further, the steps of the analysis are explained. This is followed by a presentation of the verification process of the FE-model. Finally, the chapter explains how the parametric study is performed along with a presentation of the considered parameters.

Chapter 5 presents the results from the parametric study performed with the FE-model using the matrix shown in Appendix D. The results are divided into sections of results related to ultimate load, load-deformation relationship and postbuckling mode. Furthermore, these results are presented in separated sections for each parameter.

Chapter 6 includes conclusions.

Chapter 7 presents suggestions for further research.

2 LITERATURE STUDY

This chapter is divided into four main sections; “Rectangular thin plates under compression”, “Overview of research on girders with corrugated webs”, “Parametric study based on presented models” and “Comparison between flat plate girders and girders with corrugated webs”. The initial section briefly presents certain key elements considering thin plate webs. This involves a presentation of various theories and equations developed to study the general behaviour of plates under axial compression, but also some information on the patch loading behaviour. The following section gives information on girders with corrugated webs. Here, the characteristics of the girder type are presented followed by an overview of the behaviour under shear loading and bending moment. Additionally, this section gives a more detailed presentation of the patch load behaviour of girders with corrugated webs, including a presentation of the developed design models regarding the subject. This is followed by a parametric study which is performed to investigate how changes in certain parameters affect the results using the presented design models. In the final section in this chapter, comparisons are made between girders with flat webs and corrugated webs with regard to patch load capacity and material usage.

2.1 Rectangular thin plates under compression

2.1.1 Plates under uniformly distributed load

In 1897, an analysis of the elastic critical stress σ_{cr} of a simply supported rectangular plate subjected to a uniformly distributed in-plane compressive load, Equation (2.1) was published.

$$\sigma_{cr} = k_{\sigma} \cdot \frac{\pi^2 \cdot E}{12(1 - \nu^2)} \cdot \left(\frac{t}{b}\right)^2 \quad (2.1)$$

According to this, the elastic critical stress of a plate is governed by the width-to-thickness ratio, the elastic material properties and the buckling coefficient k_{σ} . Here, k_{σ} is a function of the restraint conditions along the longitudinal boundaries and the geometry of the plate (Galambos, 1998).

Since the 1930s, extensive amount of research on the behaviour of thin steel plates has been carried out. This has increased the understanding and resulted in more accurate models on how to predict different instability problems. The various approaches developed on how to obtain the buckling behaviour of thin plates begin by defining the slenderness parameter, λ , according to Equation (2.2).

$$\lambda = \sqrt{\frac{F_y}{F_{cr}}} \quad (2.2)$$

In order to calculate λ an estimation of the yield resistance, F_y , of the plate is needed. The yield resistance is usually set to the maximum resistance without considering strain hardening.

In order to determine the buckling resistance, the elastic critical buckling load, F_{cr} , must be established. It may be written as a function of the slenderness parameter.

$$f(\lambda) = \frac{F_{cr}}{F_y} = \frac{1}{\lambda^2} \quad (2.3)$$

An important paper on the theory of the post-buckling behaviour of thin plates was published by Theodore von Kármán et al. in the early 1930s. The assumptions made by von Kármán et al. (1932) resulted in a simplified way to study a post-buckled plate and to obtain the maximum load by using an effective width approach.

The principle of the effective width approach, when studying the post-buckling behaviour of an axially loaded plate, is to assume that the ultimate load is reached when the maximum stresses at the edge of the plate are equal to the yield strength of the material.

In order to simplify the stress distribution and to achieve an easier expression of the problem, the stresses are divided uniformly into two equally sized strips along the edges subjected to the maximum load. Further, the resistance of the mid area of the plate, where the buckle develops, is assumed negligible; see Figure 2.1 (Gozzi, 2007).

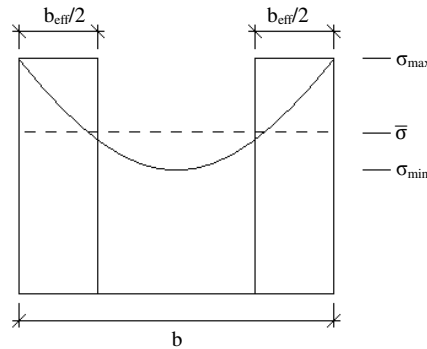


Figure 2.1: Approximate stress distribution represented by two vertical strips with an effective width, b_{eff} , along the vertical edges of the plate.

By using the effective width approach, von Kármán et al. (1932) proposed that the ultimate load in a plate would be reached when the critical buckling stress in the strips with the total width b_{eff} is equal to the yield stress, f_y , according to Equation (2.4).

$$\sigma_{cr} = f_y \rightarrow f_y = k_{\sigma} \cdot \frac{\pi^2 \cdot E}{12(1 - \nu^2)} \cdot \left(\frac{t}{b_{eff}} \right)^2 \quad (2.4)$$

Further, when dividing Equation (2.1) with (2.4), an expression for the χ -function is obtained.

$$\chi = \frac{b_{eff}}{b} = \frac{1}{\lambda} \quad (2.5)$$

However, the application of Equation (2.5) was limited to very thin plates and resulted in an overestimation of the ultimate resistance for plates in the intermediate slenderness range. Hence, there have been some modifications of the equation in order to reach better predictions of the behaviour of structural elements and the version presented by Winter (1947) is used in EN 1993-1-5 (2006) for plate buckling, Equation (2.6).

$$\chi = \frac{1}{\lambda} - \frac{0,22}{\lambda^2} \quad (2.6)$$

2.1.2 Plates with partial edge load (patch load)

The approach introduced gives rather accurate results for plates subjected to a *uniformly distributed* load. However, a *concentrated* load will result in a more complicated stress distribution. Though, as in all buckling problems, the buckling coefficient, k_F , needs to be established in order to calculate the elastic critical buckling load. The value of the buckling coefficient depends on, in similarity to k_σ , static and geometrical boundary conditions.

$$F_{cr} = k_F \cdot \frac{\pi^2 \cdot E}{12 \cdot (1 - \nu^2)} \cdot \frac{t_w^3}{h} \quad (2.7)$$

In a model established by Zetlin in 1955 the concentrated load is considered as a partly distributed load – of length s_s – acting along an edged of a plate. Further, the plate is prevented to move laterally and allowed to move in the plane of the plate. The reaction forces developed due to the applied load is defined as parabolic shear stresses along the edges parallel to the load direction, see Figure 2.2. Zetlin performed several test varying the load and plate dimensions generating different values of k_F . Several similar tests were performed throughout the 1970s introducing various modifications to the original model. One such modification, introduced by Rockey and Bagchi in 1970 was to redistribute the parabolic shear forces at the edges into uniformly distributed shear forces in order to obtain a simpler expression. Rockey and Bagchi also included the flexural and torsional properties of the flanges, thus establishing a more realistic model for the analysis of a beam under patch loading (Gozzi, 2007).

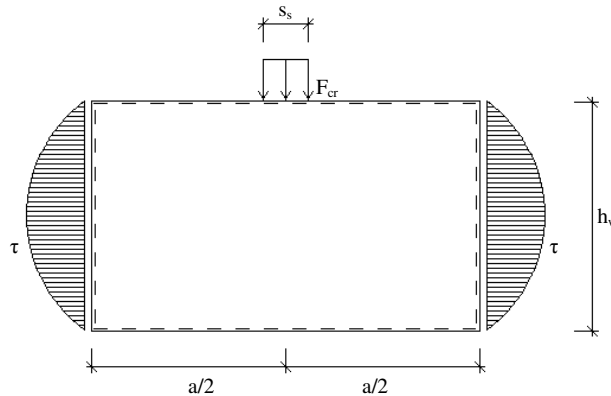


Figure 2.2: Plate model with parabolic shear reactions.

Several approaches on how to calculate the buckling coefficient has been developed based on the model introduced by Zetlin. However, the research by Lagerqvist (1994) in which he analysed the influence of a range of parameters resulted in the expression used in EN 1993-1-5 (2006). Though, this is a simplified expression where the load length is neglected and the influence from the flanges is set to a fixed value, see Equation (2.8).

$$k_F = 6 + 2 \cdot \left(\frac{h_w}{a}\right)^2 \quad (2.8)$$

The response of a steel plate girder subjected to patch loading can be described by one of three potential failure modes; yielding, buckling and crippling as seen in Figure 2.3. The mode which actually occurs is primarily dependent on the slenderness of the web and the ratio of t_f/t_w . In general, a stocky web indicates yielding failure while a slender web indicates buckling failure and a high ratio of t_f/t_w indicates buckling or crippling failure while a low ratio of t_f/t_w indicates yielding failure. In reality, crippling and buckling are usually combined and may be difficult to separate. This could however be seen as a gradual change of buckling shape as the load increases. Normally, the buckling mode initially develops and is then succeeded by crippling at larger loads (Galambos, 1998).

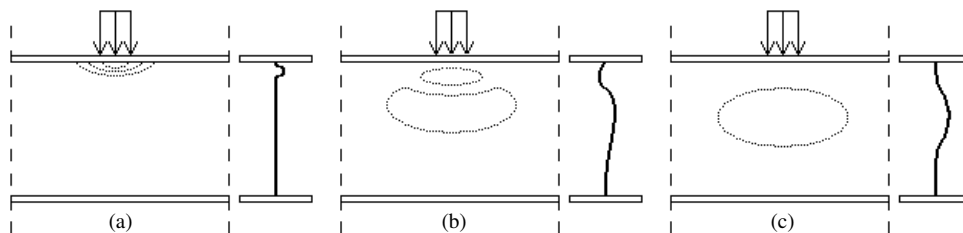


Figure 2.3: Failure modes for plate girders under concentrated load. Mode (a) is yielding, (b) is crippling and (c) is buckling.

Initially, in order to calculate the ultimate load of a steel plate girder subjected to patch loading, several empirical models were established. Many different equations have been developed since the 1960s of which the majority are somewhat complicated and not very practical to use. However, Equation (2.9) presented by Bergfelt in 1971 gives relatively accurate results while it is very easy to use (Gozzi, 2007).

$$F_R = 0,045 \cdot E \cdot t_w^2 \quad (2.9)$$

To make more accurate predictions of the ultimate resistance of steel plate girders the mechanism models were introduced in the late 1970s. These models include a plastic hinge solution where a number of plastic hinges develops in the loaded flange and the web a failure. Since 1979, when the first model, based on a four-hinge mechanism, there have been numerous similar contributions. One such model, introduced by Bergfelt in 1979, is based on a three-hinge mechanism in the flange and a uniformly distributed resistance in the web (Figure 2.4). In this model the flange initially acts as a beam resting on an elastic foundation i.e. the web. At a certain load, a plastic hinge is developed under the point of loading and the stresses in the web under the load reach the yield strength of the web. As the load increases, the yielding area of the web

expands. Finally, the ultimate load is reached when two plastic hinges are developed on each side of the load. However, since crippling failure often is preceded by elastic buckling of the web, the yield stress of the web may not be reached. This is solved by using von Kármán's approximation as the average failure stress of the web, σ_w ; see Equation (2.10). This model is sometimes called “Three-Hinge-Flange”-theory and is relatively simple to use (Gozzi, 2007).

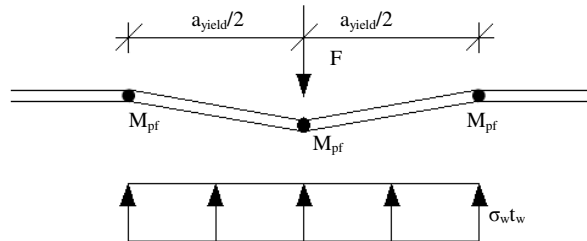


Figure 2.4: Ultimate failure model according to Bergfelt (Gozzi, 2007).

$$\sigma_w = \sqrt{\sigma_{cr} \cdot f_{yw}} \quad (2.10)$$

2.2 Overview of research on girders with corrugated webs

In order to obtain stiffer plate girders, more resistant to buckling, but without additional stiffeners or by increasing the web thickness, the concept of using webs with a corrugated profile was created. In the 1960s, the development of thin walled steel girders with corrugated webs began in Sweden, although the knowledge of the behaviour of such elements was limited. However, by rather rough estimations of the load carrying capacity, the design of corrugated webs has been carried out with a somewhat large safety margin. In addition to the economical benefits of excluding stiffeners and still being able to use very thin webs, the increased stiffness of the corrugated profile provides a series of other valuable features. One such advantage is the increased robustness during transportation and assembly which, for regular flat webs, usually requires double sided welds between web and flanges. For corrugated profiles it is sufficient to use single-sided welds. The high strength-to-weight ratio of corrugated steel webs is beneficial not only in service but also during transportation and erection (Bergfelt et al., 1985).

As mentioned earlier, the amount of published results from tests of corrugated webs is relatively limited. Nevertheless, as the concept of corrugated webs is not entirely new, the collected data from experiments performed over the past half century gives rather good conclusions concerning bending and shear capacity. As the focus of this thesis lies on the behaviour of girders with corrugated webs under patch loading, research on other load situations will only be briefly reviewed.

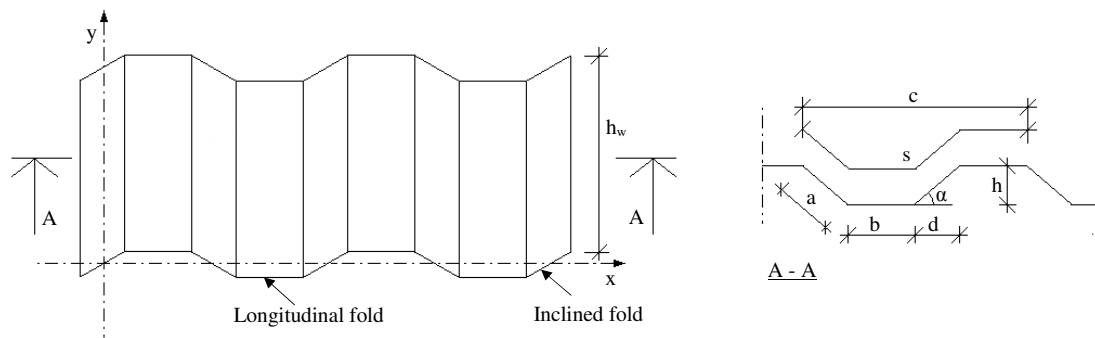


Figure 2.5: Schematic illustration of a trapezoidally corrugated web and its geometric parameters.

2.2.1 Shear capacity

According to Wang (2003), Hamilton (1993), in his Ph.D. thesis, describes that, the approximation that the web only carries shear forces is applicable due to the so-called accordion effect. Hence, the buckling behaviour of the shear force is probably the phenomenon which has been studied most when it comes to this category of girders.

In 1981, the Division of Steel and Timber Structures at Chalmers University of Technology began research on the shear behaviour of girders with trapezoidally corrugated webs. Experimental tests were performed on 15 girder of with varying depths (low, medium and deep) in order study the buckling behaviour. From the tests, it was observed that the failure mode was dependent on the depth of the girder (Bergfelt et al., 1985).

The approach and results of two series of tests carried out in the early 90s on the shear strength of girders with corrugated webs are described in an article entitled “Shear strength of beams with corrugated webs (Elgaaly et al., 1996). The former series, performed by Smith in 1992, comprised four tests on two girders. However, one of the girders failed prematurely due to too high stresses in a weld. In the second series, Hamilton (1993) did 42 tests on 21 beams of which all gave somewhat expected results as they failed due to buckling (Elgaaly et al., 1996).

In order to conduct a parametric study, Elgaaly et al. (1996) established a FE-model which was verified by the tests mentioned earlier. Overall, the comparison between the analytical model and the experimental results showed good agreement. Further, it is concluded that a coarse corrugation of the web will result in a failure controlled by local buckling of the longitudinal folds of the corrugation and global buckling will occur using a more dense corrugation profile.

An article by Sayed-Ahmed (2005) gives a rather detailed explanation of existing models describing the shear behaviour and the buckling modes of girders with corrugated webs. Based on the approximation that such webs only carry shear forces, failure of corrugated webs may only occur by shear yielding and/or shear buckling. Further, Sayed-Ahmed (2005) discusses the general behaviour of girders with corrugated webs including the two different possible boundary conditions of the web provided by the flanges; simply-supported and clamped. The former is typical for

girders with steel flanges while the latter is typical for composite girders with concrete flanges.

When discussing the stability of the web, it is stated that two buckling modes are associated with corrugated webs; a local and a global one. According to Sayed-Ahmed (2005), the local buckling mode is corresponding to the instability of a flat panel simply supported by between two folds. Here, the support is generated by corrugation profile of the web which acts as a series of flat panels mutually supporting each other along the vertical edges. Similar as for flat webs, the critical shear stress $\tau_{cr,L}$ for the local buckling mode can be derived from the theory of stationary potential energy:

$$\tau_{cr,L} = k_L \frac{\pi^2 E}{12(1 - \nu^2)} \left(\frac{t_w}{b} \right)^2 \quad (2.11)$$

Here, the buckling coefficient k_L is a function of b/h_w with b being the panel width and h_w , the web depth. Additionally, the value of k_L is dependent on the horizontal boundary conditions of the web provided by the flanges.

The buckling mode for global failure is characterized by diagonal buckling over several panels. In 1969, Easley and McFarland presented an estimation of the critical shear stress for global buckling, see Equation (2.12).

$$\tau_{cr,G} = k_G \frac{(D_y D_x^3)^{1/4}}{h_w^2 t_w} \quad (2.12)$$

In similarity to local buckling failure, the global buckling coefficient is stated as k_G but is however, only influenced by the top and bottom constraints of the web. The variables D_y and D_x are the flexural stiffness per unit-corrugation about the y - and x -axes respectively.

In a more recent report, “*Shear strength and design of trapezoidally corrugated steel webs*”, Moon et al. (2008) mention the need for a more accurate model to be used in shear buckling design and that the models presently used result in an unnecessary large margin of safety. Further, Moon et al. (2008) performed several experimental tests of which the results were compared to a design criterion. This is based on the conclusion that the interactive shear buckling is only influenced by the geometry of the corrugation profile and not by material yielding or inelasticity. The elastic interactive shear buckling stress $\tau_{cr,I}^e$ may thus be obtained from Equation (2.13) which combines the classical form of the critical shear stress for local bending and the global one described by Easley and McFarland.

$$\frac{1}{\tau_{cr,L}^e} + \frac{1}{\tau_{cr,G}^e} = \frac{1}{\tau_{cr,I}^e} \quad (2.13)$$

Consequently, the elastic interactive shear buckling stress can be written in a similar form as the classical plate buckling equation, see Equation (2.14), in which the interactive shear buckling coefficient $k_{cr,I}^e$ is defined as presented in Equation (2.15).

$$\tau_{cr,I} = k_{cr,I}^e \frac{\pi^2 E}{12(1-\nu^2)} \left(\frac{t_w}{h_w}\right)^2 \quad (2.14)$$

$$k_{cr,I}^e = \frac{k_L k_G}{\left[k_L + k_G \left(\frac{W}{h_w}\right)^2 \right]} \quad (2.15)$$

During design, the elastic interactive shear buckling stress is used by including it in the expression for the shear buckling parameter of corrugated webs, λ_s , as in Equation (2.16).

$$\lambda_s = \sqrt{\frac{\tau_y}{\tau_{cr,I}^e}} \quad (2.16)$$

Moon et al. (2008) conducted three experimental tests on girders, all in the inelastic region of $0.6 < \lambda_s \leq \sqrt{2}$, with similar dimensions but different corrugation profiles. Additionally, the initial imperfections were measured in order to investigate their influence on the shear buckling strength. Further, the results are used to verify the proposed shear buckling strength along with experimental results from tests performed earlier in Japan and South Korea. It is finally concluded that, in comparison to earlier studies, the suggestion by Moon et al. (2008) gives a better estimation of the shear strength of trapezoidally corrugated steel webs.

2.2.2 Bending capacity

Elgaaly et al. (1997) published a report on the bending strength of steel beams, in which they state: “it appears that the only tests, to examine the behaviour of girders with corrugated webs subjected to bending, were performed by Hamilton in 1993”. The results from these tests are presented and discussed in the report and in addition, a FE-model is developed in order to visualize these results.

Six specimens of similar global dimensions but with varying corrugation profile were subjected to increasing bending until failure. At maximum load, all specimens showed a sudden failure due to yielding of the compression flange followed by vertical buckling. From the results, it is concluded that strains in the web are very small while strains in the flanges increase linearly up to yield strain of the flange at failure. Hence, the contribution of the web to the bending capacity of the girder may be considered negligible. Additionally, it is stated that there is no apparent interaction between shear and bending (Elgaaly et al., 1997).

In summation, it is concluded that there is no interaction between shear forces and bending moments and additionally, the bending strength is controlled by the flanges. This master’s thesis aims at describing the behaviour of girders with corrugated webs under patch loading. Thus, there is no reason to investigate the topic of bending capacity further.

2.2.3 Overview of experimental tests on girders subjected to patch loading

In 1974, a Swedish consulting firm, Arne Johnson Ingenjörbyrå AB (Carling (1974)), performed 52 tests on two girders with corrugated webs subjected to patch loading. 36 of these tests were conducted on the undamaged parts of a girder earlier loaded up to bending failure and the other 16 tests on a girder loaded up to shear failure. The motivation of the tests was to establish an empirical basis for design values, based on the failure load. The two girders had h_w/t_w ratios of 300 and 500 and the t_w/t_f ratios of 0.2 and 0.25. The longitudinal folds of the corrugation profile had a length of 140 mm, the angle of the inclined folds was 45° and the depth of the corrugation was 40 mm.

During loading, a concentrated load of 10 mm length was placed in two different positions representing two different load scenarios. In the first scenario the load was applied over a longitudinal fold and in the other scenario the load was applied over an inclined fold. The girders were simply supported with a span of up to 1 m. The dimensions and material properties of the girders together with load length and test results are shown in Table 2.1.

Table 2.1: Girder specifications and results obtained from tests performed by Carling (1974).

| Tests | Load pos. | h_w [mm] | t_w [mm] | b_f [mm] | t_f [mm] | E [GPa] | P_u [kN] |
|-------|-----------|------------|------------|------------|------------|---------|------------|
| 18 | Long. | 600 | 2 | 200 | 10 | 210 | 86 |
| 18 | Inc. | 600 | 2 | 200 | 10 | 210 | 90 |
| 8 | Long. | 750 | 1.5 | 150 | 6 | 210 | 42 |
| 8 | Inc. | 750 | 1.5 | 150 | 6 | 210 | 51 |

Based on the results, Carling (1974) proposed an empirical model, see Equation (2.17), resulting in an ultimate load twice as large as the model Bergfelt suggested for girders with flat webs in 1971 (Carling, 1974).

$$P_u = 0,04 \cdot E t_w^2 \quad (2.17)$$

A series of tests was performed at Chalmers University of Technology in 1983 by Leiva-Aravena. Here, three girders with trapezoidally corrugated webs and varying geometries were each subjected to different scenarios of patch loading. The depths of the girders were 1.0, 1.5 and 2.0 m. The web thickness for the deepest girder was 2.0 mm while the web thickness of the other two girders was 2.5 mm, thus resulting in the h_w/t_w ratios of 400, 600 and 1000. Two different flange thicknesses were used; 10 mm in the two stockiest girders and 12 mm in the most slender girders, resulting in the t_w/t_f ratios of 0.25 and 0.21. All specimens had equal corrugation profiles where the length of the longitudinal folds was 140 mm, the angle of the inclined folds was 45° and the depth of the corrugation was 50 mm. During testing, the girders had a span length of 1 m and were supported in order to prevent transverse and vertical deflections. The tests were performed with varying load positions. These positions were: above the centre of an inclined fold, the centre of a longitudinal fold or at a corner point between two folds. The load was distributed either as a very concentrated load through a semi-cylinder –

load length about 5 mm – or through a flat plate as a concentrated load with a length of 50 mm.

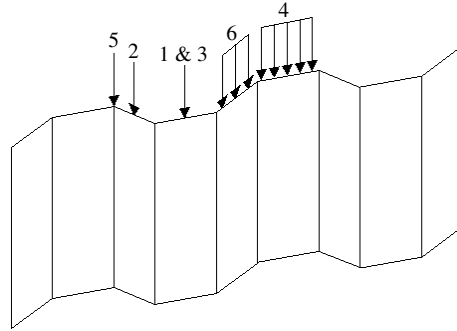


Figure 2.6: Load cases for the experimental tests performed by Leiva-Aravena in 1983 (Leiva-Aravena and Edlund, 1987).

The results from the experiments showed that web thickness is a decisive factor with a major influence on the behaviour of girders with corrugated webs subjected to patch loading. Under the circumstances present in the test, the variation in web thickness from 2.0 to 2.5 mm resulted in an increase of the ultimate strength of about 35-40 %. The variation of the of the load distribution length seemed to have a relatively small influence, showing an increase of the ultimate load of about 10 % when increasing the load distribution length from 5 to 50 mm. The variations in loading position also had an effect on the load capacity. An increase of about 10 % on the load carrying capacity was obtained when the load was positioned over an inclined fold rather than over a longitudinal fold (Leiva-Aravena and Edlund, 1987).

Table 2.2: Material and dimensional specifications of tested girders and test results.

| Case | h_w [mm] | t_w [mm] | b_f [mm] | t_f [mm] | f_{yw} [MPa] | f_{yf} [MPa] | E [GPa] | P_u [kN] |
|------|---------------|---------------|---------------|---------------|-------------------|-------------------|--------------|---------------|
| 1 | 1000 | 2.5 | 250 | 10 | 260 | 350 | 210 | 149 |
| 2 | 1000 | 2.5 | 250 | 10 | 260 | 350 | 210 | 170 |
| 3 | 1500 | 2.5 | 250 | 10 | 260 | 350 | 210 | 152 |
| 4 | 1500 | 2.5 | 250 | 10 | 260 | 350 | 210 | 168 |
| 5 | 2000 | 2 | 250 | 12 | 260 | 350 | 210 | 107 |
| 6 | 2000 | 2 | 250 | 12 | 260 | 350 | 210 | 124 |

The results of four out of the six tests published by Leiva-Aravena and Edlund were analysed further in a master’s thesis by Dahlén and Krona (1984). In the thesis, the ultimate loads obtained experimentally were compared to the ultimate loads calculated using Bergfelt’s “Three-Hinge-Flange”-theory, see Equation (2.18), with the assumption that the inclined folds of the corrugation profile act as stiffeners.

$$F_R = 0.8 \cdot t_w^2 \cdot \sqrt{E \cdot f_{yw}} \cdot \sqrt{\frac{t_i}{t_w}} \cdot f(s_s) \cdot f\left(\frac{a_{yield}}{l}\right) \quad (2.18)$$

where $\frac{t_i}{t_w} > 2$ and l is the length of the loaded fold. a_{yield} is here assumed to comprise the length of the three nearest folds.

$$t_i = t_f \sqrt[4]{\frac{b_f}{25t_f}} \quad (2.19)$$

$$f(s_s) = 1 + 40 \cdot \frac{s_s}{a_{yield}} \cdot \frac{t_w}{h_w} \quad (2.20)$$

$$f\left(\frac{a_{yield}}{l}\right) = 2 \cdot \frac{a_{yield}}{l} \cdot \sqrt{\frac{1 + \sqrt{1 + mk \cdot \left(\frac{l}{2a_{yield}}\right)^4}}{1 + \sqrt{1 + mk}}} \quad (2.21)$$

Here, m is an adjustment coefficient which is set to $m = 20$. The coefficient k is equal to $2,5\alpha^4$ with $\alpha = 1.5$.

The conclusions from the analysis made in the thesis are summed up under these few points (Dahlén and Krona, 1984).

- The test results correspond to a 20 % higher resistance than those obtained analytically with the “Three-Hinge-Flange”-theory.
- Regarding the most concentrated load, the ultimate strength is about 14 % higher when applying the load over an inclined fold than applying the load over a longitudinal fold.
- A load distributed 50 mm over a longitudinal fold will result in about the same value of the ultimate load as a load distributed 5 mm over an inclined fold. However, the latter will result in a 25 % higher value of the initial buckling load.
- In these tests, the ultimate load is not affected by h_w .
- The maximum lateral deflection of the web occurs at about 3 % of h_w below the upper flange.
- Increased load distribution will result in buckling closer to the flange.
- A load over an inclined fold will result in less local lateral deflection of the web.

In an article, Leiva-Aravena and Edlund (1987) use the results from experiments performed by Leiva-Aravena in 1983 to compare the behaviour of steel girders with corrugated webs to similar girders with flat webs. Among other conclusions, they conclude that in both the case of shear and patch loading, the load bearing capacity of the girders with corrugated webs will be of about twice that for girders with flat webs (Leiva-Aravena and Edlund, 1987).

In addition to the six experiments performed by Leiva-Aravena in 1983, Elgaaly and Seshadri (1997) carried out five similar tests in 1996. All of their five tests were performed on the same girder but with a relocation of the load between testing in order

to represent five different load cases as seen in Figure 2.7. In order to be able to conduct the testing on the same girder, only two of the cases, 1 and 2, were performed on one side. The girder was then flipped upside-down and the remaining three tests, using load cases 3, 4 and 5, could be performed. The load cases are shown in Figure 2.7.

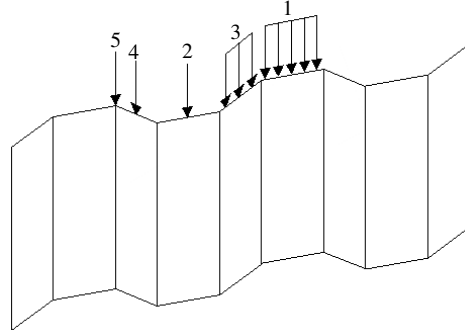


Figure 2.7: The five different cases in which the load was applied in the experiments by Elgaaly and Seshadri (1997).

The slenderness ratio, h_w/t_w , of the girder was 188 and the t_w/t_f ratio was 0.2. The girder had a corrugation profile where the length of the longitudinal folds (“horizontal” folds) was 130 mm, the angle of the inclined folds was 40° and the depth of the corrugation was 101 mm. The girder specifications and test results are given in Table 2.3.

Table 2.3: Material and dimensional properties of the tested girder and test results.

| Case | h_w [mm] | t_w [mm] | b_f [mm] | t_f [mm] | f_{yw} [MPa] | f_{yf} [MPa] | E [GPa] | P_u [kN] |
|------|---------------|---------------|---------------|---------------|-------------------|-------------------|------------|---------------|
| 1 | 376 | 2 | 120 | 10 | 379 | 389 | 200 | 131 |
| 2 | 376 | 2 | 120 | 10 | 379 | 389 | 200 | 82 |
| 3 | 376 | 2 | 120 | 10 | 379 | 389 | 200 | 102 |
| 4 | 376 | 2 | 120 | 10 | 379 | 389 | 200 | 96 |
| 5 | 376 | 2 | 120 | 10 | 379 | 389 | 200 | 73 |

2.2.4 FE-analyses performed to study girders subjected to patch loading

In 1994, Lou and Edlund (1994) performed a detailed FE-analysis of steel girders with trapezoidally corrugated webs. In the analysis, parameters considered were: strain-hardening model, corner-effects, initial imperfections (global and local), loading position, load distribution and geometric parameters. The results from the tests performed earlier by Leiva-Aravena were used to verify the analysis and finally, an empirical formula, calculating the ultimate load for girders with corrugated webs, was suggested, similar to Bergfelt and Lindgren’s formula for girders with flat webs, Equation (2.22).

$$P_u = \gamma t_f t_w \sigma_y^w \quad (2.22)$$

where the coefficient γ is given by (with new constant 10.4 as proposed by Bo Edlund):

$$\gamma = 10.4\gamma_\alpha\gamma_{s_s} \quad (2.23)$$

Here, γ_α is depending on the corrugation profile of the web, where b is the width of the longitudinal folds in the corrugation profile, α is the corrugation angle and l is the width of an inclined fold. In Equation (2.24) a misprint in the published article (which may lead to a misinterpretation) has been corrected.

$$\gamma_\alpha = \frac{b + l}{b + l \cos \alpha} \quad \text{for} \quad t_f/t_w \geq 3.82 \quad (2.24)$$

$$\gamma_\alpha = 1 \quad \text{for} \quad t_f/t_w < 3.82 \quad (2.25)$$

The value of γ_{s_s} depends on the distribution of the load (s_s is the loading length in mm) and η as a correction coefficient ($\eta = 1/240$).

$$\gamma_{s_s} = 1 + \eta s_s \quad (2.26)$$

The authors conclude that the resulting ultimate load will be 8-12 % larger when using the Ramberg-Osgood strain-hardening model instead of the elastic-perfectly plastic model. Further, it was found that corner-effects and small global imperfections will not have any significant influence on the ultimate load. However, local imperfections with amplitudes of up to half the size of the web thickness can reduce the ultimate load with up to 7 %. Another conclusion presented in the report is that the highest value of the ultimate load is obtained when applied over the centre of an inclined fold as seen in Figure 4.1. Furthermore, the lowest value is obtained when applied as a strip load on the flange over the centre of a longitudinal fold. The length of the load has a significant influence on the load-carrying capacity. In the report, it can be observed that by increasing the load length, the ultimate load will increase. Additionally, by increasing the angle of the inclined folds, the load-carrying capacity will increase. However, a corrugation angle larger than 75° will not have any further effect. Lou and Edlund also state that an increase of the web and flange thickness will increase the load-carrying capacity almost proportionally, while the panel dimensions will have almost no effect at all (Luo and Edlund, 1994).

Further, in 1997 a FE-analysis was performed by Elgaaly and Seshadri (1997). The results from the five tests by Elgaaly and Seshadri (1997) in combination with the results from the six tests by Leiva-Aravena in 1983 were used for verification of the model. Based on the FE-model, a parametric study was carried out which included the impact of changes in load length, load position, t_w/t_f ratio, web panel aspect ratio and corrugation profile.

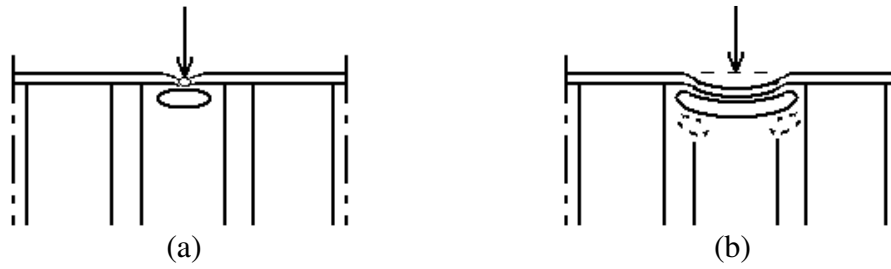


Figure 2.8: Failure modes regarding patch loading; (a) web yielding; (b) web crippling.

The analysis resulted in two different failure modes, web crippling and web yielding (see Figure 2.8), for which two different equations were presented; see Equations (2.30) and (2.31). To calculate the web crippling, Elgaaly and Seshadri (1997) suggest the following approach.

$$P_w = (E f_{yw})^{0.5} t_w^2 \quad (2.27)$$

$$P_{fl} = \frac{4 \cdot M_{pf}}{a - \frac{s_s}{4}} \quad (2.28)$$

Here, a is a function depending on the geometry and the yield strength of the profile and also the load length s_s .

$$a = \left[\frac{f_{yf} b_f t_f^2}{(2 f_{yw} t_w)^{0.5}} \right] + \frac{s_s}{4} \quad (2.29)$$

$$P_u = P_c = P_{fl} + P_w \quad (2.30)$$

To calculate the web yielding the following approach is suggested.

$$P_u = P_y = (b + b_a) t_w f_{yw} \quad (2.31)$$

Here, b_a depends on corrugation depth, flange dimensions and the yield strength ratio, while b depends on the geometry of the inclined folds (Elgaaly and Seshadri, 1997).

Additionally, Elgaaly and Seshadri (1997) studied the interaction behaviour between patch load and in-plane bending or shear. In this analysis, two different profiles were used; one with a relatively coarse corrugation (profile I) and one with more shallow corrugation (profile II). Profiles I and II were analysed using homogeneous steel properties. Additionally, profile II was also analysed using different steel properties in flange and web (hybrid). For comparison, Equations (2.32) and (2.33) were plotted together with the results from the analysis of the interaction between patch loading and shear (see Figure 2.9a).

$$\left(\frac{P}{P_u}\right)^{1.8} + \left(\frac{V}{V_u}\right)^{1.8} = 1 \quad (2.32)$$

$$\left(\frac{P}{P_u}\right)^{1.25} + \left(\frac{V}{V_u}\right)^{1.25} = 1 \quad (2.33)$$

A similar comparison was made with the results for interaction between patch loading and in-plane bending and Equations (2.34) and (2.35) (see Figure 2.9b).

$$\left(\frac{P}{P_u}\right)^2 + \left(\frac{M}{M_u}\right)^2 = 1 \quad (2.34)$$

$$\left(\frac{P}{P_u}\right)^{1.25} + \left(\frac{M}{M_u}\right)^{1.25} = 1 \quad (2.35)$$

For girders with flat webs, Equations (2.32) and (2.34) are recommended when analysing the interaction behaviour between patch loading and shear and patch loading and in-plane bending, respectively. Additionally, the curves generated by Equations (2.32) and (2.34) illustrate an average to the results of the FE-analysis and Equations (2.33) and (2.35) are proposed equations which represent lower bound solutions to the interaction situations (Egaaly and Seshadri, 1997).

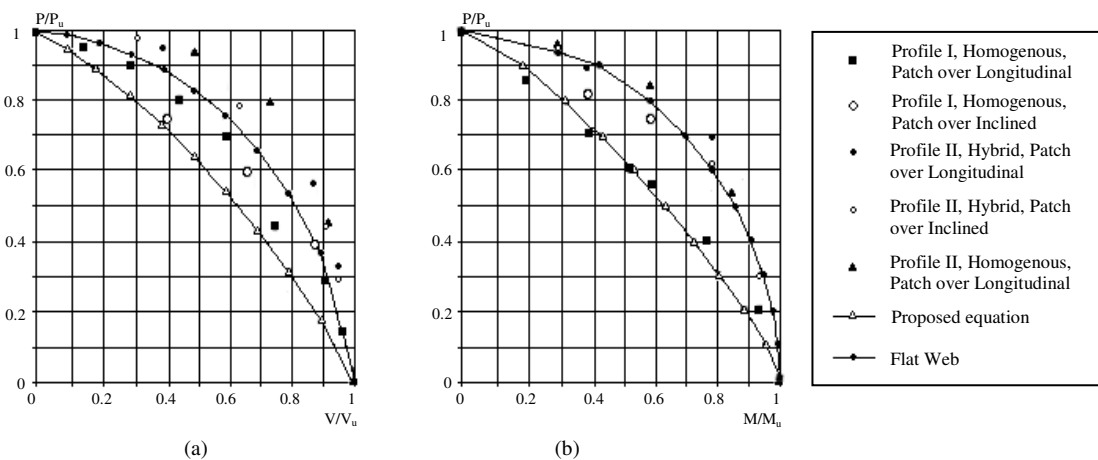


Figure 2.9: Interaction curves; (a) between shear and patch loading; (b) between bending and patch loading.

A formula for load carrying capacity based on crippling failure was presented by Pasternak and Bránka in 1999. According to verifications by Kuchta (2006), this formula proved to be rather accurate. However, since it does not include the load length, the validity of the formula is restricted to small load lengths and results in underestimations of the load carrying capacity, when the load length is increased.

At a conference in 2006, Kuchta (2006) presented results from a FE-analysis performed to study the ultimate strength on two girders with sinusoidally corrugated webs. The analysis included a rather thorough investigation on the effect of load length and web

thickness on the load-carrying capacity of girders with corrugated webs. The length of the load varied from 25 mm up to 250 mm and the three different web thicknesses were; 2 mm, 2.5 mm and 3 mm. Based on the results from the analysis, Kuchta (2006) concluded that the ultimate load increases almost linearly to the load length as seen in Figure 2.10 (Kuchta, 2006).

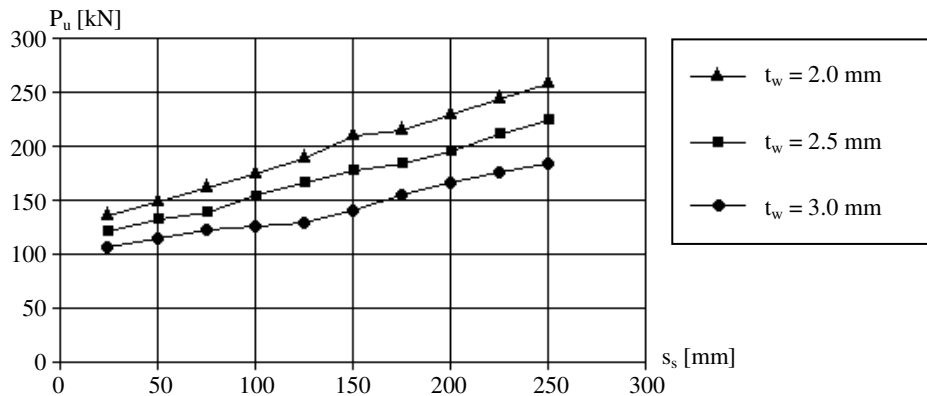


Figure 2.10: The “linear” relationship between load length and ultimate strength – for different web thicknesses – obtained by Kuchta (2006).

2.2.5 Summary of previous studies on patch loaded girders

In total, 63 experimental tests, distributed over three test series, have been presented in this thesis. These have been performed on six girders whereof 52 of the tests were performed on two of the girders in the earliest series by Arne Johnson Ingenjörbyrå AB. Due to a lack of information on material properties and test settings, this series of tests is difficult to evaluate. All test results are collected in Table 2.4.

The experimental tests and FE-analyses presented are performed on girders of relevant dimensional properties which enable verification of the FE-model introduced later in this thesis.

Girders with h_w/t_w ratios of 188, 300, 400, 500, 600 and 1000 have been tested. The relatively low value of 188 represents the girder used in the tests by Elgaaly and Seshadri (1997). By comparing the results of tests 1 and 3 by Leiva-Aravena in Table 2.4 it can be noticed that h_w/t_w does not seem to have any significant effect on the ultimate load. However, since the yield strength f_{yw} in the tests by Elgaaly and Seshadri (1997) is considerably larger than in the other tests (unknown in the tests by Arne Johnson Ingenjörbyrå AB) this comparison might be difficult. Nevertheless, based on obtained results from the experimental tests, the conclusion that the ultimate strength is not affected by h_w – made by Dahlén and Krona (1984) – seems to be relevant.

A conclusion made by Leiva-Aravena in 1983 is that the load length has a very small influence on the ultimate load of the girder (Dahlén and Krona, 1984). This is however not verified by any other researcher but is actually contradictory to the conclusion made by Lou and Edlund (1994) who stated that the load length has a large impact on the ultimate load. The latter conclusion is based on the FE-analysis by Lou and Edlund (1994). Additionally, Kuchta (2006) states that the load length has a significant effect

on the ultimate load where the ultimate load increases linearly up to rather long load length as seen in Figure 2.10.

Table 2.4: Summary of all previous experimental test results presented in this thesis.

| Load Pos. | Tests | l/t_w [mm] | $\frac{h_w}{t_w}$ | $\frac{t_w}{t_f}$ | s_s [mm] | f_{yw} [MPa] | P_b [kN] | $\frac{P_b}{Et_w^2}$ | P_u [kN] | $\frac{P_u}{Et_w^2}$ | |
|-----------|---|-----------------|-------------------|-------------------|---------------|-------------------|---------------|----------------------|---------------|----------------------|--------|
| I | Long. ** | 18 | 70 | 300 | 0.20 | 10 | - | 62* | 0.077 | 48* | 0.108 |
| | Inc. ** | 18 | 35 | 300 | 0.20 | 10 | - | 63* | 0.079 | 50* | 0.112 |
| | Long. *** | 8 | 93 | 500 | 0.25 | 10 | - | 32* | 0.071 | 75* | 0.094 |
| | Inc. *** | 8 | 47 | 500 | 0.25 | 10 | - | 40* | 0.088 | 90* | 0.113 |
| II | Long. | 1 | 56 | 400 | 0.25 | 5 | 318 | 132 | 0.106* | 149 | 0.119* |
| | Inc. | 1 | 28 | 400 | 0.25 | 5 | 318 | 157 | 0.126* | 170 | 0.136* |
| | Long. | 1 | 56 | 600 | 0.25 | 5 | 318 | 82 | 0.066* | 152 | 0.121* |
| | Long. | 1 | 56 | 600 | 0.25 | 50 | 318 | 120 | 0.096* | 168 | 0.134* |
| | Junction | 1 | 0 | 1000 | 0.21 | 5 | 285 | 75 | 0.094* | 107 | 0.133* |
| | Inc. | 1 | 36 | 1000 | 0.21 | 50 | 285 | 89 | 0.111* | 124 | 0.155* |
| III | Long. | 1 | 70 | 188 | 0.20 | 146 | 379 | - | - | 131 | 0.163* |
| | Long. | 1 | 70 | 188 | 0.20 | 0 | 379 | - | - | 82 | 0.102* |
| | Inc. | 1 | 39 | 188 | 0.20 | 104 | 379 | - | - | 102 | 0.127* |
| | Inc. | 1 | 39 | 188 | 0.20 | 0 | 379 | - | - | 96 | 0.120* |
| | Junction | 1 | 0 | 188 | 0.20 | 0 | 379 | - | - | 73 | 0.091* |
| Notes: | <p>* The value is calculated with an approximated Young's modulus of 200 GPa ** Prior to the tests, the girder was loaded up to moment failure and the undamaged parts of the girder were used *** Prior to the tests, the girder was loaded up to shear failure and the undamaged parts of the girder were used I Tests performed by Arne Johnson Ingenjörbyrå, Carling (1974) II Tests performed by Leiva-Aravena III Tests performed by Elgaaly and Seshadri (1997)</p> | | | | | | | | | | |

None of the experimental tests considers the interaction between patch loading and moment or shear forces. However, Elgaaly and Seshadri (1997) considered this in their FE-analysis and plotted the behaviour as seen in Figure 2.9. Elgaaly and Seshadri (1997) proposed Equations (2.33) and (2.35), which represent lower bound solutions to the interaction behaviour. The plotted results indicate that shallow corrugation profiles will result in higher interaction than coarse corrugation profiles will.

According to the FE-analysis by Lou and Edlund (1994), the ultimate load would increase if the corrugation angle is increased up to 75°. It can be noticed that in all the experiments, girders with a corrugation angle of 40-45° have been used, i.e. relatively small compared to 75°. Further, it is not stated which of the additional dimensional parameters of the corrugation profile that are changed as the angle is changed. Additionally, the effects of the corrugation angle when loaded over a junction between two folds do not seem to have been investigated. Thus, it may be interesting to investigate the significance of corrugation angle further and, if it is possible, to maximize the load carrying capacity with regard to corrugation angle.

The parametric study by Lou and Edlund (1994) is the only one considering the initial imperfections of the girder. They state that global imperfections will not affect the

ultimate load. However, local imperfections up to half the size of the web thickness could reduce the ultimate load with up to 7 %.

All the results presented indicate that by applying the load over an inclined fold, the highest value of the ultimate load will be obtained. According to Leiva-Aravena and Elgaaly and Seshadri (1997) the lowest value of the ultimate load will be obtained when applied over a junction between two folds. However, Luo and Edlund (1994) conclude that the lowest value will be obtained when applying the load over a longitudinal fold.

Finally, Leiva-Aravena and Edlund (1987) estimate that the shear and patch load capacity of a girder with a corrugated web will be twice as large as that of a similar girder with a flat web.

2.3 Parametric study based on presented models

In this section, a parametric study of the models presented in sections 2.2.3 and 2.2.4 will be conducted in order to examine the influence on the ultimate load for each selected parameter in the different models. Further, the results will be plotted and compared together in graphs for each studied parameter. The nine parameters considered are: web thickness, corrugation angle, corrugation depth, web depth, flange thickness, flange width, length of longitudinal folds, load length and loading position. The length and the projection length of the inclined folds will be governed by the corrugation angle and depth h .

While varying each studied parameter at a time, the other parameters of the considered girder will be kept at the following reference values:

Table 2.5: Dimensional properties used as reference values in the parametric study based on presented models.

| b_f [mm] | t_f [mm] | h_w [mm] | t_w [mm] | α [°] | b [mm] | h [mm] |
|------------|------------|------------|------------|--------------|----------|----------|
| 180 | 12 | 600 | 2 | 45 | 70 | 50 |

If nothing else is told, the load will be applied at a strip on the flange over the centre of a longitudinal fold with a load length of $s_s = 50$ mm (similar to the load illustrated in Figure 4.1). The material properties will be constant over the cross section. The values chosen are: Yield stress $f_y = 355$ MPa in flanges and web, and Young's modulus $E = 210$ GPa.

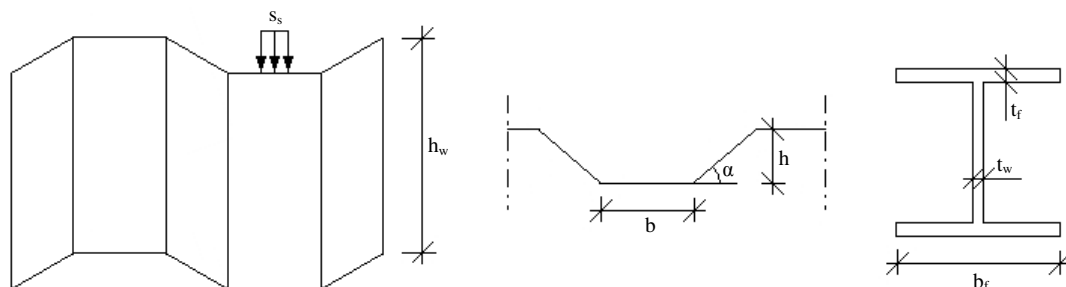


Figure 2.11: Schematic illustration of the dimensional parameters considered in the parametric study.

2.3.1 Web thickness

In all the models, the ultimate load increases as the web thickness is increased, see Figure 2.12. The models by Carling (1974), Dahlén and Krona (1984) and Elgaaly and Seshadri (1997) show similar increase patterns, although the model by Carling (1974) results in the lowest values, but not the lowest increase rate of the ultimate load. The model by Lou and Edlund (1994) has more of a linear dependence on the web thickness. However, this rate of dependence changes at a web thickness somewhere between 3 and 4 mm due to a slenderness condition. All models except Carling (1974) will result in similar ultimate loads at web thicknesses below 3 mm. At higher web thicknesses, the model by Dahlén and Krona (1984) will result in the highest values of the ultimate load.

The total increases of the ultimate load, over the range 2 to 6 mm, using each design model are: 260 kN (Carling (1974)), 560 kN (Dahlén and Krona (1984)), 195 kN (Lou and Edlund (1994)) and 370 kN (Elgaaly and Seshadri (1997)).

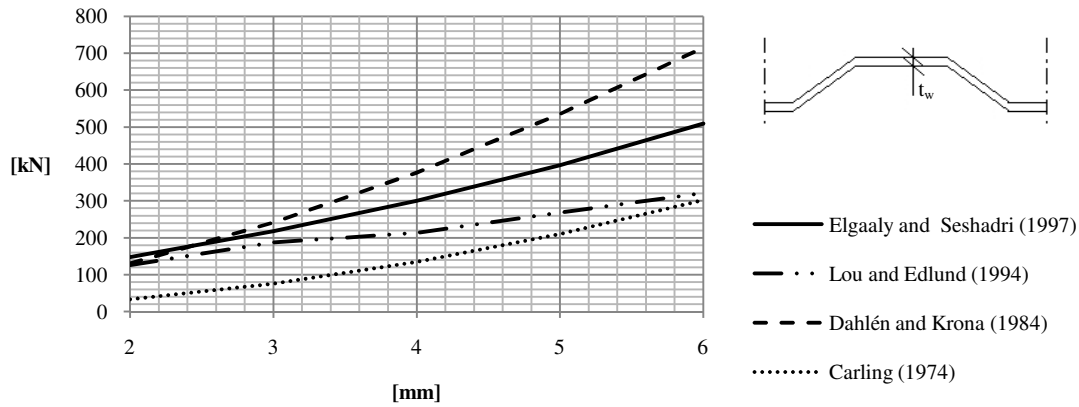


Figure 2.12: Influence of web thickness on the ultimate load using the models presented in the literature study.

2.3.2 Corrugation angle and depth

As it is mentioned in Section 2.2.3, the patch load capacity is strongly affected by the corrugation angle. However, according to Lou and Edlund (1994), this relationship is only valid at angles up to 75° at which further increase will not influence the ultimate load. As can be seen in Figure 2.13, the only model, in which changes of the corrugation angle (and corresponding corrugation depth) is included, is the one presented by Lou and Edlund (1994). At a corrugation depth of 75 mm, an increase of the corrugation angle from 30° to 75° will result in an increase in the ultimate load of almost 50 %. Similar scenarios will arise at corrugation depths of 25 and 50 mm. However, in these cases, the ultimate load will increase by 18 and 35 %, respectively. In conclusion, the ultimate load is more sensitive to changes in the corrugation angle at greater corrugation depths according to the model by Lou and Edlund (1994). Further, in that model the positive effects due to an increased corrugation angle will occur independently of load positive conditions or other dimensional parameters.

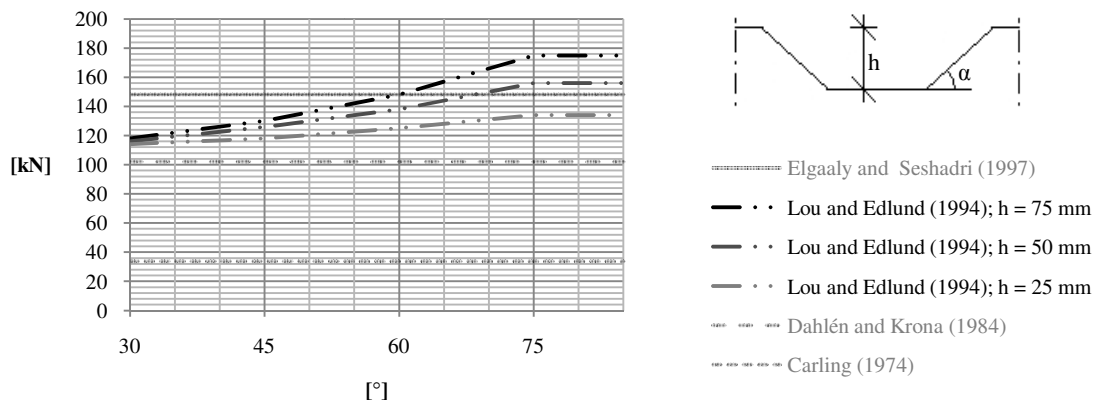


Figure 2.13: Ultimate loads at varying corrugation angles and corresponding corrugation depths using the models presented in the literature study.

2.3.3 Web depth

The only model, in which the influence of web depth on the ultimate load is included, is the one presented by Dahlén and Krona (1984). However, as can be viewed in Figure 2.14, the contribution is very small, resulting in a 2% decrease of the ultimate load when increasing the web depth from 500 mm to 2000 mm. This is also mentioned in Section 2.2.3 as a conclusion of the analysis by Dahlén and Krona (1984).

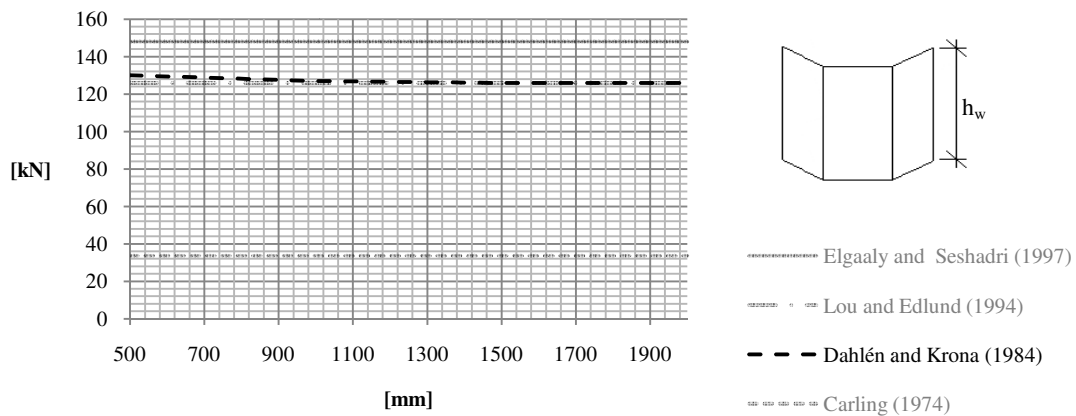


Figure 2.14: Influence of web depth on the ultimate load using the models presented in the literature study.

2.3.4 Flange thickness

As can be seen in Figure 2.15, the flange thickness has a great influence on the ultimate load in the models by Elgaaly and Seshadri (1997), Lou and Edlund (1994) and Dahlén and Krona (1984). All three models have a somewhat linear (the slope of the curve is decreasing very slightly) response to increase in the flange thickness. However, the rates at which the ultimate load increases due to increases in the flange thickness are quite different for the three models. The model by Carling (1974) does not include flange thickness as a parameter and is therefore unaffected to changes of it. The total increases of the ultimate load using each design model are: 65 kN (Dahlén and Krona (1984)), 150 kN (Elgaaly and Seshadri (1997)) and 164 kN (Lou and Edlund (1994)).

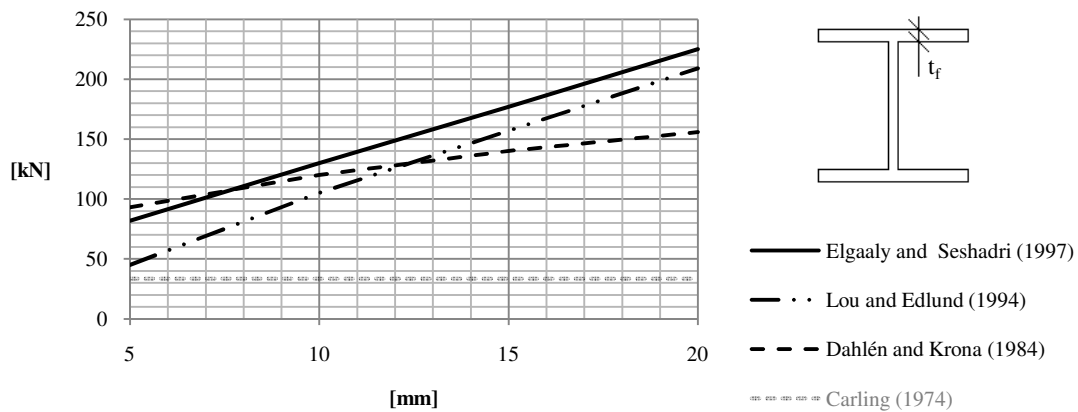


Figure 2.15: Influence of flange thickness on the ultimate load using the models presented in the literature study.

2.3.5 Flange width

Only two models consider the flange width as a parameter influencing the ultimate load. These are the models by Dahlén and Krona (1984) and Elgaaly and Seshadri (1997) of which only the latter shows significant response when varying the flange width. Changing the flange width from 100 to 200 mm, using the model by Elgaaly and Seshadri (1997), increases the ultimate load by 35 kN while as similar scenario using the model by Dahlén and Krona (1984) only increases the ultimate load by 5 kN. As the response is linear, it can be concluded that, according to Elgaaly and Seshadri (1997), an increase of the flange width will result in a relatively large increase in the ultimate load.

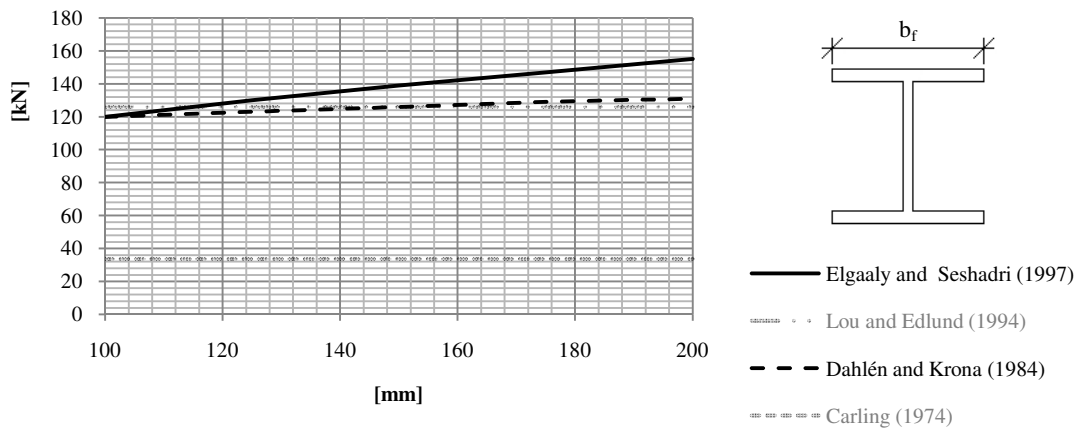


Figure 2.16: Influence of flange width on the ultimate load using the models presented in the literature study.

2.3.6 Length of longitudinal folds

As the load in this case acts on a longitudinal fold, an increase of the length of the longitudinal folds will result in a reduction of the ultimate capacity of the girder. The models presented by Dahlén and Krona (1984) and Lou and Edlund (1994) are the only

ones considering this parameter. The responses when changing the length of the longitudinal folds are shown in Figure 2.17, valid for $b \geq s_s = 50 \text{ mm}$. Here it can be observed that by increasing the length of the longitudinal folds from 50 mm to 150 mm, the ultimate load decreases by about 70 kN (44 %) using the model by Dahlén and Krona (1994) and about 20 kN (14 %) using the model by Lou and Edlund (1994). Using the model by Dahlén and Krona (1994), it seems that the response rate is exponentially decreasing with a minimum value of the ultimate load somewhere below 90 kN which is reached when the length of the longitudinal folds are somewhere above 90 mm. However, the decrease rate using the model by Lou and Edlund (1994) is linear.

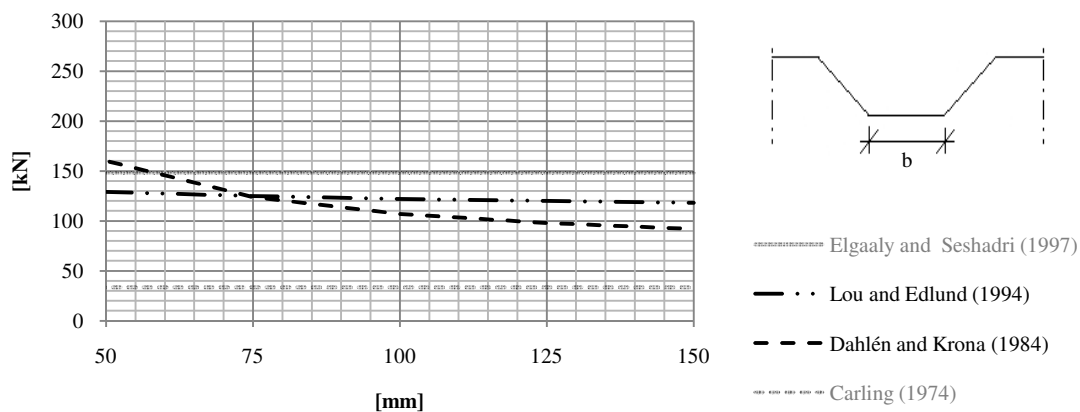


Figure 2.17: Influence of the length of the longitudinal folds on the ultimate load using the models presented in the literature study.

2.3.7 Load length

As seen in Figure 2.18, there is only one model where the patch load capacity seems to be significantly affected by the load length; the model by Lou and Edlund (1994). The relationship is linearly positive and in this case, the ultimate load increases about 43 kN when the load length increases from 0 mm to 100 mm. This is rather similar to the relationship presented by Kuchta (2005) which can be observed in Figure 2.10 in Section 2.2.4. Although the models by Dahlén and Krona (1984) and Elgaaly and Seshadri (1997) do include load length, these models do not seem to be significantly affected by changes to it. Only a small increase (about 5 kN) is obtained by using the model by Dahlén and Krona (1984).

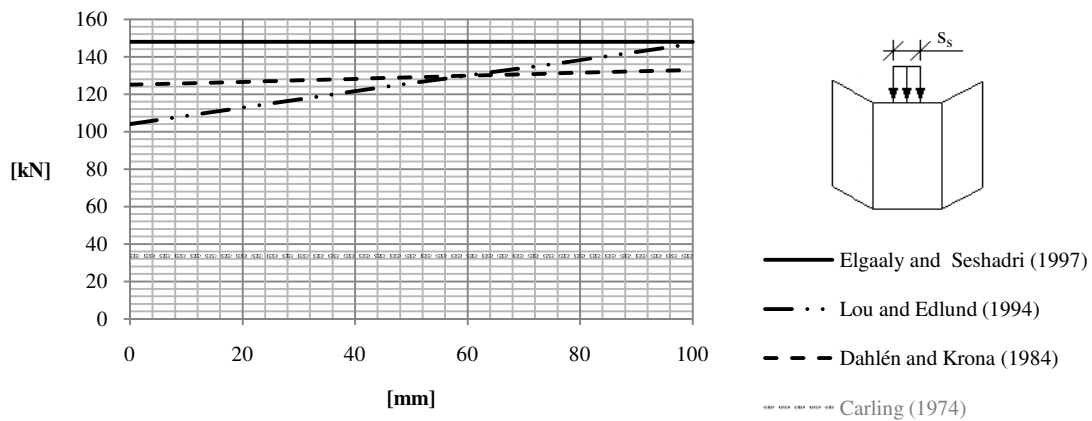


Figure 2.18: Relationship between load length and ultimate load using the models presented in the literature study.

2.3.8 Loading position

As it is proven through a series of testing, the ultimate load will be highly dependent on where on the girder the load is applied. Yet, the models by Elgaaly and Seshadri (1997) and Dahlén and Krona (1984) are the only ones considering this as a parameter. In the model by Dahlén and Krona (1984), the loading position is implemented by an approximation of the distance between the two outer plastic hinges in a failure mechanism. As can be viewed in Figure 2.19, the location which results in the lowest value of the ultimate load is – according to Dahlén and Krona (1984) – at the junction between two folds. This is consistent with the experimental results shown in Table 2.4 in Section 2.2.3. Further, according to Dahlén and Krona (1984), loading the girder over a longitudinal fold will result in the highest value of the ultimate load (almost 40 kN higher than when applied over a junction between two folds). Loading the girder over an inclined fold will result in an ultimate load of about 130 kN, i.e. about 10 kN lower than when loading the girder over a longitudinal fold and almost 30 kN higher than when loading the girder over a junction between two folds

The model by Elgaaly and Seshadri (1997) is the only one considering different failure modes – yielding and crippling. This is done by using different solutions depending on the load case. However, in this case, the difference between solutions is very small.

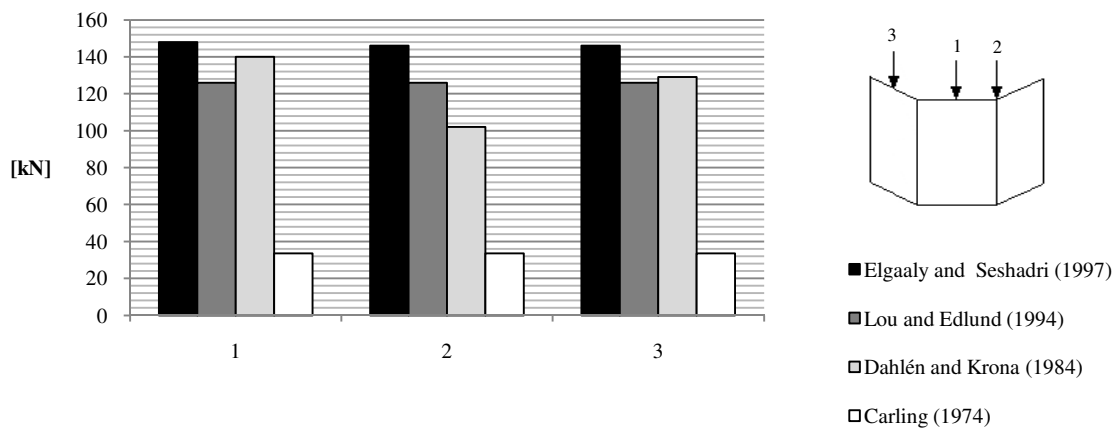








Figure 2.19: Influence of loading position on the ultimate load for the reference girder, Table 2.5, using the four models presented in the literature study; (1) longitudinal fold; (2) junction between two folds; (3) inclined fold.

2.3.9 Validity of the presented models

In order to validate the results from using the different models, a comparison with the experimental results found in the literature study need to be performed. In Table 2.6 this comparison is made between the resulting ultimate loads from the experiments, P_e [kN], and results from the different models applied on the tested girders, P_u [kN].

Table 2.6: Comparison between results from the four presented models and experimental tests.

| Test | Load pos. | P_e | Carling (1974) | | Dahlén and Krona (1984) | | Luo and Edlund (1994) | | Elgaaly and Seshadri (1997) | | |
|--------|--|-------|----------------|-----------|-------------------------|-----------|-----------------------|-----------|-----------------------------|-----------|------|
| | | | P_u | P_u/P_e | P_u | P_u/P_e | P_u | P_u/P_e | P_u | P_u/P_e | |
| I | 1 | Long. | 86 | 34 | 39% | - | - | - | - | - | - |
| I | 2 | Inc. | 90 | 34 | 38% | - | - | - | - | - | - |
| I | 3 | Long. | 42 | 19 | 45% | - | - | - | - | - | - |
| I | 4 | Inc. | 51 | 19 | 37% | - | - | - | - | - | - |
| II | 1 | Long. | 149 | 53 | 35% | 106 | 71% | 76 | 52% | 146 | 98% |
| II | 2 | Inc. | 170 | 53 | 31% | 253 | 149% | 76 | 45% | 146 | 86% |
| II | 3 | Long. | 152 | 53 | 35% | 106 | 70% | 76 | 50% | 146 | 96% |
| II | 4 | Long. | 168 | 53 | 31% | 107 | 64% | 91 | 54% | 153 | 91% |
| II | 5 | Junc. | 107 | 34 | 31% | 62 | 58% | 73 | 68% | 132 | 123% |
| II | 6 | Inc. | 124 | 34 | 27% | 196 | 158% | 87 | 70% | 144 | 116% |
| III | 1 | Long. | 131 | 34 | 26% | 130 | 99% | 152 | 116% | 119 | 91% |
| III | 2 | Long. | 82 | 34 | 41% | 120 | 146% | 96 | 117% | 119 | 145% |
| III | 3 | Inc. | 102 | 34 | 33% | 110 | 108% | 135 | 132% | 119 | 116% |
| III | 4 | Inc. | 96 | 34 | 35% | 104 | 108% | 96 | 100% | 119 | 124% |
| III | 5 | Junc. | 73 | 34 | 46% | 62 | 84% | 96 | 132% | 119 | 162% |
| Notes: | <p>* The value is calculated with an approximated Young's modulus of 210 GPa</p> <p>I Test performed by Arne Johnson Ingenjörbyrå AB, Carling (1974)</p> <p>II Test performed by Leiva-Aravena in 1983</p> <p>III Test performed by Elgaaly and Seshadri (1997)</p> <p> < 75% of experimental data</p> <p> 75-89% of experimental data</p> <p> 90-100% of experimental data</p> <p> 101-110% of experimental data</p> <p> 111-125% of experimental data</p> <p> >125% of experimental data</p> | | | | | | | | | | |

When comparing the results obtained using the various design models and the experimental tests the most conservative model by Carling (1974) gives the least varying results. Here, ultimate load from the design model will generally be about 30 % of that of the actual girder with a maximum value of 46 % and a minimum value of 26 %.

The model by Dahlén and Krona (1984) results in values of the ultimate load widely spread depending on the girder dimensions and load case. Compared to the ultimate loads obtained from the tests performed by Leiva-Aravena (1983), this model results in ultimate loads between 158 and 58 % of that of the experimental results. However, compared to the tests performed by Elgaaly and Seshadri (1997), the resulting ultimate loads obtained from this model are between 99 and 146 % of those obtained from the tests. This indicates that the model by Dahlén and Krona (1984) responds too much to variations in the dimensional parameters.

The main trends in the comparisons of the results obtained from the model by Dahlén and Krona (1984) can also be found when using the model by Lou and Edlund (1994). The latter model gives ultimate loads 45 to 70 % of those obtained from the tests performed by Leiva-Aravena (1983) and 100 to 132 % of those obtained from the tests performed by Elgaaly and Seshadri (1997).

The results closest to the experimental tests are obtained when using the model by Elgaaly and Seshadri (1997). This model results in ultimate loads of 86 to 123 % of those obtained from the tests performed by Leiva-Aravena (1983) and 91 to 162 % of those obtained from the tests performed by Elgaaly and Seshadri (1997).

In general, the models will generate the highest relative values when load is applied over an inclined fold, a junction between two folds and when the load length is very small. Why the models result in higher values when compared to the tests performed by Elgaaly and Seshadri (1997) might be due to the rather deep corrugation profile in those tests.

2.4 Comparison between flat plate girders and girders with corrugated webs

An important variable when determining the efficiency of girders with trapezoidally corrugated webs is the material need in order to achieve the required load capacity. As mentioned in section 2.2.3, a web with a corrugated profile will result in a patch load capacity of about twice that of a similar girder with a flat web. Considering this, it might seem very favourable to use these types of girders for elements subjected to patch loading. However, as a girder with a corrugated web may require more material than a regular girder with a flat web and vertical stiffeners, an analysis on the relationship between material consumption and ultimate patch load for girders with corrugated webs compared to girders with flat webs is in order.

In this section, calculations on the patch load capacity of girders with flat webs are made according to EN 1993-1-5 (2006) using five different web thicknesses, 2, 3, 4, 5 and 6 mm. The distance between the vertical stiffeners is set to 3000 mm and $\gamma_{M1} = 1.0$. Other than the web thickness, the dimensional and material parameters of the girder are set to the same values as the girder used in the parametric study in section 2.3, Table 2.5. In Table 2.7, the results from these calculations are presented along with the amount additional steel required compared to a girder with a corrugated web with a thickness of 2 mm. The details of the calculations are found in Appendix A.

Table 2.7: Patch load capacity and material consumption for flat web girders with varying web thickness (from calculations in Appendix A).

| t_w [mm] | F_{Pd} [kN] | Amount additional steel in web used compared to a girder with a corrugated web with a thickness of 2 mm |
|------------|---------------|---|
| 2 | 8 | - 10 % |
| 3 | 27 | 35 % |
| 4 | 34 | 80 % |
| 5 | 78 | 125 % |
| 6 | 147 | 170 % |

In order to evaluate these results comparisons are made with the results presented in Table 2.8 which contain the calculated patch load capacity of a girder with a corrugated web using the four different design models investigated in the parametric study in section 2.3.

Table 2.8: Patch load capacity of a girder with a corrugated web of same dimensions as the reference girder used in the parametric study performed in section 2.3. Calculations are made using the four design models investigated in the parametric study in section 2.3.

| Carling (1974) [kN] | Dahlén and Krona (1984) [kN] | Lou and Edlund (1994) [kN] | Elgaaly and Seshadri (1997) [kN] |
|---------------------|------------------------------|----------------------------|----------------------------------|
| 34 | 129 | 126 | 148 |

By comparing the ultimate loads in Table 2.7 and Table 2.8 the positive effects of using a corrugated web – with regard to patch loading – are obvious. Even when using the most conservative design model – Carling (1974) – a similar girder with a flat web requires a web thickness which is twice that of the corrugated web girder in order to obtain the same patch load capacity. This will result in a need for about 80 % more steel in the web using a flat web instead of a corrugated web.

Compared to the design model by Elgaaly and Seshadri (1997) a girder with a flat web would require a web thickness almost three times as large as that of a girder with a corrugated web in order to obtain the same patch load capacity. This will result in a need for about 170 % more steel in the web using a flat web instead of a corrugated web (the welding costs are not considered here).

Additionally, to choose girders with corrugated webs includes other positive features. One not regarded in this comparison is the need for welds between web and flanges only on one side of the girder whilst a girder with a flat web would require welds on both sides of the web. By including vertical stiffeners at the points of loading when using a girder with a flat web the patch load capacity would increase significantly. However, as this is expensive and would require additional labour, using girders with corrugated webs – without extra stiffeners – could be very profitable.

3 EXPERIMENTAL TESTS

For verification of the FE-model conducted by the authors and to increase the basis for future studies, experimental tests were performed at Chalmers University of Technology on a girder supplied by Borga Plåt AB. The dimensional properties of the tested girder are shown in Table 3.1. In this chapter, the setup and execution of these tests are presented along with results divided into sections for each load case.

Table 3.1: Dimensional properties of tested girder and load length.

| b_f [mm] | t_f [mm] | h_w [mm] | t_w [mm] | α [°] | b [mm] | h [mm] | s_s [mm] |
|------------|------------|------------|------------|--------------|----------|----------|------------|
| 160 | 12 | 578 | 3 | 45 | 140 | 50 | 50 |

3.1 Test setup and execution

The length of the two girder spans was 3 m. Vertical stiffeners were arranged at each support. In total, six tests were performed at various locations on the girder – as seen in Figure 3.1 – using a load length of 50 mm in all cases. The steel used in the girder is S355 with material properties presented in Appendix B.

By supporting the girder at each stiffener, the span during testing was 3 m with three tests conducted at each span. To separate the tests from each other, the two spans along with the corresponding test series, were named A and B. Tests A1, A2, B1 and B2 were initially performed on one edge of the girder. Further, the girder was then flipped upside down and tests A3 and B3 were performed.

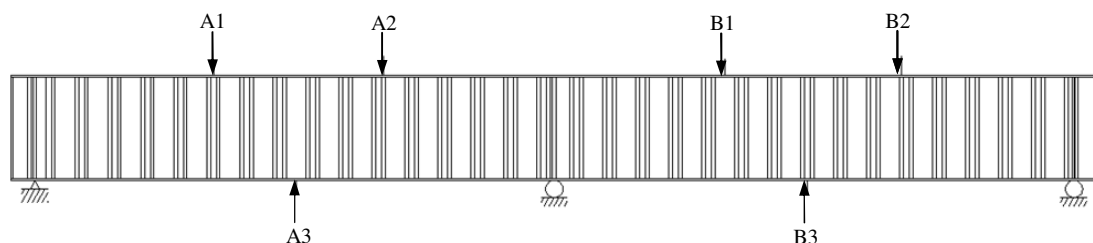


Figure 3.1: An illustration showing the tested girder and the load cases. Tests with load cases A1, A2, B1 and B2 were initially carried out and the girder was subsequently flipped upside-down enabling the two remaining tests to be performed. Total girder length: 6 m.

The loading was performed by a hydraulic jack – see Figure 3.2 – designed to create a load of up to 250 kN. The loading was displacement controlled with an increase of the vertical displacement – at the point of loading – of 0.2 mm per second. In all tests, the load increased up to the ultimate load and as the capacity decreased, the loading decreased accordingly until enough of the load-deformation behaviour had been registered. In order to avoid lateral-torsional buckling failure, the girder was laterally supported at a distance of about 500 mm from each side of the point of loading as seen in Figure 3.2. The displacements were measured at six locations; two at each support of the loaded span and two at the point of loading as seen in Figure 3.2.

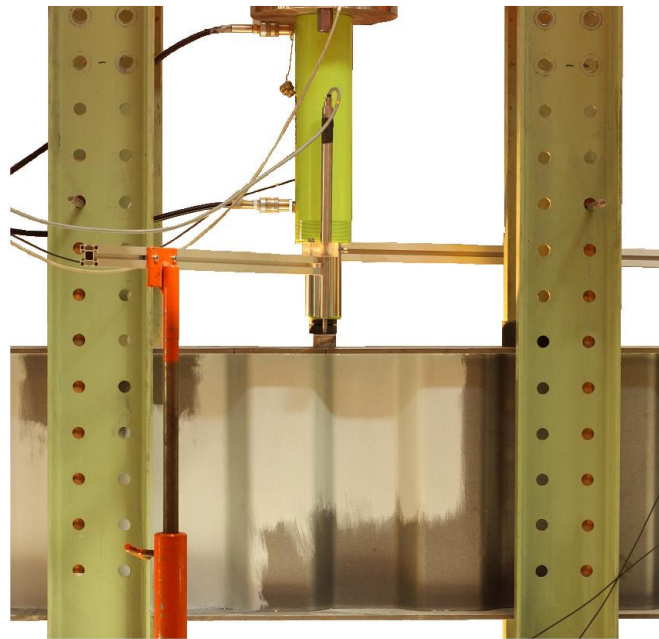


Figure 3.2: Test setup showing lateral supports, the hydraulic jack, the loading plate (200x50x30 mm) and the sensor which governs the rate of loading.

In order to measure the strains and to accurately follow the deformation development, the *Technical Research Institute of Sweden, SP*, provided their services. This involved a measuring technique using two cameras and a computer software which creates an animated three-dimensional image of the area under loading. The measuring area was about 500x500 mm which was large enough to capture the local deformation development during loading. The cameras photographed once each second which created a sequence of data that could be studied further.

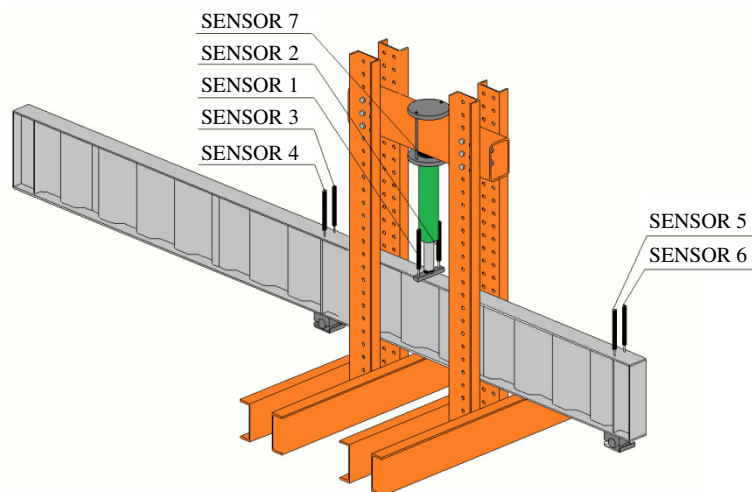


Figure 3.3: Illustration showing the test setup with the sensors measuring vertical displacements and applied load.

The local flange displacements were measured by six sensors located as seen in Figure 3.3. A seventh sensor was also included to measure the applied load. After the tests

were performed, the displacements measured by sensors 1 and 2 were weighted against each other based on the location of the load strip. For load cases A3 and B1 (longitudinal fold) this weighting proved to be very important in order to get results comparable with the FE-analysis performed later. The weighting was carried out by interpolation between the two sensors to the point where the centre of the loading strip encounters the web as seen in Figure 3.4. The load is applied at the centre of the loading strip, i.e. at the centre of the flange.

To eliminate possible disturbances at loading initiation, due to support conditions, the weighted values of the displacement measured by sensor 1 and 2 were reduced by the value of the displacements measured by sensors 3 to 6.

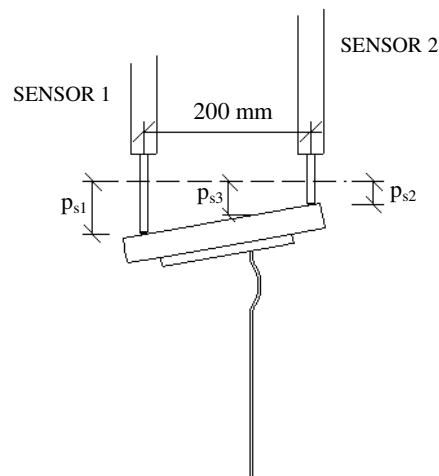


Figure 3.4: Schematic illustration on how the weighting of the displacements p_{s1} and p_{s2} is performed by interpolation into p_{s3} .

3.2 Load case A1 and B3: Position over an inclined fold

The load case which resulted in the highest ultimate load was the one loaded over an inclined fold (A1 and B3). Here, the ultimate load reached about 218 and 219 kN which also makes it the load case which resulted in the most steady values of the ultimate load, varying only by about 0.5 %.

In this load case, the visual buckling was initiated as a small buckle in the fold directly below the load. This buckle then spread through the adjacent longitudinal folds where two additional buckles developed. The maximum lateral deflection of the buckles occurred at about 35 to 55 mm from the inner face of the upper flange. The direction of the lateral deflection in each buckle was so that the two secondary buckles in the longitudinal folds had their convex side facing the same way while the main buckle in the inclined fold was faced the opposite way. From figures in sections C.6.1 and C.6.6 in Appendix C, it can be distinguished that the buckling initiated at a load of about 215 kN.

3.3 Load case A2 and B2: Position over a junction between two folds

At about 217 and 213 kN, a load applied over a junction between two folds (A2 and B2) resulted in the second highest ultimate values. The results in this case were not as

consistent as the previous case, varying by about 1.8 %. Furthermore, this load case resulted in the highest stiffness and the most dramatic decrease of capacity after reaching the ultimate load.

The buckling propagation in the web when applying the load over the junction between two folds (A2 and B2) was very similar to the behaviour when loading over an inclined fold and visual differences are not easily determined. Based on the figures in sections C.6.2 and C.6.5 in Appendix C it can be observed that no buckling is initiated until reaching a load just below the ultimate load.

3.4 Load case A3 and B1: Position over the centre of a longitudinal fold

By applying the load over a longitudinal fold (A3 and B1), the lowest resulting ultimate loads were obtained. An important notice is that, due to the great distance between one edge of the flange and the web, the load induced a rotation around the connection between the web and the flange. Consequently, very large displacements at one edge of the flange were obtained. This load case also resulted in the lowest stiffness of all tests. However, the behaviour obtained with this load case was the most ductile. Additionally, this case resulted in the most differed values of the ultimate load, 181 and 192 kN, varying by 5.7 %.

When loading the girder over a longitudinal fold (A3 and B1), the visible buckle was mainly restricted to the fold which is directly below the load, with the exception of small areas very close to the flange. Here, very small lateral deformations can be observed which has spread to the adjacent folds. The main buckle is in both cases shaped so that the convex side of the buckle is facing the same direction as the convex side of the corrugation profile in that area. This might be because of the rotational movement around the connection between the flange and the web which was mentioned earlier. The maximum lateral deflection of the web occurs at 27 to 30 mm from the inner face of the upper flange. In the same manner as for the other two load cases, figures in sections C.6.3 and C.6.4 in Appendix C indicate that buckling is initiated long before reaching the ultimate load.

3.5 Summary of test results

The collected values of the ultimate loads from the tests are shown in Table 3.2. For more detailed results on the load-deformation curves, strains and buckling modes, see Appendix C.

Table 3.2: *Ultimate loads obtained from tests.*

| Test | Load case | P_e [kN] |
|------|------------|------------|
| A1 | Inc. fold | 219 |
| A2 | Junction | 217 |
| A3 | Long. fold | 181 |
| B1 | Long. fold | 188 |
| B2 | Junction | 213 |
| B3 | Inc. fold | 218 |

4 FINITE ELEMENT ANALYSIS

In this chapter, the FE-modelling process and analysis is presented. The chapter is divided into four sections. Initially, section 4.1 describes the details of the model regarding: dimensions, material properties, element types, mesh, boundary conditions and load. Further, section 4.1 also explains the steps of the analysis. This is followed by section 4.2 which presents the verification process of the FE-model and section 4.3 which mentions some approximations and limitations in the analysis. Finally, section 4.4 describes how the parametric study in chapter 5 is performed along with a presentation of the considered parameters.

4.1 Modelling

The girder consists of three parts (top and bottom flange and a web with stiffeners) modelled with quadratic shell elements S8R with 5 integration points through the plate thickness. Only one span of the girder is modelled as the influence of the self weight of the other part of the girder is considered negligible. The corrugation profile of the web has the dimensional properties listed in Table 3.1 with the exception that only 3 m of the girder is modelled as mentioned earlier. The radius R of the curved shape between adjacent folds is set to 30 mm based on measurements on the tested girder as seen in Figure 4.1.

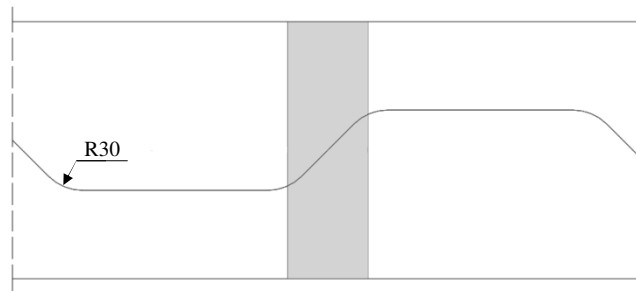


Figure 4.1: Detail of the corrugation profile with R30 as the radius of the curved shape at the junctions between folds. The area highlighted in gray is an example on how the load is applied on the flange. In this figure, a load over an inclined fold is depicted, i.e. load cases A1 and B3 in the tests.

As the interaction between patch loading and shear force or patch loading and bending moment does not seem to have any significant influence on the results, it is sufficient to choose one point of loading which represents one of the locations used in the experimental tests and run all numerical simulated tests in that area of the girder and still get comparable results. Hence, the load is applied as pressure on an area of $50 \times 160 \text{ mm}^2$, i.e. $s_s b_f$ about one meter from a support.

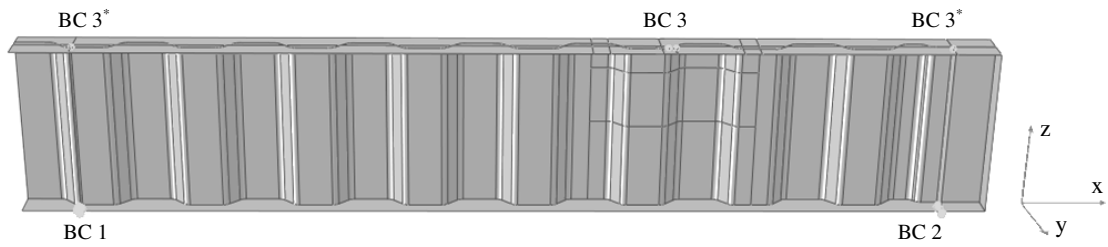


Figure 4.2: Boundary conditions used in the FE-model. Further descriptions are made in Table 4.1.

The supports are introduced as boundary conditions at the edges of the girder as seen in Figure 4.2. To avoid lateral torsional buckling, a boundary condition at the area of loading is applied, preventing movement along the y-axis, see Figure 4.2. The connection between web and flanges are modelled as rigid.

Table 4.1: Explanations of the boundary conditions shown in Figure 4.2.

| | x | y | z |
|-------|---------------------------|--------|--------|
| BC 1 | Locked | Locked | Locked |
| BC 2 | Free | Locked | Locked |
| BC 3 | Free | Locked | Free |
| Note: | * Locked just in one node | | |

Before establishing a material model, material testing was performed. However, as measurements of the plastic strain were not included, only the Young's modulus and yield stress were possible to obtain for each test. The yield stresses were estimated according to EN 1993-1-5 (2006) by removing 0.2 % of the elastic strain as seen in Figure 4.3a. Further, a bilinear behaviour with a plastic hardening following a reduced modulus of $E/100$, as seen in Figure 4.3b, was implemented in ABAQUS CAE.

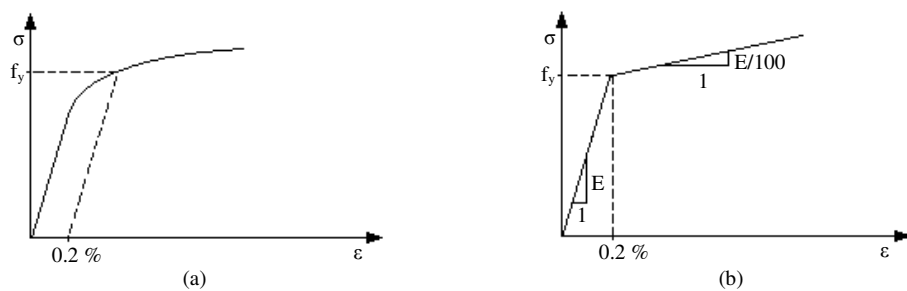


Figure 4.3: Material models; (a) illustration on how the yield stress is obtained; (b) the bilinear material model used in the FE-analysis with a hardening modulus of $E/100$.

By following the approach in Figure 4.3 with the material models presented in Appendix B, the yield stresses in the web and the flange are approximated to 375 and 406 MPa, respectively. Furthermore, the corresponding ultimate stresses are approximated to 491 and 568 MPa. The Young's moduli for the web and flanges are

calculated to 193 and 195 GPa, respectively, using Hooke's law with the stress-strain relationship from Appendix B.

Table 4.2: Material properties estimated from Appendix B.

| f_{yw} [MPa] | f_{yf} [MPa] | f_{uf} [MPa] | f_{uw} [MPa] | E_w [GPa] | E_f [GPa] |
|----------------|----------------|----------------|----------------|-------------|-------------|
| 375 | 406 | 491 | 568 | 193 | 195 |

4.1.1 Linear buckling analysis

In order to obtain an appropriate mesh for the FE-model, detailed enough to simulate the behaviour of a real girder, a mesh convergence study is made through a linear buckling analysis. Here, a load is applied as mentioned earlier and using only the elastic material properties in ABAQUS CAE, the behaviour of the FE-model is studied.

In Figure 4.4, the mesh convergence for the three first eigenvalues and each load case is plotted as the eigenvalue/element size relationship. Here, it can be seen that, for each load case and for each eigenvalue, the FE-model starts to converge (starts to reach the final eigenvalue) at a mesh element size of about 20 to 30 mm. This gives a rather helpful guideline when constructing the global mesh.

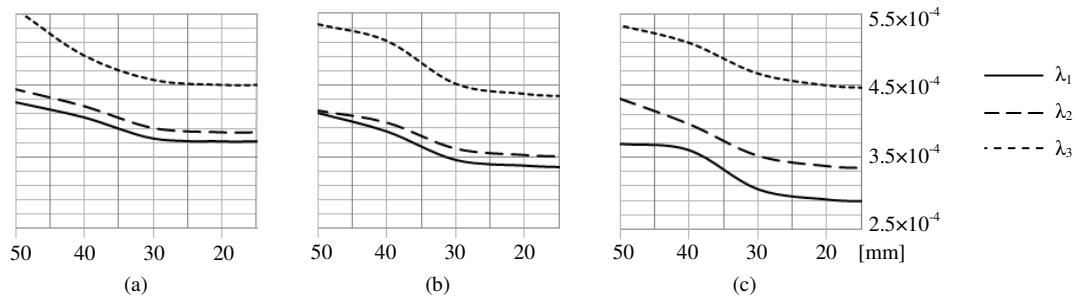


Figure 4.4: Eigenvalues vs. finite element size [mm]. Convergence study of different element sizes at different load positions: (a) inclined fold; (b) junction between two folds; (c) longitudinal fold.

Further, the linear buckling analysis is performed in order to obtain the eigenmodes at each load case. The shape of the first eigenmode for each of the three load positions is then used as the shapes of the initial imperfection in the non-linear buckling analysis. These eigenmodes are shown in Figure 4.5.

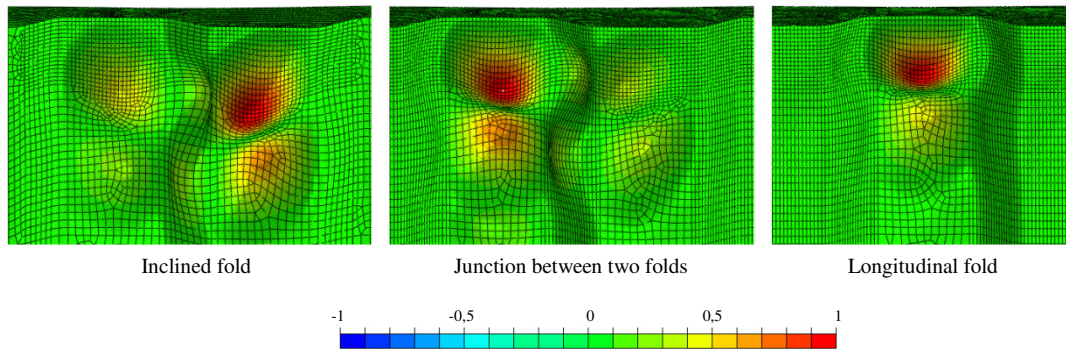


Figure 4.5: Shapes of the first eigenmode for the three load positions used as shapes of the assumed initial imperfections in the non-linear FE-model.

4.1.2 Non-linear buckling analysis

Following the linear buckling analysis of the girder a non-linear buckling analysis was performed. Here, an increasing load on girders with small initial web imperfections (Figure 4.5) was simulated and both the linear and non-linear behaviour of the girder could be analysed. The method of the non-linear buckling analysis was used during verification of the model (section 4.2) and during the parametric study (section 4.4). The default settings in ABAQUS CAE – such as using Simpson integration and automatic arc-length iteration with Riks’ method– were utilized.

As mentioned in section 4.1.1, it would be sufficient to use a mesh with element sizes around 30 mm, in both web and flanges. However, this was only when concerning the global behaviour of the girder. When analyzing the local behaviour in the web just below the loaded area, a more detailed mesh was required. Hence, a refined mesh was constructed in this area while the remaining part of the girder still used a mesh with the original element size of 30 mm. The refinement of the mesh was performed in steps – as seen in Figure 4.6 – with “outer” areas using element sizes of 10 and 20 mm and an inner area – where the main part of the buckling deformation occurs – using an element size of 5 mm.

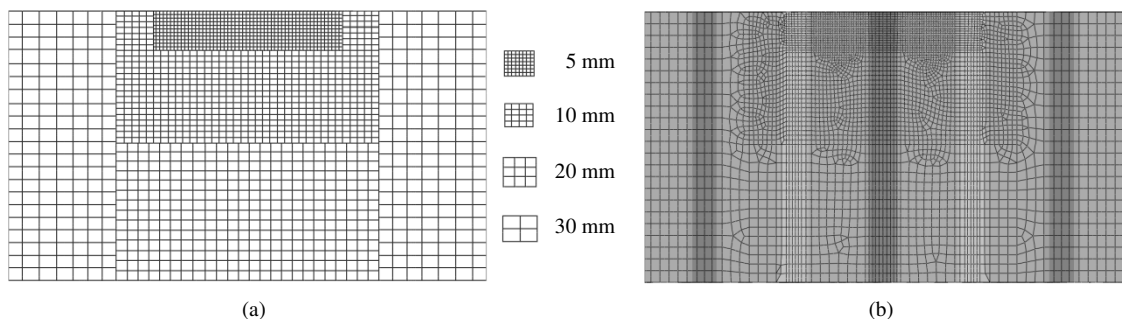


Figure 4.6: Local refined mesh in the web below the loaded area; (a) schematic illustration on how the element size is gradually decreased closer to the loaded portion; (b) resulting mesh used in ABAQUS CAE. The mesh of the flanges is governed by the element sizes in adjacent areas of the web.

To obtain realistic results for the verification, an approximation of the initial imperfections of the tested girder was performed. These values were extracted by Mathias Flansbjer at the *Technical Research Institute of Sweden (SP)* using the software ARAMIS by applying a path – as seen in Figure 4.7 – which extended across the measuring area of the web where the maximum out-of-plane deformations would occur. From this path, the initial shape of the cross section of the tested girder could be plotted (see Appendix C) and the resulting maximum *magnitude* of initial imperfection used in the FE-model, which was estimated at 0.5 mm. To generate a *shape* of the assumed initial imperfections, the first eigenmode of the linear buckling analysis (see Figure 4.5) was implemented in the non-linear buckling analysis.

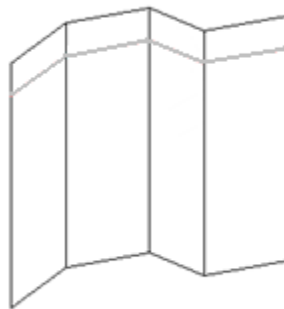


Figure 4.7: Measuring area using ARAMIS. The red line indicates the path at which the initial cross-section shape and consequently, the magnitude of the initial imperfections was obtained.

After each job was performed in ABAQUS CAE, the desired results were extracted and analysed further in either the verification process or the parametric study. Most of the data are collected in the appendices in the end of the thesis.

4.2 Verification of the model

In order to verify the reliability of the results obtained from the FE-model, comparisons between experimental test results and calculations are appropriate. In this thesis, the FE-model was developed with the same geometrical and material properties as the girder used in the experimental tests presented in section 3. Hence, these tests results are to be the main source for verification of the developed FE-model.

4.2.1 Beam theory – vertical deflection

To get an initial verification of the FE-model, it is common to compare the vertical deflection of the girder at a certain load obtained from the FE-model and from regular beam theory. Here, it is assumed that the girder is 3 m and simply supported, i.e. the response due to the remaining part of the girder is neglected. Further, only the contribution of the flanges is considered when calculating the second moment of inertia I . The equation for calculating the vertical deflection at the point of loading is as follows.

$$p_{bt} = P \cdot \frac{a^2 b^2}{3EIL} \quad (4.1)$$

The load P is set to 100 kN in order to get an elastic response for all load cases. Young's modulus is the same as used in the flanges in the FE-model.

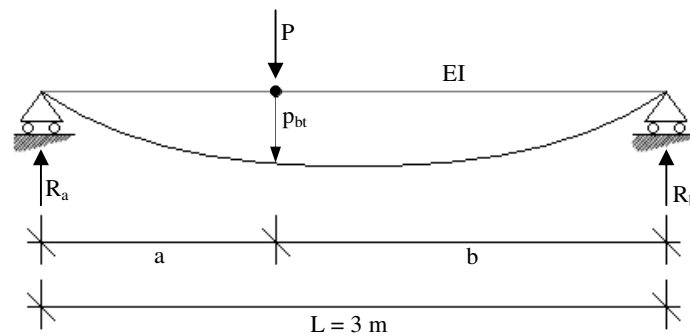


Figure 4.8: Simplified illustration of one span used to calculate vertical deflection p_{bt} due to load P in beam theory.

In Table 4.3 the results using Equation (4.1) are compared with the vertical deflections obtained from the FE-model. Even though the difference in vertical deflection is about 70 %, the results obtained by the beam theory and the FE-model might not entirely correlate due to the simplicity and estimations of the beam theory and the geometry of the FE-model. However, the results could be considered to be in the vicinity of each other – around 1 mm – and are therefore acceptable. Further, the results from the experimental tests are even larger than the results from the FE-analysis – around 2 mm – which gives an indication of that the beam theory does not include local deformations.

Table 4.3: Comparison between vertical deflections at the point of loading obtained from beam theory and obtained from the FE-model. Load $P = 100$ kN.

| p_{bt} [mm] | p_{FEM} [mm] | p_{test} [mm] |
|---------------|----------------|-----------------|
| 0.70 | 1.20 | ~ 2 |

4.2.2 Load-displacement curves and ultimate load

To achieve a reliable FE-model, a comparison between load-displacement diagrams obtained from experimental testing and from the FE-model is made. Here, it can be established if the resulting ultimate loads of the FE-model and the tests show some agreement. Furthermore, the general behaviour under loading can be studied to judge whether the response of the FE-model is satisfactory or not.

Table 4.4: Comparison between the ultimate loads obtained from test results and results from the FE-model.

| Test | Load pos. | P_e [kN] | P_{u_FEM} [kN] | P_{u_FEM}/P_e |
|------|------------|------------|-------------------|------------------|
| A1 | Inc. fold | 219 | 210 | 0.9589 |
| A2 | Junction | 217 | 202 | 0.9309 |
| A3 | Long. fold | 181 | 164 | 0.9061 |
| B1 | Long. fold | 188 | 164 | 0.8723 |
| B2 | Junction | 213 | 202 | 0.9484 |
| B3 | Inc. fold | 218 | 210 | 0.9633 |

Load case A1 and B3: Position over an inclined fold

The ultimate loads obtained from the experimental test are 219 and 218 kN. As seen in Table 4.4, the ultimate load obtained with the FE-model is 210 kN resulting in deviations of only 4.1 and 3.7 % from the ultimate loads from the test. Such small deviations are very satisfying when aiming to verify the FE-model.

In Figure 4.9 the load-displacement curves of cases A1 and B3 are plotted together with the results from a similar load case using the FE-model. The curves representing experimental test B3 and the result from the FE-analysis show very similar behaviour with a rather sudden dip in capacity after reaching the ultimate load. However, the curve obtained from experimental test A1 indicates a less dramatic behaviour after reaching the ultimate load.

Furthermore, the elastic behaviour obtained with the FE-model is significantly stiffer than the behaviour of the tested girder. However, this is to be expected as the tests are performed with an amount of “uncertain” variables which may affect the results, such as supports, variations of the material properties etc.

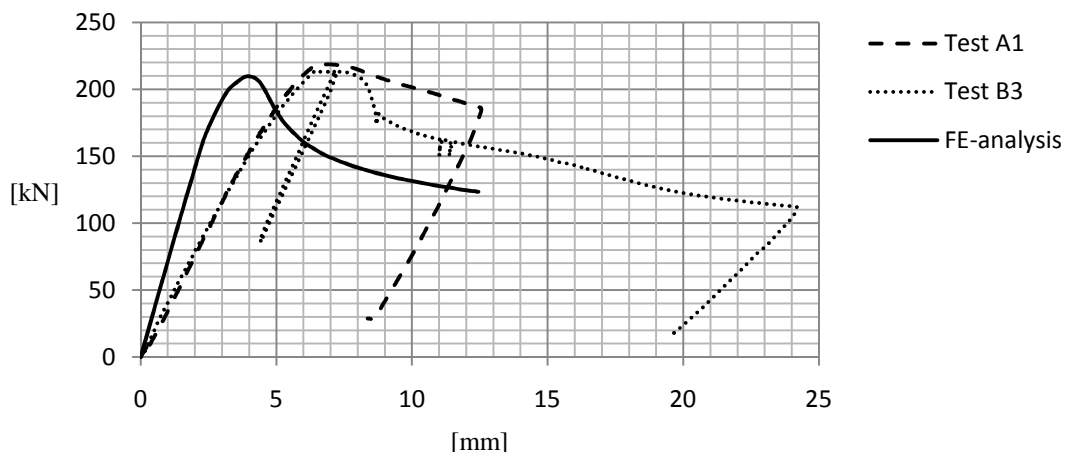


Figure 4.9: Load-displacement relationship for the FE-analysis and the experimental tests A1 and B3.

Load case A2 and B2: Position over a junction between two folds

The resulting ultimate loads from the experimental tests are 217 and 213 kN. Simulating a similar load case with the FE-model resulted in an ultimate load of 202 kN. This corresponds rather well with the results of test B2 from which it deviates by 5.2 %. Compared to the results from test A2 and the FE-model the ultimate load obtained with the FE-model is 6.9 % lower, i.e. also a good result.

The load-deformation curves obtained from the experimental tests and the FE-model correspond very well throughout the entire loading range. The rather drastic drop in capacity after reaching the ultimate load is present in all three curves. This behaviour reveals a structure with high stiffness sensitive to imperfections.

Similarly as for the load cases A1 and B3, the FE-model is stiffer in the elastic part of the loading range than the tested girder. However, in this case, the difference is comparatively small.

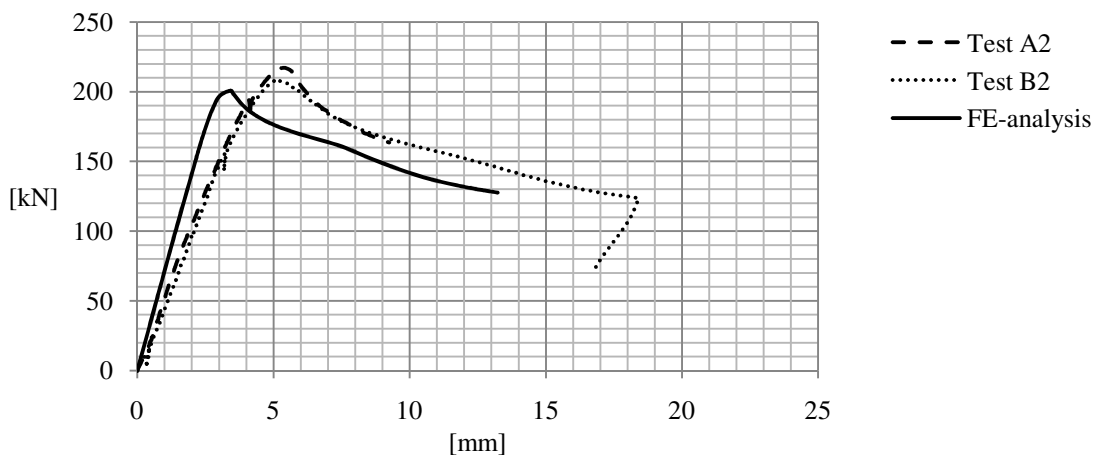


Figure 4.10: Load-displacement relationship for the FE-analysis and the experimental tests A2 and B2.

Load case A3 and B1: Position over the centre of a longitudinal fold

The test results on the ultimate load when loading over a longitudinal fold and the results from the FE-analysis do not correspond as well compared to the results from the other two load cases. As seen in Table 4.4, the ultimate loads obtained from experiments are 181 and 188 kN while the ultimate load obtained from the FE-analysis is 164 kN, resulting in differences of 9.4 and 12.8 %. As the latter difference is greater than 10 %, it may be considered somewhat large. However, as explained in section 3.4, the tests with load cases A3 and B1 resulted in a response where the eccentricity of the longitudinal fold induced a rotation of the flange. The response achieved by the FE-model – where the load is applied as a pressure directly on the flange – is one where the flange deflects on each side of the web. Since these behaviours are rather different it is bound to affect the results (see Figure 4.18).

The shapes of the load-deformation curves obtained from the tests and from the FE-analysis share the same characteristics. As seen in Figure 4.11, the load increases linearly up to a point where the rate of increase starts to decline. This occurs rather smoothly up to and beyond the ultimate load, representing a somewhat ductile behaviour.

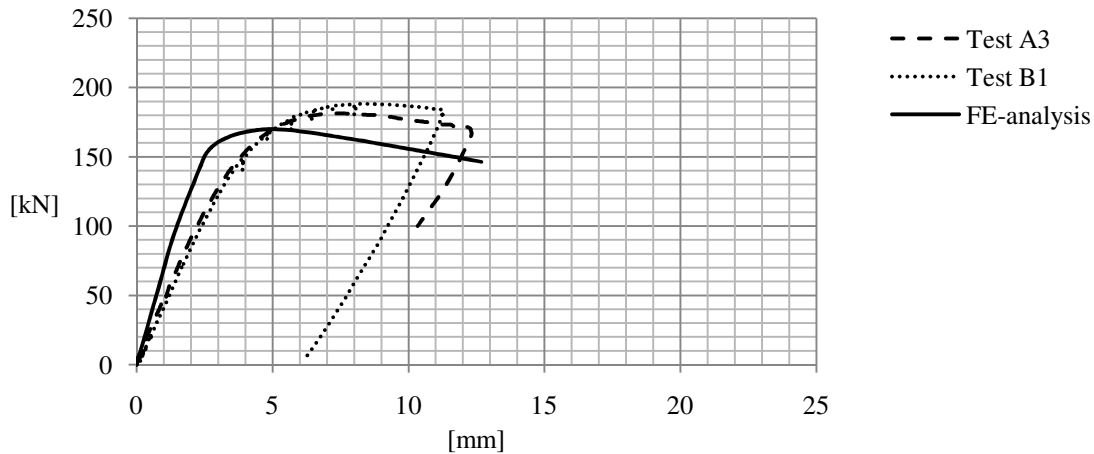


Figure 4.11: Load-displacement relationship for the FE-analysis and the experimental tests A3 and B1.

4.2.3 Buckling behaviour

A comparison of the more detailed buckling characteristics obtained from the tests and the FE-analysis is made in order to further evaluate the FE-model. Here, the amount of buckles, magnitude of out-of-plane deformations, the shape and propagation of the buckles are analysed. Due to approximations in the FE-model (such as material properties and initial imperfections of the tested girder) and limitations within the testing equipment, one should not expect to obtain very close agreement of the real behaviour with a FE-model. However, it is rather important that the behaviour is simulated as correctly as possible in order to rely on the model during the parametric study.

Load case A1 and B3: Position over an inclined fold

When loading the girder over an inclined fold, three buckles are prominent at the ultimate load in both the tests and in the FE-analysis. The buckles are located in the three folds closest to the point of loading and very close to the top flange. In the experimental tests, the distance between the maximum out-of-plane deformation and the top flange was about 50 mm (centre buckle). Corresponding value obtained from the FE-analysis was 24 mm. The magnitudes of the maximum out-of-plane deformations, at the ultimate load, in each buckle (see Figure 4.12) were about 0.70, 0.80 – 1.9 and 0.80 mm on the tested girder while related values obtained from the FE-analysis were about 0.5, 2.5 and 1.0 mm.

In Figure 4.12 the deformed shape of the tested girder is displayed together with the corresponding result from the FE-analysis. Judging from Figure 4.12, the shapes and in-plane distribution of the buckles, at ultimate load, obtained by FE-analysis and by real tests are very similar. Furthermore, the buckles obtained in both the experimental tests and the FE-analysis transcend the junction between folds.

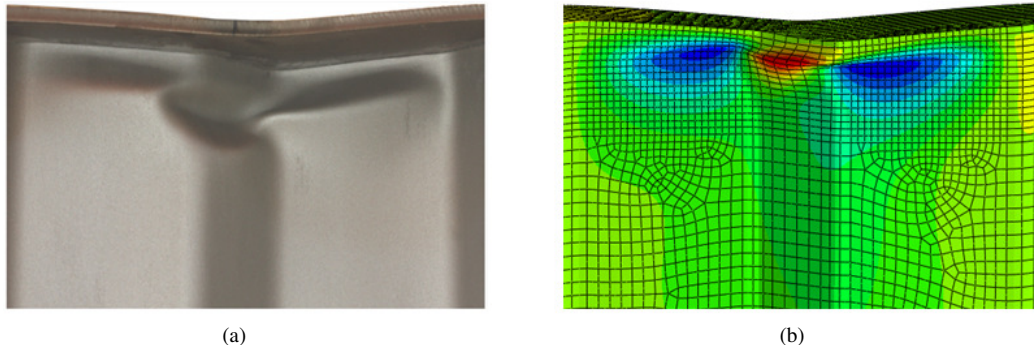


Figure 4.12: Comparison of buckle distribution; (a) obtained from experimental test B3; (b) obtained from FE-analysis. Blue colour represents outward deformations while red colour represents inward deformations (away from the reader).

As mentioned in section 3.1, the buckling propagation at the points where maximum out-of-plane deformations in the web occurred during the experimental testing were measured with help from SP using the software ARAMIS (cf. section 4.1.2). In Figure 4.13, the propagation of the out-of-plane deformations obtained in test A1 and B3 is compared to equivalent results obtained with the FE-model. Here, it can be observed that the out-of-plane deformations develop very instantly at the ultimate load in the experimental tests.

The FE-model results in a rather smooth behaviour while the results from the tests display a significant amount of disturbance – such as irregularities in the behaviour. However, as there are numerous amounts of uncertainties in the tests and FE-analysis, this scenario is more or less unavoidable.

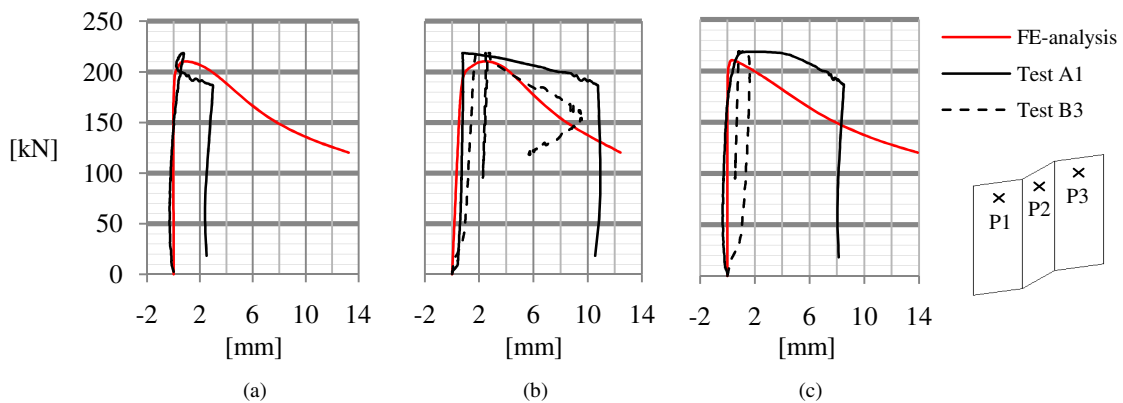


Figure 4.13: Load/out-of-plane deformations at locations P1 (a), P2 (b) and P3 (c) when applying the load over an inclined fold.

Load case A2 and B2: Position over a junction between two folds

Similar to the results in load case A1 and B3, three main buckles develops in the web when loading over a junction between two folds in both the experimental tests and the

FE-analysis. These are located very close to the top flange and distributed over two longitudinal folds and one inclined fold.

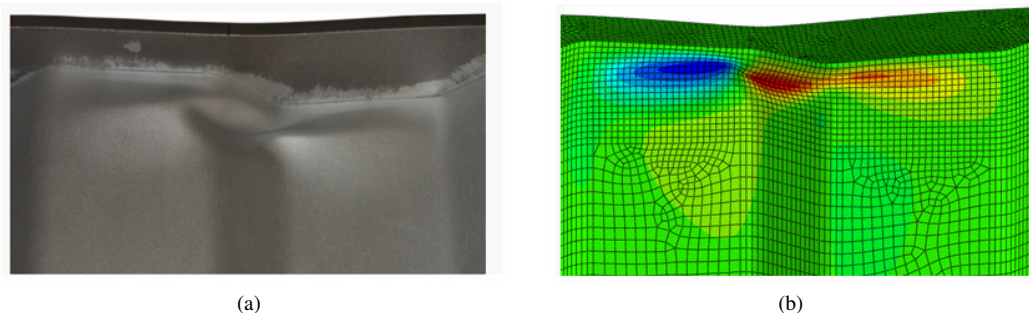


Figure 4.14: Comparison of buckle distribution; (a) obtained from experimental test B2; (b) obtained from FE-analysis. Blue colour represents outward deformations while red colour represents inward deformations (away from the reader).

Measured in the real tests, the distance between the top flange and the maximum out-of-plane deformation in the web was 37 mm (buckle in the inclined fold) while the corresponding value obtained from the FE-analysis was 22 mm. At ultimate load, the maximum out-of-plane deformations in each buckle – obtained from the real tests (load case A2) – were about 3, 1 and 2.3 mm. The corresponding values obtained from FE-analysis were 1, 0.8 and 0.1 mm.

The behaviour of the out-of-plane deflections at each buckle obtained from the FE-analysis and the actual tests are very similar in locations P1 and P2 as seen in Figure 4.15 (load case A2). However, at location P3 the FE-analysis results in a very drastic decrease in capacity when the buckle develops while the results from the tests show a much more smooth behaviour.

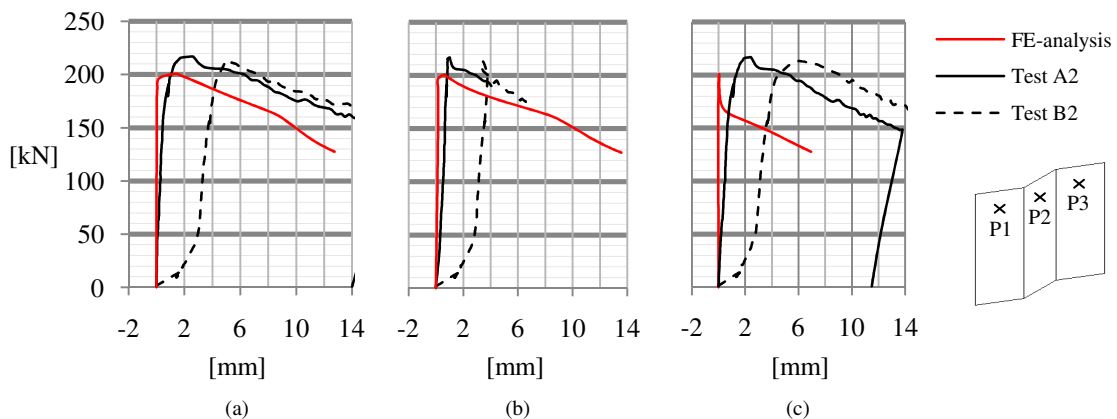


Figure 4.15: Load/out-of-plane deformations at locations P1 (a), P2 (b) and P3 (c) when applying the load over a junction between two folds.

Load case A3 and B1: Position over the centre of a longitudinal fold

In contrast to the other load cases, the number of buckles in the web when loading the girder over a longitudinal fold is only one. This is located directly below the point of loading and spreads across the longitudinal fold. In the experimental tests, the maximum out-of-plane deformation at ultimate load is about 10 mm located about 15 mm from the top flange. Related values obtained from the FE-analysis are 5 mm and 12 mm correspondingly. As seen in Figure 4.16, the shape and distribution of the buckle obtained from tests is very similar to the one obtained by FE-analysis.

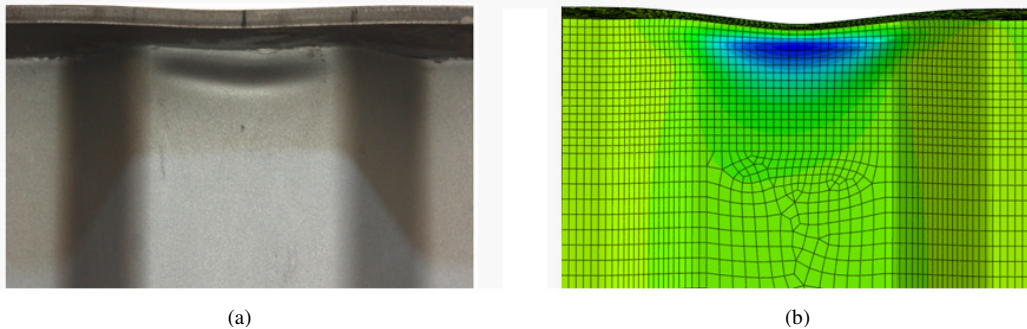


Figure 4.16: Comparison of buckle distribution; (a) obtained from experimental test A3; (b) obtained from FE-analysis. Blue colour represents outward deformations (toward the reader)

Due to the stiff metal bar between the hydraulic jack and the top flange which distributed the load over the flange width and load length, the load during testing was only able to rotate around one axis close to the web. However, the load in the FE-analysis was evenly distributed over the area of loading and set to follow the deformations during loading. This enabled the load to act uniformly over the loading area even though large vertical flange deformations on each side on the web occurred. This difference in behaviour is very prominent in the case when the load acts over a longitudinal fold with negative vertical deformations on each side of the web in the FE-analysis, while the experimental tests resulted in a rotation around the web, see Figure 4.18.

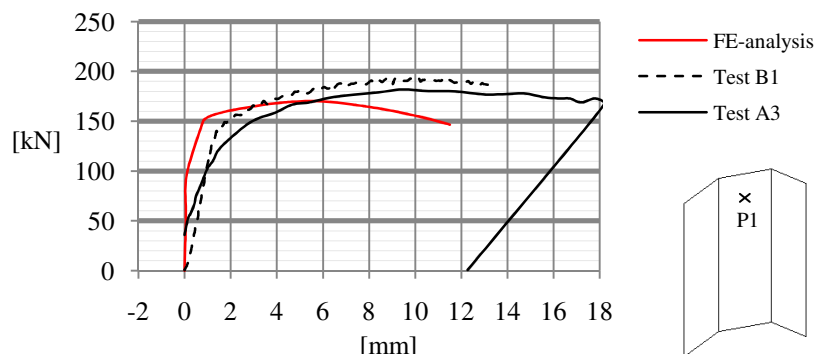


Figure 4.17: Load/out-of-plane deformations at location P1 when the girder is loaded over a longitudinal fold.

As only one buckle develops in the web when the girder is loaded over a longitudinal fold only one location, P1, is considered when comparing the out-of-plane deformations of the FE-analysis and the experimental tests. As seen in Figure 4.17, the response is rather similar with deformations slowly increasing until approaching the ultimate load. However, the main difference between tests and FE-analysis is that the deformation obtained from the FE-analysis is so that there are no deformations until the load reaches about 90 kN, but the tests show deformations well below that.

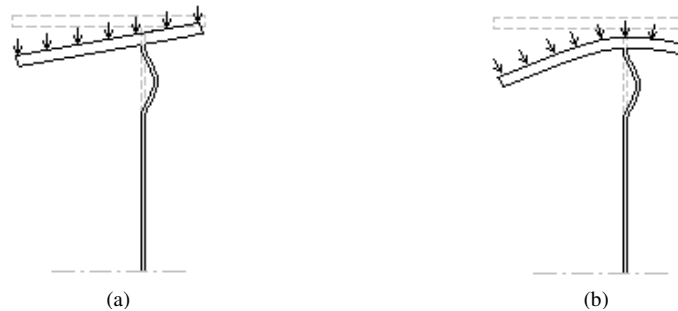


Figure 4.18: Schematic illustration on how the upper flange responds during loading; (a) response during experimental testing; (b) response during FE-analysis.

4.3 Approximations and limitations

In order to reduce calculation time and complexity of the FE-analysis, a number of approximations are made during the modelling procedure. Mostly, these approximations should not influence the results significantly, while the modelling is simplified considerably. At times, however, limitations in information make approximations necessary in order to obtain an operating FE-model. Such approximations are sometimes prone to affect the results and are therefore important to mention and be aware of. Listed below are various assumptions and approximations made during the analysis.

- No regard to variations in material properties in the web at the junctions between two folds due to strain hardening. The effects of such variations have been examined earlier (Lou and Edlund (1994)) with the conclusion that it does not affect the results significantly. However, as this conclusion is based on girders with other material and dimensional properties, it may not be applicable to the girder tested in this analysis.
- Due to limitations in the knowledge of the material properties used in the real girder, the approach presented in section 4.1 was used. As this is an estimation of the material properties, the behaviour of the material used in the FE-model will be different from that of the material used in the real girder. Consequently, there may be some apparent differences of the results obtained by experimental tests and FE-analysis.
- The additional stiffness of the loaded area provided by the loading plate used in the experimental tests is not considered in the FE-analysis. This may primarily affect the behaviour of the upper flange as the distribution of the load will differ.

This is discussed more in detail in section 4.2.3 under “Load case A3 and B1: Longitudinal fold”.

- Only the magnitudes of the initial imperfections used in the FE-model are determined by measurements of the actual girder. The shapes of the initial imperfections are based on the first eigenmode obtained by a linear buckling analysis at each load case.
- Only one span is modelled in ABAQUS CAE in order to shorten the calculation time. As the magnitudes of the loads provided by the hydraulic jack are overwhelming compared to any response from the unloaded span, this choice should not affect the results significantly.
- Due to multiple testing on the real girder, the stiffness of the girder might be reduced. This is not taken into account in the FE-analysis. However, as focus is on local behaviour, this should not affect the results significantly.
- Effects from welds between flange and web are not taken into consideration. However, an attempt to include this was made, but with unsuccessful results.
- As with all comparisons between real tests and FE-modelling, possible errors during execution of the experimental tests cannot be predicted and hence, not be taken into account.

4.4 Parametric study

As told in section 4.1.2, the parametric study is performed in ABAQUS CAE in the same manner as the non-linear buckling analysis. This means to simulate a case with an increasing deformation up to and beyond the ultimate load in order to track the behaviour of the girder at each increment of the load.

The parameters considered in the parametric study are: t_w , t_f and the initial imperfection amplitude e_o . These are varied within a range of reasonable values to obtain useful results. Three different web thicknesses are considered; 2, 3 and 4 mm. The flange thicknesses considered are 10, 12, 16 and 20 mm. Besides the initial imperfection of $e_o = 0.5$ mm used in the verification process, the initial imperfection will be changed to simulate different types of scenarios. By setting the initial imperfection to 0 mm a stiffer response is to be expected. Further, the response using larger initial imperfections amplitudes of 1 mm, 2 mm and 5 mm will be investigated. Here, smoother responses are to be expected. Furthermore, the effects of different loading positions (inclined fold, junction between two folds and longitudinal fold) will be investigated. If nothing else is mentioned, the dimensional parameters, material model and initial imperfections of the girder used in the parametric study will be kept to the original values of the FE-model, see Tables 3.1 and 4.2. The results in chapter 5 can thus be regarded as an extension of the simulation results in sections 4.2.2 and 4.2.3.

Appendix D includes a matrix describing the parameter changes in each job in ABAQUS CAE.

5 RESULTS

This chapter presents the results from the parametric study, cf. section 4.4, performed with the FE-model using the matrix shown in Appendix D. The results are presented in separate sections, one for each parameter (t_w , t_f , and e_0). Furthermore, the results are subdivided into sections of results related to ultimate load, load-deformation (here mostly meaning load-displacement) relationship and postbuckling mode. For more detailed results, see Appendix D.

5.1 Influence of web thickness

Based on information presented earlier, the parameter having the greatest influence on the ultimate load is the web thickness. In most model formulas, the ultimate load increases at a quadratic rate when increasing the web thickness. Hence, this parameter is the most critical to investigate in order to obtain good understanding of the girder type in regard.

As seen in section D.1 in Appendix D, the web thicknesses considered in the investigation are 2, 3 and 4 mm. The results will be presented in terms of ultimate load, load-deformation behaviour and postbuckling mode. Further, the results will be compared with results obtained from the models established by Lou and Edlund (1994) and Elgaaly and Seshadri (1997) due to their good agreement with actual tests.

5.1.1 Ultimate load

In order to distinguish the actual influence of the web thickness, the various results at different load cases must be studied. Hence, Figure 5.1 plots the ultimate loads at various web thicknesses for the load cases: inclined fold, junction between two folds and longitudinal fold along with results using models established by Lou and Edlund (1994) and Elgaaly and Seshadri (1997).

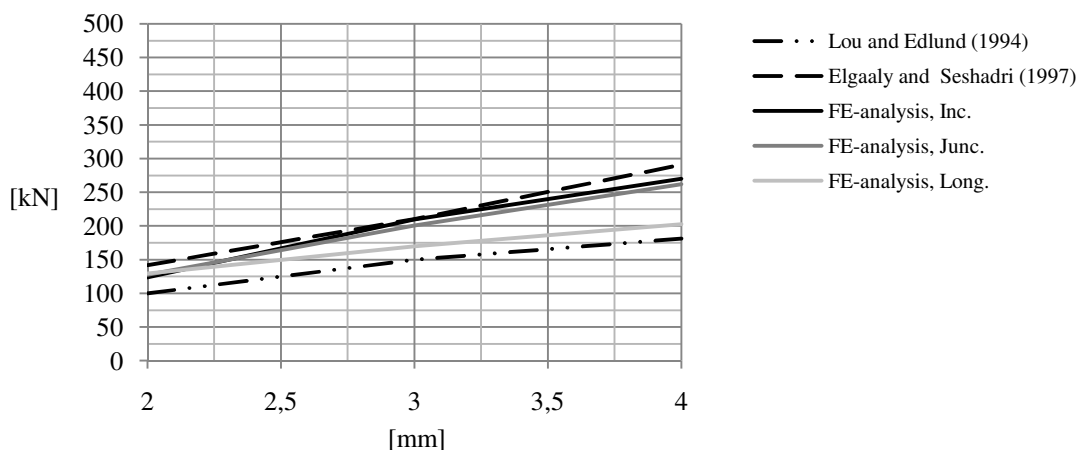


Figure 5.1: Influence of the web thickness on the ultimate load at various load cases. Results from the FE-analysis are plotted along with results using the models established by Lou and Edlund (1994) and Elgaaly and Seshadri (1997).

As seen in Figure 5.1, the ultimate patch load of thin webs does not seem to be affected by the load position. At greater web thicknesses, the ultimate load increases for all load cases. However, as the web thickness increases, the rate at which the ultimate load increases will be significantly lower in the case at which the load is applied over a longitudinal fold than in the other two load cases. The total increase of the ultimate load after increasing the web thickness from 2 mm to 4 mm will be about 115 % over an inclined fold, 110 % over a junction between two folds and 60 % over a longitudinal fold.

The ultimate loads obtained by the model by Elgaaly and Seshadri (1997) are rather close to those obtained from the FE-model loading the girder over an inclined fold at web thicknesses close to 3 mm. However, at web thicknesses well above 3 mm, the difference is greater due to the different increase rates.

The model by Lou and Edlund (1994) results in values of the ultimate load lower than the results obtained from the FE-analysis. The behaviour is especially similar to the case when the load is applied over a longitudinal fold (about 10 to 20 % lower). (Compare the result in Figure 2.12, which is for a girder with b half as wide and a little wider flange. There the behaviour changes somewhat at web thicknesses above 4 mm and the increase rate is expected to increase.)

5.1.2 Load-deformation relationship

In order to investigate how the stiffness behaviour is influenced by changes in the web thickness, the load-deformation behaviour is investigated. The results from the FE-analysis are presented in different figures for each load case comparing the behaviour at various web thicknesses.

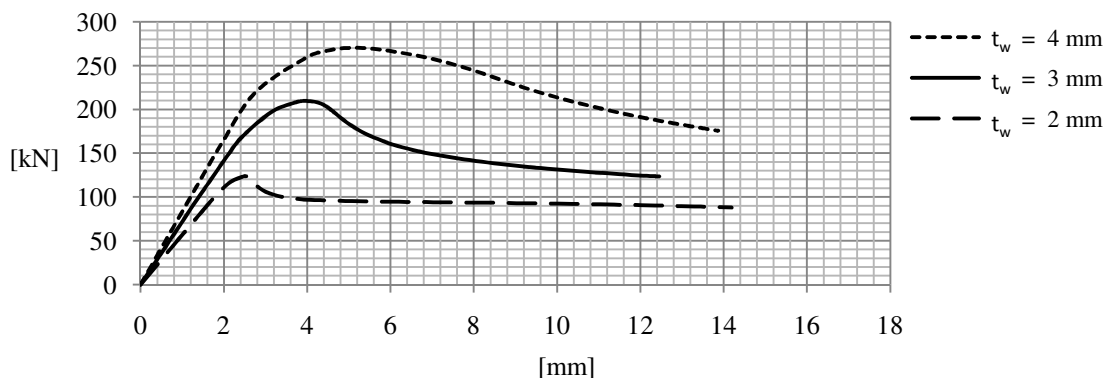


Figure 5.2: Load-deformation relationship at various web thicknesses when the load is applied over an inclined fold.

Increasing the web thickness will not only increase the ultimate load of the girder. In Figure 5.7, the influence of changes in web thickness is plotted. Here it can be seen that an increased web thickness will result in a stiffer girder in the elastic range of loading. Further, it is obvious that an increased web thickness will result in a more ductile behaviour. At a small web thickness however, the failure has a somewhat brittle character. At a web thickness of 2 mm, the postbuckling capacity remains rather constant compared to that of girders with thicker webs.

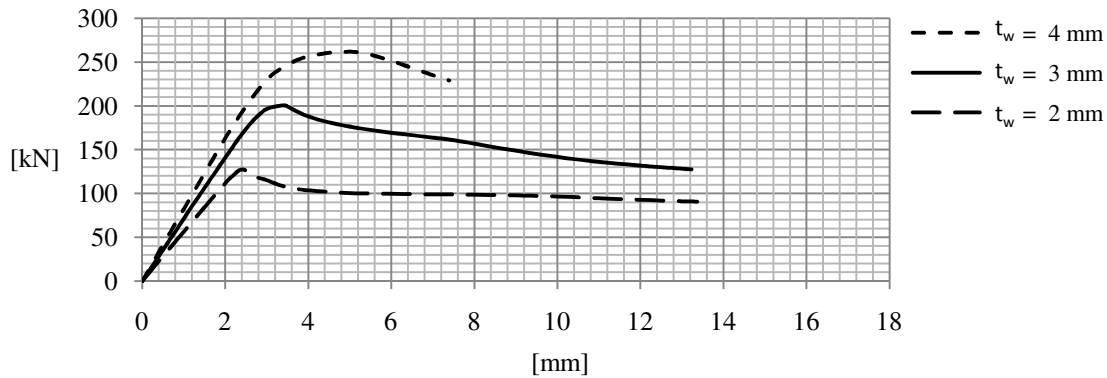


Figure 5.3: Load-deformation relationship at various web thicknesses when the load is applied over a junction between two folds.

The changes in behaviour – due to varying web thicknesses – of a girder loaded over a junction between two folds is rather similar to that of a girder loaded over an inclined fold. A thicker web will result in a stiffer response in the elastic range which decreases in a smooth manner closer to the ultimate load resulting in a ductile failure. Decreasing the web thickness will result in a girder with lower stiffness and a more brittle failure. Additionally, as when the load is applied over an inclined fold, the postbuckling capacity is more prominent at thinner webs.

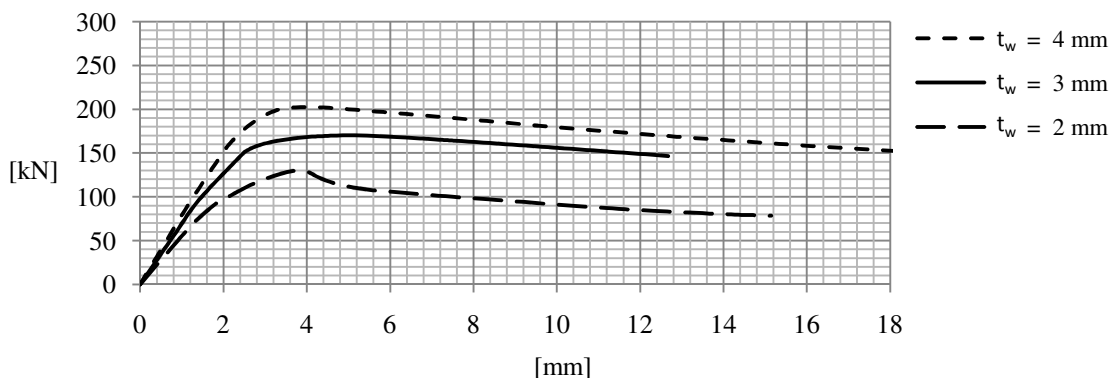


Figure 5.4: Load-deformation relationship at various web thicknesses when the load is applied over a longitudinal fold.

When applying the load over a longitudinal fold, changes in web thickness will induce similar changes in the load-deformation behaviour as when applying the load over an inclined fold or over a junction between two folds. In this case however, the changes will not be as obvious. Further, the most ductile behaviour seems to be possessed by the girder with the intermediate web thickness instead of the girder with the thicker web. Additionally, the postbuckling capacity using thin webs is not as notable as that of the other two load cases.

5.1.3 Postbuckling behaviour

The buckling behaviour is strongly influenced by the web thickness. Although the shape of the buckling mode is mainly governed by the load case (Girder 10X, Girder 20X and Girder 30X in Figure 5.5), the propagation of it is heavily dependent on the slenderness

of the web. Hence, Figure 5.5 depicts the various buckling modes at the end of the loading process using different web thicknesses and load cases.

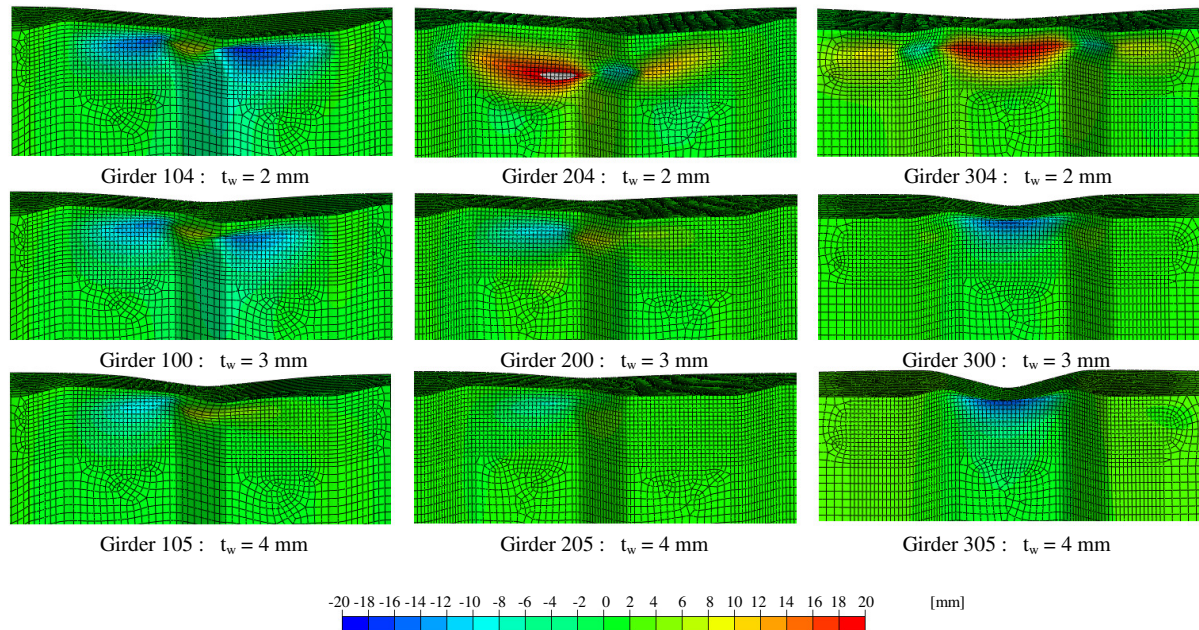


Figure 5.5: Buckling shapes and magnitudes at different load cases with varying web thicknesses and at the end of a loading process of 50 increments in ABAQUS CAE. Flange thickness $t_f = 12$ mm.

The propagation of the buckling mode, when loading over an inclined fold (Girder 10X in Figure 5.5) is more or less proportional to the change in web thickness. Further, the main shapes of the buckling modes are very similar at a web thickness of 2 and 3 mm. However, when increasing the web thickness to 4 mm, the rightmost buckle “disappears” into the mid-buckle. The buckle propagation is far more influenced by the web thickness when the load is applied over a junction between two folds (Girder 20X in Figure 5.5). At a web thickness 2 mm (Girder 204) the leftmost buckle reaches over and beyond the adjacent junctions. Further, at the smallest web thickness, the buckling seems to occur farther from the upper flange than when increasing the web thickness.

The buckling shape when applying the load over a longitudinal fold (Girder 30X in Figure 5.5) varies greatly when changing the web thickness from 2 to 3 mm. As it can be seen in Figure 5.5, using the two larger web thicknesses – 3 and 4 mm – will result in a single buckle directly below the loaded area. However, at a web thickness of 2 mm (Girder 304), the buckle propagation will reach beyond the longitudinal fold and create two buckles in the adjacent inclined folds and two additional buckles in the following longitudinal folds. Furthermore, as the load at the end of the loading cycle is higher using girders with thicker webs (see Appendix D) the deformation of the flange will be greater. This is most apparent comparing the flange deformations in Girder 300 and Girder 305 in Figure 5.5.

5.2 Influence of flange thickness

The design models by Lou and Edlund (1994) and Elgaaly and Seshadri (1997) indicate that the flange thickness has a great influence on the ultimate load. According to Lou and Edlund (1994) this influence is proportional while Elgaaly and Seshadri (1997) estimate a more linearly increasing ultimate load as the flange thickness increases. However, to the knowledge of the authors, the actual influence of the flange thickness is yet to be investigated through experimental tests.

As seen in Appendix D, the flange thicknesses used in the study are 10, 12, 16 and 20 mm. In this section the influence of the flange thickness (based on the current FE-model) will be presented in terms of ultimate load, load-deformation relationship and buckling modes.

5.2.1 Ultimate load

As when studying the results considering the influence of web thickness, the results at different load cases must be regarded when studying the influence of flange thickness on the ultimate load. Further, the results from the FE-analysis are plotted in Figure 5.6 together with results using the models established by Lou and Edlund (1994) and Elgaaly and Seshadri (1997).

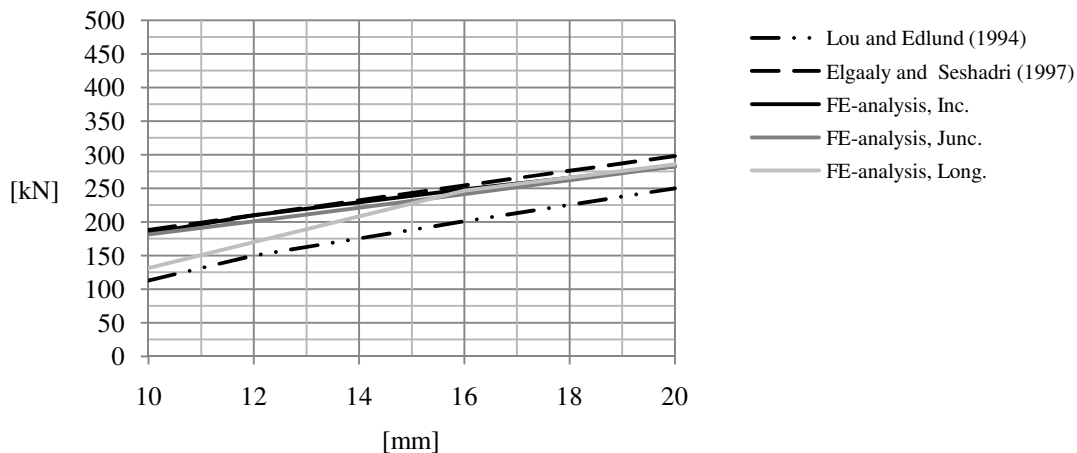


Figure 5.6: Influence of the flange thickness on the ultimate load at various load cases. Results from the FE-analysis are plotted along with results using the models established by Lou and Edlund (1994) and Elgaaly and Seshadri (1997).

As seen in Figure 5.6, the increase of the ultimate load when increasing the flange thickness is almost linear when loading the girder over an inclined fold or over a junction between two folds. The increase for these two load cases are almost identical and changing the flange thickness from 10 to 20 mm results in an increase of the ultimate load from about 180 kN to 280 kN, i.e. an increase of 55 %.

At a flange thickness of 10 mm, a girder loaded over a longitudinal fold will generate an ultimate load of about 130 kN (about 30 % less than a girder loaded over an inclined

fold or over a junction between two folds). However, as the flange thickness increases, the rate at which the ultimate load increases will be higher than for the two other load cases and at a flange thickness of 16 mm, the resulting ultimate loads are equal. When further increasing the flange thickness, the resulting ultimate loads – for all three load cases – are equal. In conclusion, the case at which the girder is loaded over a longitudinal fold is most sensitive to changes in flange thickness in the range $10 \text{ mm} < t_f < 16 \text{ mm}$.

The model by Elgaaly and Seshadri (1997) corresponds very well with the results from the FE-analysis, when loading the girder over an inclined fold and over a junction between two folds. At flange thicknesses above 16 mm this model also corresponds well with the FE-model loaded over a longitudinal fold.

The model by Lou and Edlund (1994) also corresponds well with the FE-model. For the case, when loading the girder over a longitudinal fold and for flange thickness up to almost 14 mm, the response of this model is the most similar to that of the FE-analysis, see Figure 5.6. The increase rate of this model is very similar to that of the model by Elgaaly and Seshadri (1997).

5.2.2 Load-deformation relationship

Similar to when varying the web thickness, the influence of flange thickness on the load-deformation relationship is analysed. The results from the FE-analysis are presented in one figure for each load case comparing the behaviour at various flange thicknesses.

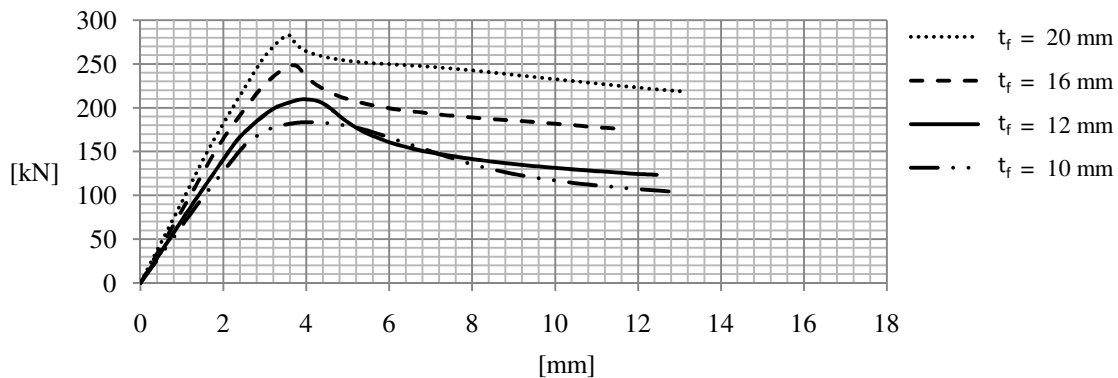


Figure 5.7: Load-deformation relationship at various flange thicknesses when the load is applied over an inclined fold.

In Figure 5.7 the influence of changes in flange thickness when the load is applied over an inclined fold is plotted. Here it can be seen that an increased flange thickness will result in a stiffer girder in the elastic range of loading. Further, an increased flange thickness will result in a more brittle behaviour with a rather fast decrease in capacity after reaching the ultimate load. At a small flange thickness, however, the failure is more ductile with more smooth characteristics.

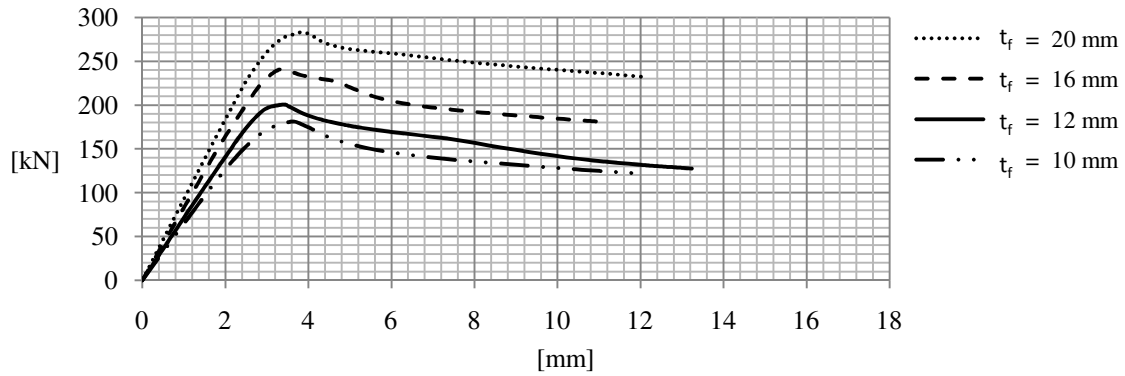


Figure 5.8: Load-deformation relationship at various flange thicknesses when the load is applied over a junction between two folds.

Except for differences in the ultimate load and the stiffness at the elastic loading range, the load-deformation behaviour is not considerably affected by changes in the flange thickness when the load is applied over a junction between two folds. Again, the stiffer girders are those with the thicker flanges. After the ultimate load is reached, however, the behaviour is somewhat brittle, independently on the flange thickness.

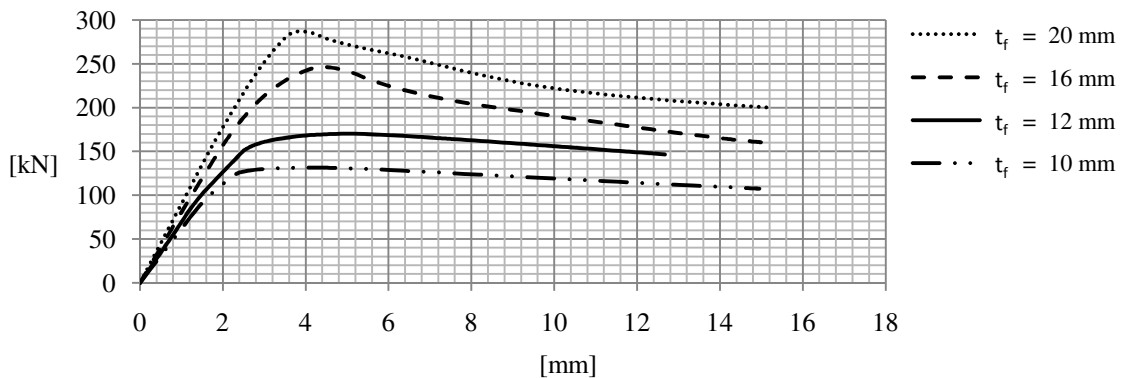


Figure 5.9: Load-deformation relationship at various flange thicknesses when the load is applied over a longitudinal fold.

Loading the girder over a longitudinal fold shows more similarities with a load applied over an inclined fold regarding responses to changes in flange thickness. The lowest initial stiffness is possessed within girders using flanges of small thickness. Using girders with thin flanges results in very ductile behaviour and along with increasing flange thicknesses, the behaviour becomes more brittle with a more pronounced decrease of the capacity after reaching the ultimate load.

5.2.3 Postbuckling behaviour

As mentioned earlier, the shape of the buckling mode is mainly governed by the load case (10X, 20X and 30X in Figure 5.10). In similarity to the web thickness, the flange thickness has a strong influence on the buckling propagation. Hence, Figure 5.10 depicts the various buckling modes at the end of the loading process using different flange thicknesses and load cases.

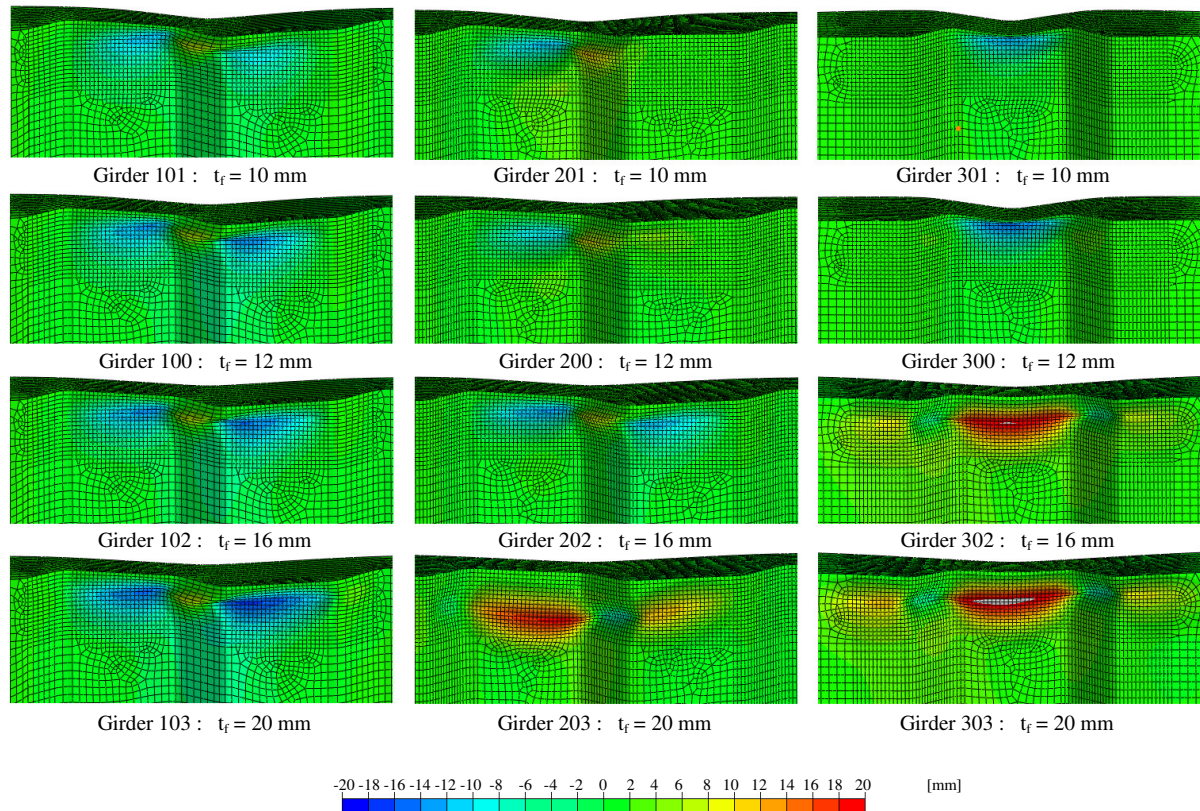


Figure 5.10: Buckling shapes and magnitudes at different load cases with a varying flange thickness and at the end of a loading process of 50 increments in ABAQUS CAE. Web thickness $t_w = 3$ mm.

When applying the load over an inclined fold (Girder 10X in Figure 5.10), the variations in flange thickness do not seem to have any great influence on the buckle propagation, only a slight increase when increasing the flange thickness. For all cases, three obvious buckles appear in the three folds closest to the applied load.

A similar behaviour is present when loading the girder over a junction between two folds (Girder 20X in Figure 5.10). However, in this case, the changes in flange thickness seem to have a stronger influence on the buckle propagation. Using the thinnest flange, $t_f = 10$ mm, will result in only two obvious buckles in the adjacent folds on each side of the loaded junction. Increasing the flange thickness will increase the capacity of the flange thus spreading the buckling of the web to the unaffected longitudinal fold closest to the loaded area. At a flange thickness of 20 mm these three folds have become highly affected with a buckle in the leftmost fold which stretches over the junctions on each side of the fold. Further, at a flange thickness of 20 mm the buckling appears to occur farther from the upper flange than at thinner flanges.

When loading the girder over a longitudinal fold while using a flange thickness of 10 mm only a small buckle just below the loaded area is obvious after the loading cycle in ABAQUS CAE (Girder 301 in Figure 5.10). Increasing the flange thickness to 12 mm will not affect the buckling propagation significantly. However, increasing the flange thickness from 12 mm to 16 mm will increase the propagation of the buckling through the adjacent inclined folds and to the following longitudinal folds (Girder 302 in Figure

5.10). A further increase of the flange thickness to 20 mm will not have any considerable effect on the shape or the propagation of the buckling, but only increase the magnitude of the out-of-plane deformations.

5.3 Influence of local initial imperfections

According to Lou and Edlund (1994) local initial imperfections up to half the size of the web thickness could reduce the ultimate load with up to 7 %. As the web in the reference girder used in this analysis has a thickness of only 3 mm, imperfections half the size of the web are reasonable in a real scenario. Hence, this parameter is valid for further investigation. However, the shapes of the initial imperfections are here set to the shape of the first eigenmode obtained from the linear buckling analysis for each loading case. Hence, the results when changing the local initial imperfections may not represent a worst case scenario.

As seen in Appendix D, the imperfections used in the study are 0, 0.5, 1, 2 and 5 mm. In this section the influence of the local initial imperfections will be presented in terms of ultimate load, load-deformation relationship and postbuckling mode.

5.3.1 Ultimate load

As mentioned earlier, a 7 % reduction in the ultimate load may be expected when increasing the local initial imperfection amplitude from zero to of half the size of the web thickness. Though this may seem large for such small imperfections, the behaviour at larger local initial imperfections is yet to be investigated. Hence, local initial imperfections up to almost twice the size of the web thickness are considered in this analysis. The results from the FE-analysis are plotted in Figure 5.11 together with results from the models by Lou and Edlund (1994) and Elgaaly and Seshadri (1997).

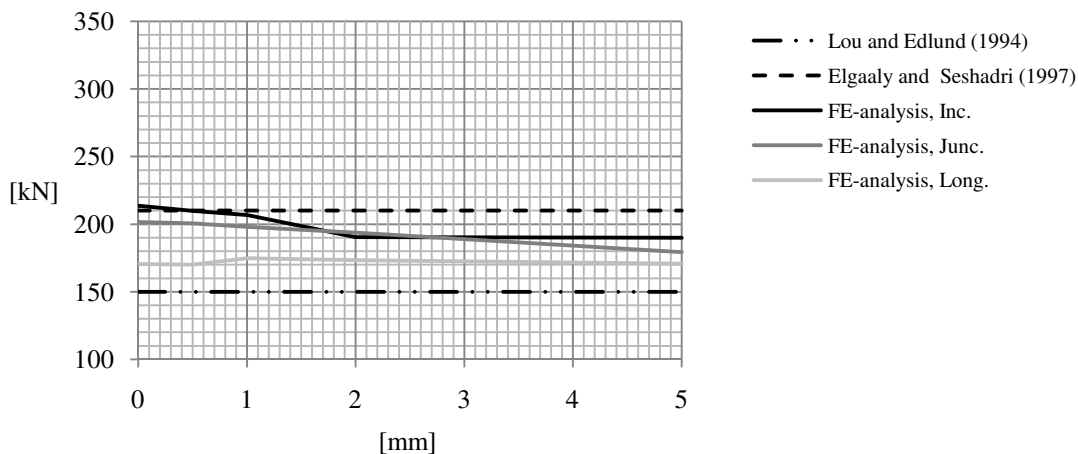


Figure 5.11: Influence of the local initial imperfection size on the ultimate load. Results from the FE-analysis are plotted along with results using the models by Lou and Edlund (1994) and Elgaaly and Seshadri (1997).

When applying the load over an inclined panel, setting the local initial imperfections to 0 mm will result in the highest ultimate load, about 213 kN. Increasing the local initial imperfection will then gradually decrease the resulting ultimate load until reaching a local initial imperfection amplitude of about 2 mm, from which the ultimate load does

not change significantly up to a very large local initial imperfection of 5 mm. The reference girder used in the analysis had a local initial imperfection of 0.5 mm which – in this case – resulted in a 1.4 % decrease of the ultimate load. At a local initial imperfection of 1.5 mm (which is half the size of the thickness of the web and should, according to Lou and Edlund (1994), result in a decrease in the ultimate load of about 7 %) the ultimate load decreases about 7.5 %, which is very close to the statement made by Lou and Edlund (1994).

Increasing the local initial imperfections when the girder is loaded over a junction between two folds will result in a more constant decrease rate in the ultimate load. A maximum ultimate load of 202 kN is obtained at a local initial imperfection of 0 mm. As the local initial imperfection increases up to the maximum value of 5 mm the ultimate load decreases about 13 %. Using the reference value of the local initial imperfection (0.5 mm) will result in a 1 % decrease in the ultimate load. At a local initial imperfection of half the size of the web thickness, the decrease in the ultimate load will only be about 3.1 %.

The load case which is least affected by changes in the initial imperfections – regarding ultimate load – is when the load is applied over a longitudinal fold. Here, a maximum load of 174 kN is reached at a local initial imperfection of about 1 mm, i.e. 3 % higher than the ultimate load when having no local initial imperfection. However, at a local initial imperfection of 0.5 mm, the resulting ultimate load is less than that obtained with no local initial imperfection. Increasing the local initial imperfections from 1 to 5 mm will result in a 3 % decrease of the ultimate, i.e. the ultimate load at a local initial imperfection of 0 mm and 5 mm are more or less equal.

As none of the models by Lou and Edlund (1994) or Elgaaly and Seshadri (1997) takes local initial imperfections into account, the results are constant at the values for the considered girder type. Though, the model by Elgaaly and Seshadri (1997) corresponds quite well with results from the FE-model when loading the girder over an inclined fold and while: $0 \text{ mm} < e_0 < 1 \text{ mm}$.

5.3.2 Load-deformation relationship

In this section, the influence of changes in the local initial imperfection magnitude on the load-deformation relationship is analysed. This is made by comparing the FE-results obtained when varying the local initial imperfections at different load cases. The results are presented in figures for each load case.

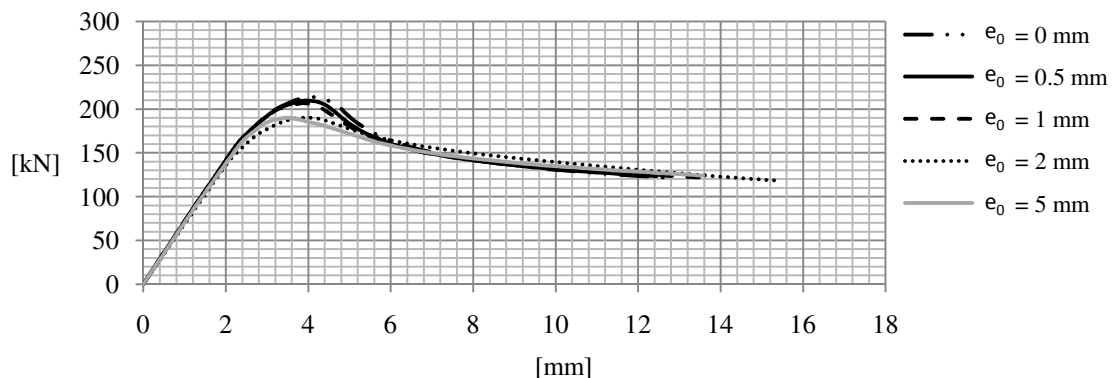


Figure 5.12: Load-deformation relationship at various local initial imperfections when the load is applied over an inclined fold.

By looking at Figure 5.12 it can be noticed that changes in the local initial imperfections will not affect the initial stiffness of the girder when it is loaded over an inclined fold. However, at higher loads, the stiffness of the girders with larger local initial imperfections will start to decrease earlier and a somewhat ductile behaviour is obtained. At lower local initial imperfections, the stiffness remains larger at higher loads until the ultimate load is reached and a somewhat faster decrease in capacity indicates a more brittle behaviour. However, after some unloading, the curves in Figure 5.12 reconnect and the postbuckling capacities of these girders are rather similar.

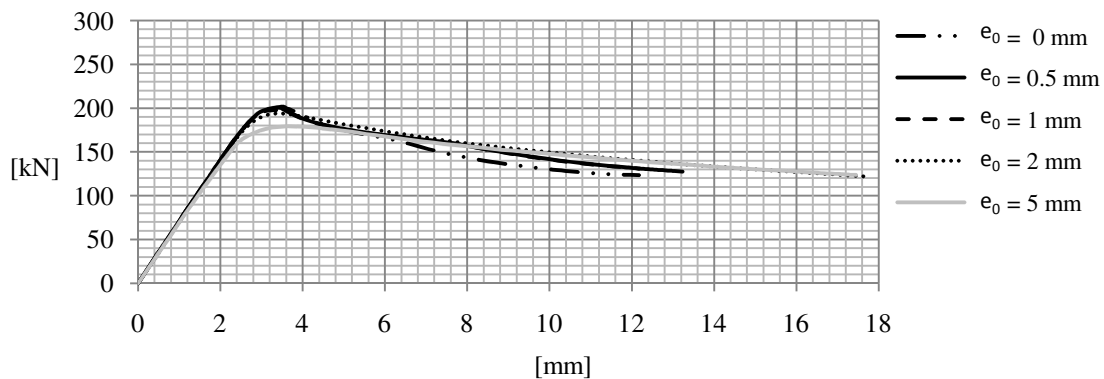


Figure 5.13: Load-deformation relationship at various local initial imperfections when the load is applied over a junction between two folds.

The effects on the load-deformation behaviour due to variations in the local initial imperfections when applying the load over a junction between two folds are very similar to those when applying the load over an inclined fold. Again, variations in the local initial imperfections have no significant influence on the initial stiffness. Furthermore, larger local initial imperfections will result in a more ductile behaviour and the postbuckling capacities of most configurations are rather similar (though the postbuckling capacity of Girder 206 is a little lower).

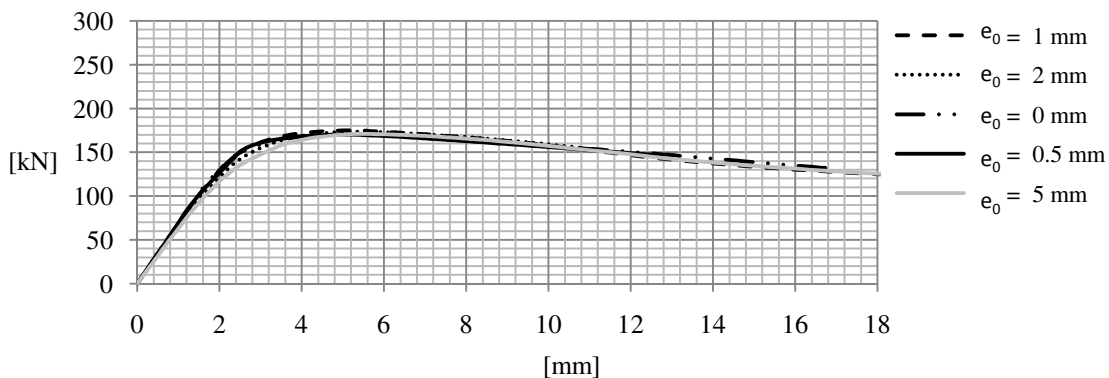


Figure 5.14: Load-deformation relationship at various local initial imperfections when the load is applied over a longitudinal fold.

When applying the load over a longitudinal fold the changes in the load-deformation relationship due to initial imperfections are not as obvious as those of the other two load

cases. Here, all girder configurations exhibit rather ductile behaviour. However, there are some differences most easily observed at deformations between 2 and 4 mm in Figure 5.14. As when loading the girder over an inclined fold or over a junction between two folds, larger local initial imperfections result in a more ductile behaviour. Though in this case, all girder configurations will result in a more or less ductile behaviour.

5.3.3 Postbuckling behaviour

As the results concerning ultimate load when changing the local initial imperfections were not as consistent as when considering the parameters studied earlier (web thickness and flange thickness), the results concerning the postbuckling modes may be more difficult to predict. Though the local initial imperfections should not affect the general shape of the buckling mode, they should affect the magnitude of the out-of-plane deformations.

Similar as for the previous parameters considered in this study, the postbuckling modes (after one loading process in ABAQUS CAE) as a response to changes in the local initial imperfection are presented for different load cases (10X, 20X and 30X in Figure 5.15).

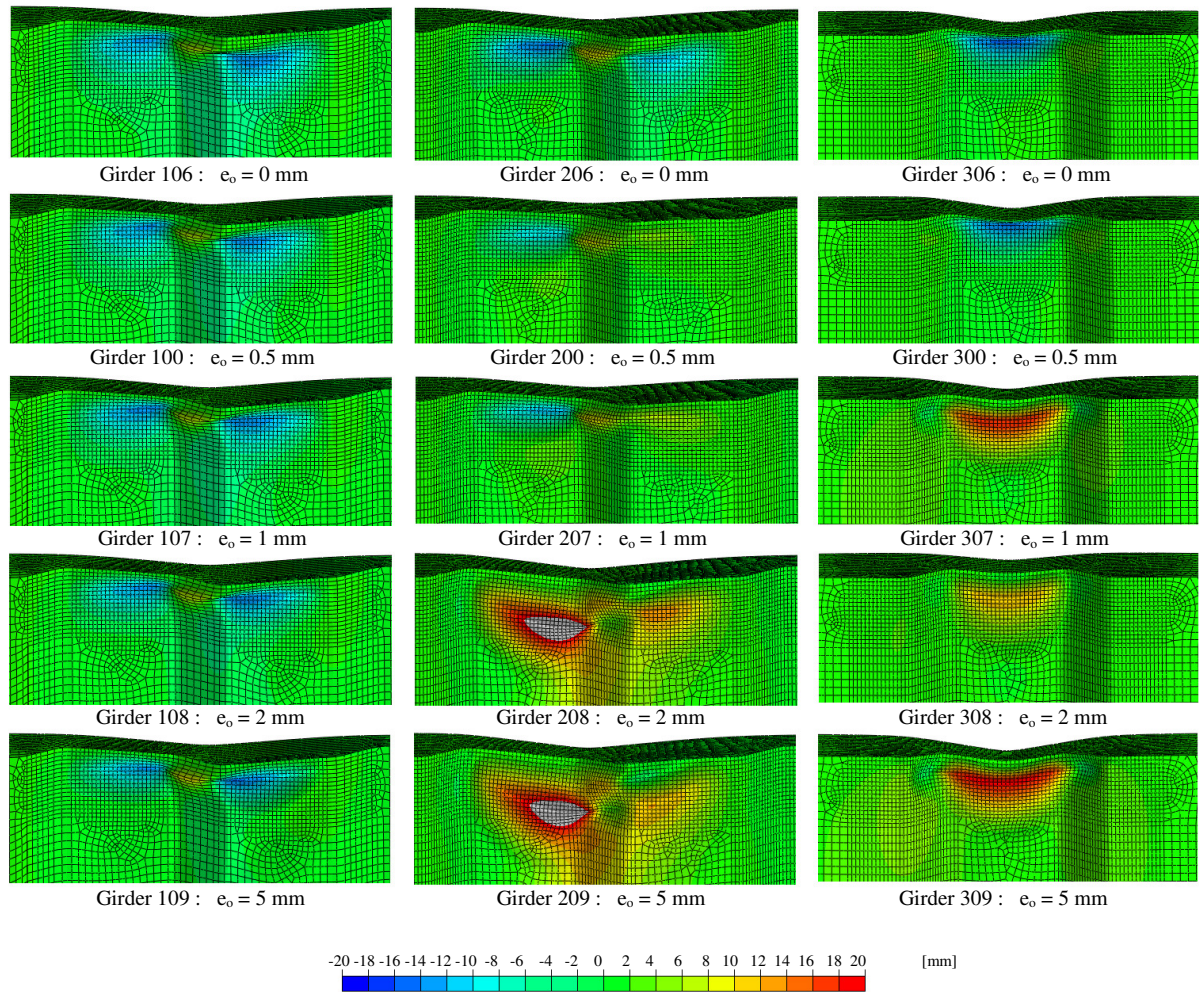


Figure 5.15: Buckling shapes and magnitudes at different load cases with varying local initial imperfections and at the end of a loading process of 50 increments in ABAQUS CAE.

As seen in Figure 5.15, changing the local initial imperfections when applying the load over an inclined fold (Girder 10X) will not essentially affect the buckling shape or the magnitude of the buckling. At the end of the loading cycle, the deformations in each case vary between 13 mm and 16 mm (see Figure 5.12) and yet, no significant difference due to variations in the local initial imperfections is obtained.

When loading the girder over a junction between two folds, the results for the three smallest e_o values (Girder 206, Girder 200 and Girder 207 in Figure 5.15) seem quite consistent. Here, three buckles develop at same locations and same directions (except for the rightmost buckles in Girder 200 and Girder 207). Increasing the initial imperfections to 2 mm and 5 mm will increase the distance from the buckles to the upper flange (Girder 208 and Girder 209). Further, all three buckles – in this case – will develop in the same direction and the buckle in the longitudinal fold closest to the loaded junction is the largest. Though the vertical displacements of Girder 208 and Girder 209, at the end of the loading cycle, were about 6 mm larger than that when using smaller initial local imperfections (Figure 5.13), it seems as if the buckle

propagation tends to increase vertically when considering larger initial local imperfections.

Applying the load over a longitudinal fold will result in no significant difference in the postbuckling modes if the initial local imperfections are set to 0 mm or 0.5 mm. This buckling shape and direction is very similar to what was obtained during the experimental testing, i.e. in a direction opposite to the initial imperfection mode. However, when increasing the initial local imperfection size above $e_o = 0.5$ mm, the buckle develops in the opposite direction and farther from the upper flange. This is a strong indication that the eigenmode used for this load case is not the shape easiest obtained during loading. The larger initial local imperfections force the girder to deform in another shape more similar to the first eigenmode from the linear buckling analysis. This may also be the reason why the ultimate load increases in the range $0.5 \text{ mm} < e_o < 1 \text{ mm}$ as seen in Figure 5.11.

5.4 Influence of load position

According to the models and the experimental tests presented in section 2.1.2, the load position has a rather large influence on the ultimate load of the girder. The load positions considered in the earlier studies are: over an inclined fold, over a junction between two folds and over a longitudinal fold. However, as the available tests on each load position – particularly over the junctions between two folds – are few, this parameter is included in the parametric study in order to obtain more information on how it may affect the ultimate capacity of the girder.

The effects of varying load positions are – in this section – only presented in terms of ultimate load. For information about the effects that varying load positions may have on the buckling mode, see sections concerning load-deformation relationship.

5.4.1 Ultimate load

In Figure 5.16, the resulting ultimate loads with varying load positions are compared for all girder types considered in the parametric study. Generally, a load positioned over an inclined fold will result in the largest ultimate load, followed closely by a load over a junction between two folds. A load over a longitudinal fold will most often result in an ultimate load 10 – 20 % smaller than that of a girder loaded over an inclined fold. However, this is mostly related to results using the reference girder or only changing the initial imperfections.

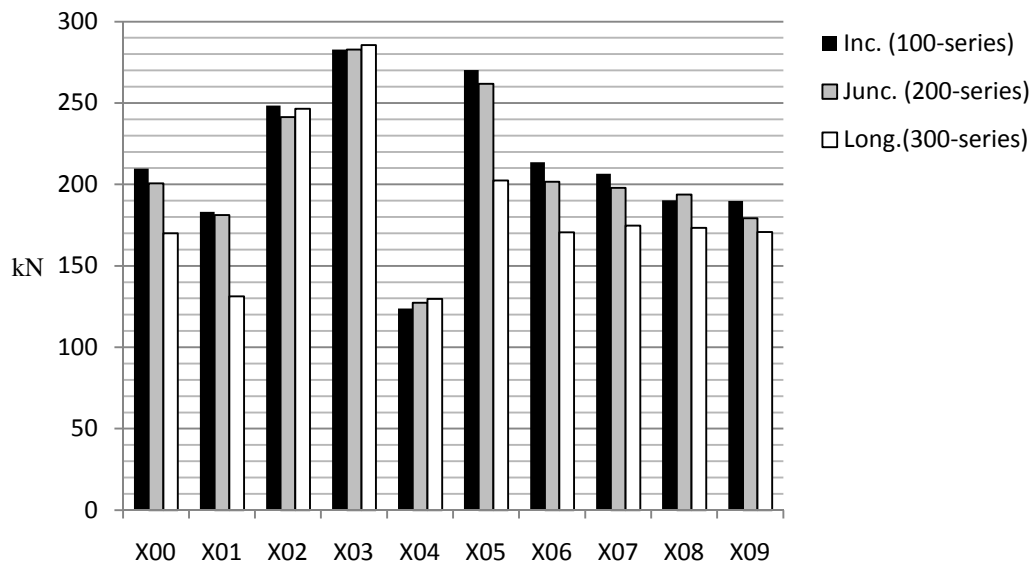


Figure 5.16: Influence of the load position on the ultimate load of different girders.

According to the results presented in Figure 5.16, load position has a very strong influence on the ultimate load using girders with thin flanges (about 30 % smaller ultimate load when loaded over a longitudinal fold at a flange thickness of 10 mm). However, at large flange thicknesses (16 - 20 mm) changes in the load position will have almost no effect at all on the ultimate load (about 1 - 3 %).

When using a girder with a small web thickness (X04: $t_w = 2$ mm) the influence of the load position on the ultimate load will be trivial. As the web thickness increases, the resulting ultimate loads will increase rather equally when loaded over an inclined fold or over a junction between two folds. However, the ultimate load is not as sensitive to changes in the web thickness when loading the girder over a longitudinal fold. Hence, for this case, the difference in ultimate load when using a girder with a thick web (X05: $t_w = 4$ mm) is quite large (about 25 % smaller ultimate load when loaded over a longitudinal fold).

Furthermore, as initial imperfections increase (X06, X07, X08 and X09) the resulting ultimate load decreases only when loaded over an inclined fold and over a junction between two folds while it remains rather stable when the girder is loaded over a longitudinal fold. However, as mentioned earlier, as the initial imperfections are set to the shape of the first eigenmodes – i.e. not necessarily the “worst case scenario” – the actual effects of the initial imperfections might yet remain to be investigated.

6 CONCLUSIONS

6.1 On design models and comparison with FE-simulation results

In section 2.3.9, where results using the present design models were compared with experimental tests, it was concluded that the two design models developed by Lou and Edlund (1994) and Elgaaly and Seshadri (1997) were most promising. Hence, these two design models were used for comparison when analysing the results from the parametric study performed with the Finite Element model in chapter 5.

Model by Elgaaly and Seshadri (1997).- In comparison, the results obtained from the FE-analysis and the model by Elgaaly and Seshadri (1997) show very good agreement when loading the girder over an inclined fold or over a junction between folds. However, when applying the load over a longitudinal fold the results are heavily dependent on the ratio t_w/t_f . The design model seems to correspond well with the FE-model, when $t_w/t_f < 0.2$. As t_w/t_f is increased, the ultimate loads using the design model will be larger than those of the FE-model.

Modified semi-empirical formula set by Lou and Edlund, Equations (2.22) to (2.26).- The study of the influence of the *web thickness* on the ultimate load in Figure 5.1 shows that the ultimate loads obtained by the design model of Lou and Edlund (1994) has similar characteristics – although somewhat lower – as the results from the FE-analysis when loading the girder over a longitudinal fold. Further, when studying the influence of the flange thickness in Figure 5.6 it can be observed that the design model by Lou and Edlund (1994) corresponds well with the FE-model. Using the design model by Lou and Edlund (1994) will mostly generate ultimate loads on the safe side.

6.2 Influence of increasing plate thickness

When the load is applied over an inclined fold or over a junction between folds the FE-analysis indicates that, when increasing the *web thickness* with 1 mm, the ultimate load increases with about 60 kN. The corresponding increase, when loading the girder over the centre of a longitudinal fold, is about 50 kN.

Loading the girder over an inclined fold or over a junction between folds the FE-analysis indicates that, when increasing the *flange thickness* with 1 mm, the ultimate load increases with about 10 kN. The corresponding increase, when loading the girder over the centre of a longitudinal fold, is about 20 kN for $t_f < 15$ mm and 10 kN for $t_f > 15$ mm.

6.3 Influence of the load position

As indicated by the observations in all experimental tests, the load position has a great influence on the ultimate load. Generally, it seems that a load over the centre of a longitudinal fold will result in the lowest values of the ultimate load. However, a worst case position, which is applicable in every situation, cannot be distinguished. As observed in section 5.4.1, it seems that the influence of the load position on the ultimate load is very small for $t_w/t_f < 0.2$.

6.4 Influence of initial imperfections

Lou and Edlund (1994) conclude that a local initial imperfection of up to half the size of the web thickness could reduce the ultimate load with up to 7 %. This agrees with observations made in section 5.3.1.

The results from the FE-analysis, when loading the girder over a longitudinal fold, are that increased local initial imperfections cause a small increase of the ultimate load. This indicates that the assumed shape of the imperfections might not be the actual worst case scenario. Choosing another shape – more similar to the buckling mode obtained using a non-linear analysis of an imperfection free structure – is likely to result in decreased carrying capacity, when increasing the magnitude of the local initial imperfection. For the other two load cases (over an inclined fold and over a junction between folds) the ultimate load decreases when increasing the size of the local initial imperfection.

6.5 Load-deformation behaviour

The load-deformation behaviour is heavily dependent on both the load case and the ratio t_w/t_f . For all load cases, an increased value of t_w/t_f will result in a more ductile behaviour of the girder under patch loading. The rate of change of the load-deformation curve, due to changes in t_w/t_f , is dependent on the load position.

7 SUGGESTIONS FOR FURTHER RESEARCH

The present knowledge on the patch load behaviour of plate girders with corrugated webs is limited. Hence, further studies are required in order to obtain a reliable design model. Based on the information presented in the thesis, there are certain “key areas”, which these further studies should include.

Experimental tests by different researchers on the behaviour of girders should be performed with a larger variation in dimensional properties. So far, the experimental tests have been performed on girders of rather similar geometry. Hence, for a more complete knowledge, tests on girders with a larger variation in thicknesses and corrugation profile are needed.

The loading lengths used in the experimental tests by different researchers presented in this thesis have varied between 5 and 100 mm. However, these tests have been performed on girders of different dimensions or with different load positions. Hence, comparing the results may be difficult. Therefore, conducting experimental tests with similar configurations but with varying loading length is required.

As the problem illustrated by Fig. 4.18 may have a significant effect on the results it would be desirable with a more realistic modelling of the load application details, e.g. by including the loading bar in the FEM model.

Additionally, experimental tests on the *interaction* behaviour between both patch loading and bending and patch loading and shear need to be investigated. To the authors' knowledge, this interaction behaviour has only been studied through a FE-analysis performed by Elgaaly and Seshadri (1997).

Furthermore, a more thorough investigation of the effects of initial imperfections is required. In the parametric study performed in this master's thesis, only the variation of the *magnitude* of the initial imperfections was considered. However, the effects of different shapes of the initial imperfections are yet to be studied, e.g. using the non-linear buckling mode.

8 REFERENCES

- Bergfelt, A., Edlund, B. and Leiva-Aravena, L., 1985. Trapezoidally corrugated girder webs: Shear buckling. Patch loading. *Ingenieurs et architectes suisses*, 111, pp.22-27.
- Carling, O., 1974. *Rana balken typgodkännande; Belastningsförsök på svetsade stålbalkar med veckat liv*. Stockholm: Ingenjörbyrå AB.
- Dahlén, A. and Krona, K.-M., 1984. *Lokal intryckning av veckat liv*. Publ. 84:5. Göteborg: Chalmers University of Technology, Division of Steel and Timber Structures.
- Egaaly, M. and Seshadri, A., 1997. Girders with corrugated webs under partial compressive edge loading. *Journal of Structural Engineering*, pp.783-91.
- Elgaaly, M., Seshadri, A. and Hamilton, R.W., 1996. Shear strength of beam with corrugated webs. *Journal of Structural Engineering*, pp.390-98.
- Elgaaly, M., Seshadri, A. and Hamilton, R.W., 1997. Bending strength of steel beams with corrugated webs. *Journal of structural engineering*, pp.772-82.
- EN 1993-1-5, 2006. *Eurocode 3: Design of Steel Structures, Part 1.5: Plated structural elements*. Brussels, Belgium: CEN, European Committee for standardization.
- Galambos, T.V., 1998. *Guide to Stability Design Criteria for Metal Structures*. New York: John Wiley & Sons Inc.
- Gozzi, J., 2007. *Patch Loading Resistance of Plated Girders: Ultimate and serviceability limit state*. PhD Thesis. Luleå: Luleå University of Technology.
- Hamilton, R., 1993. *Behavior of Welded Girders with Corrugated Webs*. Orono: University of Maine.
- Kuchta, K.R., 2006. Patch load carrying capacity of corrugated web. In *ICMS-2006 - Progress in Steel, Composite and Aluminium Structures*. London: Taylor & Francis Group.
- Lagerqvist, O., 1994. *Patch Loading: Resistance of steel girders subjected to concentrated forces*. Ph.D. Thesis. Luleå, Sweden: Luleå University of Technology.
- Leiva-Aravena, L. and Edlund, B., 1987. Buckling of Trapezoidally Corrugated Webs. *Colloquium on Stability of Plate and Shell Structures, ECCS*, pp.107-16, Ghent University.
- Luo, R. and Edlund, B., 1994. Ultimate Strength of Girders with Trapezoidally Corrugated Webs Under Patch Loading. *Thin-Walled Structures*, vol. 24, pp.135-56.
- Moon, J., Yi, J., Choi, B.H. and Lee, H.-E., 2008. Shear strength and design of trapezoidally corrugated steel webs. *Journal of constructional steel research*, Vol. 65, pp.1198-205.

Sayed-Ahmed, E.Y., 2005. Plate girders with corrugated steel webs. *Canadian Journal of Civil Engineering*, 1st Quarter, pp.656-72.

Wang, X., 2003. *Behavior of Steel Members with Trapezoidally Corrugated Webs and Tubular Flanges under Static Loading*. Ph.D. Thesis. Philadelphia: Drexel University.

Winter, G., 1947. Strength of thin steel compression flanges. *Trans. A.S.C.E.*, (112), pp.527-44.

von Kármán, T., Sechler, E.E. and Donnell, L.H., 1932. The strength of thin plates in compression. *Trans. A.S.M.E.*, 54(APM-54-5), pp.53-57.

APPENDIX A - Comparison of Earlier Models (Mathcad)

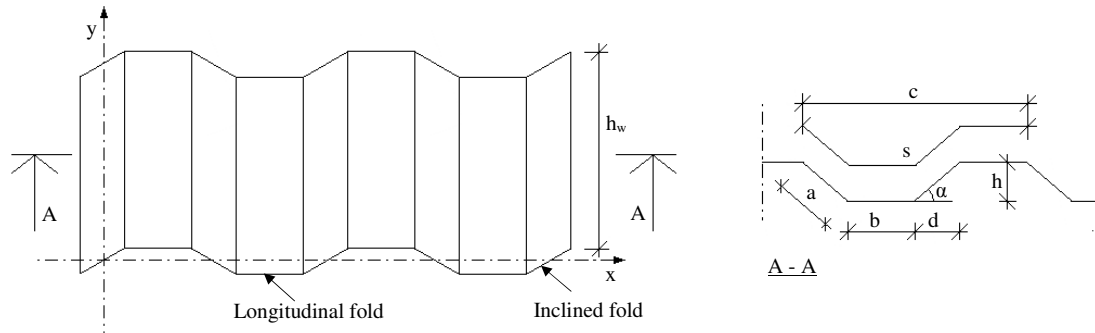
| | | |
|-------|---|----|
| A.1 | Standard parameters | 1 |
| A.1.1 | Literature study | 1 |
| A.1.2 | FE-analysis | 1 |
| A.2 | Invariants | 2 |
| A.2.1 | Dahlén och Krona (1984) | 2 |
| A.2.2 | Lou and Edlund (1994) | 2 |
| A.3 | Varying web thickness, t_w | 3 |
| A.3.1 | Arne Johnson Ingenjörbyrå AB, Carling (1974) | 3 |
| A.3.2 | Rana (1982) | 3 |
| A.3.3 | Dahlén and Krona (1984) | 3 |
| A.3.4 | Lou and Edlund (1994) | 5 |
| A.3.5 | Elgaaly and Seshadri (1997) | 6 |
| A.4 | Varying corrugation angle α and depth of inclination h | 8 |
| A.4.1 | Arne Johnson Ingenjörbyrå AB, Carling (1974) | 8 |
| A.4.2 | Rana (1982) | 8 |
| A.4.3 | Dahlén and Krona (1984) | 8 |
| A.4.4 | Lou and Edlund (1994) | 9 |
| A.4.5 | Elgaaly and Seshadri (1997) | 12 |
| A.5 | Varying web depth, h_w | 13 |
| A.5.1 | Arne Johnson Ingenjörbyrå AB, Carling (1974) | 13 |
| A.5.2 | Rana (1982) | 13 |
| A.5.3 | Dahlén and Krona (1984) | 13 |
| A.5.4 | Lou and Edlund (1994) | 13 |
| A.5.5 | Elgaaly and Seshadri (1997) | 13 |
| A.6 | Varying flange thickness, t_f | 14 |
| A.6.1 | Arne Johnson Ingenjörbyrå AB, Carling (1974) | 14 |
| A.6.2 | Rana (1982) | 14 |
| A.6.3 | Dahlén and Krona (1984) | 14 |
| A.6.4 | Lou and Edlund (1994) | 15 |
| A.6.5 | Elgaaly and Seshadri (1997) | 16 |
| A.7 | Varying flange width, b_f | 17 |

| | | |
|----------|---|----|
| A.7.1 | Arne Johnson Ingenjörbyrå AB, Carling (1974) | 17 |
| A.7.2 | Rana (1982) | 17 |
| A.7.3 | Dahlén och Krona (1984) | 17 |
| A.7.4 | Lou and Edlund (1994) | 18 |
| A.7.5 | Elgaaly and Seshadri (1997) | 18 |
| A.8 | Varying length of the longitudinal fold, b | 19 |
| A.8.1 | Arne Johnson Ingenjörbyrå AB, Carling (1974) | 19 |
| A.8.2 | Rana (1982) | 19 |
| A.8.3 | Dahlén and Krona (1984) | 19 |
| A.8.4 | Lou and Edlund (1994) | 22 |
| A.8.5 | Elgaaly and Seshadri (1997) | 23 |
| A.9 | Varying loading length, s_s | 24 |
| A.9.1 | Arne Johnson Ingenjörbyrå AB, Carling (1974) | 24 |
| A.9.2 | Rana (1982) | 24 |
| A.9.3 | Dahlén and Krona (1984) | 24 |
| A.9.4 | Lou and Edlund (1994) | 25 |
| A.9.5 | Elgaaly and Seshadri (1997) | 25 |
| A.10 | Varying load position | 27 |
| A.10.1 | Arne Johnson Ingenjörbyrå AB, Carling (1974) | 27 |
| A.10.2 | Rana (1982) | 27 |
| A.10.3 | Dahlén and Krona (1984) | 27 |
| A.10.3.1 | Load applied over inclined fold | 27 |
| A.10.3.2 | Load applied over junction between folds | 27 |
| A.10.3.3 | Load applied over longitudinal fold | 28 |
| A.10.4 | Lou and Edlund (1994) | 28 |
| A.10.5 | Elgaaly and Seshadri (1997) | 28 |
| A.10.5.1 | Load applied over inclined fold | 29 |
| A.10.5.2 | Load applied over junction between folds | 29 |
| A.10.5.3 | Load applied over longitudinal fold | 29 |
| A.11 | Calculation for a girder with a flat web subjected to patch loading | 30 |
| A.11.1 | Ultimate load with varying web thicknesses | 30 |
| A.11.2 | Comparison of steel amount | 34 |

A.1 Standard parameters

A.1.1 Literature study

The values of the parameters listed below represent the dimensional and material properties of the girder used in the parametric study in chapter 2.



| | |
|-------------------------------|--|
| $b_{f_std} = 180 \text{ mm}$ | (flange width) |
| $t_{f_std} = 12 \text{ mm}$ | (flange thickness) |
| $h_{w_std} = 600 \text{ mm}$ | (web height) |
| $t_{w_std} = 2 \text{ mm}$ | (web thickness) |
| $\alpha_{std} = 45^\circ$ | (corrugation angle) |
| $b_{std} = 70 \text{ mm}$ | (length of longitudinal fold) |
| $h_{std} = 50 \text{ mm}$ | (corrugation depth) |
| $a_{std} = 70,771 \text{ mm}$ | (length of inclined fold) |
| $d_{std} = 50 \text{ mm}$ | (length of the projection of an inclined fold) |

| | |
|----------------------------|---------------------------------|
| $f_{yw} = 355 \text{ MPa}$ | (yield strength of the web) |
| $f_{yf} = 355 \text{ MPa}$ | (yield strength of the flanges) |
| $E = 210 \text{ GPa}$ | (Young's modulus) |

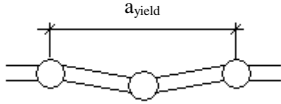
A.1.2 FE-analysis

In the FE-analysis, most of the dimensional and material properties were set to the same values as those presented in A.1.1. However, the following parameters were modified in order to be able to verify the model against the experimental tests performed in this thesis.

| | |
|-------------------------------|---------------------------------|
| $b_{f_std} = 160 \text{ mm}$ | (flange width) |
| $t_{w_std} = 3 \text{ mm}$ | (web thickness) |
| $b_{std} = 140 \text{ mm}$ | (length of longitudinal fold) |
| $f_{yw} = 375 \text{ MPa}$ | (yield strength of the web) |
| $f_{yf} = 406 \text{ MPa}$ | (yield strength of the flanges) |

A.2 Invariants

A.2.1 Dahlén och Krona (1984)



$$a_{yield} := b_{std} + 2d_{std} + 2t_{f_std}$$

$$a_{yield} = 194 \text{ mm}$$

$$mk := 1.5^4 \cdot 2.5 \cdot 20$$

$$mk = 253.125$$

Value of mk is assumed to be the same as Bergfelt proposed for flat girders

A.2.2 Lou and Edlund (1994)

$$\eta := \frac{1}{240 \text{ mm}}$$

A.3 Varying web thickness, t_w

$$t_w := \begin{pmatrix} 2\text{mm} \\ 3\text{mm} \\ 4\text{mm} \\ 5\text{mm} \\ 6\text{mm} \end{pmatrix}$$

A.3.1 Arne Johnson Ingenjörbyrå AB, Carling (1974)

$$P_{1974_tw} := 0.04 \cdot E \cdot t_w^2 \qquad P_{1974_tw} = \begin{pmatrix} 33.6 \\ 75.6 \\ 134.4 \\ 210 \\ 302.4 \end{pmatrix} \cdot \text{kN}$$

A.3.2 Rana (1982)

$$P_{1982_tw} := 0.75 \cdot f_{yw} \cdot t_w \cdot (2t_{f_std} + s_{s_std}) \qquad P_{1982_tw} = \begin{pmatrix} 39.405 \\ 59.108 \\ 78.81 \\ 98.513 \\ 118.215 \end{pmatrix} \cdot \text{kN}$$

A.3.3 Dahlén and Krona (1984)

$$t_w := t_{f_std} \cdot \sqrt[4]{\frac{b_{f_std}}{25 \cdot t_{f_std}}} \qquad t_i = 0.011 \text{ m}$$

$$f_{cv} := 1 + 40 \cdot \frac{s_{s_std}}{a_{yield}} \cdot \frac{t_w}{h_{w_std}} \qquad f_c = \begin{pmatrix} 1.034 \\ 1.052 \\ 1.069 \\ 1.086 \\ 1.103 \end{pmatrix}$$

$$f_{al} := 2 \cdot \frac{a_{yield}}{b_{std}} \cdot \frac{\sqrt{1 + \sqrt{1 + mk \cdot \left(\frac{b_{std}}{2 \cdot a_{yield}}\right)^4}}}{1 + \sqrt{1 + mk}} \quad f_{al} = 1.964$$

$$P_{1984_tw} := \begin{bmatrix} 0.8 \cdot \sqrt{\frac{t_i}{t_{w0}}} \cdot (t_{w0})^2 \cdot \sqrt{f_{yw} \cdot E} \cdot f_{c0} \cdot f_{al} \\ 0.8 \cdot \sqrt{\frac{t_i}{t_{w1}}} \cdot (t_{w1})^2 \cdot \sqrt{f_{yw} \cdot E} \cdot f_{c1} \cdot f_{al} \\ 0.8 \cdot \sqrt{\frac{t_i}{t_{w2}}} \cdot (t_{w2})^2 \cdot \sqrt{f_{yw} \cdot E} \cdot f_{c2} \cdot f_{al} \\ 0.8 \cdot \sqrt{\frac{t_i}{t_{w3}}} \cdot (t_{w3})^2 \cdot \sqrt{f_{yw} \cdot E} \cdot f_{c3} \cdot f_{al} \\ 0.8 \cdot \sqrt{\frac{t_i}{t_{w4}}} \cdot (t_{w4})^2 \cdot \sqrt{f_{yw} \cdot E} \cdot f_{c4} \cdot f_{al} \end{bmatrix} \quad P_{1984_tw} = \begin{pmatrix} 128.958 \\ 240.846 \\ 376.865 \\ 535.152 \\ 714.607 \end{pmatrix} \cdot \text{kN}$$

A.3.4 Lou and Edlund (1994)

$$\gamma_{\alpha} := \left(\begin{array}{l} \left| \begin{array}{l} \frac{b_{\text{std}} + a_{\text{std}}}{b_{\text{std}} + a_{\text{std}} \cdot \cos(\alpha_{\text{std}})} \text{ if } \frac{t_{f_std}}{t_{w_0}} \geq 3.82 \\ 1 \text{ otherwise} \end{array} \right. \\ \left| \begin{array}{l} \frac{b_{\text{std}} + a_{\text{std}}}{b_{\text{std}} + a_{\text{std}} \cdot \cos(\alpha_{\text{std}})} \text{ if } \frac{t_{f_std}}{t_{w_1}} \geq 3.82 \\ 1 \text{ otherwise} \end{array} \right. \\ \left| \begin{array}{l} \frac{b_{\text{std}} + a_{\text{std}}}{b_{\text{std}} + a_{\text{std}} \cdot \cos(\alpha_{\text{std}})} \text{ if } \frac{t_{f_std}}{t_{w_2}} \geq 3.82 \\ 1 \text{ otherwise} \end{array} \right. \\ \left| \begin{array}{l} \frac{b_{\text{std}} + a_{\text{std}}}{b_{\text{std}} + a_{\text{std}} \cdot \cos(\alpha_{\text{std}})} \text{ if } \frac{t_{f_std}}{t_{w_3}} \geq 3.82 \\ 1 \text{ otherwise} \end{array} \right. \\ \left| \begin{array}{l} \frac{b_{\text{std}} + a_{\text{std}}}{b_{\text{std}} + a_{\text{std}} \cdot \cos(\alpha_{\text{std}})} \text{ if } \frac{t_{f_std}}{t_{w_4}} \geq 3.82 \\ 1 \text{ otherwise} \end{array} \right. \end{array} \right) \gamma_{\alpha} = \begin{pmatrix} 1.173 \\ 1.173 \\ 1 \\ 1 \\ 1 \end{pmatrix}$$

$$\gamma_{\text{cov}} := 1 + \eta \cdot s_{s_std}$$

$$\gamma_c = 1.208$$

$$\gamma_{\text{min}} := 10.4 \cdot \gamma_{\alpha} \cdot \gamma_c$$

$$\gamma = \begin{pmatrix} 14.736 \\ 14.736 \\ 12.567 \\ 12.567 \\ 12.567 \end{pmatrix}$$

$$P_{1994_tw} := \begin{pmatrix} \gamma_0 \cdot t_{f_std} \cdot t_{w_0} \cdot f_{yw} \\ \gamma_1 \cdot t_{f_std} \cdot t_{w_1} \cdot f_{yw} \\ \gamma_2 \cdot t_{f_std} \cdot t_{w_2} \cdot f_{yw} \\ \gamma_3 \cdot t_{f_std} \cdot t_{w_3} \cdot f_{yw} \\ \gamma_4 \cdot t_{f_std} \cdot t_{w_4} \cdot f_{yw} \end{pmatrix} \quad P_{1994_tw} = \begin{pmatrix} 125.547 \\ 188.32 \\ 214.136 \\ 267.67 \\ 321.204 \end{pmatrix} \cdot \text{kN}$$

A.3.5 Elgaaly and Seshadri (1997)

Type I Failure - Web Crippling

$$M_{pf} := \frac{b_{f_std} \cdot f_{yf} \cdot t_{f_std}^2}{4} \quad M_{pf} = 2.3 \text{ kN} \cdot \text{m}$$

$$a := \left(\frac{f_{yf} \cdot b_{f_std} \cdot t_{f_std}^2}{2 \cdot f_{yw} \cdot t_w} \right)^{0.5} + \frac{s_{s_std}}{4} \quad a = \begin{pmatrix} 0.093 \\ 0.078 \\ 0.069 \\ 0.063 \\ 0.059 \end{pmatrix} \text{ m}$$

$$P_{fl} := \frac{4 \cdot M_{pf}}{a - \frac{s_{s_std}}{4}} \quad P_{fl} = \begin{pmatrix} 114.308 \\ 139.998 \\ 161.656 \\ 180.736 \\ 197.987 \end{pmatrix} \text{ kN}$$

$$P_w := (E \cdot f_{yw})^{0.5} \cdot t_w^2 \quad P_w = \begin{pmatrix} 34.537 \\ 77.708 \\ 138.148 \\ 215.856 \\ 310.832 \end{pmatrix} \text{ kN}$$

$$P_{1997_tw} := P_w + P_{fl}$$

$$P_{1997_tw} = \begin{pmatrix} 148.845 \\ 217.706 \\ 299.803 \\ 396.592 \\ 508.819 \end{pmatrix} \cdot \text{kN}$$

A.4 Varying corrugation angle α and depth of inclination h

$$\alpha := \begin{pmatrix} 30 \\ 45 \\ 60 \\ 75 \\ 80 \\ 85 \end{pmatrix} \cdot \frac{\pi}{180} \qquad h := \begin{pmatrix} 25\text{mm} \\ 50\text{mm} \\ 75\text{mm} \end{pmatrix}$$

A.4.1 Arne Johnson Ingenjörbyrå AB, Carling (1974)

$$P_{1974_\alpha} := 0.04 \cdot E \cdot t_{w_std}^2 \qquad P_{1974_\alpha} = 33.6 \cdot \text{kN}$$

A.4.2 Rana (1982)

$$P_{1982} := 0.75 \cdot f_{yw} \cdot t_{w_std} \cdot (2t_{f_std} + s_{s_std}) \qquad P_{1982} = 39.405 \cdot \text{kN}$$

A.4.3 Dahlén and Krona (1984)

$$t_i := t_{f_std} \cdot \sqrt[4]{\frac{b_{f_std}}{25 \cdot t_{f_std}}} \qquad t_i = 0.011 \text{ m}$$

$$f_c := 1 + 40 \cdot \frac{s_{s_std}}{a_{yield}} \cdot \frac{t_{w_std}}{h_{w_std}} \qquad f_{al} = 1.964$$

$$f_{al} := 2 \cdot \frac{a_{yield}}{b_{std}} \cdot \frac{1 + \sqrt{1 + mk \cdot \left(\frac{b_{std}}{2 \cdot a_{yield}}\right)^4}}{1 + \sqrt{1 + mk}} \qquad f_{al} = 1.281$$

$$P_{1984_\alpha} := 0.8 \cdot \sqrt{\frac{t_i}{t_{w_std}}} \cdot t_{w_std}^2 \cdot \sqrt{f_{yw} \cdot E \cdot f_c \cdot f_{al}} \qquad P_{1984_\alpha} = 128.958 \cdot \text{kN}$$

A.4.4 Lou and Edlund (1994)

$$\gamma_{\alpha h1} := \left(\begin{array}{l} \frac{b_{\text{std}} + \frac{h_0}{\sin(\alpha_0)}}{b_{\text{std}} + \frac{h_0}{\sin(\alpha_0)} \cdot \cos(\alpha_0)} \quad \text{if } \frac{t_{f_std}}{t_{w_std}} \geq 3.82 \\ 1 \quad \text{otherwise} \\ \frac{b_{\text{std}} + \frac{h_0}{\sin(\alpha_1)}}{b_{\text{std}} + \frac{h_0}{\sin(\alpha_1)} \cdot \cos(\alpha_1)} \quad \text{if } \frac{t_{f_std}}{t_{w_std}} \geq 3.82 \\ 1 \quad \text{otherwise} \\ \frac{b_{\text{std}} + \frac{h_0}{\sin(\alpha_2)}}{b_{\text{std}} + \frac{h_0}{\sin(\alpha_2)} \cdot \cos(\alpha_2)} \quad \text{if } \frac{t_{f_std}}{t_{w_std}} \geq 3.82 \\ 1 \quad \text{otherwise} \\ \frac{b_{\text{std}} + \frac{h_0}{\sin(\alpha_3)}}{b_{\text{std}} + \frac{h_0}{\sin(\alpha_3)} \cdot \cos(\alpha_3)} \quad \text{if } \frac{t_{f_std}}{t_{w_std}} \geq 3.82 \\ 1 \quad \text{otherwise} \\ \frac{b_{\text{std}} + \frac{h_0}{\sin(\alpha_4)}}{b_{\text{std}} + \frac{h_0}{\sin(\alpha_4)} \cdot \cos(\alpha_4)} \quad \text{if } \frac{t_{f_std}}{t_{w_std}} \geq 3.82 \\ 1 \quad \text{otherwise} \\ \frac{b_{\text{std}} + \frac{h_0}{\sin(\alpha_5)}}{b_{\text{std}} + \frac{h_0}{\sin(\alpha_5)} \cdot \cos(\alpha_5)} \quad \text{if } \frac{t_{f_std}}{t_{w_std}} \geq 3.82 \\ 1 \quad \text{otherwise} \end{array} \right) \quad \gamma_{\alpha h1} = \left(\begin{array}{l} 1.059 \\ 1.109 \\ 1.171 \\ 1.25 \\ 1.282 \\ 1.317 \end{array} \right)$$

$$\gamma_{\alpha h2} := \left(\begin{array}{l}
\frac{b_{\text{std}} + \frac{h_1}{\sin(\alpha_0)}}{b_{\text{std}} + \frac{h_1}{\sin(\alpha_0)} \cdot \cos(\alpha_0)} \quad \text{if } \frac{t_{f_std}}{t_{w_std}} \geq 3.82 \\
1 \quad \text{otherwise} \\
\frac{b_{\text{std}} + \frac{h_1}{\sin(\alpha_1)}}{b_{\text{std}} + \frac{h_1}{\sin(\alpha_1)} \cdot \cos(\alpha_1)} \quad \text{if } \frac{t_{f_std}}{t_{w_std}} \geq 3.82 \\
1 \quad \text{otherwise} \\
\frac{b_{\text{std}} + \frac{h_1}{\sin(\alpha_2)}}{b_{\text{std}} + \frac{h_1}{\sin(\alpha_2)} \cdot \cos(\alpha_2)} \quad \text{if } \frac{t_{f_std}}{t_{w_std}} \geq 3.82 \\
1 \quad \text{otherwise} \\
\frac{b_{\text{std}} + \frac{h_1}{\sin(\alpha_3)}}{b_{\text{std}} + \frac{h_1}{\sin(\alpha_3)} \cdot \cos(\alpha_3)} \quad \text{if } \frac{t_{f_std}}{t_{w_std}} \geq 3.82 \\
1 \quad \text{otherwise} \\
\frac{b_{\text{std}} + \frac{h_1}{\sin(\alpha_4)}}{b_{\text{std}} + \frac{h_1}{\sin(\alpha_4)} \cdot \cos(\alpha_4)} \quad \text{if } \frac{t_{f_std}}{t_{w_std}} \geq 3.82 \\
1 \quad \text{otherwise} \\
\frac{b_{\text{std}} + \frac{h_1}{\sin(\alpha_5)}}{b_{\text{std}} + \frac{h_1}{\sin(\alpha_5)} \cdot \cos(\alpha_5)} \quad \text{if } \frac{t_{f_std}}{t_{w_std}} \geq 3.82 \\
1 \quad \text{otherwise}
\end{array} \right) \quad \gamma_{\alpha h2} = \begin{pmatrix} 1.086 \\ 1.173 \\ 1.292 \\ 1.46 \\ 1.532 \\ 1.616 \end{pmatrix}$$

$$\gamma_{\alpha h3} := \left(\begin{array}{l}
\frac{b_{\text{std}} + \frac{h_2}{\sin(\alpha_0)}}{\frac{b_{\text{std}} + \frac{h_2}{\sin(\alpha_0)} \cdot \cos(\alpha_0)}{1}} \text{ if } \frac{t_{f_std}}{t_{w_std}} \geq 3.82 \\
1 \text{ otherwise} \\
\frac{b_{\text{std}} + \frac{h_2}{\sin(\alpha_1)}}{\frac{b_{\text{std}} + \frac{h_2}{\sin(\alpha_1)} \cdot \cos(\alpha_1)}{1}} \text{ if } \frac{t_{f_std}}{t_{w_std}} \geq 3.82 \\
1 \text{ otherwise} \\
\frac{b_{\text{std}} + \frac{h_2}{\sin(\alpha_2)}}{\frac{b_{\text{std}} + \frac{h_2}{\sin(\alpha_2)} \cdot \cos(\alpha_2)}{1}} \text{ if } \frac{t_{f_std}}{t_{w_std}} \geq 3.82 \\
1 \text{ otherwise} \\
\frac{b_{\text{std}} + \frac{h_2}{\sin(\alpha_3)}}{\frac{b_{\text{std}} + \frac{h_2}{\sin(\alpha_3)} \cdot \cos(\alpha_3)}{1}} \text{ if } \frac{t_{f_std}}{t_{w_std}} \geq 3.82 \\
1 \text{ otherwise} \\
\frac{b_{\text{std}} + \frac{h_2}{\sin(\alpha_4)}}{\frac{b_{\text{std}} + \frac{h_2}{\sin(\alpha_4)} \cdot \cos(\alpha_4)}{1}} \text{ if } \frac{t_{f_std}}{t_{w_std}} \geq 3.82 \\
1 \text{ otherwise} \\
\frac{b_{\text{std}} + \frac{h_2}{\sin(\alpha_5)}}{\frac{b_{\text{std}} + \frac{h_2}{\sin(\alpha_5)} \cdot \cos(\alpha_5)}{1}} \text{ if } \frac{t_{f_std}}{t_{w_std}} \geq 3.82 \\
1 \text{ otherwise}
\end{array} \right) \gamma_{\alpha h3} = \begin{pmatrix} 1.101 \\ 1.214 \\ 1.382 \\ 1.639 \\ 1.756 \\ 1.898 \end{pmatrix}$$

$$\gamma_c := 1 + \eta \cdot s_{s_std}$$

$$\gamma_c = 1.208$$

$$\gamma := \begin{pmatrix} 10.4 \cdot \gamma_{\alpha h1} \cdot \gamma_c \\ 10.4 \cdot \gamma_{\alpha h2} \cdot \gamma_c \\ 10.4 \cdot \gamma_{\alpha h3} \cdot \gamma_c \end{pmatrix}$$

$$\gamma = \begin{pmatrix} \{6,1\} \\ \{6,1\} \\ \{6,1\} \end{pmatrix}$$

$$P_{ult_1994} := (\gamma_0 \cdot t_{f_std} \cdot t_{w_std} \cdot f_{yw} \quad \gamma_1 \cdot t_{f_std} \cdot t_{w_std} \cdot f_{yw} \quad \gamma_2 \cdot t_{f_std} \cdot t_{w_std} \cdot f_{yw})$$

$$P_{ult_1994_{0,0}} = \begin{pmatrix} 113.398 \\ 118.739 \\ 125.371 \\ 133.847 \\ 137.253 \\ 141.046 \end{pmatrix} \cdot kP_{ult_1994_{0,1}} = \begin{pmatrix} 116.228 \\ 125.547 \\ 138.33 \\ 156.324 \\ 164.062 \\ 173.025 \end{pmatrix} \cdot lP_{ult_1994_{0,2}} = \begin{pmatrix} 117.831 \\ 130.007 \\ 147.987 \\ 175.458 \\ 188.03 \\ 203.177 \end{pmatrix} \cdot kN$$

A.4.5 Elgaaly and Seshadri (1997)

Type I Failure - Web Crippling

$$M_{pf} := \frac{b_{f_std} \cdot f_{yf} \cdot t_{f_std}^2}{4}$$

$$M_{pf} = 2.3 \text{ kN} \cdot \text{m}$$

$$a := \left(\frac{f_{yf} \cdot b_{f_std} \cdot t_{f_std}^2}{2 \cdot f_{yw} \cdot t_{w_std}} \right)^{0.5} + \frac{s_{s_std}}{4}$$

$$a = 0.093 \text{ m}$$

$$P_{fl} := \frac{4 \cdot M_{pf}}{a - \frac{s_{s_std}}{4}}$$

$$P_{fl} = 114.308 \cdot \text{kN}$$

$$P_w := (E \cdot f_{yw})^{0.5} \cdot t_{w_std}^2$$

$$P_w = 34.537 \cdot \text{kN}$$

$$P_{T1ult_1997} := P_w + P_{fl}$$

$$P_{T1ult_1997} = 148.845 \cdot \text{kN}$$

A.5 Varying web depth, h_w

$$h_w := \begin{pmatrix} 500\text{mm} \\ 1000\text{mm} \\ 1500\text{mm} \\ 2000\text{mm} \end{pmatrix}$$

A.5.1 Arne Johnson Ingenjörbyrå AB, Carling (1974)

The design model by Arne Johnson Ingenjörbyrå AB is not affected by this parameter.

A.5.2 Rana (1982)

The design model by Rana is not affected by this parameter.

A.5.3 Dahlén and Krona (1984)

$$t_i := t_{f_std} \cdot \sqrt[4]{\frac{b_{f_std}}{25 \cdot t_{f_std}}} \quad t_i = 0.011 \text{ m}$$

$$f_{c} := 1 + 40 \cdot \frac{s_{s_std}}{a_{yield}} \cdot \frac{t_{w_std}}{h_w} \quad f_c = \begin{pmatrix} 1.041 \\ 1.021 \\ 1.014 \\ 1.01 \end{pmatrix}$$

$$f_{al} := 2 \cdot \frac{a_{yield}}{b_{std}} \cdot \frac{\sqrt{1 + \sqrt{1 + mk \cdot \left(\frac{b_{std}}{2 \cdot a_{yield}}\right)^4}}}{1 + \sqrt{1 + mk}} \quad f_{al} = 1.964$$

$$P_{1984_hw} := 0.8 \cdot \sqrt{\frac{t_i}{t_{w_std}}} \cdot t_{w_std}^2 \cdot \sqrt{f_{yw} \cdot E} \cdot f_c \cdot f_{al} \quad P_{1984_hw} = \begin{pmatrix} 129.814 \\ 127.244 \\ 126.387 \\ 125.959 \end{pmatrix} \cdot \text{kN}$$

A.5.4 Lou and Edlund (1994)

The design model by Lou and Edlund is not affected by this parameter.

A.5.5 Elgaaly and Seshadri (1997)

The design model by Elgaaly and Seshadri is not affected by this parameter.

A.6 Varying flange thickness, t_f

$$t_f := \begin{pmatrix} 5\text{mm} \\ 10\text{mm} \\ 15\text{mm} \\ 20\text{mm} \end{pmatrix}$$

A.6.1 Arne Johnson Ingenjörbyrå AB, Carling (1974)

The design model by Arne Johnson Ingenjörbyrå AB is not affected by this parameter.

A.6.2 Rana (1982)

$$P_{1982_tf} := 0.75 \cdot f_{yw} \cdot t_{w_std} \cdot (2t_f + s_{s_std}) \quad P_{1982_tf} = \begin{pmatrix} 31.95 \\ 37.275 \\ 42.6 \\ 47.925 \end{pmatrix} \cdot \text{kN}$$

A.6.3 Dahlén and Krona (1984)

$$t_{w_std} := \begin{pmatrix} t_{f_0} \cdot \sqrt[4]{\frac{b_{f_std}}{25 \cdot t_{f_0}}} \\ t_{f_1} \cdot \sqrt[4]{\frac{b_{f_std}}{25 \cdot t_{f_1}}} \\ t_{f_2} \cdot \sqrt[4]{\frac{b_{f_std}}{25 \cdot t_{f_2}}} \\ t_{f_3} \cdot \sqrt[4]{\frac{b_{f_std}}{25 \cdot t_{f_3}}} \end{pmatrix} \quad t_i = \begin{pmatrix} 5.477 \times 10^{-3} \\ 9.212 \times 10^{-3} \\ 0.012 \\ 0.015 \end{pmatrix} \text{m}$$

$$f_{cov} := 1 + 40 \cdot \frac{s_{s_std}}{a_{yield}} \cdot \frac{t_{w_std}}{h_{w_std}} \quad f_c = 1.034$$

$$f_{alv} := 2 \cdot \frac{a_{yield}}{b_{std}} \cdot \sqrt{\frac{1 + \sqrt{1 + mk \cdot \left(\frac{b_{std}}{2 \cdot a_{yield}}\right)^4}}{1 + \sqrt{1 + mk}}} \quad f_{al} = 1.964$$

$$P_{1984_tf} := 0.8 \cdot \sqrt{\frac{t_i}{t_{w_std}}} \cdot t_{w_std}^2 \cdot \sqrt{f_{yw} \cdot E \cdot f_c \cdot f_{al}} \quad P_{1984_tf} = \begin{pmatrix} 92.868 \\ 120.435 \\ 140.213 \\ 156.185 \end{pmatrix} \cdot \text{kN}$$

A.6.4 Lou and Edlund (1994)

$$\gamma_{\alpha} := \begin{pmatrix} \left| \begin{array}{l} \frac{b_{std} + a_{std}}{b_{std} + a_{std} \cdot \cos(\alpha_{std})} \text{ if } \frac{t_{f_0}}{t_{w_std}} \geq 3.82 \\ 1 \text{ otherwise} \\ \frac{b_{std} + a_{std}}{b_{std} + a_{std} \cdot \cos(\alpha_{std})} \text{ if } \frac{t_{f_1}}{t_{w_std}} \geq 3.82 \\ 1 \text{ otherwise} \\ \frac{b_{std} + a_{std}}{b_{std} + a_{std} \cdot \cos(\alpha_{std})} \text{ if } \frac{t_{f_2}}{t_{w_std}} \geq 3.82 \\ 1 \text{ otherwise} \\ \frac{b_{std} + a_{std}}{b_{std} + a_{std} \cdot \cos(\alpha_{std})} \text{ if } \frac{t_{f_3}}{t_{w_std}} \geq 3.82 \\ 1 \text{ otherwise} \end{array} \right. \right. \end{pmatrix} \quad \gamma_{\alpha} = \begin{pmatrix} 1 \\ 1.173 \\ 1.173 \\ 1.173 \end{pmatrix}$$

$$\gamma_{\alpha} := 1 + \eta \cdot s_{s_std}$$

$$\gamma_c = 1.208$$

$$\gamma_{\alpha} := 10.4 \cdot \gamma_{\alpha} \cdot \gamma_c$$

$$\gamma = \begin{pmatrix} 12.567 \\ 14.736 \\ 14.736 \\ 14.736 \end{pmatrix}$$

$$P_{1994_tf} := \begin{pmatrix} \gamma_0 \cdot t_{f_0} \cdot t_{w_std} \cdot f_{yw} \\ \gamma_1 \cdot t_{f_1} \cdot t_{w_std} \cdot f_{yw} \\ \gamma_2 \cdot t_{f_2} \cdot t_{w_std} \cdot f_{yw} \\ \gamma_3 \cdot t_{f_3} \cdot t_{w_std} \cdot f_{yw} \end{pmatrix} \quad P_{1994_tf} = \begin{pmatrix} 44.612 \\ 104.622 \\ 156.933 \\ 209.245 \end{pmatrix} \cdot \text{kN}$$

A.6.5 Elgaaly and Seshadri (1997)

Type I Failure - Web Crippling

$$M_{pf} := \frac{b_{f_std} \cdot f_{yf} \cdot t_f^2}{4}$$

$$M_{pf} = \begin{pmatrix} 0.399 \\ 1.597 \\ 3.594 \\ 6.39 \end{pmatrix} \text{ kN} \cdot \text{m}$$

$$a := \left(\frac{f_{yf} \cdot b_{f_std} \cdot t_{f_std}^2}{2 \cdot f_{yw} \cdot t_{w_std}} \right)^{0.5} + \frac{s_{s_std}}{4}$$

$$a = \begin{pmatrix} 0.046 \\ 0.08 \\ 0.113 \\ 0.147 \end{pmatrix} \text{ m}$$

$$P_{fl} := \frac{4 \cdot M_{pf}}{a - \frac{s_{s_std}}{4}}$$

$$P_{fl} = \begin{pmatrix} 47.628 \\ 95.256 \\ 142.885 \\ 190.513 \end{pmatrix} \cdot \text{kN}$$

$$P_w := (E \cdot f_{yw})^{0.5} \cdot t_{w_std}^2$$

$$P_w = 34.537 \cdot \text{kN}$$

$$P_{1997_tf} := P_w + P_{fl}$$

$$P_{1997_tf} = \begin{pmatrix} 82.165 \\ 129.793 \\ 177.422 \\ 225.05 \end{pmatrix} \cdot \text{kN}$$

A.7 Varying flange width, b_f

$$b_f := \begin{pmatrix} 100\text{mm} \\ 125\text{mm} \\ 150\text{mm} \\ 175\text{mm} \\ 200\text{mm} \end{pmatrix}$$

A.7.1 Arne Johnson Ingenjörbyrå AB, Carling (1974)

The design model by Arne Johnson Ingenjörbyrå AB is not affected by this parameter.

A.7.2 Rana (1982)

The design model by Rana is not affected by this parameter.

A.7.3 Dahlén och Krona (1984)

$$f_{w, \text{std}} := t_{f_std} \cdot \sqrt[4]{\frac{b_f}{25 \cdot t_{f_std}}} \quad t_i = \begin{pmatrix} 9.118 \times 10^{-3} \\ 9.641 \times 10^{-3} \\ 0.01 \\ 0.01 \\ 0.011 \end{pmatrix} \text{m}$$

$$f_{c, \text{std}} := 1 + 40 \cdot \frac{s_{s_std} \cdot t_{w_std}}{a_{\text{yield}} \cdot h_{w_std}} \quad f_c = 1.034$$

$$f_{al, \text{std}} := 2 \cdot \frac{a_{\text{yield}}}{b_{\text{std}}} \cdot \frac{\sqrt{1 + \sqrt{1 + mk \cdot \left(\frac{b_{\text{std}}}{2 \cdot a_{\text{yield}}}\right)^4}}}{1 + \sqrt{1 + mk}} = 1.281 \quad f_{al} = 1.964$$

$$P_{1984_bf} := 0.8 \cdot \sqrt{\frac{t_i}{t_{w_std}}} \cdot t_{w_std}^2 \cdot \sqrt{f_{yw} \cdot E} \cdot f_c \cdot f_{al} \quad P_{1984_bf} = \begin{pmatrix} 119.822 \\ 123.212 \\ 126.052 \\ 128.504 \\ 130.667 \end{pmatrix} \cdot \text{kN}$$

A.7.4 Lou and Edlund (1994)

The design model by Lou and Edlund is not affected by this parameter.

A.7.5 Elgaaly and Seshadri (1997)

Type I Failure - Web Crippling

$$M_{pf} := \frac{b_{f_std} \cdot f_{yf} \cdot t_{f_std}^2}{4}$$

$$M_{pf} = \begin{pmatrix} 1.278 \\ 1.597 \\ 1.917 \\ 2.237 \\ 2.556 \end{pmatrix} \text{ kN} \cdot \text{m}$$

$$a := \left(\frac{f_{yf} \cdot b_f \cdot t_{f_std}^2}{2 \cdot f_{yw} \cdot t_{w_std}} \right)^{0.5} + \frac{s_{s_std}}{4}$$

$$a = \begin{pmatrix} 0.073 \\ 0.08 \\ 0.086 \\ 0.092 \\ 0.097 \end{pmatrix} \text{ m}$$

$$P_{fl} := \frac{4 \cdot M_{pf}}{a - \frac{s_{s_std}}{4}}$$

$$P_{fl} = \begin{pmatrix} 85.2 \\ 95.256 \\ 104.348 \\ 112.709 \\ 120.491 \end{pmatrix} \cdot \text{kN}$$

$$P_{ww} := (E \cdot f_{yw})^{0.5} \cdot t_{w_std}^2$$

$$P_w = 34.537 \cdot \text{kN}$$

$$P_{1997_bf} := P_w + P_{fl}$$

$$P_{1997_bf} = \begin{pmatrix} 119.737 \\ 129.793 \\ 138.885 \\ 147.246 \\ 155.028 \end{pmatrix} \cdot \text{kN}$$

A.8 Varying length of the longitudinal fold, b

$$b := \begin{pmatrix} 25\text{mm} \\ 50\text{mm} \\ 75\text{mm} \\ 100\text{mm} \\ 125\text{mm} \\ 150\text{mm} \end{pmatrix}$$

A.8.1 Arne Johnson Ingenjörbyrå AB, Carling (1974)

The design model by Arne Johnson Ingenjörbyrå AB is not affected by this parameter.

A.8.2 Rana (1982)

The design model by Rana is not affected by this parameter.

A.8.3 Dahlén and Krona (1984)

$$a_{\text{yield}} := b + 2 \cdot d_{\text{std}} + 2t_{\text{f_std}} \quad a_{\text{yield}} = \begin{pmatrix} 0.149 \\ 0.174 \\ 0.199 \\ 0.224 \\ 0.249 \\ 0.274 \end{pmatrix} \text{ m}$$

$$t_{\text{w}} := t_{\text{f_std}} \cdot \sqrt[4]{\frac{b_{\text{f_std}}}{25 \cdot t_{\text{f_std}}}} \quad t_{\text{f}} = 0.011 \text{ m}$$

$$f_{\text{cv}} := 1 + 40 \cdot \frac{s_{\text{s_std}}}{a_{\text{yield}}} \cdot \frac{t_{\text{w_std}}}{h_{\text{w_std}}} \quad f_{\text{c}} = \begin{pmatrix} 1.045 \\ 1.038 \\ 1.034 \\ 1.03 \\ 1.027 \\ 1.024 \end{pmatrix}$$

$$f_{al} := \left[\begin{array}{l} 2 \cdot \frac{a_{yield_0}}{b_0} \cdot \frac{1 + \sqrt{1 + mk \cdot \left(\frac{b_0}{2 \cdot a_{yield_0}} \right)^4}}{1 + \sqrt{1 + mk}} \\ 2 \cdot \frac{a_{yield_1}}{b_1} \cdot \frac{1 + \sqrt{1 + mk \cdot \left(\frac{b_1}{2 \cdot a_{yield_1}} \right)^4}}{1 + \sqrt{1 + mk}} \\ 2 \cdot \frac{a_{yield_2}}{b_2} \cdot \frac{1 + \sqrt{1 + mk \cdot \left(\frac{b_2}{2 \cdot a_{yield_2}} \right)^4}}{1 + \sqrt{1 + mk}} \\ 2 \cdot \frac{a_{yield_3}}{b_3} \cdot \frac{1 + \sqrt{1 + mk \cdot \left(\frac{b_3}{2 \cdot a_{yield_3}} \right)^4}}{1 + \sqrt{1 + mk}} \\ 2 \cdot \frac{a_{yield_4}}{b_4} \cdot \frac{1 + \sqrt{1 + mk \cdot \left(\frac{b_4}{2 \cdot a_{yield_4}} \right)^4}}{1 + \sqrt{1 + mk}} \\ 2 \cdot \frac{a_{yield_5}}{b_5} \cdot \frac{1 + \sqrt{1 + mk \cdot \left(\frac{b_5}{2 \cdot a_{yield_5}} \right)^4}}{1 + \sqrt{1 + mk}} \end{array} \right] \quad f_{al} = \begin{pmatrix} 4.102 \\ 2.423 \\ 1.89 \\ 1.642 \\ 1.504 \\ 1.419 \end{pmatrix}$$

$$P_{1984_b} := \begin{bmatrix} 0.8 \cdot \sqrt{\frac{t_i}{t_{w_std}}} \cdot (t_{w_std})^2 \cdot \sqrt{f_{yw} \cdot E} \cdot f_{c_0} \cdot f_{al_0} \\ 0.8 \cdot \sqrt{\frac{t_i}{t_{w_std}}} \cdot (t_{w_std})^2 \cdot \sqrt{f_{yw} \cdot E} \cdot f_{c_1} \cdot f_{al_1} \\ 0.8 \cdot \sqrt{\frac{t_i}{t_{w_std}}} \cdot (t_{w_std})^2 \cdot \sqrt{f_{yw} \cdot E} \cdot f_{c_2} \cdot f_{al_2} \\ 0.8 \cdot \sqrt{\frac{t_i}{t_{w_std}}} \cdot (t_{w_std})^2 \cdot \sqrt{f_{yw} \cdot E} \cdot f_{c_3} \cdot f_{al_3} \\ 0.8 \cdot \sqrt{\frac{t_i}{t_{w_std}}} \cdot (t_{w_std})^2 \cdot \sqrt{f_{yw} \cdot E} \cdot f_{c_4} \cdot f_{al_4} \\ 0.8 \cdot \sqrt{\frac{t_i}{t_{w_std}}} \cdot (t_{w_std})^2 \cdot \sqrt{f_{yw} \cdot E} \cdot f_{c_5} \cdot f_{al_5} \end{bmatrix}$$

$$P_{1984_b} = \begin{pmatrix} 272.097 \\ 159.709 \\ 124.008 \\ 107.363 \\ 98.079 \\ 92.289 \end{pmatrix} \text{ kN}$$

A.8.4 Lou and Edlund (1994)

$$\gamma_{\alpha} := \left(\begin{array}{l} \frac{b_0 + a_{std}}{b_0 + a_{std} \cdot \cos(\alpha_{std})} \text{ if } \frac{t_{f_std}}{t_{w_std}} \geq 3.82 \\ 1 \text{ otherwise} \\ \frac{b_1 + a_{std}}{b_1 + a_{std} \cdot \cos(\alpha_{std})} \text{ if } \frac{t_{f_std}}{t_{w_std}} \geq 3.82 \\ 1 \text{ otherwise} \\ \frac{b_2 + a_{std}}{b_2 + a_{std} \cdot \cos(\alpha_{std})} \text{ if } \frac{t_{f_std}}{t_{w_std}} \geq 3.82 \\ 1 \text{ otherwise} \\ \frac{b_3 + a_{std}}{b_3 + a_{std} \cdot \cos(\alpha_{std})} \text{ if } \frac{t_{f_std}}{t_{w_std}} \geq 3.82 \\ 1 \text{ otherwise} \\ \frac{b_4 + a_{std}}{b_4 + a_{std} \cdot \cos(\alpha_{std})} \text{ if } \frac{t_{f_std}}{t_{w_std}} \geq 3.82 \\ 1 \text{ otherwise} \\ \frac{b_5 + a_{std}}{b_5 + a_{std} \cdot \cos(\alpha_{std})} \text{ if } \frac{t_{f_std}}{t_{w_std}} \geq 3.82 \\ 1 \text{ otherwise} \end{array} \right) \quad \gamma_{\alpha} = \left(\begin{array}{l} 1.276 \\ 1.207 \\ 1.166 \\ 1.138 \\ 1.118 \\ 1.104 \end{array} \right)$$

$$\gamma_{wv} := 1 + \eta \cdot s_{s_std}$$

$$\gamma_c = 1.208$$

$$\gamma_{ww} := 10.4 \cdot \gamma_{\alpha} \cdot \gamma_c$$

$$\gamma = \left(\begin{array}{l} 16.037 \\ 15.169 \\ 14.649 \\ 14.302 \\ 14.054 \\ 13.868 \end{array} \right)$$

$$P_{1994_tw} := \gamma \cdot t_{f_std} \cdot t_{w_std} \cdot f_{yw}$$

$$P_{1994_tw} = \begin{pmatrix} 136.634 \\ 129.243 \\ 124.808 \\ 121.851 \\ 119.739 \\ 118.155 \end{pmatrix} \cdot \text{kN}$$

A.8.5 Elgaaly and Seshadri (1997)

The design model by Elgaaly and Seshadri is not affected by this parameter.

A.9 Varying loading length, s_s

$$s_s := \begin{pmatrix} 0\text{mm} \\ 25\text{mm} \\ 50\text{mm} \\ 75\text{mm} \\ 100\text{mm} \end{pmatrix}$$

A.9.1 Arne Johnson Ingenjörbyrå AB, Carling (1974)

The design model by Arne Johnson Ingenjörbyrå AB is not affected by this parameter.

A.9.2 Rana (1982)

$$P_{1982_ss} := 0.75 \cdot f_{yw} \cdot t_{w_std} \cdot (2t_{f_std} + s_s) \quad P_{1982_ss} = \begin{pmatrix} 12.78 \\ 26.093 \\ 39.405 \\ 52.718 \\ 66.03 \end{pmatrix} \cdot \text{kN}$$

A.9.3 Dahlén and Krona (1984)

$$t_{w_std} := t_{f_std} \cdot \sqrt[4]{\frac{b_f}{25 \cdot t_{f_std}}} \quad t_i = 0.011 \text{ m}$$

$$f_{ev} := 1 + 40 \cdot \frac{s_s}{a_{yield}} \cdot \frac{t_{w_std}}{h_{w_std}} \quad f_c = \begin{pmatrix} 1 \\ 1.016 \\ 1.031 \\ 1.047 \\ 1.062 \end{pmatrix}$$

$$f_{alv} := 2 \cdot \frac{a_{yield}}{b_{std}} \cdot \frac{1 + \sqrt{1 + mk \cdot \left(\frac{b_{std}}{2 \cdot a_{yield}}\right)^4}}{1 + \sqrt{1 + mk}} \quad f_{al} = 1.964$$

$$P_{1984_Ss} := 0.8 \cdot \sqrt{\frac{t_i}{t_{w_std}}} \cdot t_{w_std}^2 \cdot \sqrt{f_{yw} \cdot E} \cdot f_c \cdot f_{al} \quad P_{1984_Ss} = \begin{pmatrix} 124.673 \\ 126.815 \\ 128.958 \\ 131.1 \\ 133.242 \end{pmatrix} \cdot \text{kN}$$

A.9.4 Lou and Edlund (1994)

$$\gamma_{\alpha} := \begin{cases} \frac{b_{std} + a_{std}}{b_{std} + a_{std} \cdot \cos(\alpha_{std})} & \text{if } \frac{t_{f_std}}{t_{w_std}} \geq 3.82 \\ 1 & \text{otherwise} \end{cases} \quad \gamma_{\alpha} = 1.173$$

$$\gamma_{\alpha} := 1 + \eta \cdot s_s \quad \gamma_c = \begin{pmatrix} 1 \\ 1.104 \\ 1.208 \\ 1.313 \\ 1.417 \end{pmatrix}$$

$$\gamma := 10.4 \cdot \gamma_{\alpha} \cdot \gamma_c \quad \gamma = \begin{pmatrix} 12.195 \\ 13.465 \\ 14.736 \\ 16.006 \\ 17.276 \end{pmatrix}$$

$$P_{1994_Ss} := \gamma \cdot t_{f_std} \cdot t_{w_std} \cdot f_{yw} \quad P_{1994_Ss} = \begin{pmatrix} 103.901 \\ 114.724 \\ 125.547 \\ 136.37 \\ 147.193 \end{pmatrix} \cdot \text{kN}$$

A.9.5 Elgaaly and Seshadri (1997)

Type I Failure - Web Crippling

$$M_{pf} := \frac{b_{f_std} \cdot f_{yf} \cdot t_{f_std}^2}{4} \quad M_{pf} = 2.3 \text{ kN} \cdot \text{m}$$

$$a_{ww} := \left(\frac{f_{yf} \cdot b_{f_std} \cdot t_{f_std}^2}{2 \cdot f_{yw} \cdot t_{w_std}} \right)^{0.5} + \frac{s_s}{4}$$

$$a = \begin{pmatrix} 0.08 \\ 0.087 \\ 0.093 \\ 0.099 \\ 0.105 \end{pmatrix} \text{ m}$$

$$P_{fl} := \frac{4 \cdot M_{pf}}{a - \frac{s_s}{4}}$$

$$P_{fl} = \begin{pmatrix} 114.308 \\ 114.308 \\ 114.308 \\ 114.308 \\ 114.308 \end{pmatrix} \cdot \text{kN}$$

$$P_{ww} := (E \cdot f_{yw})^{0.5} \cdot t_{w_std}^2$$

$$P_w = 34.537 \cdot \text{kN}$$

$$P_{1997_Ss} := P_w + P_{fl}$$

$$P_{1997_Ss} = 148.845 \cdot \text{kN}$$

A.10 Varying load position

A.10.1 Arne Johnson Ingenjörbyrå AB, Carling (1974)

The design model by Arne Johnson Ingenjörbyrå AB is not affected by this parameter.

A.10.2 Rana (1982)

The design model by Rana is not affected by this parameter.

A.10.3 Dahlén and Krona (1984)

A.10.3.1 Load applied over inclined fold

$$a_{\text{yield}} := 2b_{\text{std}} + d_{\text{std}} + 2t_{f_std} \quad a_{\text{yield}} = 214\text{mm}$$

$$t_i := t_{f_std} \cdot \sqrt[4]{\frac{b_{f_std}}{25 \cdot t_{f_std}}} \quad t_i = 0.011\text{m}$$

$$f_{\text{max}} := 1 + 40 \cdot \frac{s_{s_std}}{a_{\text{yield}}} \cdot \frac{t_{w_std}}{h_{w_std}} \quad f_c = 1.031$$

$$f_{\text{al}} := 2 \cdot \frac{a_{\text{yield}}}{b_{\text{std}}} \cdot \sqrt{\frac{1 + \sqrt{1 + mk \left(\frac{b_{\text{std}}}{2 \cdot a_{\text{yield}}} \right)^4}}{1 + \sqrt{1 + mk}}} \quad f_{\text{al}} = 2.146$$

$$P_{1984_inc} := 0.8 \cdot \sqrt{\frac{t_i}{t_{w_std}}} \cdot (f_{yw} \cdot E)^{0.5} \cdot t_{w_std}^2 \cdot f_c \cdot f_{\text{al}} \quad P_{1984_inc} = 140.492\text{kN}$$

A.10.3.2 Load applied over junction between folds

$$a_{\text{yield}} := b_{\text{std}} + d_{\text{std}} + 2t_{f_std} \quad a_{\text{yield}} = 144\text{mm}$$

$$t_i := t_{f_std} \cdot \sqrt[4]{\frac{b_{f_std}}{25 \cdot t_{f_std}}} \quad t_i = 0.011\text{m}$$

$$f_{\text{max}} := 1 + 40 \cdot \frac{s_{s_std}}{a_{\text{yield}}} \cdot \frac{t_{w_std}}{h_{w_std}} \quad f_c = 1.046$$

$$f_{\text{al}} := 2 \cdot \frac{a_{\text{yield}}}{b_{\text{std}}} \cdot \sqrt{\frac{1 + \sqrt{1 + mk \left(\frac{b_{\text{std}}}{2 \cdot a_{\text{yield}}} \right)^4}}{1 + \sqrt{1 + mk}}} \quad f_{\text{al}} = 1.54$$

$$P_{1984_junc} := 0.8 \cdot \sqrt{\frac{t_i}{t_{w_std}}} \cdot (f_{yw} \cdot E)^{0.5} \cdot t_{w_std}^2 \cdot f_c \cdot f_{al} \quad P_{1984_junc} = 102.279 \text{ kN}$$

A.10.3.3 Load applied over longitudinal fold

$$a_{yield} := b_{std} + 2d_{std} + 2t_{f_std} \quad a_{yield} = 194 \text{ mm}$$

$$t_i := t_{f_std} \cdot \sqrt[4]{\frac{b_{f_std}}{25 \cdot t_{f_std}}} \quad t_i = 0.011 \text{ m}$$

$$f_c := 1 + 40 \cdot \frac{s_{s_std}}{a_{yield}} \cdot \frac{t_{w_std}}{h_{w_std}} \quad f_c = 1.034$$

$$f_{al} := 2 \cdot \frac{a_{yield}}{b_{std}} \cdot \frac{1 + \sqrt{1 + mk \left(\frac{b_{std}}{2 \cdot a_{yield}} \right)^4}}{1 + \sqrt{1 + mk}} \quad f_{al} = 1.964$$

$$P_{1984_long} := 0.8 \cdot \sqrt{\frac{t_i}{t_{w_std}}} \cdot (f_{yw} \cdot E)^{0.5} \cdot t_{w_std}^2 \cdot f_c \cdot f_{al} \quad P_{1984_long} = 128.958 \text{ kN}$$

A.10.4 Lou and Edlund (1994)

The design model by Lou and Edlund is not affected by this parameter.

A.10.5 Elgaaly and Seshadri (1997)

Type I Failure - Web Crippling

$$M_{pf} := \frac{b_{f_std} \cdot f_{yf} \cdot t_{f_std}^2}{4} \quad M_{pf} = 2.3 \text{ kN} \cdot \text{m}$$

$$a := \left(\frac{f_{yf} \cdot b_{f_std} \cdot t_{f_std}^2}{2 \cdot f_{yw} \cdot t_{w_std}} \right)^{0.5} + \frac{s_s}{4} \quad a = 0.093 \text{ m}$$

$$P_{fl} := \frac{4 \cdot M_{pf}}{a - \frac{s_s}{4}} \quad P_{fl} = 114.308 \text{ kN}$$

$$P_{www} := (E \cdot f_{yw})^{0.5} \cdot t_{w_std}^2$$

$$P_w = 34.537 \cdot \text{kN}$$

$$P_{1997_wc} := P_w + P_{fl}$$

$$P_{1997_wc} = 148.845 \text{ kN}$$

Type II Failure - Web yielding

$$b := \left(\frac{a_{std}}{\frac{b_{std} + d_{std}}{2}} \right)$$

$$b = \begin{pmatrix} 0.071 \\ 0.06 \end{pmatrix} \text{ m}$$

$$\beta_{II} := \frac{h_{std}}{b_{f_std}}$$

$$\beta_{II} = 0.278$$

$$\alpha_I := 14 + 3.5 \beta_{II} - 37 \beta_{II}^2$$

$$\alpha_I = 12.117$$

$$\alpha_{II} := \begin{cases} \alpha_I & \text{if } \alpha_I \geq 5.5 \\ 5.5 & \text{otherwise} \end{cases} = 12.117$$

$$\alpha_{II} = 12.117$$

$$b_a := \alpha_{II} t_{f_std} \cdot \left(\frac{f_{yf}}{f_{yw}} \right)^{0.5}$$

$$b_a = 0.145 \text{ m}$$

$$P_{1997_wy} := (b + b_a) \cdot t_{w_std} \cdot f_{yw}$$

$$P_{1997_wy} = \begin{pmatrix} 153.444 \\ 145.839 \end{pmatrix} \cdot \text{kN}$$

A.10.5.1 Load applied over inclined fold

$$P_{1997_wy_1} = 145.839 \text{ kN}$$

A.10.5.2 Load applied over junction between folds

$$P_{1997_wy_1} = 145.839 \text{ kN}$$

A.10.5.3 Load applied over longitudinal fold

$$P_{1997_wc} = 148.845 \text{ kN}$$

A.11 Calculation for a girder with a flat web subjected to patch loading

The girder with a flat web has the same standard parameters as a the girder with a corrugated web. The calculations of the ultimate load are made according to EN 1993-1-5 (2006).

A.11.1 Ultimate load with varying web thicknesses

$$t_w := \begin{pmatrix} 2\text{mm} \\ 3\text{mm} \\ 4\text{mm} \\ 5\text{mm} \\ 6\text{mm} \end{pmatrix}$$

$$a_{\text{stiffeners}} := 3000\text{mm}$$

$$\gamma_{M1} := 1.0$$

$$\kappa_F := 6 + 2 \cdot \frac{h_w}{a_{\text{stiffeners}}}$$

$$\kappa_F = 6.4$$

$$F_{\text{cr}} := \begin{bmatrix} 0.9 \kappa_F \cdot E \cdot \frac{(t_{w0})^3}{h_w} \\ 0.9 \kappa_F \cdot E \cdot \frac{(t_{w1})^3}{h_w} \\ 0.9 \kappa_F \cdot E \cdot \frac{(t_{w2})^3}{h_w} \\ 0.9 \kappa_F \cdot E \cdot \frac{(t_{w3})^3}{h_w} \\ 0.9 \kappa_F \cdot E \cdot \frac{(t_{w4})^3}{h_w} \end{bmatrix}$$

$$F_{\text{cr}} = \begin{pmatrix} 16.128 \\ 54.432 \\ 129.024 \\ 252 \\ 435.456 \end{pmatrix} \cdot \text{kN}$$

$$\lambda_F := 0.6$$

$$m_1 := \begin{pmatrix} \frac{f_{yf} \cdot b_f}{f_{yw} \cdot t_{w0}} \\ \frac{f_{yf} \cdot b_f}{f_{yw} \cdot t_{w1}} \\ \frac{f_{yf} \cdot b_f}{f_{yw} \cdot t_{w2}} \\ \frac{f_{yf} \cdot b_f}{f_{yw} \cdot t_{w3}} \\ \frac{f_{yf} \cdot b_f}{f_{yw} \cdot t_{w4}} \end{pmatrix} \quad m_1 = \begin{pmatrix} 90 \\ 60 \\ 45 \\ 36 \\ 30 \end{pmatrix}$$

$$m_2 := \begin{cases} 0.02 \left(\frac{h_w}{t_f} \right)^2 & \text{if } \lambda_F > 0.5 \\ 0 & \text{otherwise} \end{cases} \quad m_2 = 50$$

$$l_y := \begin{pmatrix} \begin{cases} s_s + 2 \cdot t_f \cdot \left(1 + \sqrt{m_{10} + m_2} \right) & \text{if } a_{\text{stiffeners}} \geq s_s + 2 \cdot t_f \cdot \left(1 + \sqrt{m_{10} + m_2} \right) \\ a_{\text{stiffeners}} & \text{otherwise} \end{cases} \\ \begin{cases} s_s + 2 \cdot t_f \cdot \left(1 + \sqrt{m_{11} + m_2} \right) & \text{if } a_{\text{stiffeners}} \geq s_s + 2 \cdot t_f \cdot \left(1 + \sqrt{m_{11} + m_2} \right) \\ a_{\text{stiffeners}} & \text{otherwise} \end{cases} \\ \begin{cases} s_s + 2 \cdot t_f \cdot \left(1 + \sqrt{m_{12} + m_2} \right) & \text{if } a_{\text{stiffeners}} \geq s_s + 2 \cdot t_f \cdot \left(1 + \sqrt{m_{12} + m_2} \right) \\ a_{\text{stiffeners}} & \text{otherwise} \end{cases} \\ \begin{cases} s_s + 2 \cdot t_f \cdot \left(1 + \sqrt{m_{13} + m_2} \right) & \text{if } a_{\text{stiffeners}} \geq s_s + 2 \cdot t_f \cdot \left(1 + \sqrt{m_{13} + m_2} \right) \\ a_{\text{stiffeners}} & \text{otherwise} \end{cases} \\ \begin{cases} s_s + 2 \cdot t_f \cdot \left(1 + \sqrt{m_{14} + m_2} \right) & \text{if } a_{\text{stiffeners}} \geq s_s + 2 \cdot t_f \cdot \left(1 + \sqrt{m_{14} + m_2} \right) \\ a_{\text{stiffeners}} & \text{otherwise} \end{cases} \end{pmatrix} \quad l_y = \begin{pmatrix} 0.358 \\ 0.326 \\ 0.308 \\ 0.297 \\ 0.289 \end{pmatrix} \text{ m}$$

$$\lambda_{F_i} := \left(\begin{array}{c} \frac{l_{y_0} \cdot t_{w_0} \cdot f_{yw}}{F_{cr_0}} \\ \frac{l_{y_1} \cdot t_{w_1} \cdot f_{yw}}{F_{cr_1}} \\ \frac{l_{y_2} \cdot t_{w_2} \cdot f_{yw}}{F_{cr_2}} \\ \frac{l_{y_3} \cdot t_{w_3} \cdot f_{yw}}{F_{cr_3}} \\ \frac{l_{y_4} \cdot t_{w_4} \cdot f_{yw}}{F_{cr_4}} \end{array} \right) \quad \lambda_F = \left(\begin{array}{c} 15.759 \\ 6.373 \\ 3.389 \\ 2.089 \\ 1.412 \end{array} \right)$$

$$m_2 := \left[\begin{array}{l} \left| \begin{array}{l} 0.02 \left(\frac{h_w}{t_f} \right)^2 \text{ if } \lambda_{F_0} > 0.5 \\ 0 \text{ otherwise} \end{array} \right. \\ \left| \begin{array}{l} 0.02 \left(\frac{h_w}{t_f} \right)^2 \text{ if } \lambda_{F_1} > 0.5 \\ 0 \text{ otherwise} \end{array} \right. \\ \left| \begin{array}{l} 0.02 \left(\frac{h_w}{t_f} \right)^2 \text{ if } \lambda_{F_2} > 0.5 \\ 0 \text{ otherwise} \end{array} \right. \\ \left| \begin{array}{l} 0.02 \left(\frac{h_w}{t_f} \right)^2 \text{ if } \lambda_{F_3} > 0.5 \\ 0 \text{ otherwise} \end{array} \right. \\ \left| \begin{array}{l} 0.02 \left(\frac{h_w}{t_f} \right)^2 \text{ if } \lambda_{F_4} > 0.5 \\ 0 \text{ otherwise} \end{array} \right. \end{array} \right] \quad m_2 = \left(\begin{array}{c} 50 \\ 50 \\ 50 \\ 50 \\ 50 \end{array} \right)$$

$$l_y := \left[\begin{array}{l} \left| \begin{array}{l} s_s + 2 \cdot t_f \cdot \left(1 + \sqrt{m_{1_0} + m_{2_0}} \right) \text{ if } a_{\text{stiffeners}} \geq s_s + 2 \cdot t_f \cdot \left(1 + \sqrt{m_{1_0} + m_{2_0}} \right) \\ a_{\text{stiffeners}} \text{ otherwise} \end{array} \right. \\ \left| \begin{array}{l} s_s + 2 \cdot t_f \cdot \left(1 + \sqrt{m_{1_1} + m_{2_1}} \right) \text{ if } a_{\text{stiffeners}} \geq s_s + 2 \cdot t_f \cdot \left(1 + \sqrt{m_{1_1} + m_{2_1}} \right) \\ a_{\text{stiffeners}} \text{ otherwise} \end{array} \right. \\ \left| \begin{array}{l} s_s + 2 \cdot t_f \cdot \left(1 + \sqrt{m_{1_2} + m_{2_2}} \right) \text{ if } a_{\text{stiffeners}} \geq s_s + 2 \cdot t_f \cdot \left(1 + \sqrt{m_{1_2} + m_{2_2}} \right) \\ a_{\text{stiffeners}} \text{ otherwise} \end{array} \right. \\ \left| \begin{array}{l} s_s + 2 \cdot t_f \cdot \left(1 + \sqrt{m_{1_3} + m_{2_3}} \right) \text{ if } a_{\text{stiffeners}} \geq s_s + 2 \cdot t_f \cdot \left(1 + \sqrt{m_{1_3} + m_{2_3}} \right) \\ a_{\text{stiffeners}} \text{ otherwise} \end{array} \right. \\ \left| \begin{array}{l} s_s + 2 \cdot t_f \cdot \left(1 + \sqrt{m_{1_4} + m_{2_4}} \right) \text{ if } a_{\text{stiffeners}} \geq s_s + 2 \cdot t_f \cdot \left(1 + \sqrt{m_{1_4} + m_{2_4}} \right) \\ a_{\text{stiffeners}} \text{ otherwise} \end{array} \right. \end{array} \right] l_y = \begin{pmatrix} 0.358 \\ 0.326 \\ 0.308 \\ 0.297 \\ 0.289 \end{pmatrix} \text{ m}$$

$$\lambda_F := \left(\begin{array}{l} \frac{l_{y_0} \cdot t_{w_0} \cdot f_{yw}}{F_{cr_0}} \\ \frac{l_{y_1} \cdot t_{w_1} \cdot f_{yw}}{F_{cr_1}} \\ \frac{l_{y_1} \cdot t_{w_1} \cdot f_{yw}}{F_{cr_1}} \\ \frac{l_{y_2} \cdot t_{w_2} \cdot f_{yw}}{F_{cr_2}} \\ \frac{l_{y_3} \cdot t_{w_3} \cdot f_{yw}}{F_{cr_3}} \end{array} \right) \lambda_F = \begin{pmatrix} 15.759 \\ 6.373 \\ 3.389 \\ 2.089 \\ 1.412 \end{pmatrix}$$

$$\chi_f := \begin{pmatrix} \frac{0.5}{\lambda_{F_0}} \\ \frac{0.5}{\lambda_{F_1}} \\ \frac{0.5}{\lambda_{F_2}} \\ \frac{0.5}{\lambda_{F_3}} \\ \frac{0.5}{\lambda_{F_4}} \end{pmatrix} \quad \chi_f = \begin{pmatrix} 0.032 \\ 0.078 \\ 0.078 \\ 0.148 \\ 0.239 \end{pmatrix}$$

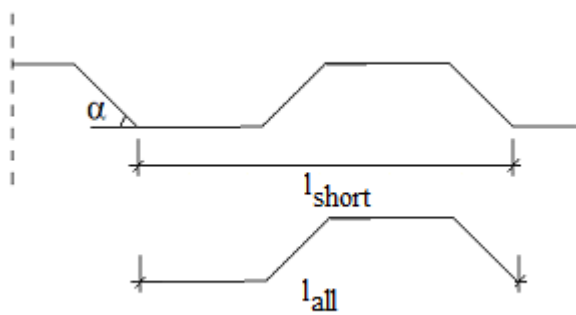
$$L_{\text{eff}} := \begin{pmatrix} \chi_{f_0} \cdot l_{y_0} \\ \chi_{f_1} \cdot l_{y_1} \\ \chi_{f_2} \cdot l_{y_2} \\ \chi_{f_3} \cdot l_{y_3} \\ \chi_{f_4} \cdot l_{y_4} \end{pmatrix} \quad L_{\text{eff}} = \begin{pmatrix} 0.011 \\ 0.026 \\ 0.024 \\ 0.044 \\ 0.069 \end{pmatrix} \text{ m}$$

$$F_{\text{flatEC3}} := \begin{pmatrix} \frac{f_{yw} \cdot L_{\text{eff}_0} \cdot t_{w_0}}{\gamma_{M1}} \\ \frac{f_{yw} \cdot L_{\text{eff}_1} \cdot t_{w_1}}{\gamma_{M1}} \\ \frac{f_{yw} \cdot L_{\text{eff}_2} \cdot t_{w_2}}{\gamma_{M1}} \\ \frac{f_{yw} \cdot L_{\text{eff}_3} \cdot t_{w_3}}{\gamma_{M1}} \\ \frac{f_{yw} \cdot L_{\text{eff}_4} \cdot t_{w_4}}{\gamma_{M1}} \end{pmatrix} \quad F_{\text{flatEC3}} = \begin{pmatrix} 8.064 \\ 27.216 \\ 34.306 \\ 77.666 \\ 147.17 \end{pmatrix} \cdot \text{kN}$$

A.11.2 Comparison of steel amount

In this section, the amount steel required in a girder with a flat web (with various web thicknesses) is compared to that of a similar girder with a corrugated web (with a thickness of 2 mm). Other varying web thicknesses, the dimensions and material

properties of the girders are set to the same values as the reference girder used in the parametric study performed in section 2.3 in the thesis.



$$\alpha := \frac{\pi}{4} \text{ rad}$$

$$l_{short} := 2 \cdot a_{in} + 2 \cdot a_{long}$$

$$l_{short} = 0.38 \text{ m}$$

$$l_{all} := \frac{2 \cdot a_{in}}{\cos(\alpha)} + 2 \cdot a_{long}$$

$$l_{all} = 0.421 \text{ m}$$

$$\text{Amount}_{fw} := \frac{l_{short} \cdot t_w}{l_{all} \cdot 2 \text{ mm}}$$

$$\text{Amount}_{fw} = \begin{pmatrix} 0.902 \\ 1.353 \\ 1.803 \\ 2.254 \\ 2.705 \end{pmatrix} [-]$$

APPENDIX B- Material properties

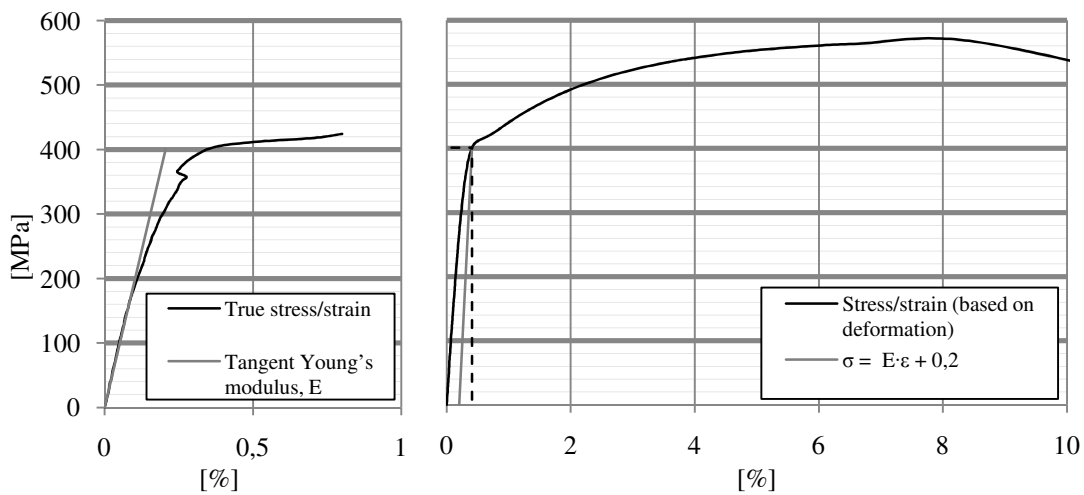
| | | |
|-------|------------------|---|
| B.1 | MATERIAL TESTS | 1 |
| B.1.1 | Test I – flange | 1 |
| B.1.2 | Test II – flange | 1 |
| B.1.3 | Test III –web | 2 |
| B.1.4 | Test IV – web | 2 |
| B.1.5 | Test V – web | 2 |
| B.2 | MATERIAL MODELS | 3 |

B.1 Material tests

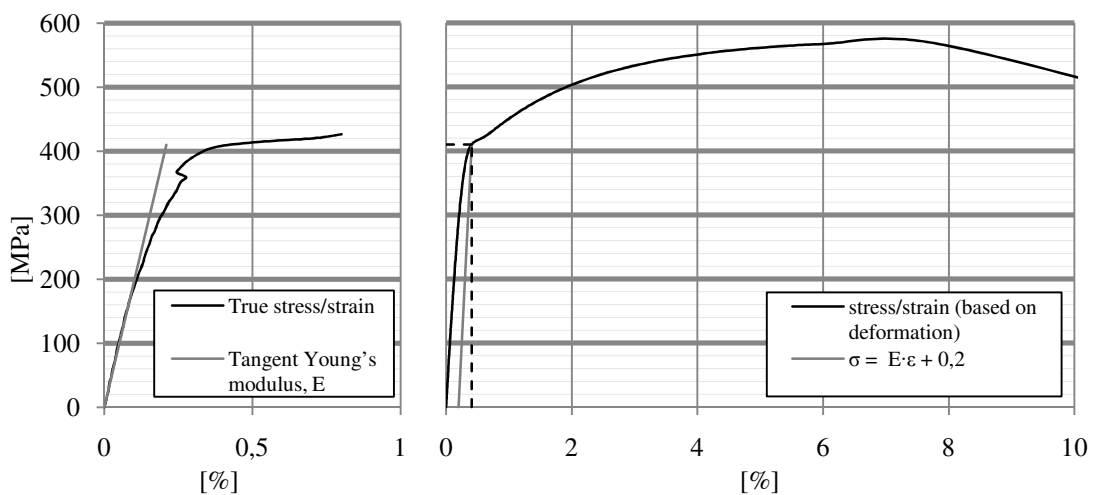
Five different pull tests were performed, two on the flange material and three on the web material. The material was cutout with water to reduce the residual stresses. As mentioned in the thesis, only the Young's modulus and yield stress were possible to obtain. The yield stresses were estimated according to EUROCODE by removing 0.2 % of the elastic strain as seen in Figure 4.3a. Further, a bilinear behaviour with a plastic hardening following a reduced modulus of $E/100$, as seen in Figure 4.3b, was implemented in Abaqus CAE.

Each test included a true stress/strain graph from where the Young's modulus was obtained. And a stress/strain graph biased on the total deformation of the test sample.

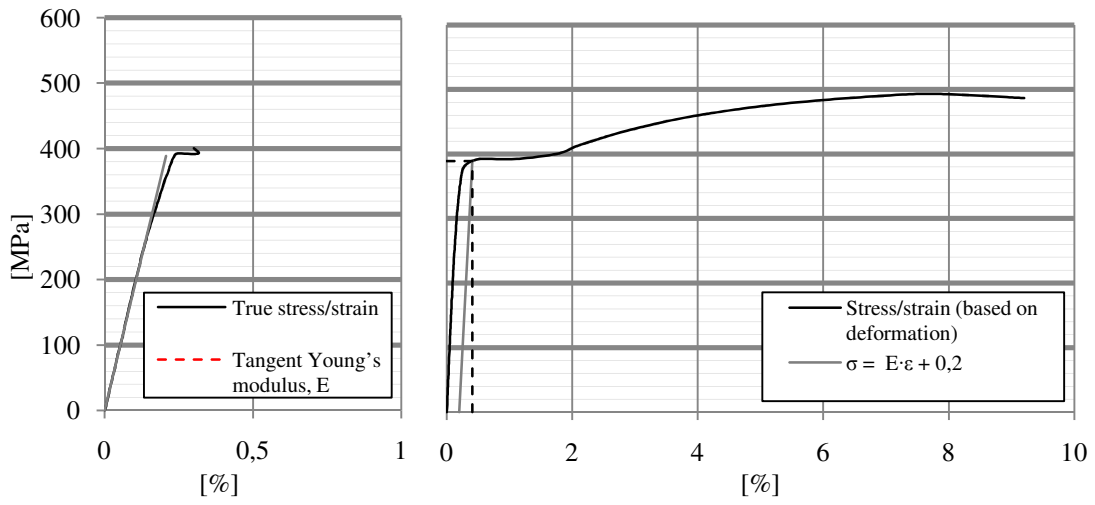
B.1.1 Test I – flange



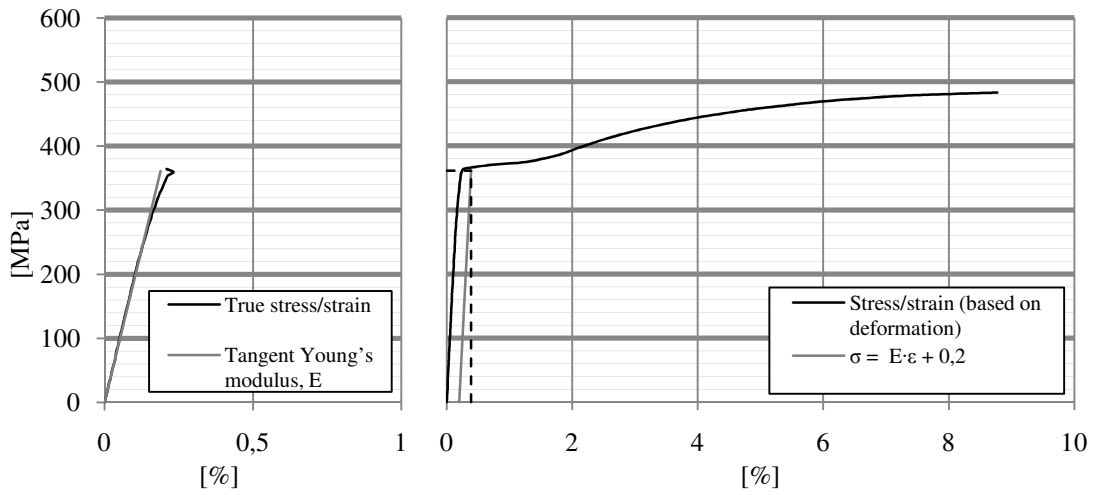
B.1.2 Test II – flange



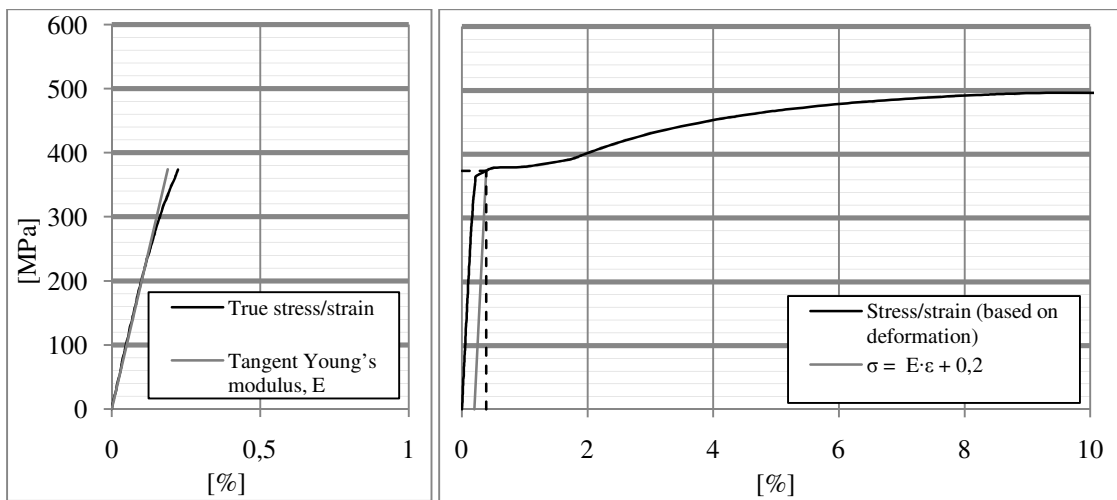
B.1.3 Test III –web



B.1.4 Test IV – web



B.1.5 Test V – web

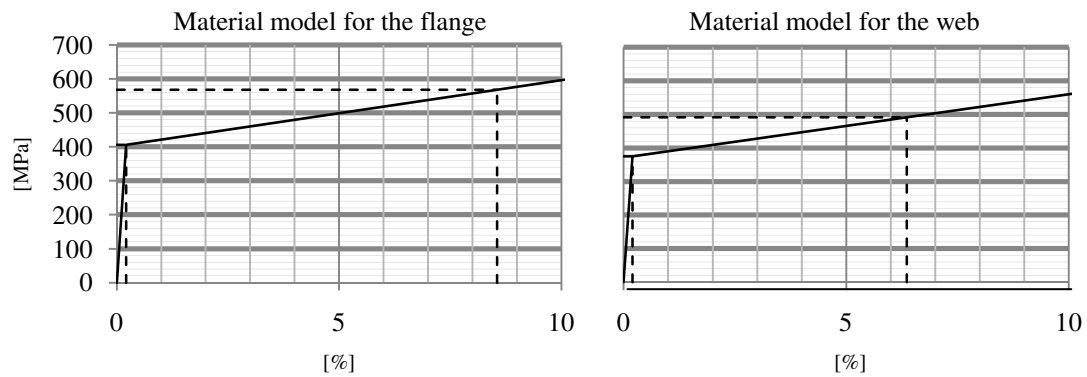


B.2 Material models

To establish the material models, a mean value of the flange tests and the web test were calculated.

| Test | Flange | | Web | | |
|---------------------------|--------|-----|-----|-----|-----|
| | I | II | III | IV | V |
| E [GPa] | 194 | 196 | 188 | 191 | 188 |
| E_{mean} [GPa] | 195 | | 189 | | |
| f_y [MPa] | 401 | 410 | 389 | 361 | 374 |
| $f_{y,\text{mean}}$ [MPa] | 406 | | 375 | | |
| f_u [MPa] | 567 | 570 | 493 | 483 | 496 |
| $f_{u,\text{mean}}$ [MPa] | 568 | | 491 | | |

The material models are as follow:



APPENDIX C- Test results

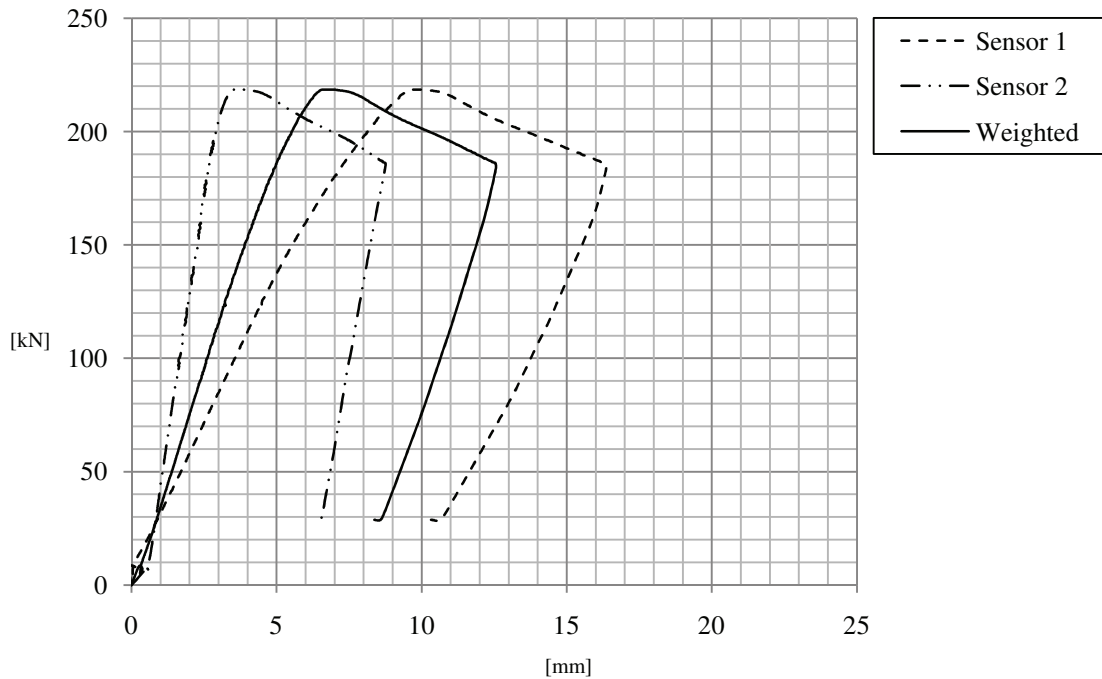
| | | |
|-------|--|----|
| C.1 | LOAD/DEFORMATION DIAGRAM | 1 |
| C.1.1 | Test A1 – Loaded over an inclined fold | 1 |
| C.1.2 | Test A2 – Loaded over a junction between two folds | 1 |
| C.1.3 | Test A3 – Loaded over a longitudinal fold | 2 |
| C.1.4 | Test B1 – Loaded over a longitudinal fold | 2 |
| C.1.5 | Test B2 – Loaded over a junction between two folds | 3 |
| C.1.6 | Test B3 – Loaded over an inclined fold | 3 |
| C.2 | LOAD/DEFORMATION DATA | 4 |
| C.2.1 | Test A1, A2 and A3 | 4 |
| C.2.2 | Test B1, B2 and B3 | 5 |
| C.3 | FAILURE MODES | 6 |
| C.3.1 | Test A1 – Loaded over an inclined fold | 6 |
| C.3.2 | Test A2 – Loaded over a junction between two folds | 6 |
| C.3.3 | Test A3 – Loaded over a longitudinal fold | 6 |
| C.3.4 | Test B1 – Loaded over a longitudinal fold | 7 |
| C.3.5 | Test B2 – Loaded over a junction between two folds | 7 |
| C.3.6 | Test B3 – Loaded over an inclined fold | 7 |
| C.4 | LOAD/OUT-OF-PLANE DEFORMATION, W_{PI} | 8 |
| C.4.1 | Test A1 – Loaded over an inclined fold | 8 |
| C.4.2 | Test A2 – Loaded over a junction between two folds | 9 |
| C.4.3 | Test A3 – Loaded over a longitudinal fold | 10 |
| C.4.4 | Test B1 – Loaded over a longitudinal fold | 10 |
| C.4.5 | Test B2 – Loaded over a junction between two folds | 11 |
| C.4.6 | Test B3 – Loaded over an inclined fold | 12 |
| C.5 | OUT-OF-PLANE DEFORMATION DATA | 13 |
| C.5.1 | Tests A1 and A2 | 13 |
| C.5.2 | Tests A3 and B1 | 15 |
| C.5.3 | Tests B2 and B3 | 16 |
| C.6 | INITIAL IMPERFECTIONS | 18 |
| C.6.1 | Test A1 | 18 |
| C.6.2 | Test A2 | 18 |

| | |
|--|----|
| C.6.3 Test A3 | 19 |
| C.6.4 Test B1 | 19 |
| C.6.5 Test B2 | 19 |
| C.6.6 Test B3 | 20 |
| C.7 STRAIN CONTOUR-PLOTS | 21 |
| C.7.1 Test A1 – Loaded over an inclined fold | 21 |
| C.7.2 Test A2 – Loaded over a junction between two folds | 21 |
| C.7.3 Test B1 – Loaded over a longitudinal fold | 22 |
| C.7.4 Test B2 – Loaded over a junction between two folds | 23 |
| C.7.5 Test B3 – Loaded over an inclined fold | 23 |

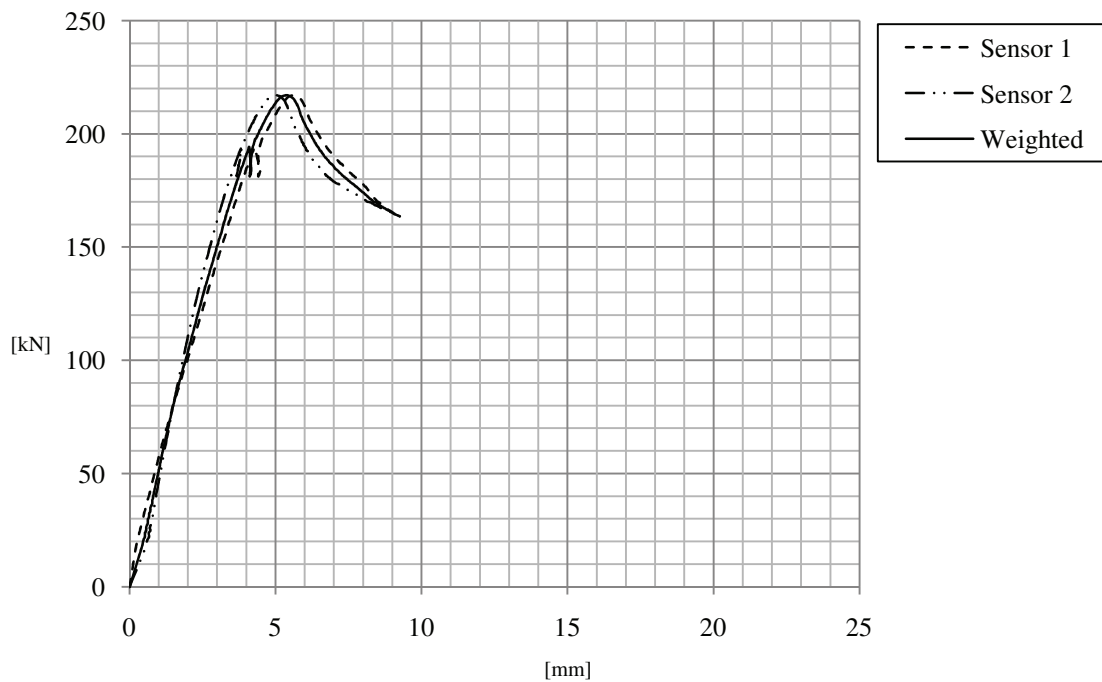
C.1 Load/deformation diagram

In this section, load/deformation diagrams are presented. Sensor 1, Sensor 2 are show in Figure 3.3 and the weighting process is described in section 3.1

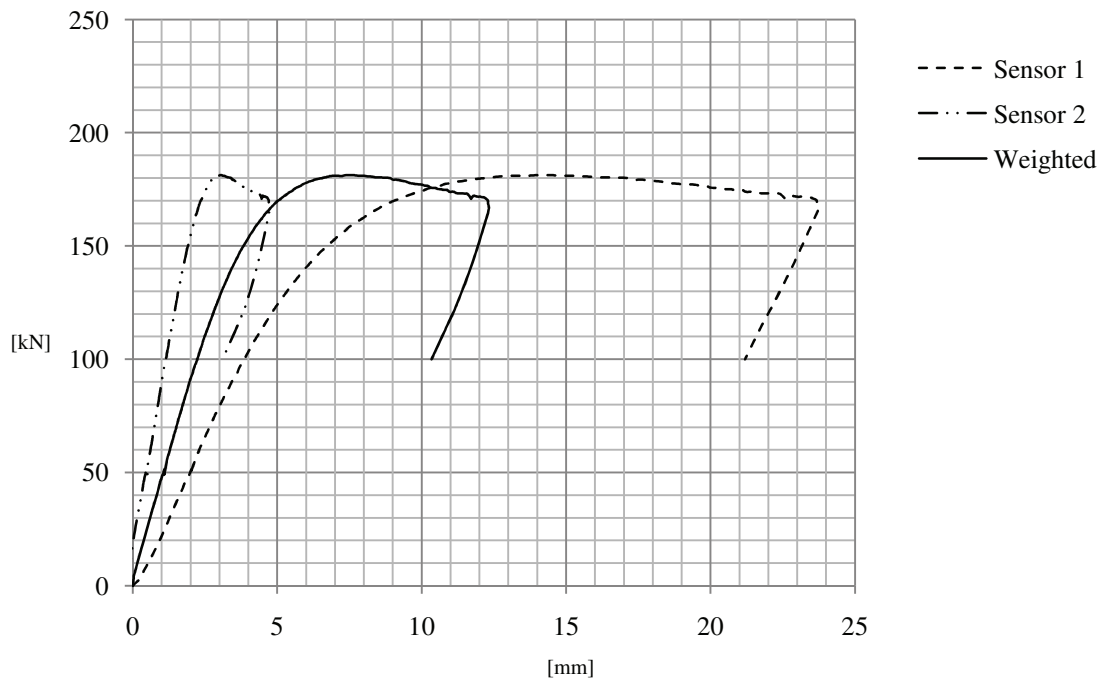
C.1.1 Test A1 – Loaded over an inclined fold



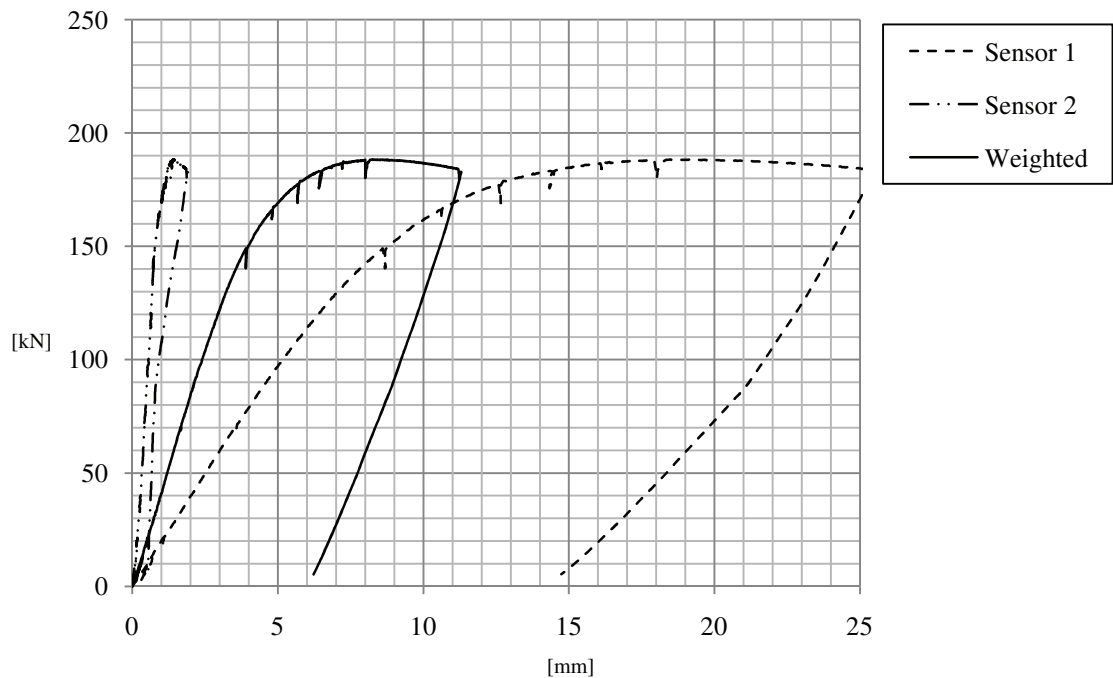
C.1.2 Test A2 – Loaded over a junction between two folds



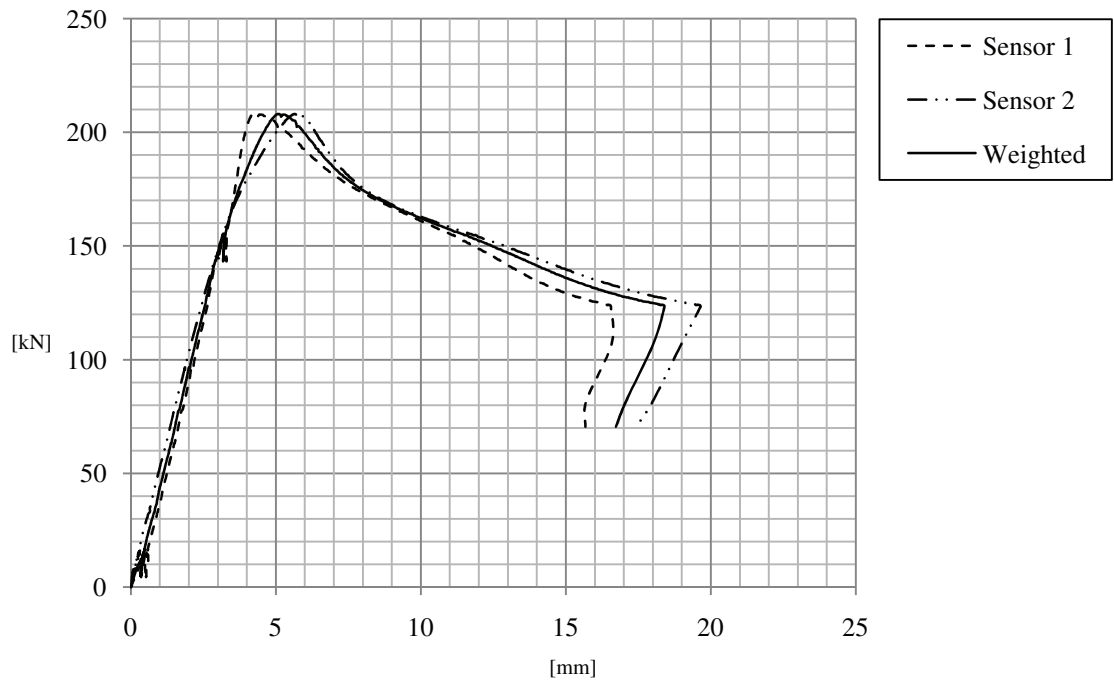
C.1.3 Test A3 – Loaded over a longitudinal fold



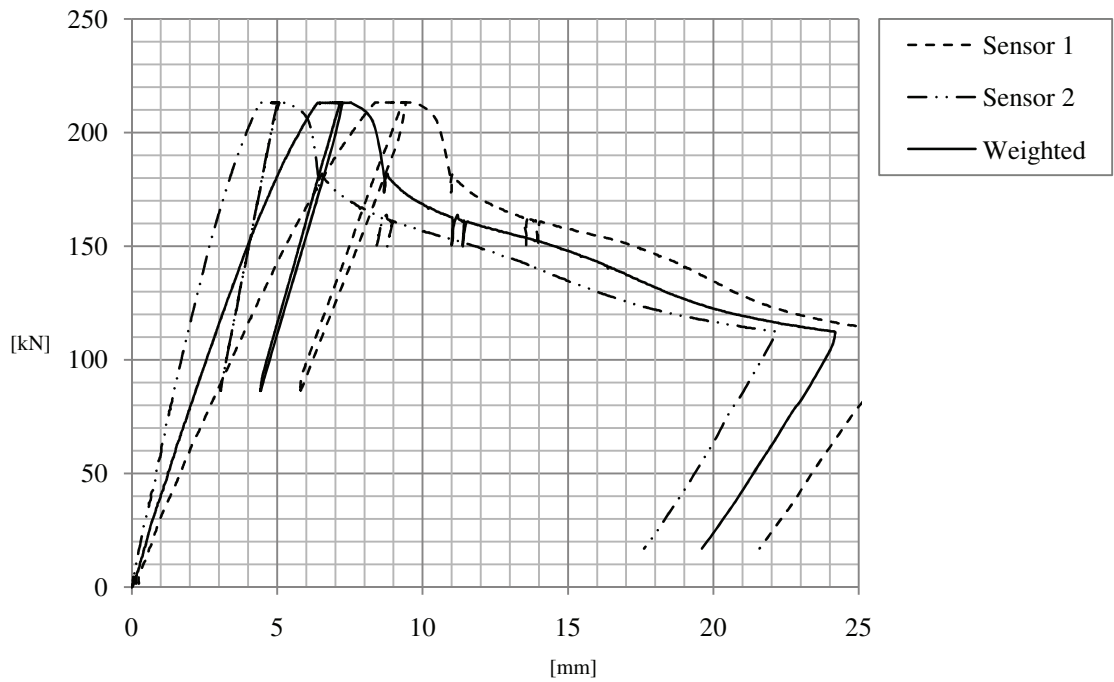
C.1.4 Test B1 – Loaded over a longitudinal fold



C.1.5 Test B2 – Loaded over a junction between two folds



C.1.6 Test B3 – Loaded over an inclined fold



C.2 Load/deformation data

In this section, a downsized amount collected data for the graphs shown in the previous section is presented.

C.2.1 Test A1, A2 and A3

| Test A1 | | | | Test A2 | | | | Test A3 | | | |
|-----------|----------|----------|---------|-----------|----------|----------|---------|-----------|----------|----------|---------|
| Load [kN] | ps1 [mm] | ps2 [mm] | pw [mm] | Load [kN] | ps1 [mm] | ps2 [mm] | pw [mm] | Load [kN] | ps1 [mm] | ps2 [mm] | pw [mm] |
| 0 | 0,00 | 0,00 | 0,00 | 0 | 0,00 | 0,00 | 0,00 | 0 | 0,00 | 0,00 | 0,00 |
| 46 | 1,54 | 1,02 | 1,28 | 30 | 0,45 | 0,75 | 0,63 | 51 | 0,47 | 2,03 | 1,10 |
| 92 | 3,28 | 1,55 | 2,41 | 41 | 0,69 | 0,92 | 0,83 | 40 | 0,31 | 1,64 | 0,84 |
| 108 | 3,84 | 1,77 | 2,81 | 54 | 0,94 | 1,11 | 1,04 | 65 | 0,68 | 2,47 | 1,39 |
| 116 | 4,15 | 1,87 | 3,01 | 67 | 1,20 | 1,30 | 1,26 | 65 | 0,68 | 2,47 | 1,39 |
| 138 | 5,02 | 2,14 | 3,58 | 79 | 1,46 | 1,48 | 1,47 | 84 | 0,92 | 3,18 | 1,82 |
| 152 | 5,63 | 2,29 | 3,96 | 90 | 1,72 | 1,66 | 1,70 | 93 | 1,03 | 3,57 | 2,05 |
| 171 | 6,53 | 2,47 | 4,50 | 101 | 1,99 | 1,83 | 1,93 | 101 | 1,16 | 3,90 | 2,25 |
| 193 | 7,70 | 2,76 | 5,23 | 112 | 2,27 | 2,03 | 2,18 | 110 | 1,27 | 4,28 | 2,48 |
| 198 | 8,00 | 2,89 | 5,45 | 124 | 2,54 | 2,24 | 2,42 | 118 | 1,41 | 4,71 | 2,73 |
| 203 | 8,30 | 2,95 | 5,62 | 136 | 2,82 | 2,46 | 2,67 | 128 | 1,54 | 5,20 | 3,00 |
| 207 | 8,58 | 3,04 | 5,81 | 147 | 3,08 | 2,70 | 2,93 | 136 | 1,66 | 5,68 | 3,27 |
| 211 | 8,86 | 3,14 | 6,00 | 159 | 3,35 | 2,93 | 3,19 | 144 | 1,79 | 6,22 | 3,56 |
| 214 | 9,15 | 3,26 | 6,20 | 170 | 3,61 | 3,18 | 3,44 | 151 | 1,92 | 6,78 | 3,86 |
| 217 | 9,44 | 3,39 | 6,42 | 181 | 3,90 | 3,45 | 3,72 | 158 | 2,06 | 7,43 | 4,21 |
| 219 | 9,70 | 3,59 | 6,65 | 190 | 4,17 | 3,72 | 3,99 | 164 | 2,19 | 8,14 | 4,57 |
| 219 | 10,03 | 3,88 | 6,95 | 194 | 4,45 | 3,84 | 4,21 | 169 | 2,32 | 8,87 | 4,94 |
| 218 | 10,38 | 4,17 | 7,27 | 202 | 4,73 | 4,11 | 4,48 | 173 | 2,47 | 9,69 | 5,36 |
| 217 | 10,73 | 4,47 | 7,60 | 209 | 5,01 | 4,38 | 4,76 | 177 | 2,60 | 10,64 | 5,82 |
| 215 | 11,09 | 4,78 | 7,94 | 214 | 5,25 | 4,64 | 5,00 | 179 | 2,73 | 11,66 | 6,30 |
| 213 | 11,45 | 5,09 | 8,27 | 217 | 5,50 | 4,88 | 5,25 | 181 | 2,85 | 12,63 | 6,76 |
| 210 | 11,81 | 5,40 | 8,60 | 215 | 5,90 | 5,31 | 5,66 | 181 | 2,97 | 13,60 | 7,23 |
| 208 | 12,14 | 5,68 | 8,91 | 202 | 6,37 | 5,70 | 6,10 | 181 | 3,02 | 14,07 | 7,44 |
| 206 | 12,50 | 5,98 | 9,24 | 217 | 5,50 | 4,88 | 5,25 | 181 | 3,20 | 15,51 | 8,13 |
| 204 | 12,83 | 6,26 | 9,54 | 195 | 6,72 | 5,98 | 6,43 | 180 | 3,36 | 16,81 | 8,74 |
| 202 | 13,18 | 6,55 | 9,87 | 189 | 7,08 | 6,26 | 6,75 | 179 | 3,53 | 18,03 | 9,33 |
| 200 | 13,51 | 6,83 | 10,17 | 184 | 7,42 | 6,52 | 7,06 | 177 | 3,70 | 19,19 | 9,90 |
| 199 | 13,85 | 7,10 | 10,47 | 180 | 7,77 | 6,87 | 7,41 | 176 | 3,88 | 20,20 | 10,41 |
| 197 | 14,18 | 7,36 | 10,77 | 176 | 8,13 | 7,39 | 7,83 | 175 | 4,05 | 20,94 | 10,81 |
| 195 | 14,49 | 7,60 | 11,05 | 170 | 8,48 | 8,12 | 8,33 | 173 | 4,38 | 22,40 | 11,58 |
| 188 | 15,83 | 8,46 | 12,14 | 167 | 8,80 | 8,66 | 8,74 | 169 | 4,70 | 23,68 | 12,29 |
| 114 | 14,32 | 7,72 | 11,02 | 164 | 9,14 | 9,19 | 9,17 | 165 | 4,71 | 23,67 | 12,29 |

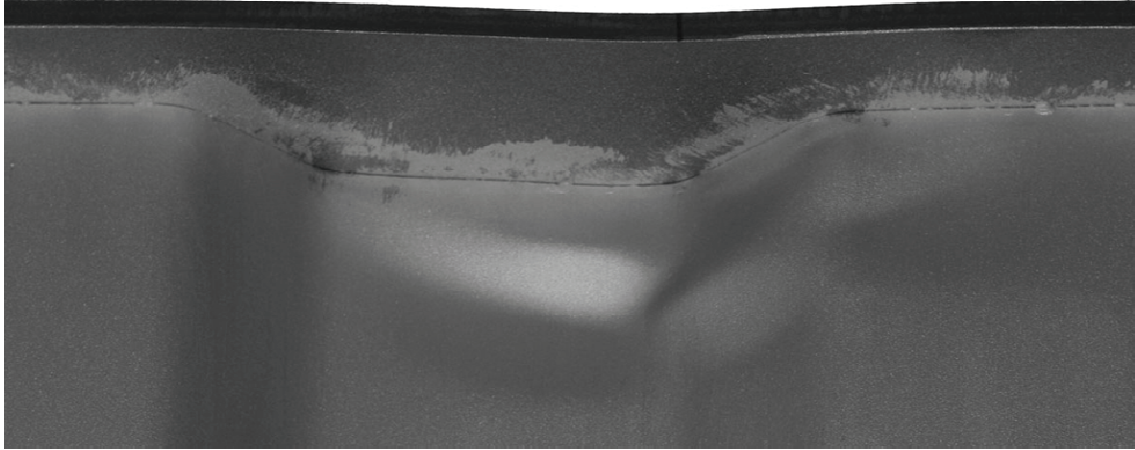
C.2.2 Test B1, B2 and B3

| Test B1 | | | | Test B2 | | | | Test B3 | | | |
|-----------|----------|----------|---------|-----------|----------|----------|---------|-----------|----------|----------|---------|
| Load [kN] | ps1 [mm] | ps2 [mm] | pw [mm] | Load [kN] | ps1 [mm] | ps2 [mm] | pw [mm] | Load [kN] | ps1 [mm] | ps2 [mm] | pw [mm] |
| 0 | 0,00 | 0,00 | 0,00 | 0 | 0,00 | 0,00 | 0,00 | | 0,00 | 0,00 | 0,00 |
| 33 | 1,67 | 0,26 | 0,82 | 5 | 0,52 | 0,08 | 0,35 | 56 | 1,85 | 0,94 | 1,40 |
| 73 | 3,68 | 0,42 | 1,72 | 6 | 0,51 | 0,10 | 0,35 | 103 | 3,53 | 1,75 | 2,64 |
| 100 | 5,18 | 0,55 | 2,40 | 5 | 0,51 | 0,11 | 0,35 | 156 | 5,53 | 2,81 | 4,17 |
| 120 | 6,40 | 0,66 | 2,95 | 12 | 0,49 | 0,20 | 0,37 | 170 | 6,12 | 3,12 | 4,62 |
| 129 | 6,99 | 0,67 | 3,20 | 15 | 0,56 | 0,28 | 0,45 | 189 | 6,98 | 3,60 | 5,29 |
| 137 | 7,61 | 0,70 | 3,47 | 16 | 0,57 | 0,30 | 0,46 | 200 | 7,56 | 3,94 | 5,75 |
| 148 | 8,52 | 0,76 | 3,86 | 26 | 0,76 | 0,44 | 0,63 | 209 | 8,09 | 4,25 | 6,17 |
| 157 | 9,46 | 0,85 | 4,29 | 37 | 1,01 | 0,72 | 0,90 | 213 | 8,34 | 4,40 | 6,37 |
| 165 | 10,41 | 0,94 | 4,73 | 51 | 1,25 | 0,96 | 1,14 | 213 | 8,96 | 4,73 | 6,85 |
| 171 | 11,33 | 1,03 | 5,15 | 63 | 1,51 | 1,22 | 1,40 | 198 | 9,18 | 4,76 | 6,97 |
| 173 | 11,66 | 1,02 | 5,28 | 78 | 1,78 | 1,50 | 1,67 | 183 | 8,76 | 4,54 | 6,65 |
| 175 | 11,96 | 1,06 | 5,42 | 93 | 2,04 | 1,80 | 1,95 | 169 | 8,33 | 4,32 | 6,32 |
| 176 | 12,28 | 1,08 | 5,56 | 106 | 2,31 | 2,06 | 2,21 | 147 | 7,68 | 3,97 | 5,82 |
| 169 | 12,65 | 1,02 | 5,67 | 121 | 2,57 | 2,36 | 2,49 | 134 | 7,28 | 3,77 | 5,53 |
| 179 | 12,95 | 1,14 | 5,86 | 138 | 2,83 | 2,75 | 2,80 | 119 | 6,80 | 3,53 | 5,16 |
| 180 | 13,27 | 1,15 | 6,00 | 151 | 3,10 | 3,06 | 3,09 | 103 | 6,31 | 3,29 | 4,80 |
| 182 | 13,91 | 1,19 | 6,28 | 160 | 3,38 | 3,33 | 3,36 | 101 | 6,06 | 3,27 | 4,66 |
| 184 | 14,55 | 1,20 | 6,54 | 177 | 3,62 | 3,91 | 3,79 | 113 | 6,41 | 3,44 | 4,92 |
| 185 | 15,20 | 1,23 | 6,82 | 195 | 3,85 | 4,73 | 4,38 | 125 | 6,75 | 3,64 | 5,20 |
| 186 | 15,52 | 1,25 | 6,96 | 205 | 4,08 | 5,35 | 4,84 | 146 | 7,38 | 3,97 | 5,67 |
| 186 | 15,83 | 1,26 | 7,09 | 207 | 4,39 | 5,74 | 5,20 | 174 | 8,16 | 4,39 | 6,27 |
| 185 | 16,12 | 1,27 | 7,21 | 206 | 4,73 | 5,99 | 5,49 | 195 | 8,80 | 4,71 | 6,75 |
| 187 | 16,48 | 1,33 | 7,39 | 202 | 5,07 | 6,18 | 5,74 | 206 | 9,10 | 4,88 | 6,99 |
| 187 | 16,81 | 1,34 | 7,53 | 199 | 5,44 | 6,40 | 6,01 | 213 | 9,10 | 4,88 | 6,99 |
| 188 | 17,12 | 1,36 | 7,67 | 195 | 5,80 | 6,62 | 6,29 | 213 | 9,48 | 5,11 | 7,29 |
| 188 | 18,59 | 1,40 | 8,28 | 191 | 6,14 | 6,85 | 6,57 | 173 | 11,67 | 7,11 | 9,39 |
| 188 | 21,15 | 1,51 | 9,37 | 187 | 6,48 | 7,08 | 6,84 | 166 | 12,67 | 7,97 | 10,32 |
| 187 | 21,82 | 1,54 | 9,65 | 180 | 7,17 | 7,59 | 7,42 | 165 | 12,90 | 8,15 | 10,53 |
| 187 | 22,47 | 1,58 | 9,94 | 177 | 7,50 | 7,86 | 7,72 | 154 | 16,24 | 10,77 | 13,51 |
| 186 | 23,76 | 1,70 | 10,52 | 160 | 10,17 | 10,62 | 10,44 | 137 | 19,54 | 14,45 | 17,00 |
| 174 | 25,10 | 1,79 | 11,12 | 158 | 10,49 | 11,03 | 10,81 | 120 | 22,87 | 18,67 | 20,77 |

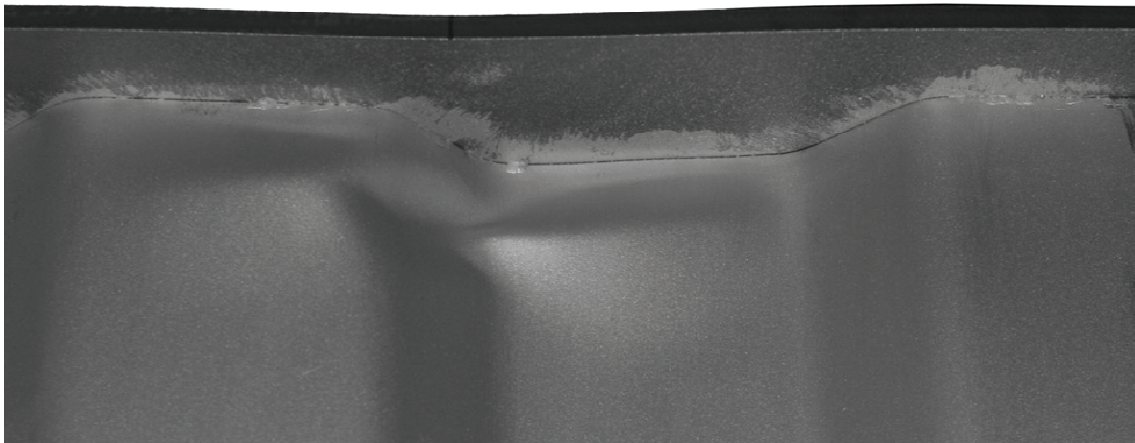
C.3 Failure modes

This section includes images of the buckling after the girder has been unloaded.

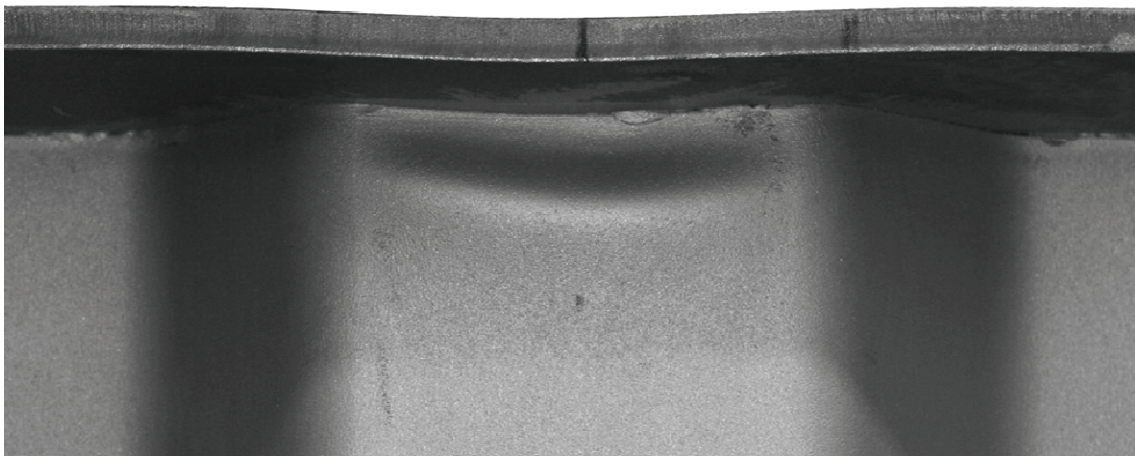
C.3.1 Test A1 – Loaded over an inclined fold



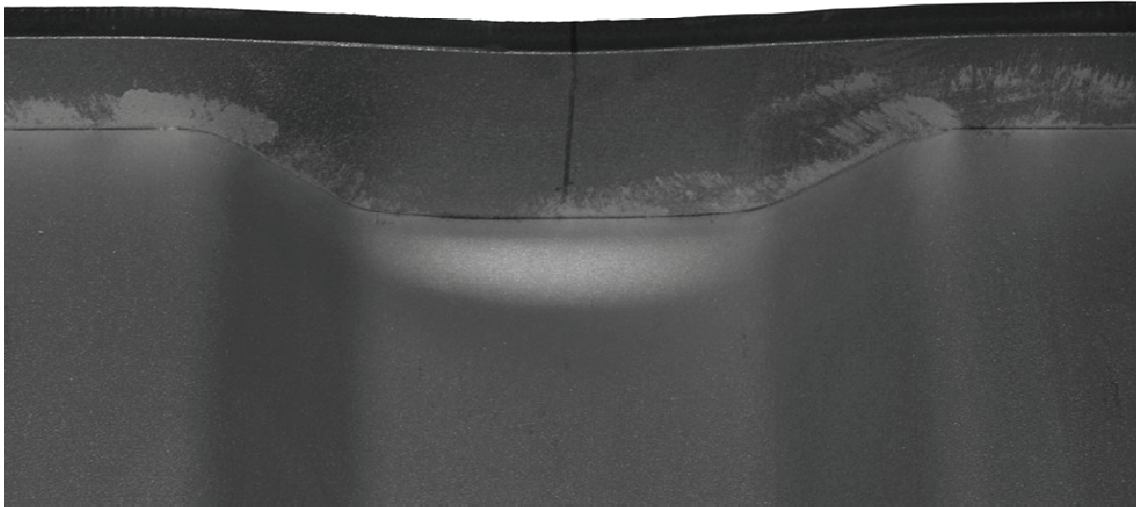
C.3.2 Test A2 – Loaded over a junction between two folds



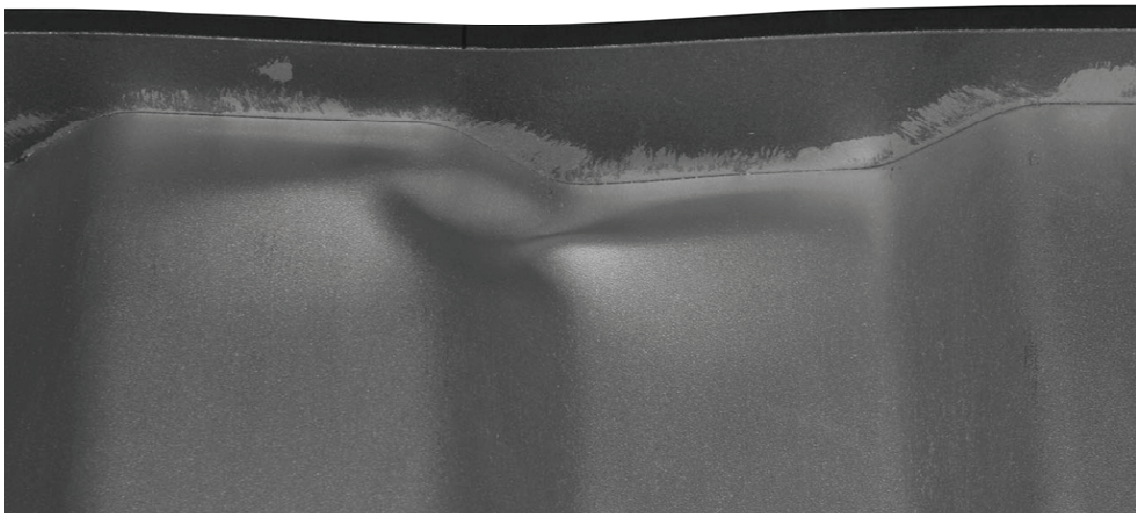
C.3.3 Test A3 – Loaded over a longitudinal fold



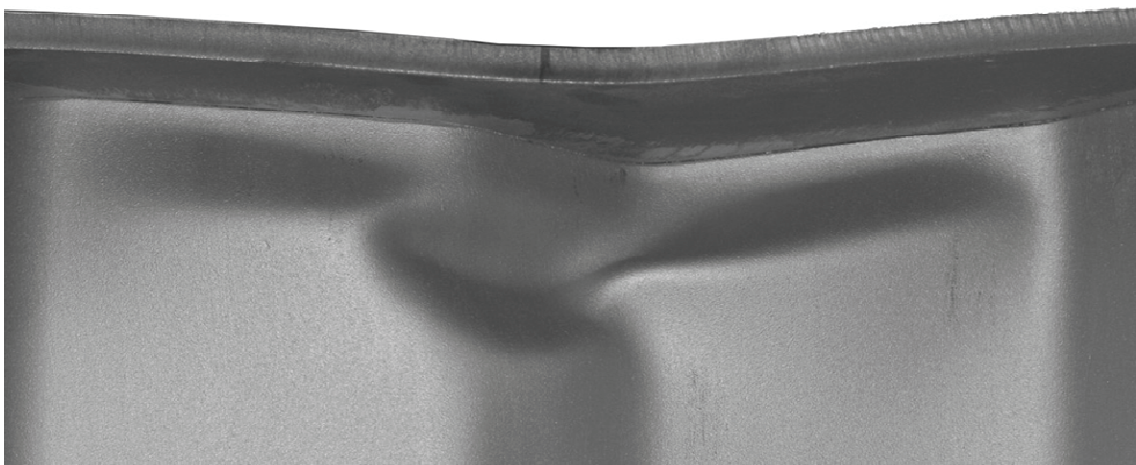
C.3.4 Test B1 – Loaded over a longitudinal fold



C.3.5 Test B2 – Loaded over a junction between two folds



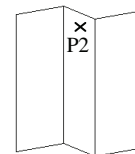
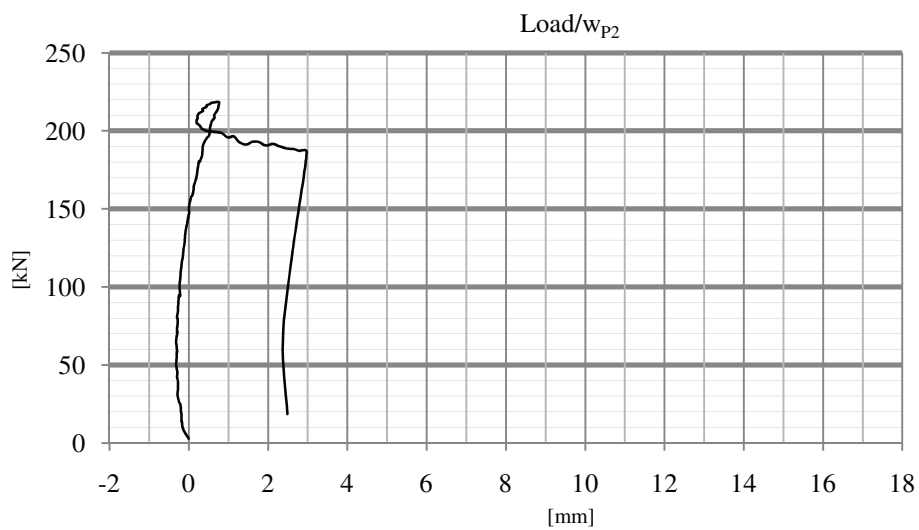
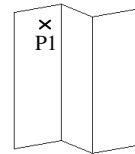
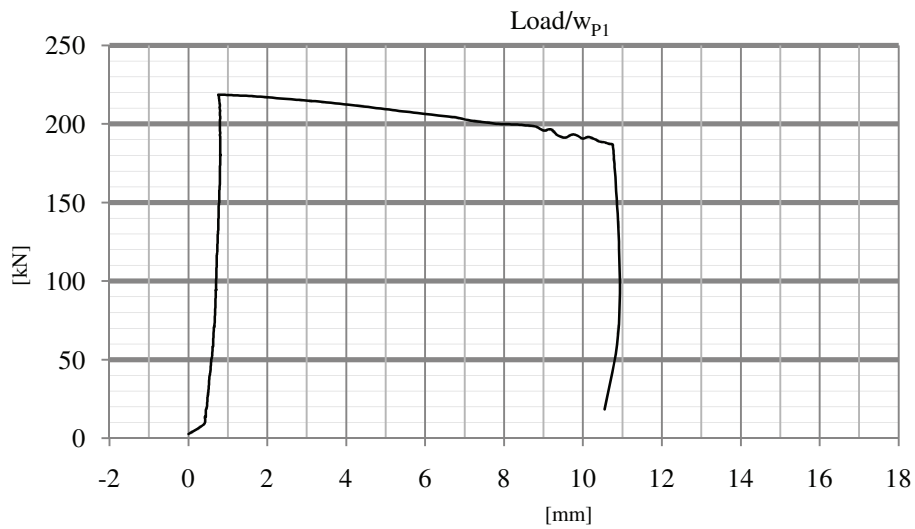
C.3.6 Test B3 – Loaded over an inclined fold

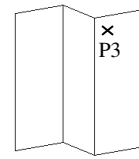


C.4 Load/Out-of-plane deformation, w_{Pi}

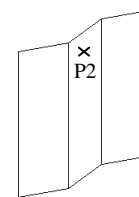
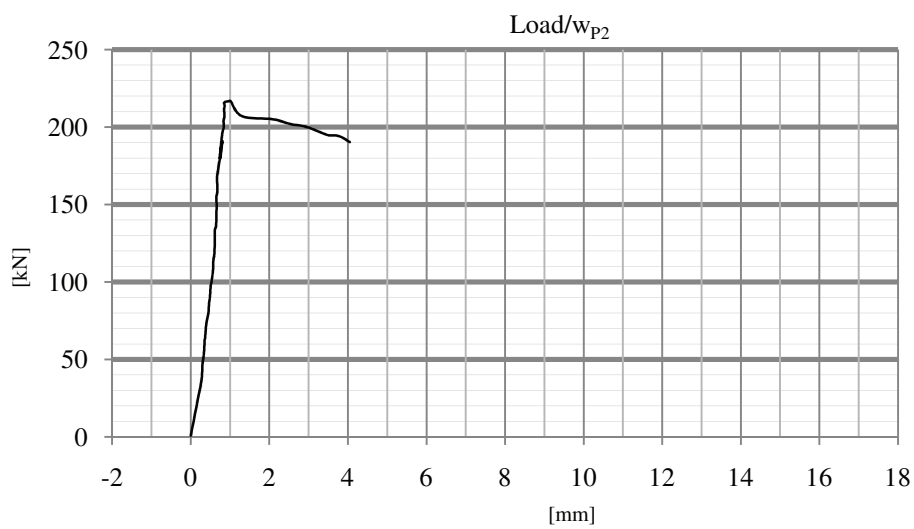
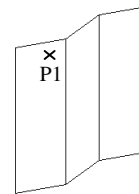
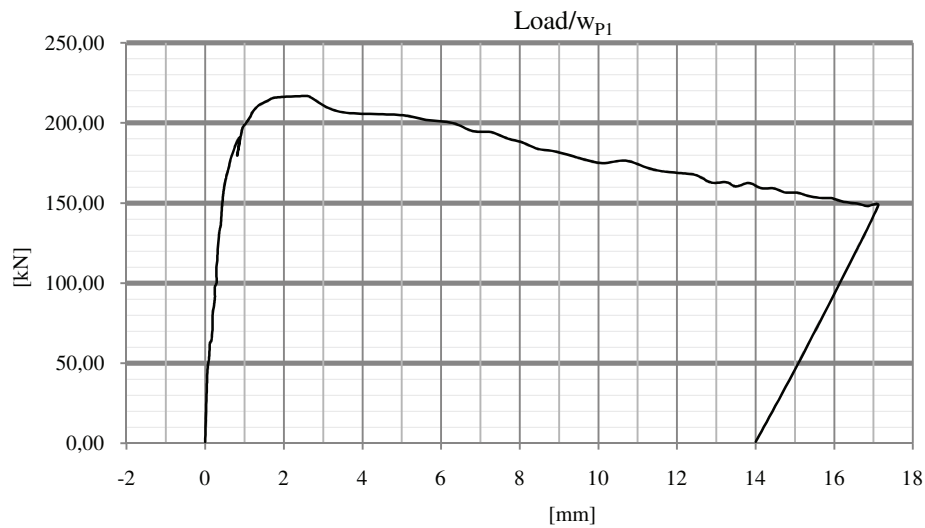
In this section, the out-of-plane deformation at the points where the maximum deformations were obtained is presented.

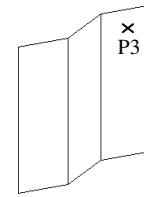
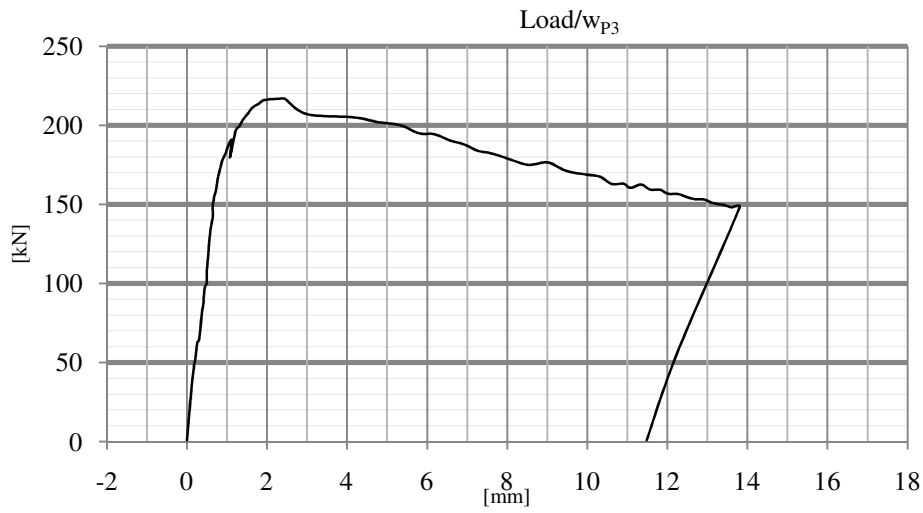
C.4.1 Test A1 – Loaded over an inclined fold



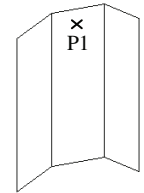
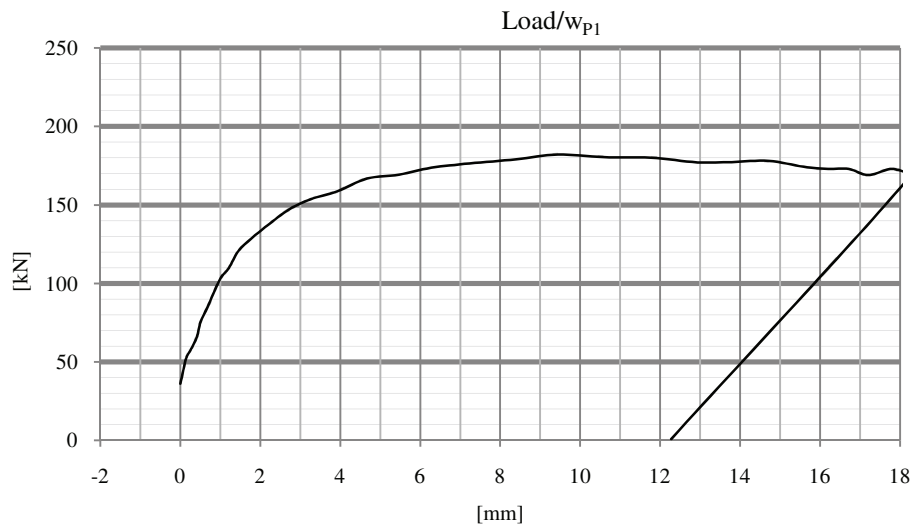


C.4.2 Test A2 – Loaded over a junction between two folds

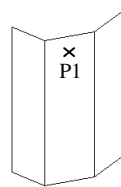
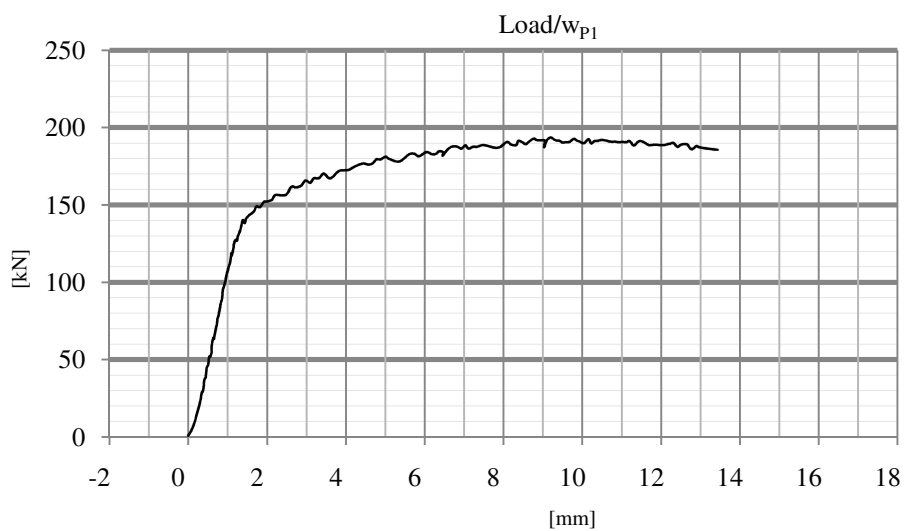




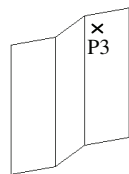
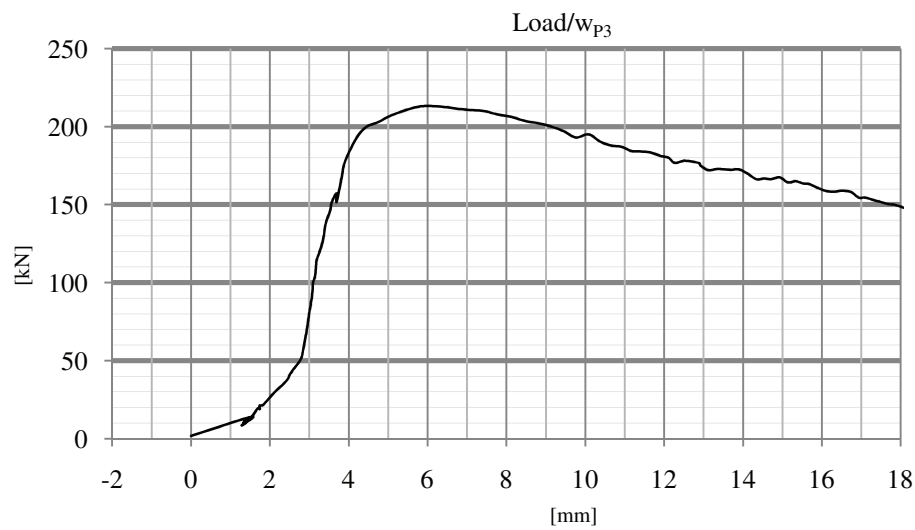
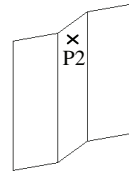
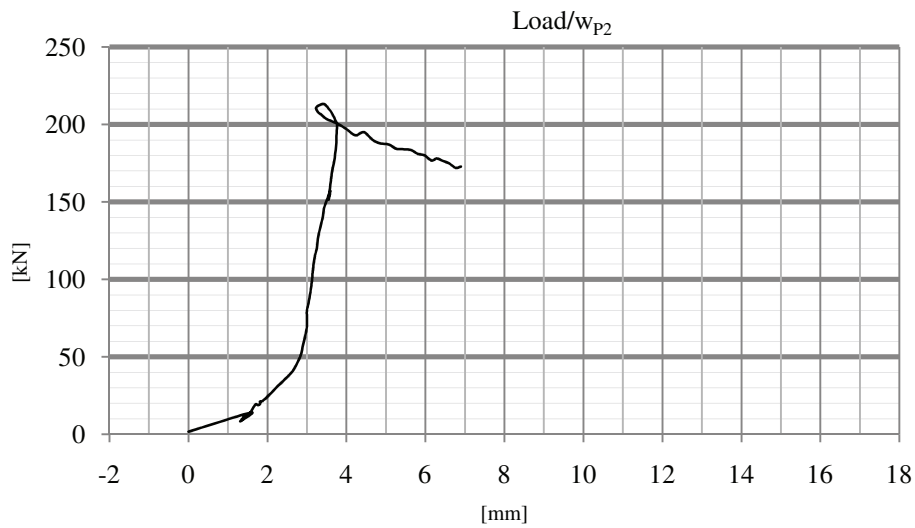
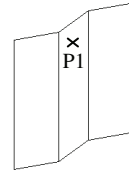
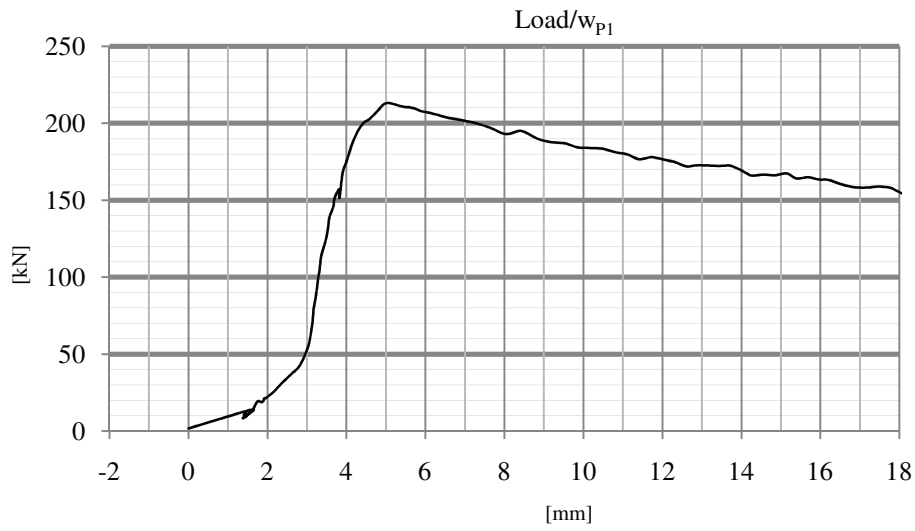
C.4.3 Test A3 – Loaded over a longitudinal fold



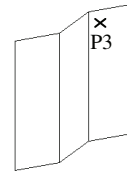
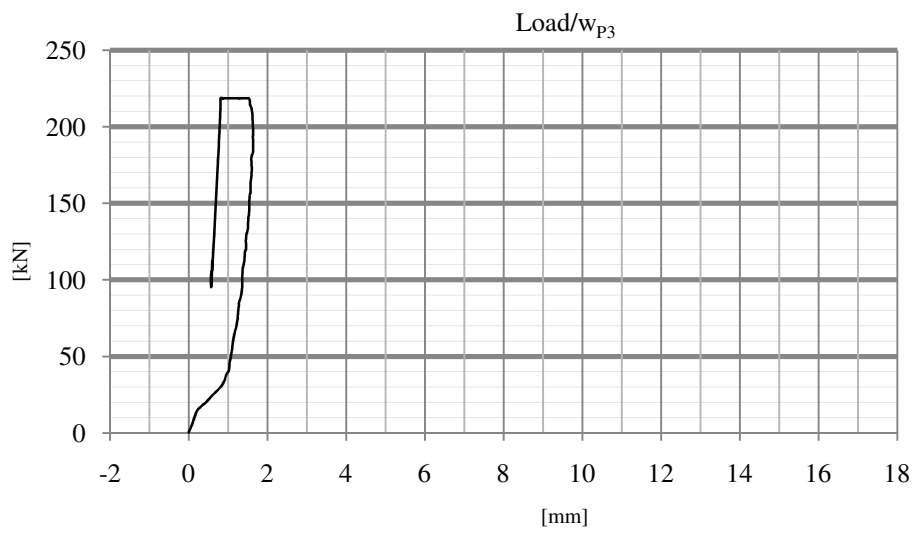
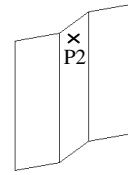
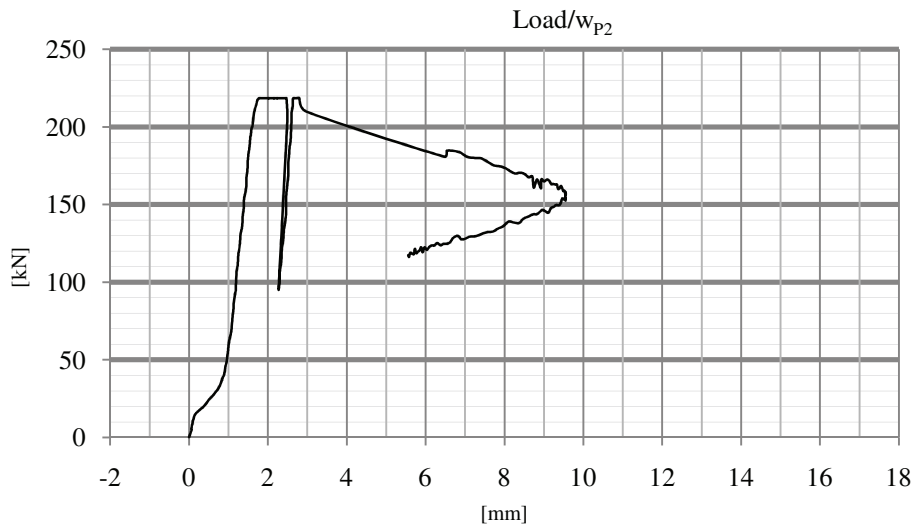
C.4.4 Test B1 – Loaded over a longitudinal fold



C.4.5 Test B2 – Loaded over a junction between two folds



C.4.6 Test B3 – Loaded over an inclined fold



C.5 Out-of-plane deformation data

In this section, a downsized amount collected data for the graphs shown in the previous section is presented.

C.5.1 Tests A1 and A2

| Test A1 | | | | Test A2 | | | |
|-----------|-------|------|-------|-----------|------|------|------|
| Load [kN] | WP1 | WP2 | WP3 | Load [kN] | WP1 | WP2 | WP3 |
| 3 | 0,00 | 0,00 | 0,00 | 1 | 0,00 | 0,00 | 0,00 |
| 14 | -0,17 | 0,41 | -0,18 | 41 | 0,05 | 0,29 | 0,14 |
| 18 | -0,18 | 0,44 | -0,22 | 54 | 0,10 | 0,33 | 0,22 |
| 25 | -0,21 | 0,48 | -0,27 | 64 | 0,16 | 0,37 | 0,30 |
| 31 | -0,28 | 0,50 | -0,30 | 80 | 0,19 | 0,45 | 0,36 |
| 39 | -0,27 | 0,53 | -0,32 | 91 | 0,25 | 0,49 | 0,42 |
| 46 | -0,29 | 0,56 | -0,31 | 100 | 0,29 | 0,53 | 0,50 |
| 53 | -0,31 | 0,60 | -0,35 | 114 | 0,31 | 0,57 | 0,52 |
| 58 | -0,29 | 0,62 | -0,34 | 125 | 0,33 | 0,61 | 0,55 |
| 71 | -0,28 | 0,65 | -0,34 | 136 | 0,40 | 0,64 | 0,60 |
| 79 | -0,27 | 0,67 | -0,33 | 149 | 0,43 | 0,66 | 0,64 |
| 84 | -0,27 | 0,68 | -0,32 | 159 | 0,48 | 0,68 | 0,73 |
| 95 | -0,25 | 0,70 | -0,29 | 172 | 0,59 | 0,69 | 0,82 |
| 101 | -0,23 | 0,70 | -0,27 | 182 | 0,71 | 0,77 | 0,96 |
| 109 | -0,20 | 0,71 | -0,27 | 191 | 0,88 | 0,81 | 1,12 |
| 116 | -0,17 | 0,72 | -0,24 | 196 | 0,94 | 0,80 | 1,22 |
| 123 | -0,14 | 0,73 | -0,19 | 204 | 1,14 | 0,83 | 1,40 |
| 131 | -0,10 | 0,74 | -0,16 | 211 | 1,36 | 0,85 | 1,63 |
| 139 | -0,06 | 0,75 | -0,17 | 216 | 1,78 | 0,86 | 1,93 |
| 148 | 0,01 | 0,77 | -0,11 | 216 | 2,67 | 1,03 | 2,47 |
| 153 | 0,02 | 0,78 | -0,08 | 207 | 3,43 | 1,30 | 2,99 |
| 159 | 0,09 | 0,78 | -0,07 | 205 | 4,96 | 2,10 | 4,16 |
| 165 | 0,13 | 0,79 | -0,04 | 202 | 5,62 | 2,53 | 4,75 |
| 171 | 0,20 | 0,80 | 0,01 | 200 | 6,30 | 2,96 | 5,33 |
| 180 | 0,26 | 0,81 | 0,08 | 195 | 6,80 | 3,47 | 5,79 |
| 183 | 0,32 | 0,81 | 0,14 | 194 | 7,28 | 3,76 | 6,19 |
| 190 | 0,36 | 0,80 | 0,22 | 190 | 7,70 | 4,05 | 6,58 |
| 194 | 0,41 | 0,80 | 0,26 | 188 | 8,06 | 0,00 | 6,92 |
| 197 | 0,52 | 0,80 | 0,36 | 184 | 8,45 | 0,00 | 7,26 |
| 204 | 0,56 | 0,80 | 0,47 | 183 | 8,82 | 0,00 | 7,52 |
| 208 | 0,65 | 0,80 | 0,54 | 180 | 9,20 | 0,00 | 7,84 |

| | | | | | | | |
|-----|------|-------|------|-----|-------|------|-------|
| 212 | 0,69 | 0,80 | 0,65 | 178 | 9,57 | 0,00 | 8,14 |
| 216 | 0,75 | 0,77 | 0,78 | 175 | 10,09 | 0,00 | 8,55 |
| 218 | 0,77 | 0,76 | 1,10 | 176 | 10,69 | 0,00 | 9,01 |
| 219 | 0,74 | 0,79 | 2,00 | 172 | 11,28 | 0,00 | 9,41 |
| 218 | 0,67 | 1,05 | 2,95 | 170 | 11,69 | 0,00 | 9,75 |
| 218 | 0,56 | 1,54 | 3,67 | 169 | 12,16 | 0,00 | 10,05 |
| 216 | 0,45 | 2,23 | 4,26 | 167 | 12,50 | 0,00 | 10,33 |
| 214 | 0,35 | 3,36 | 4,83 | 163 | 12,88 | 0,00 | 10,61 |
| 212 | 0,28 | 4,25 | 5,29 | 163 | 13,26 | 0,00 | 10,91 |
| 209 | 0,22 | 5,08 | 5,68 | 160 | 13,49 | 0,00 | 11,07 |
| 207 | 0,20 | 5,80 | 6,04 | 163 | 13,82 | 0,00 | 11,35 |
| 205 | 0,20 | 6,50 | 6,31 | 159 | 14,14 | 0,00 | 11,57 |
| 202 | 0,30 | 7,09 | 6,62 | 159 | 14,46 | 0,00 | 11,81 |
| 201 | 0,39 | 7,63 | 6,85 | 157 | 14,74 | 0,00 | 12,02 |
| 200 | 0,53 | 8,13 | 7,05 | 156 | 15,05 | 0,00 | 12,28 |
| 199 | 0,74 | 8,55 | 7,27 | 155 | 15,32 | 0,00 | 12,48 |
| 196 | 0,99 | 9,00 | 7,47 | 153 | 15,62 | 0,00 | 12,69 |
| 193 | 1,27 | 9,36 | 7,66 | 153 | 15,92 | 0,00 | 12,91 |
| 193 | 1,62 | 9,72 | 7,83 | 151 | 16,24 | 0,00 | 13,13 |
| 191 | 1,94 | 10,00 | 8,03 | 150 | 16,57 | 0,00 | 13,38 |
| 190 | 2,28 | 10,31 | 8,18 | 148 | 16,85 | 0,00 | 13,61 |
| 188 | 2,65 | 10,54 | 8,34 | 148 | 17,11 | 0,00 | 13,80 |
| 187 | 2,97 | 10,76 | 8,52 | 57 | 15,24 | 0,00 | 12,26 |
| 66 | 2,37 | 10,89 | 8,05 | 1 | 14,00 | 0,00 | 11,48 |

C.5.2 Tests A3 and B1

| Test A3 | | Test B1 | |
|-----------|-----------------|-----------|-----------------|
| Load [kN] | W _{P1} | Load [kN] | W _{P1} |
| 36 | 0,00 | 0 | 0,00 |
| 52 | 0,15 | 78 | -0,02 |
| 57 | 0,25 | 150 | 0,56 |
| 66 | 0,41 | 162 | 1,53 |
| 75 | 0,50 | 170 | 2,71 |
| 85 | 0,68 | 174 | 3,81 |
| 93 | 0,82 | 177 | 4,79 |
| 104 | 1,01 | 178 | 5,69 |
| 110 | 1,21 | 178 | 6,55 |
| 121 | 1,45 | 176 | 7,35 |
| 129 | 1,78 | 174 | 8,08 |
| 137 | 2,17 | 172 | 8,76 |
| 147 | 2,72 | 170 | 9,39 |
| 154 | 3,25 | 168 | 9,99 |
| 159 | 3,93 | 166 | 10,55 |
| 167 | 4,67 | 164 | 11,09 |
| 169 | 5,47 | 161 | 11,61 |
| 174 | 6,28 | 159 | 12,11 |
| 176 | 7,23 | 156 | 12,60 |
| 179 | 8,40 | 154 | 13,08 |
| 182 | 9,44 | | |
| 180 | 10,58 | | |
| 180 | 11,76 | | |
| 177 | 12,93 | | |
| 177 | 13,79 | | |
| 178 | 14,71 | | |
| 174 | 15,59 | | |
| 173 | 16,20 | | |
| 173 | 16,71 | | |
| 169 | 17,21 | | |
| 173 | 17,82 | | |
| 166 | 18,18 | | |
| 1 | 12,27 | | |

C.5.3 Tests B2 and B3

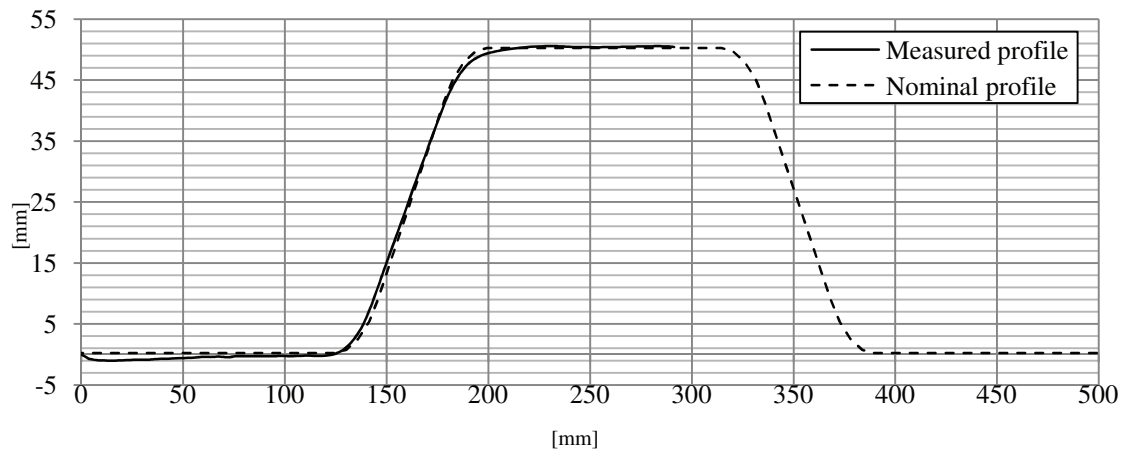
| Test B2 | | | | Test B3 | | |
|-----------|-------|------|-------|-----------|------|-------|
| Load [kN] | WP1 | WP2 | WP3 | Load [kN] | WP2 | WP3 |
| 2 | 0,00 | 0,00 | 0,00 | 0 | 0,00 | 0,00 |
| 8 | 1,38 | 1,31 | 1,29 | 17 | 0,24 | 0,30 |
| 12 | 1,45 | 1,40 | 1,36 | 49 | 0,95 | 1,06 |
| 10 | 1,42 | 1,36 | 1,33 | 66 | 1,05 | 1,17 |
| 19 | 1,75 | 1,69 | 1,69 | 83 | 1,13 | 1,27 |
| 20 | 1,90 | 1,82 | 1,74 | 113 | 1,24 | 1,41 |
| 21 | 1,96 | 1,87 | 1,82 | 130 | 1,30 | 1,46 |
| 42 | 2,81 | 2,67 | 2,53 | 143 | 1,36 | 1,53 |
| 70 | 3,14 | 3,00 | 2,94 | 172 | 1,48 | 1,60 |
| 100 | 3,29 | 3,13 | 3,09 | 185 | 1,52 | 1,63 |
| 114 | 3,36 | 3,19 | 3,18 | 200 | 1,59 | 1,63 |
| 128 | 3,51 | 3,29 | 3,35 | 209 | 1,65 | 1,61 |
| 146 | 3,67 | 3,43 | 3,52 | 219 | 1,77 | 1,52 |
| 157 | 3,82 | 3,59 | 3,68 | 219 | 1,89 | 1,43 |
| 168 | 3,90 | 3,62 | 3,82 | 219 | 1,99 | 1,35 |
| 186 | 4,13 | 3,74 | 4,05 | 219 | 2,07 | 1,27 |
| 200 | 4,42 | 3,76 | 4,46 | 219 | 2,14 | 1,22 |
| 208 | 4,77 | 3,62 | 5,12 | 219 | 2,18 | 1,15 |
| 213 | 5,05 | 3,43 | 5,97 | 219 | 2,23 | 1,10 |
| 211 | 5,39 | 3,24 | 6,86 | 219 | 2,27 | 1,05 |
| 208 | 5,89 | 3,28 | 7,74 | 219 | 2,32 | 0,98 |
| 204 | 6,56 | 3,48 | 8,44 | 219 | 2,37 | 0,94 |
| 200 | 7,34 | 3,83 | 9,18 | 219 | 2,40 | 0,85 |
| 193 | 8,04 | 4,23 | 9,76 | 219 | 2,47 | 0,81 |
| 190 | 8,81 | 4,65 | 10,38 | 107 | 2,30 | 0,59 |
| 187 | 9,53 | 5,07 | 10,91 | 127 | 2,39 | 0,61 |
| 184 | 9,87 | 5,26 | 11,17 | 146 | 2,46 | 0,62 |
| 183 | 10,51 | 5,64 | 11,64 | 167 | 2,51 | 0,61 |
| 180 | 11,10 | 5,98 | 12,11 | 188 | 2,55 | 0,61 |
| 178 | 11,72 | 6,29 | 12,52 | 205 | 2,60 | 0,61 |
| 175 | 12,30 | 6,60 | 12,92 | 219 | 2,64 | 0,58 |
| 173 | 12,87 | 6,90 | 13,33 | 219 | 2,74 | 0,47 |
| 172 | 13,44 | 0,00 | 13,70 | 185 | 6,53 | -4,76 |
| 169 | 14,01 | 0,00 | 14,14 | 180 | 7,41 | -6,22 |
| 167 | 14,55 | 0,00 | 14,52 | 173 | 8,04 | -7,30 |
| 167 | 15,15 | 0,00 | 14,93 | 170 | 8,50 | -8,25 |

| | | | | | | |
|-----|-------|------|-------|-----|------|--------|
| 165 | 15,68 | 0,00 | 15,33 | 166 | 8,82 | -9,09 |
| 163 | 16,21 | 0,00 | 15,67 | 166 | 9,07 | -9,74 |
| 159 | 16,84 | 0,00 | 16,11 | 163 | 9,29 | -10,47 |
| 159 | 17,45 | 0,00 | 16,51 | 162 | 9,43 | -11,16 |
| 154 | 18,09 | 0,00 | 16,93 | 159 | 9,52 | -11,88 |
| 153 | 18,64 | 0,00 | 17,33 | 153 | 9,55 | -12,58 |
| 150 | 19,18 | 0,00 | 17,68 | 154 | 9,48 | -13,27 |
| 148 | 19,78 | 0,00 | 18,07 | 150 | 9,31 | -13,96 |
| 146 | 20,32 | 0,00 | 18,44 | 146 | 9,02 | -14,72 |
| 144 | 20,94 | 0,00 | 18,80 | 142 | 8,61 | -15,50 |
| 142 | 21,49 | 0,00 | 19,15 | 139 | 8,11 | -16,33 |
| 138 | 22,08 | 0,00 | 19,51 | 132 | 7,58 | -17,07 |
| 138 | 22,62 | 0,00 | 19,82 | 129 | 7,11 | -17,77 |
| 135 | 23,12 | 0,00 | 20,17 | 129 | 6,70 | -18,41 |
| 133 | 23,65 | 0,00 | 20,45 | 124 | 6,38 | -18,93 |
| 131 | 24,08 | 0,00 | 20,77 | 123 | 6,09 | -19,47 |
| 132 | 24,55 | 0,00 | 21,08 | 123 | 5,88 | -19,93 |
| 132 | 24,95 | 0,00 | 21,32 | 122 | 5,73 | -20,37 |
| 130 | 25,34 | 0,00 | 21,55 | 119 | 5,62 | -20,78 |

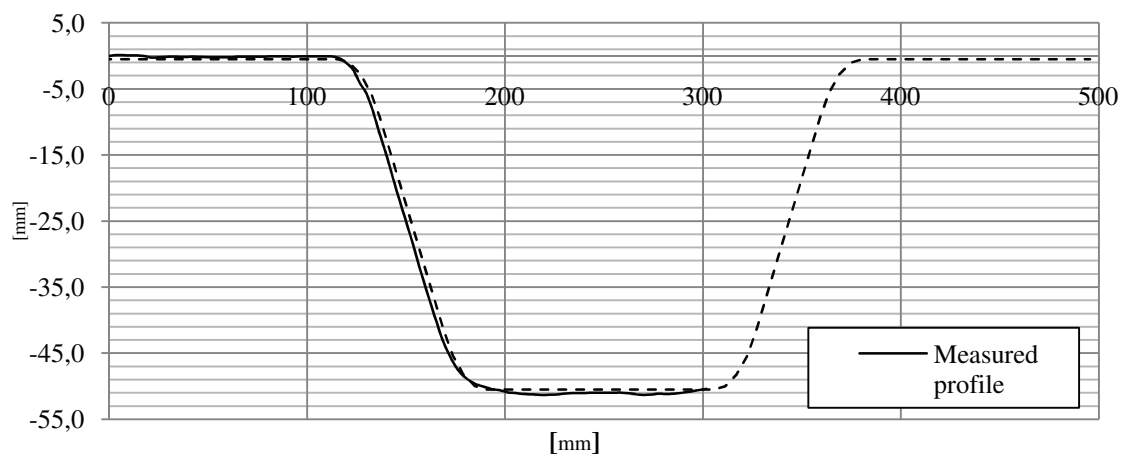
C.6 Initial imperfections

The true shape of the profile along the measuring path – shown in Figure 4.7 – is plotted against a nominal profile shape.

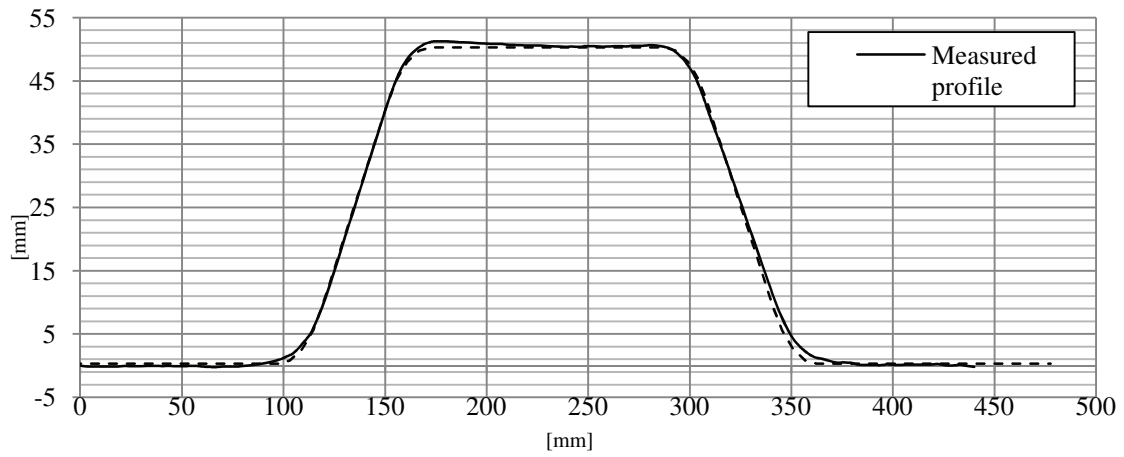
C.6.1 Test A1



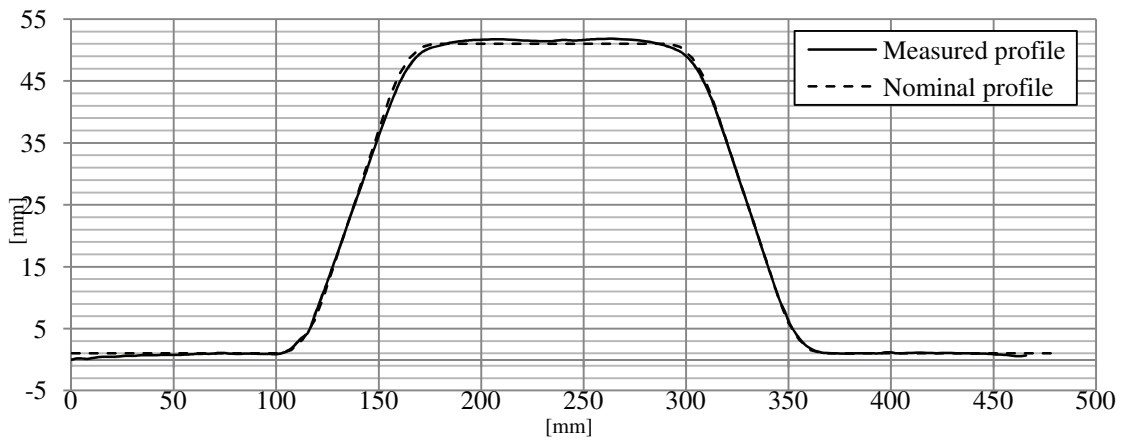
C.6.2 Test A2



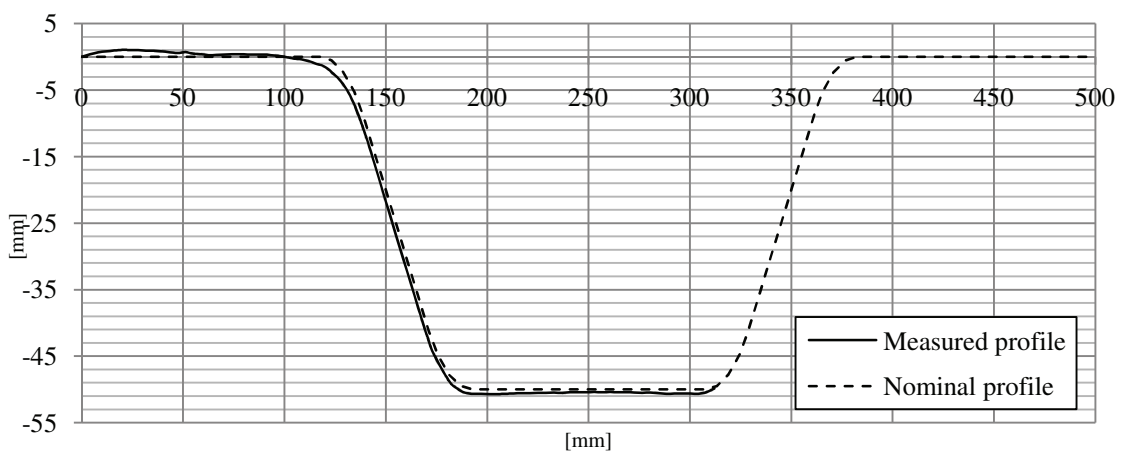
C.6.3 Test A3



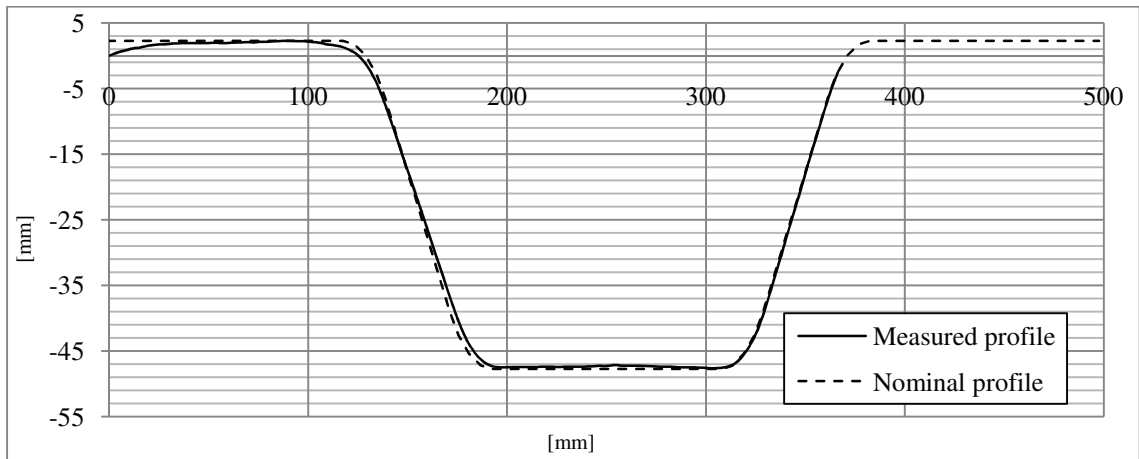
C.6.4 Test B1



C.6.5 Test B2



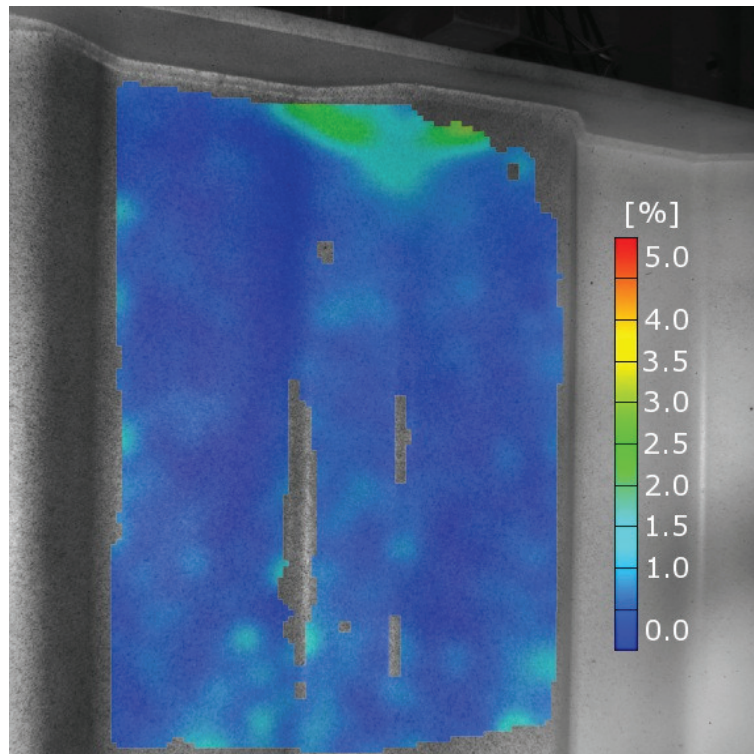
C.6.6 Test B3



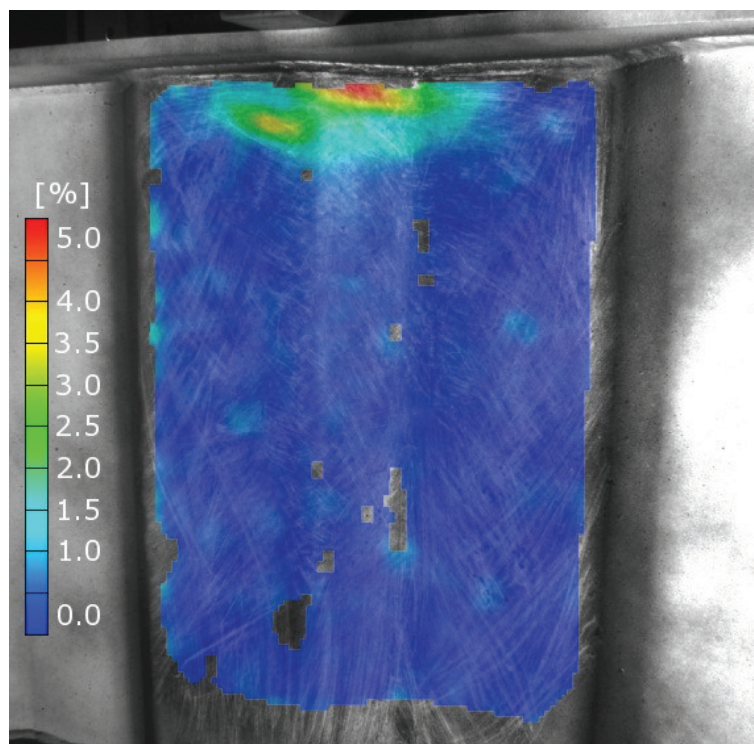
C.7 Strain contour-plots

In this section, contour-plots of the strains at maximum load are presented.

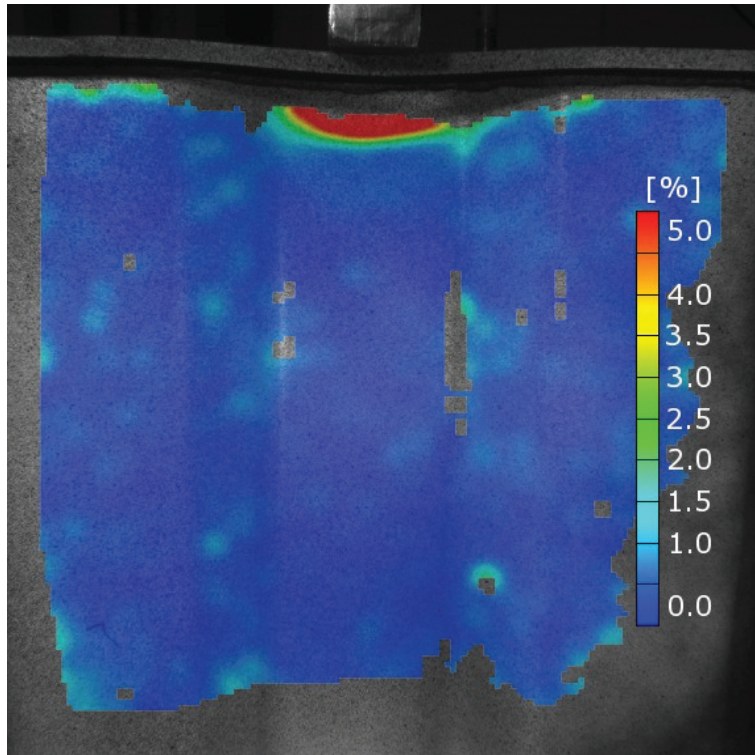
C.7.1 Test A1 – Loaded over an inclined fold



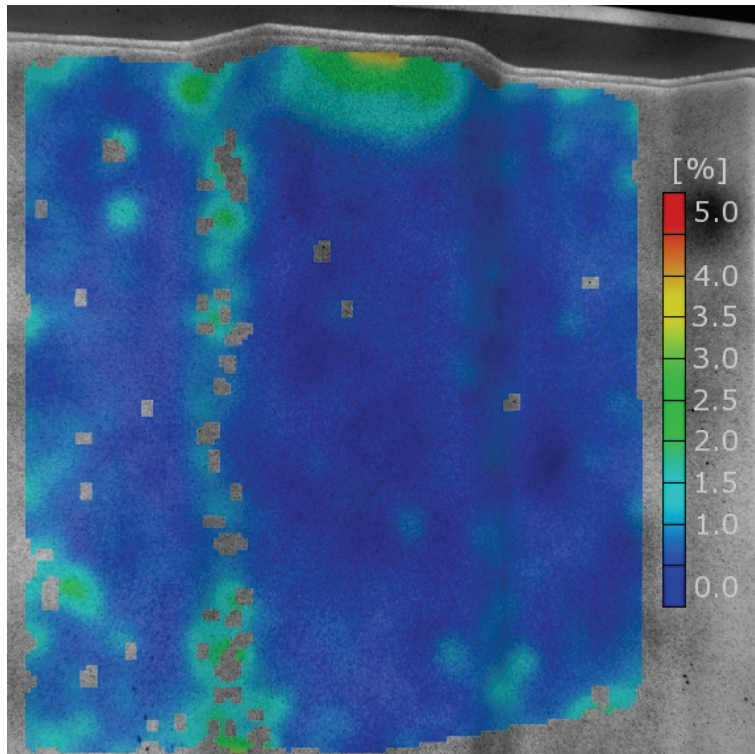
C.7.2 Test A2 – Loaded over a junction between two folds



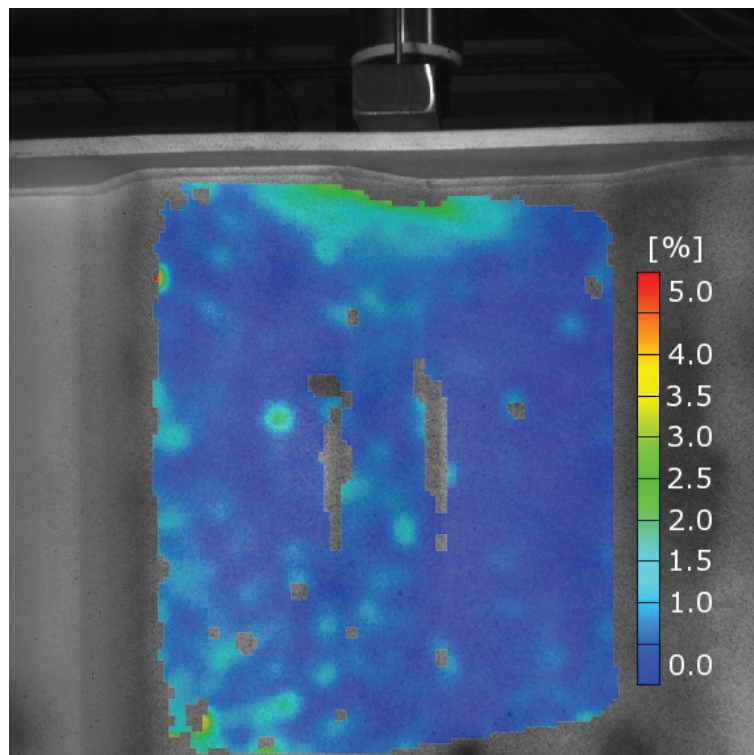
Test A3 – Loaded over a longitudinal fold



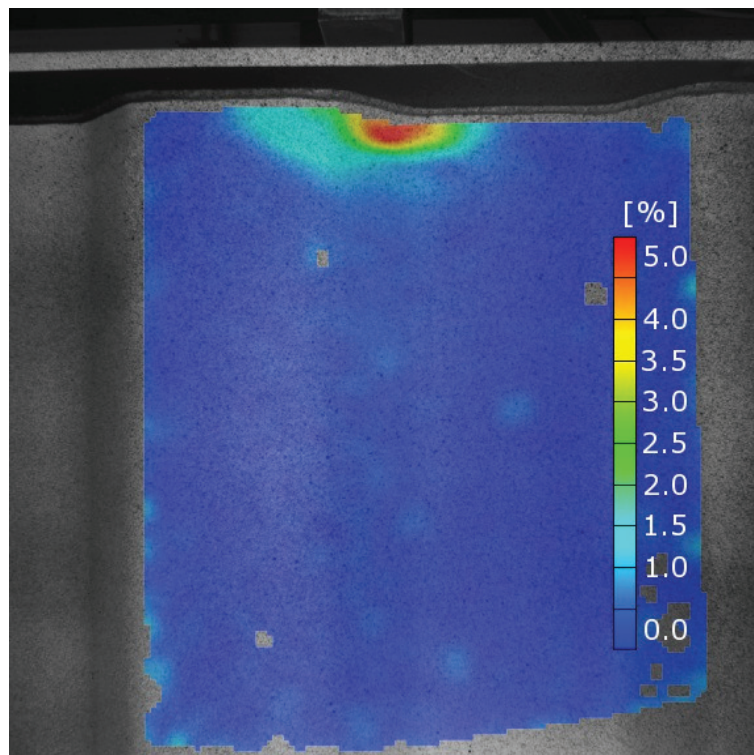
C.7.3 Test B1 – Loaded over a longitudinal fold



C.7.4 Test B2 – Loaded over a junction between two folds



C.7.5 Test B3 – Loaded over an inclined fold



APPENDIX D – Result obtained using ABAQUS CAE

| | | |
|----------|--------------------------------------|----|
| D.1 | Parameters | 1 |
| D.1.1 | Load over inclined fold | 1 |
| D.1.2 | Load over junction between two folds | 1 |
| D.1.3 | Load over longitudinal folds | 2 |
| D.2 | Results from the FE-anaslysis | 3 |
| D.2.1 | Load/ Vertical-deformation diagrams | 3 |
| D.2.2 | Girder 100 | 3 |
| D.2.2.1 | Girder 101 | 3 |
| D.2.2.2 | Girder 102 | 4 |
| D.2.2.3 | Girder 103 | 4 |
| D.2.2.4 | Girder 104 | 4 |
| D.2.2.5 | Girder 105 | 5 |
| D.2.2.6 | Girder 106 | 5 |
| D.2.2.7 | Girder 107 | 5 |
| D.2.2.8 | Girder 108 | 6 |
| D.2.2.9 | Girder 109 | 6 |
| D.2.2.10 | Girder 200 | 6 |
| D.2.2.11 | Girder 201 | 7 |
| D.2.2.12 | Girder 202 | 7 |
| D.2.2.13 | Girder 203 | 7 |
| D.2.2.14 | Girder 204 | 8 |
| D.2.2.15 | Girder 205 | 8 |
| D.2.2.16 | Girder 206 | 8 |
| D.2.2.17 | Girder 207 | 9 |
| D.2.2.18 | Girder 208 | 9 |
| D.2.2.19 | Girder 209 | 9 |
| D.2.2.20 | Girder 300 | 10 |
| D.2.2.21 | Girder 301 | 10 |
| D.2.2.22 | Girder 302 | 10 |
| D.2.2.23 | Girder 303 | 11 |
| D.2.2.24 | Girder 304 | 11 |
| D.2.2.25 | Girder 305 | 11 |
| D.2.2.26 | Girder 306 | 12 |

| | | |
|----------|---|----|
| D.2.2.27 | Girder 307 | 12 |
| D.2.2.28 | Girder 308 | 12 |
| D.2.2.29 | Girder 309 | 13 |
| D.2.3 | Load/ Vertical-deformation data | 14 |
| D.2.3.1 | Girder 100-104 | 14 |
| D.2.3.2 | Girder 105-109 | 15 |
| D.2.3.3 | Girder 200-204 | 16 |
| D.2.3.4 | Girder 205-209 | 17 |
| D.2.3.5 | Girder 300-304 | 18 |
| D.2.3.6 | Girder 305-309 | 20 |
| D.2.4 | Load/ out-of-plane deformation diagrams | 21 |
| D.2.4.1 | Girder 100 | 21 |
| D.2.4.2 | Girder 200 | 22 |
| D.2.4.3 | Girder 300 | 24 |

D.1 Parameters

The dimensions and label on the girders that are used in the parametric study. Each job has a notation based on load case and in what order it is performed. The notation used is Girder 10X when loaded over an inclined fold, Girder 20X when loaded over a junction between two folds and 30X when loaded over a longitudinal fold. X varies from 0 to 9 with 0 representing a girder with same dimensions as the test girder for each load case. The detailed results from each job are presented in Appendix D and diagrams along with descriptions of the results are presented in chapter 5.

D.1.1 Load over inclined fold

| | t_{f1} 10 mm | t_{f3} 12 mm | t_{f4} 16 mm | t_{f5} 20 mm | t_{w1} 2 mm | t_{w2} 3 mm | t_{w3} 4 mm | e_{01} 0 mm | e_{01} 0,5 mm | e_{02} 1 mm | e_{03} 2 mm | e_{04} 5 mm |
|-----------------------|-------------------|-------------------|-------------------|-------------------|------------------|------------------|------------------|------------------|--------------------|------------------|------------------|------------------|
| Girder ₁₀₀ | | X | | | | X | | | X | | | |
| Girder ₁₀₁ | X | | | | | X | | | X | | | |
| Girder ₁₀₂ | | | X | | | X | | | X | | | |
| Girder ₁₀₃ | | | | X | | X | | | X | | | |
| Girder ₁₀₄ | | X | | | X | | | | X | | | |
| Girder ₁₀₅ | | X | | | | | X | | X | | | |
| Girder ₁₀₆ | | X | | | | X | | X | | | | |
| Girder ₁₀₇ | | X | | | | X | | | | X | | |
| Girder ₁₀₈ | | X | | | | X | | | | | X | |
| Girder ₁₀₉ | | X | | | | X | | | | | | X |

D.1.2 Load over junction between two folds

| | t_{f1} 10 mm | t_{f3} 12 mm | t_{f4} 16 mm | t_{f5} 20 mm | t_{w1} 2 mm | t_{w2} 3 mm | t_{w3} 4 mm | e_{01} 0 mm | e_{01} 0,5 mm | e_{02} 1 mm | e_{03} 2 mm | e_{04} 5 mm |
|-----------------------|-------------------|-------------------|-------------------|-------------------|------------------|------------------|------------------|------------------|--------------------|------------------|------------------|------------------|
| Girder ₂₀₀ | | X | | | | X | | | X | | | |
| Girder ₂₀₁ | X | | | | | X | | | X | | | |
| Girder ₂₀₂ | | | X | | | X | | | X | | | |
| Girder ₂₀₃ | | | | X | | X | | | X | | | |
| Girder ₂₀₄ | | X | | | X | | | | X | | | |
| Girder ₂₀₅ | | X | | | | | X | | X | | | |
| Girder ₂₀₆ | | X | | | | X | | X | | | | |
| Girder ₂₀₇ | | X | | | | X | | | | X | | |
| Girder ₂₀₈ | | X | | | | X | | | | | X | |
| Girder ₂₀₉ | | X | | | | X | | | | | | X |

D.1.3 Load over longitudinal folds

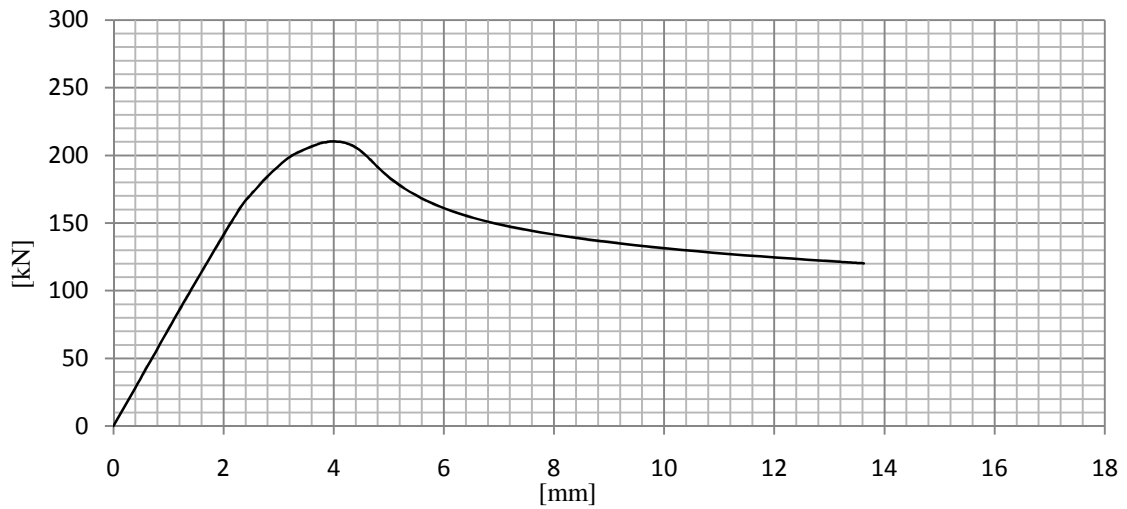
| | t_{f1} 10 mm | t_{f3} 12 mm | t_{f4} 16 mm | t_{f5} 20 mm | t_{w1} 2 mm | t_{w2} 3 mm | t_{w3} 4 mm | e_{01} 0 mm | e_{01} 0,5 mm | e_{02} 1 mm | e_{03} 2 mm | e_{04} 5 mm |
|-----------------------|-------------------|-------------------|-------------------|-------------------|------------------|------------------|------------------|------------------|--------------------|------------------|------------------|------------------|
| Girder ₃₀₀ | | X | | | | X | | | X | | | |
| Girder ₃₀₁ | X | | | | | X | | | X | | | |
| Girder ₃₀₂ | | | X | | | X | | | X | | | |
| Girder ₃₀₃ | | | | X | | X | | | X | | | |
| Girder ₃₀₄ | | X | | | X | | | | X | | | |
| Girder ₃₀₅ | | X | | | | | X | | X | | | |
| Girder ₃₀₆ | | X | | | | X | | X | | | | |
| Girder ₃₀₇ | | X | | | | X | | | | X | | |
| Girder ₃₀₈ | | X | | | | X | | | | | X | |
| Girder ₃₀₉ | | X | | | | X | | | | | | X |

D.2 Results from the FE-analysis

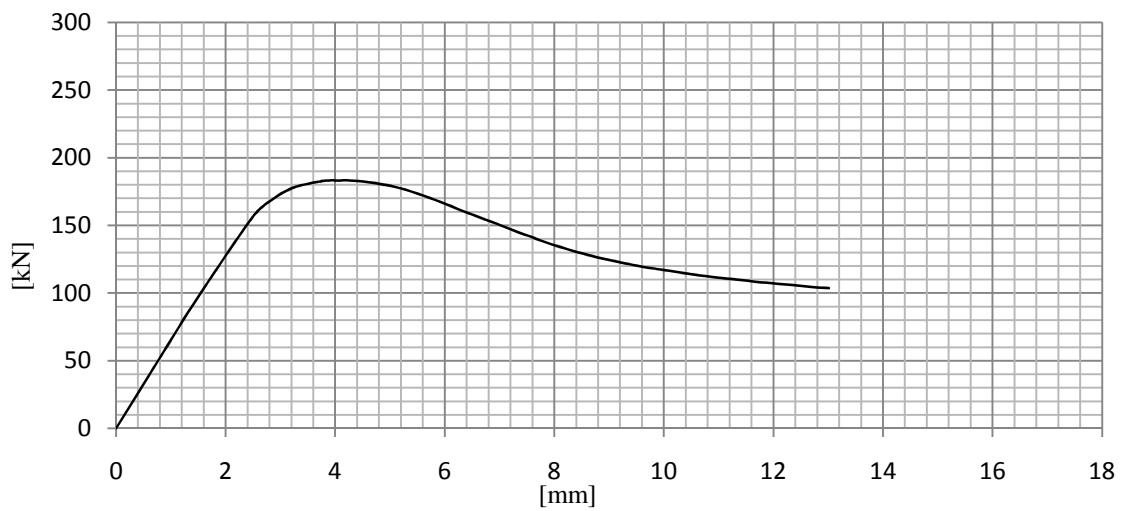
D.2.1 Load/ Vertical-deformation diagrams

In this section, load/deformation diagrams for each girder configuration are presented.

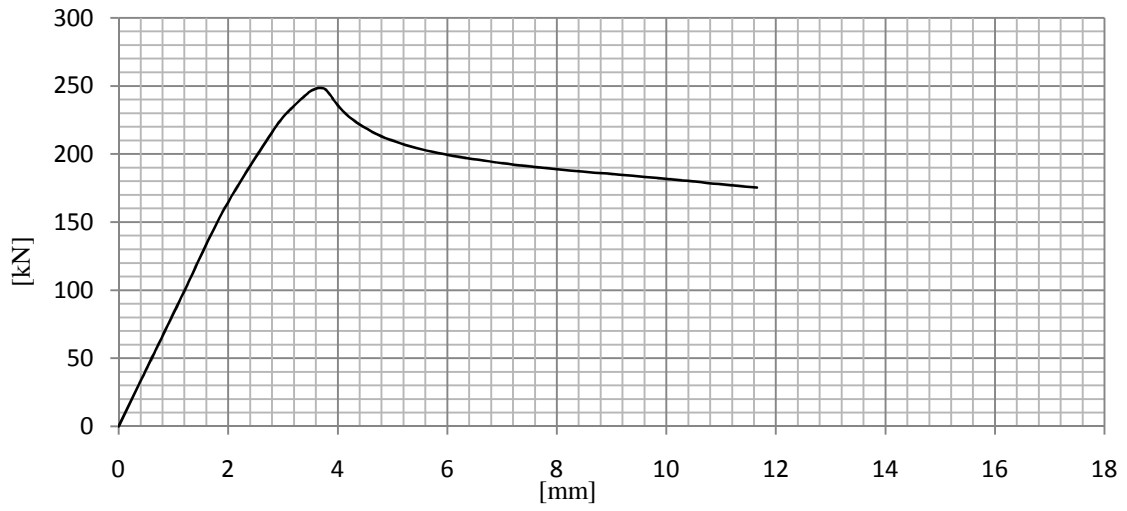
D.2.1.1 Girder 100



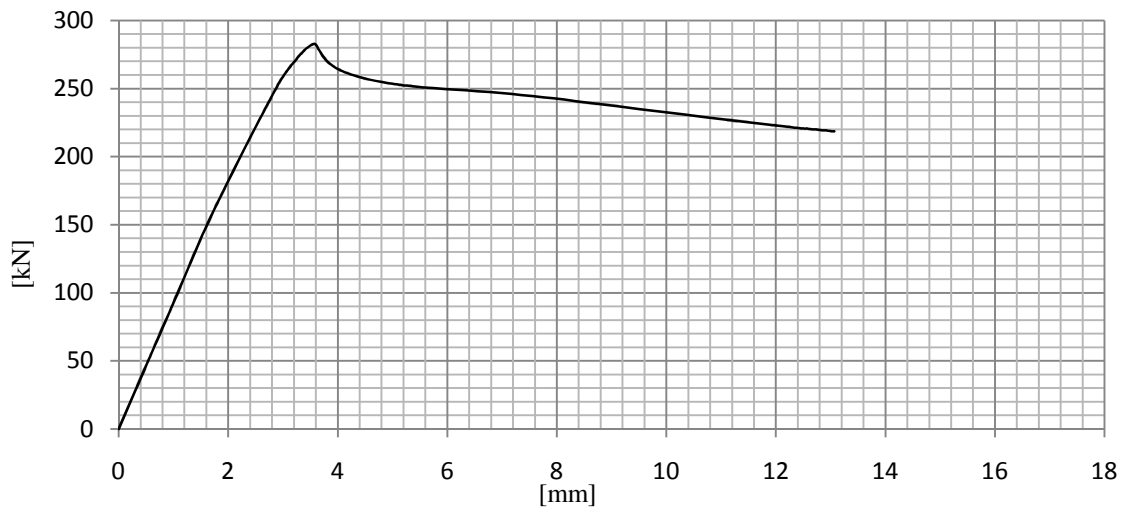
D.2.1.2 Girder 101



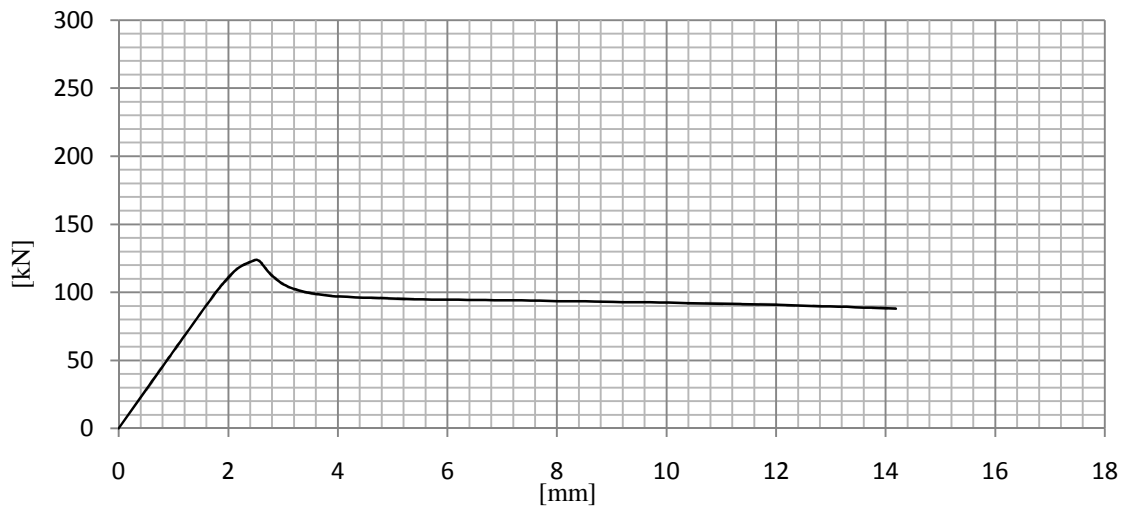
D.2.1.3 Girder 102



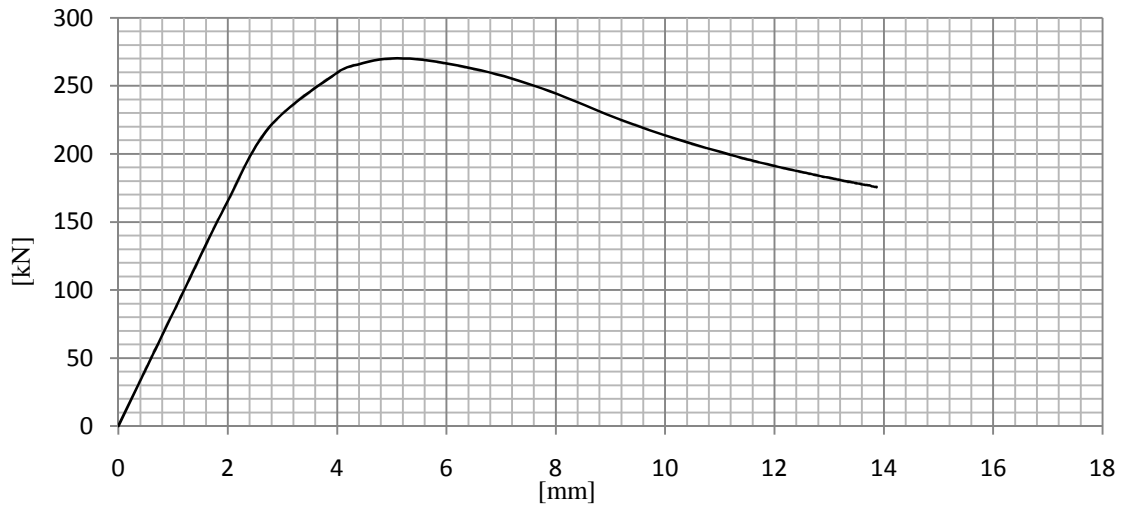
D.2.1.4 Girder 103



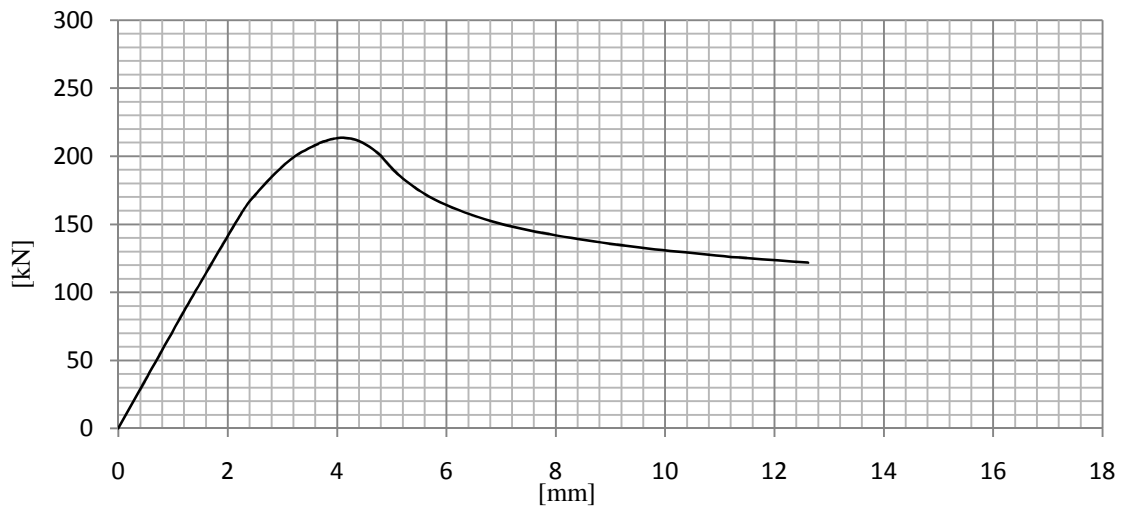
D.2.1.5 Girder 104



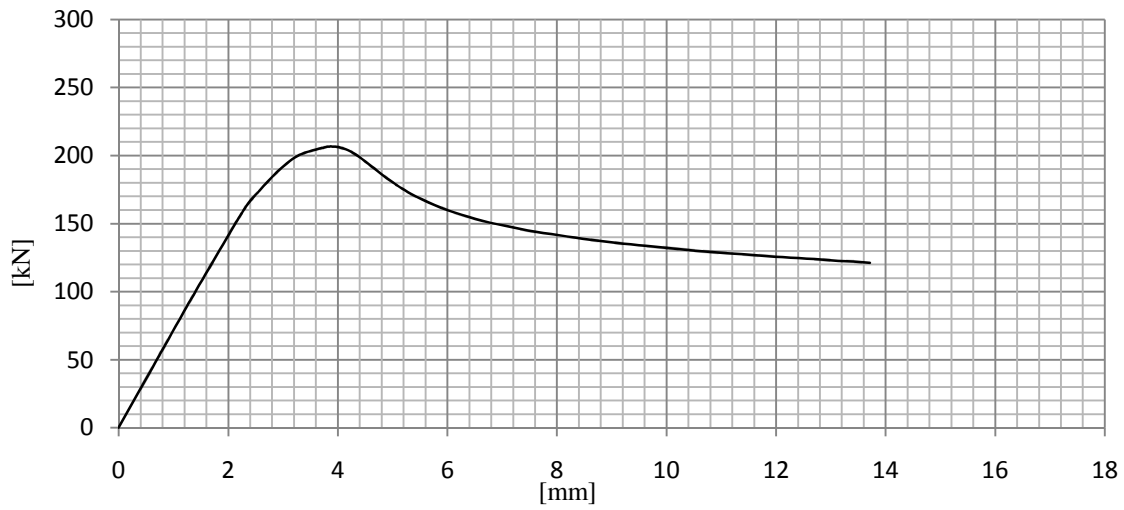
D.2.1.6 Girder 105



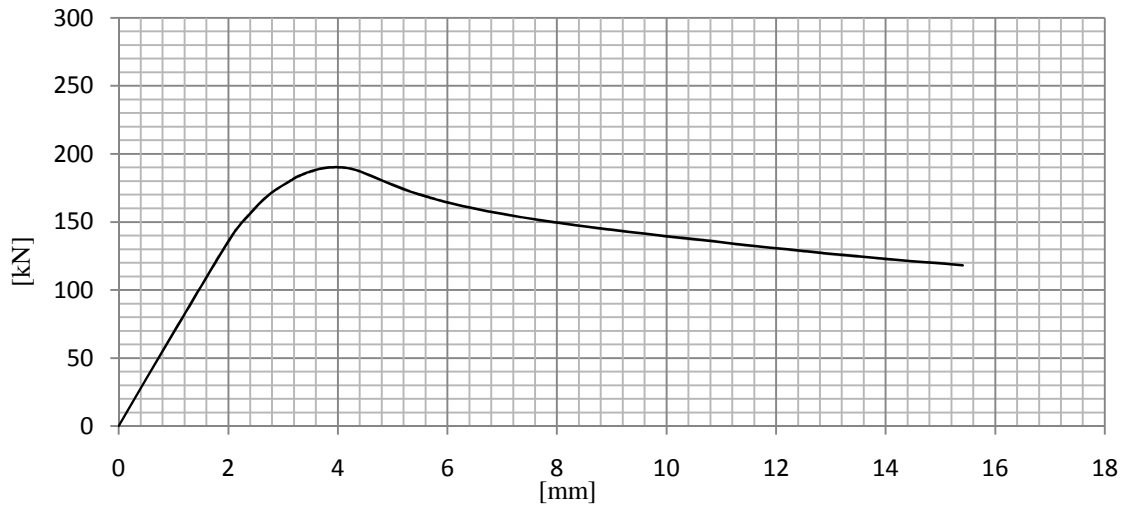
D.2.1.7 Girder 106



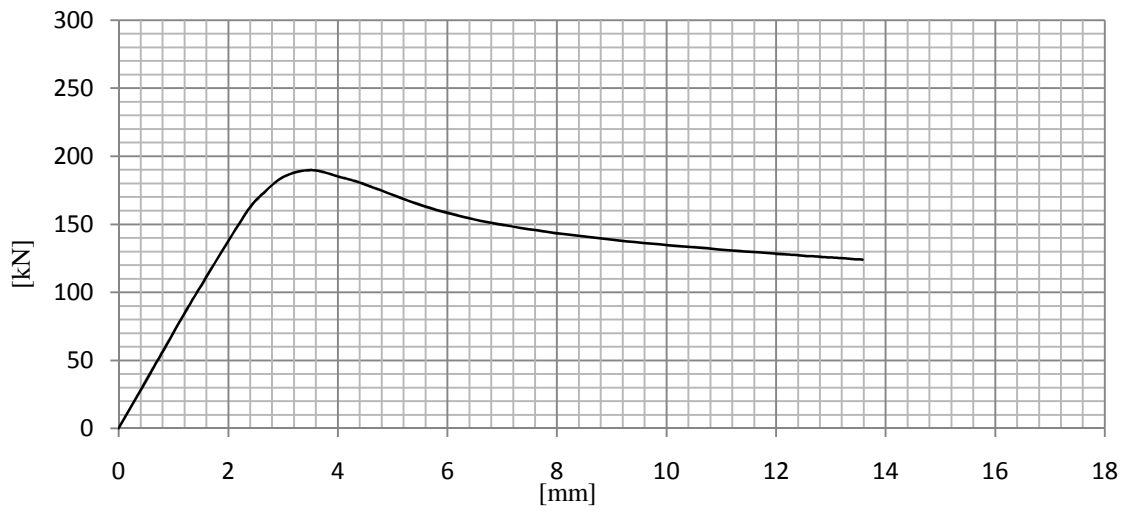
D.2.1.8 Girder 107



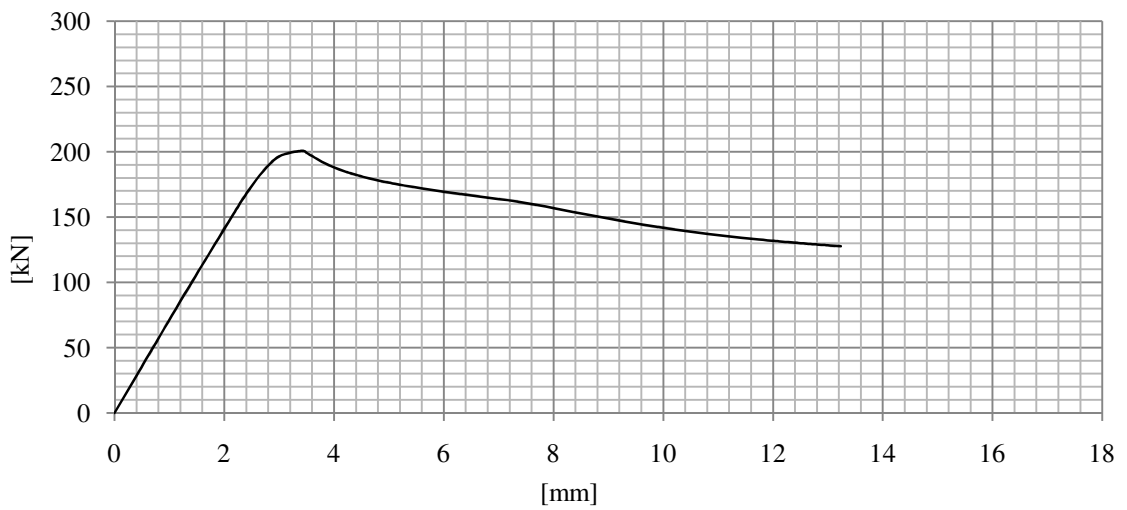
D.2.1.9 Girder 108



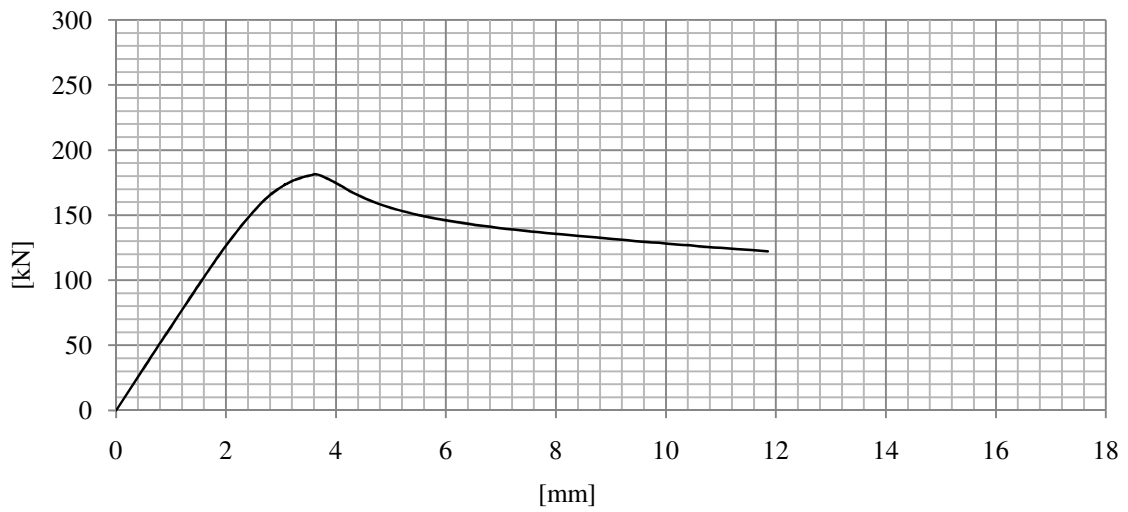
D.2.1.10 Girder 109



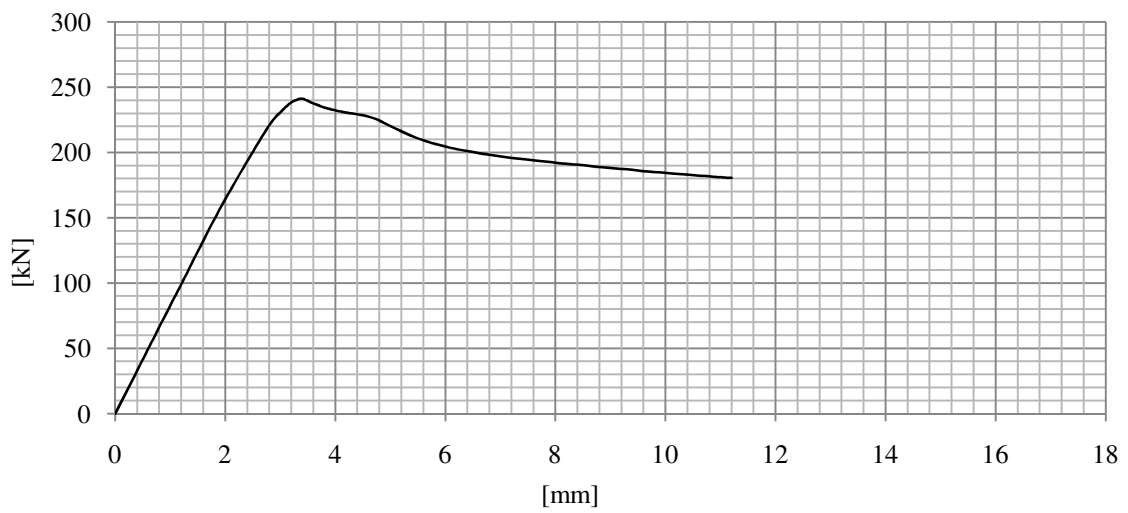
D.2.1.11 Girder 200



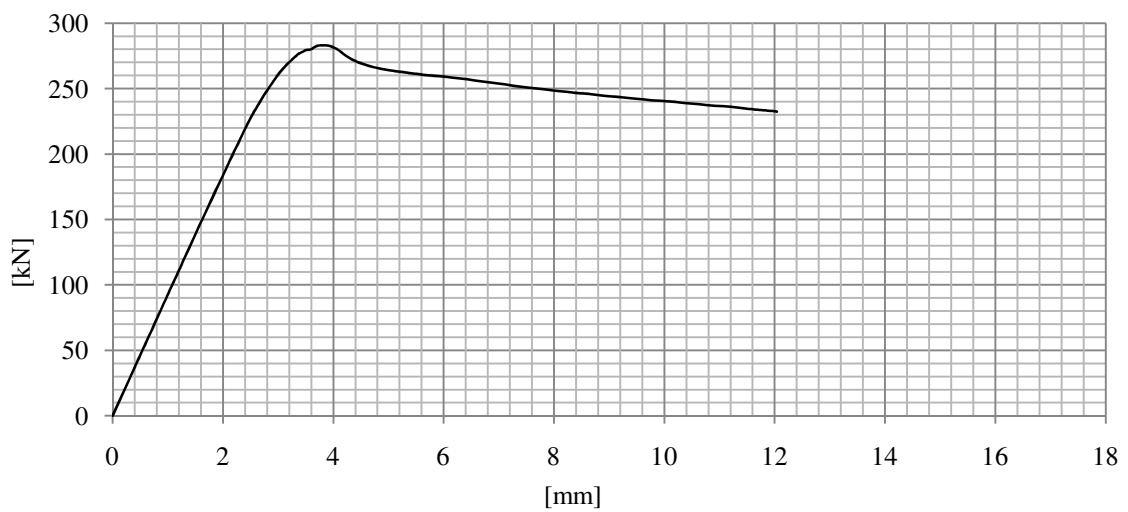
D.2.1.12 Girder 201



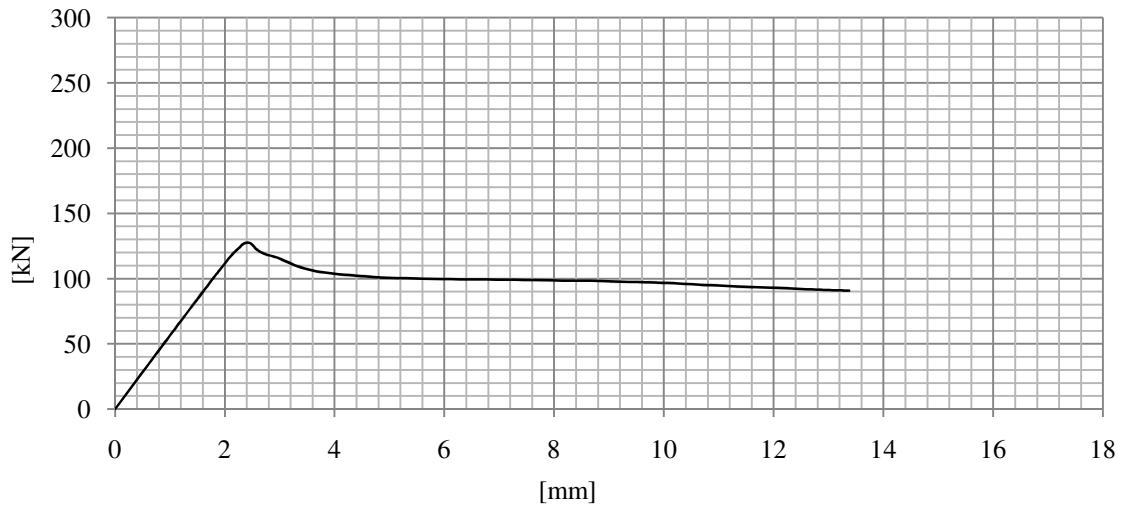
D.2.1.13 Girder 202



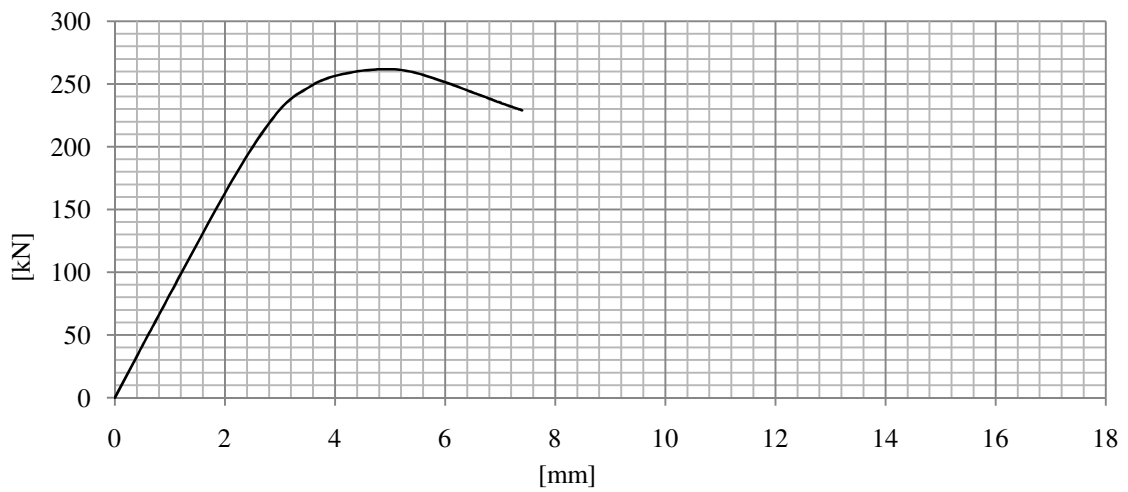
D.2.1.14 Girder 203



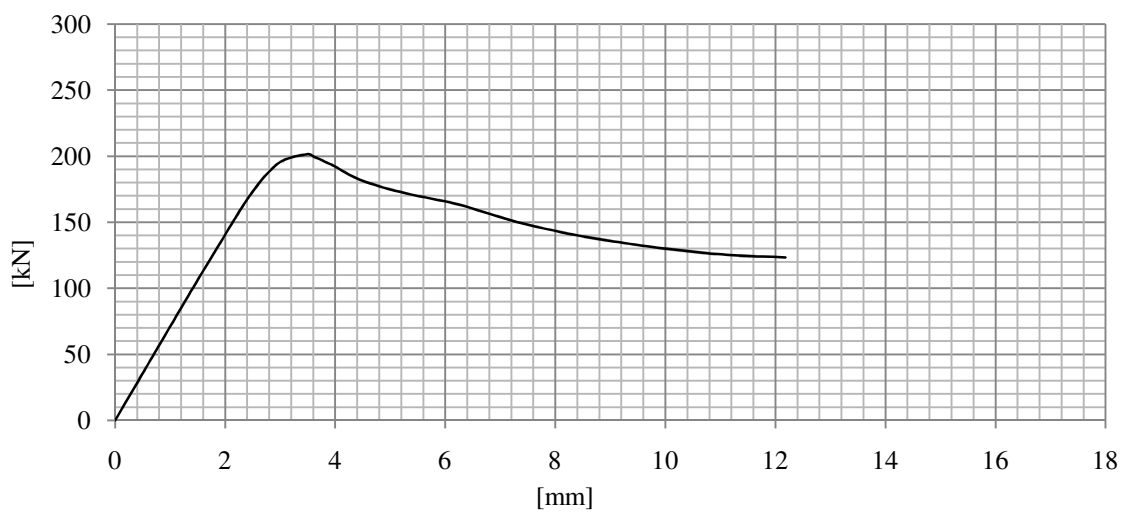
D.2.1.15 Girder 204



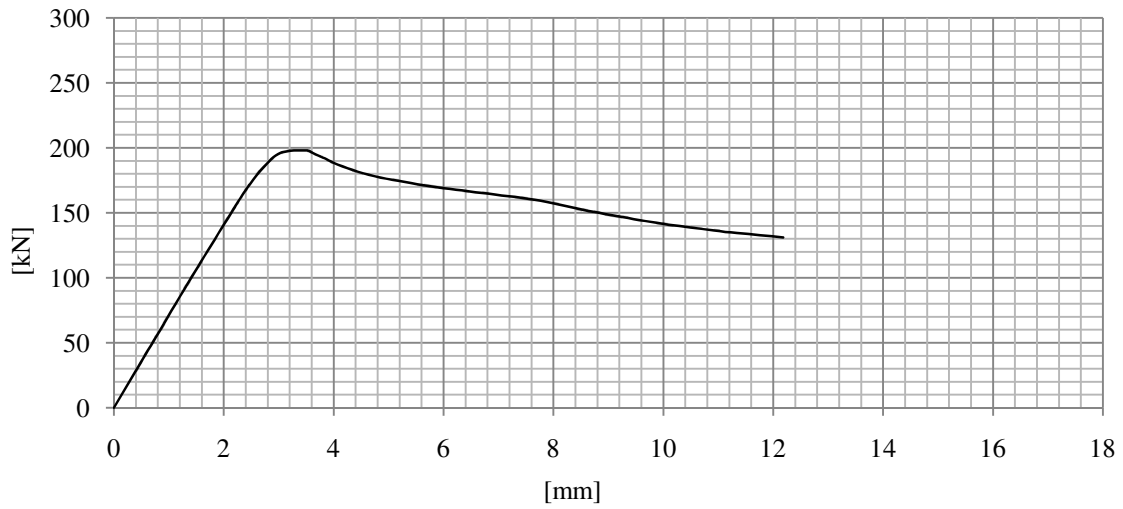
D.2.1.16 Girder 205



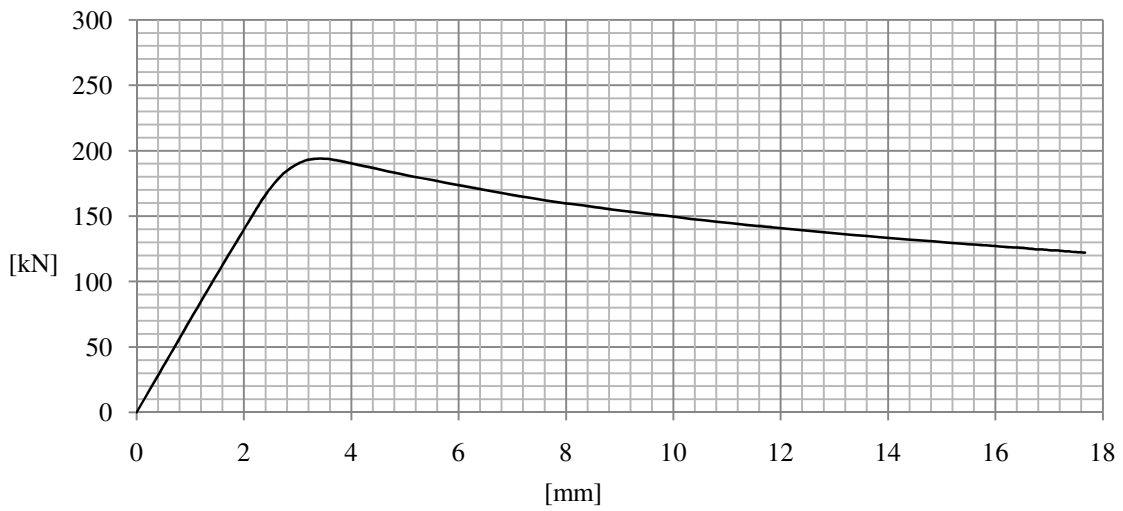
D.2.1.17 Girder 206



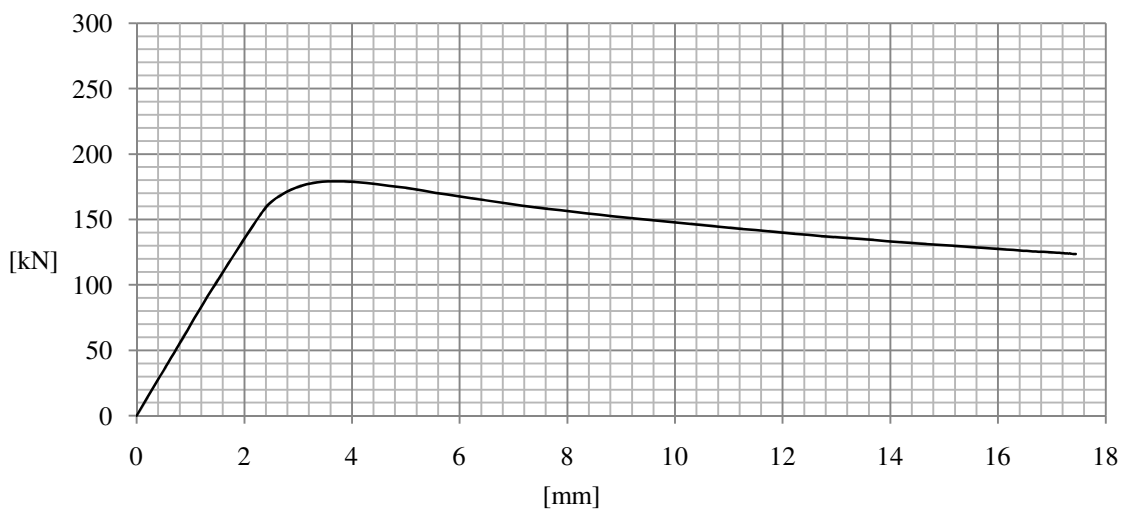
D.2.1.18 Girder 207



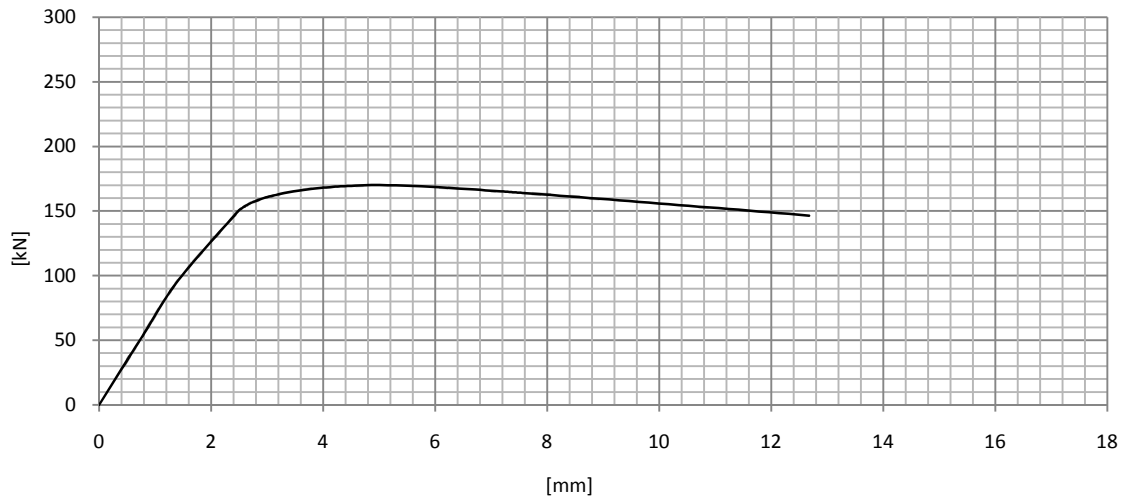
D.2.1.19 Girder 208



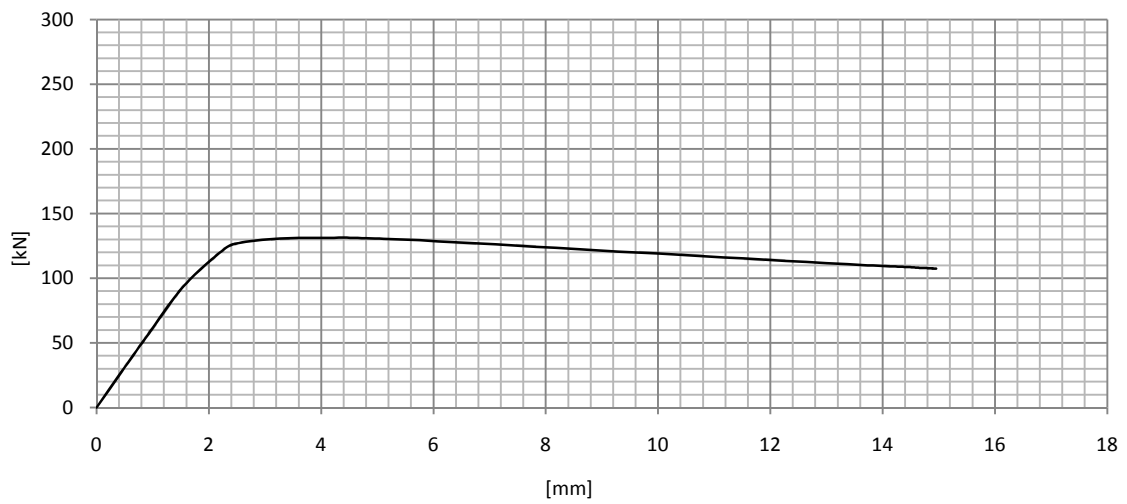
D.2.1.20 Girder 209



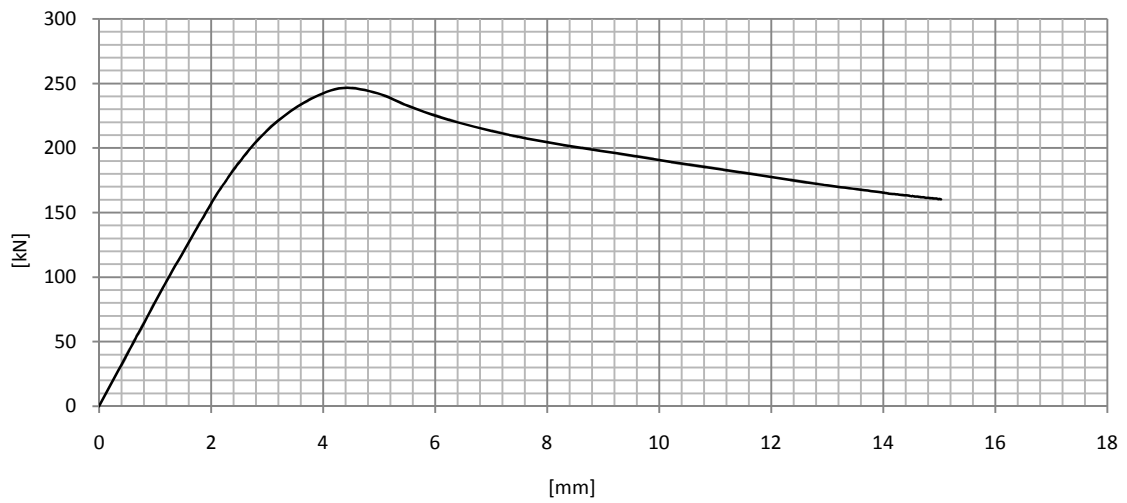
D.2.1.21 Girder 300



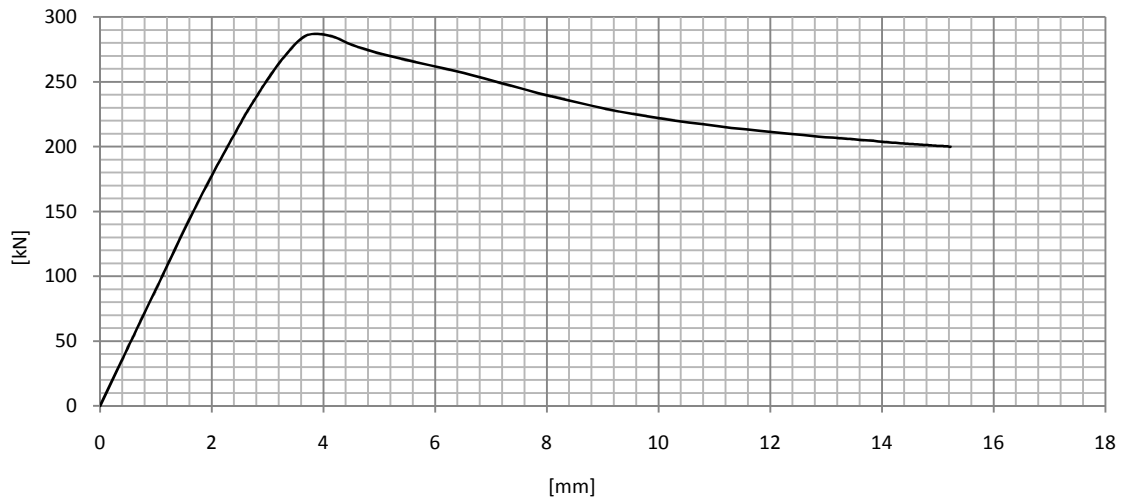
D.2.1.22 Girder 301



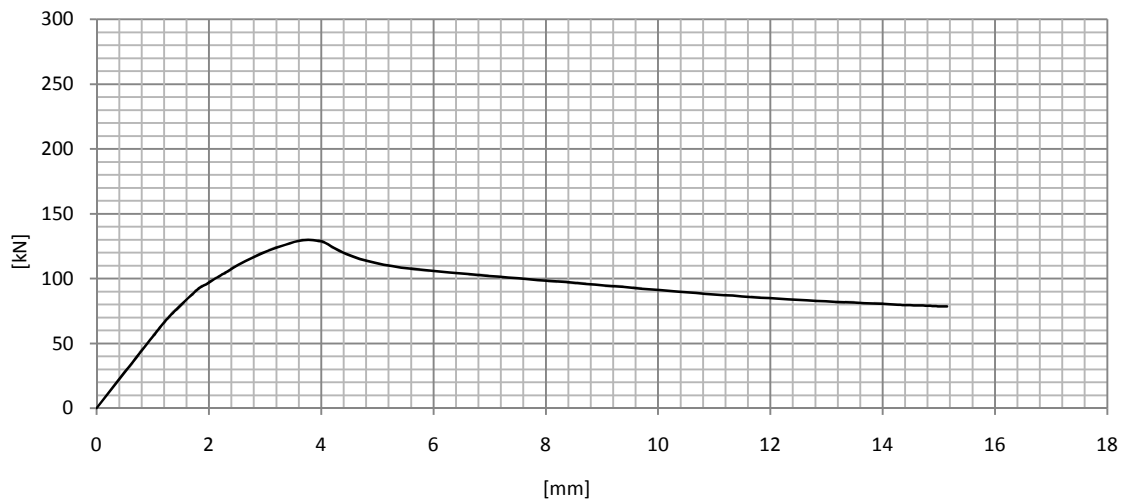
D.2.1.23 Girder 302



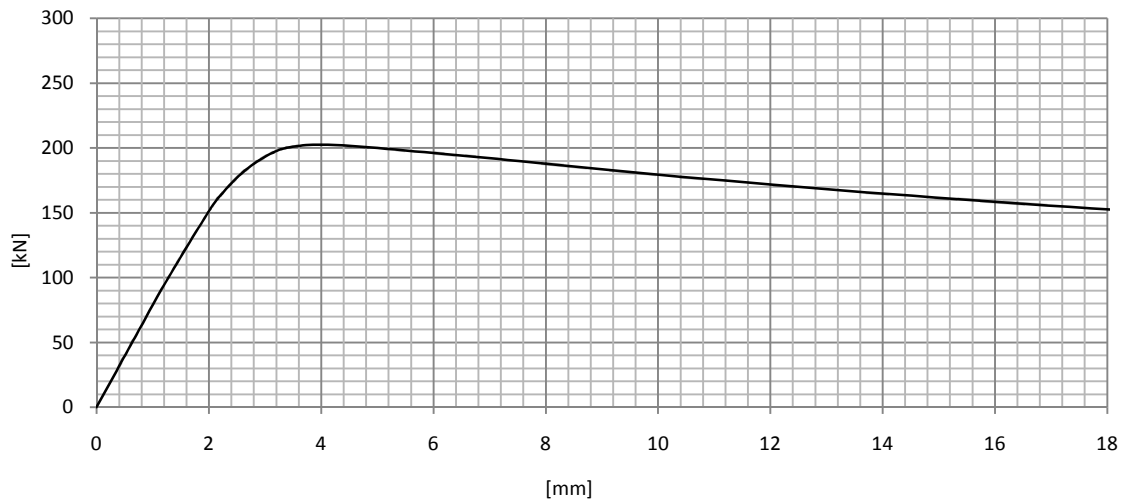
D.2.1.24 Girder 303



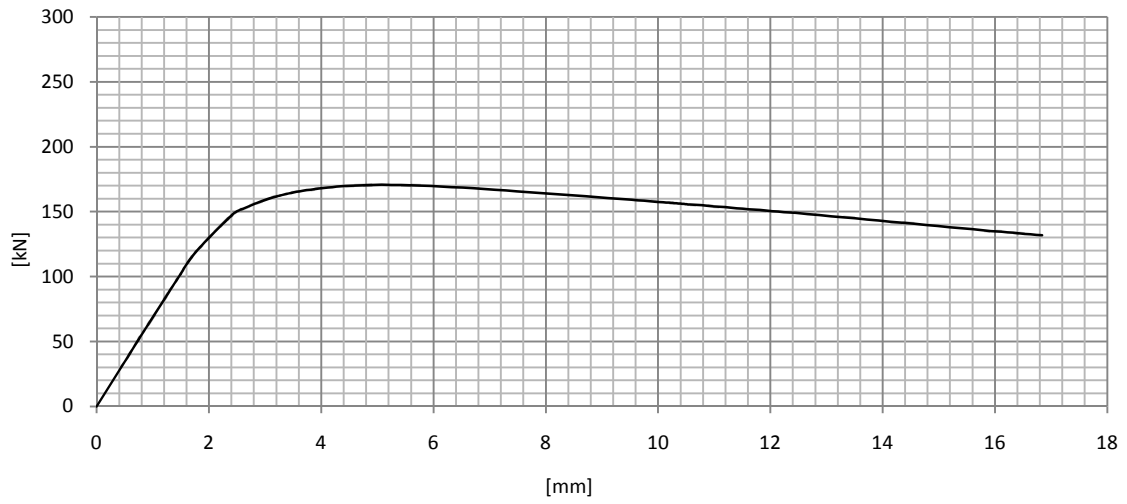
D.2.1.25 Girder 304



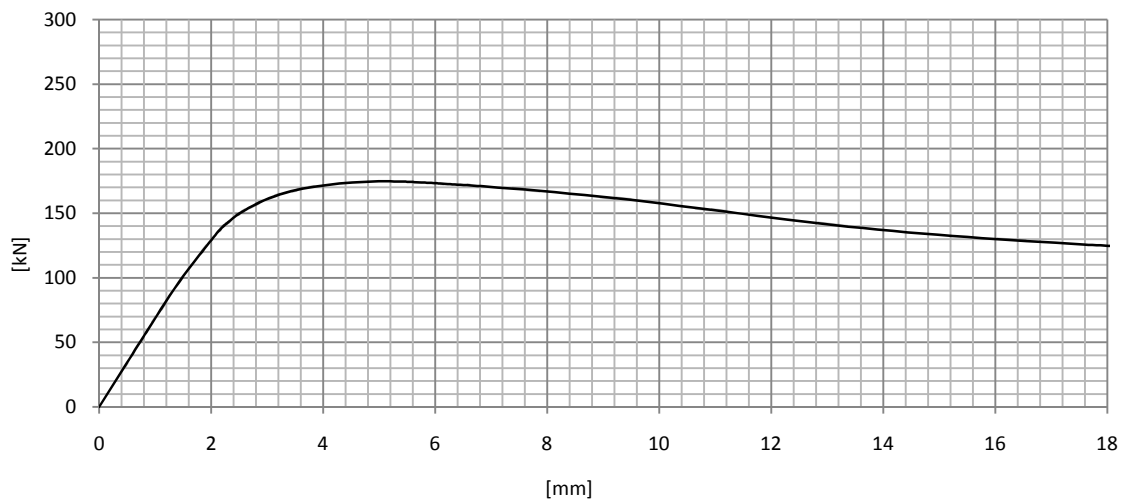
D.2.1.26 Girder 305



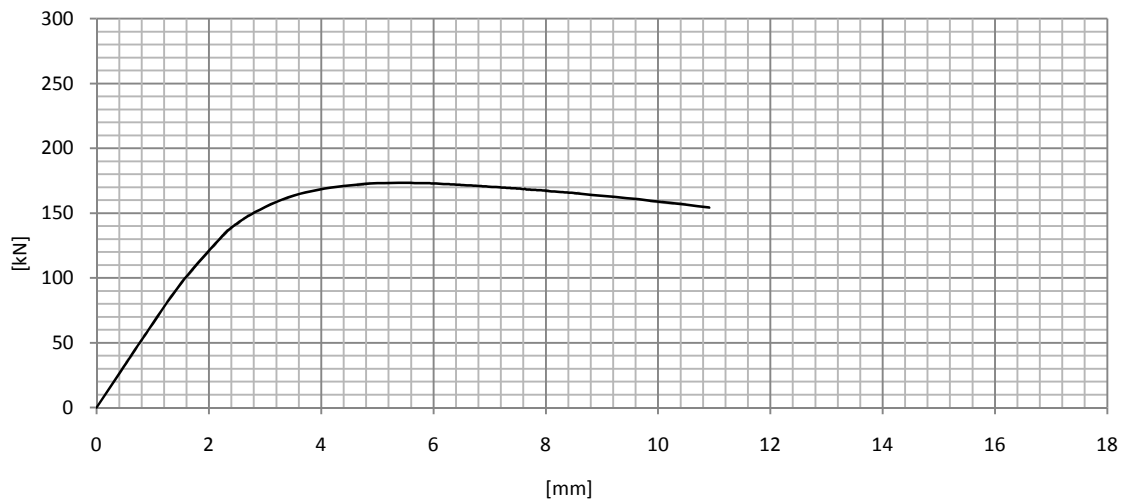
D.2.1.27 Girder 306



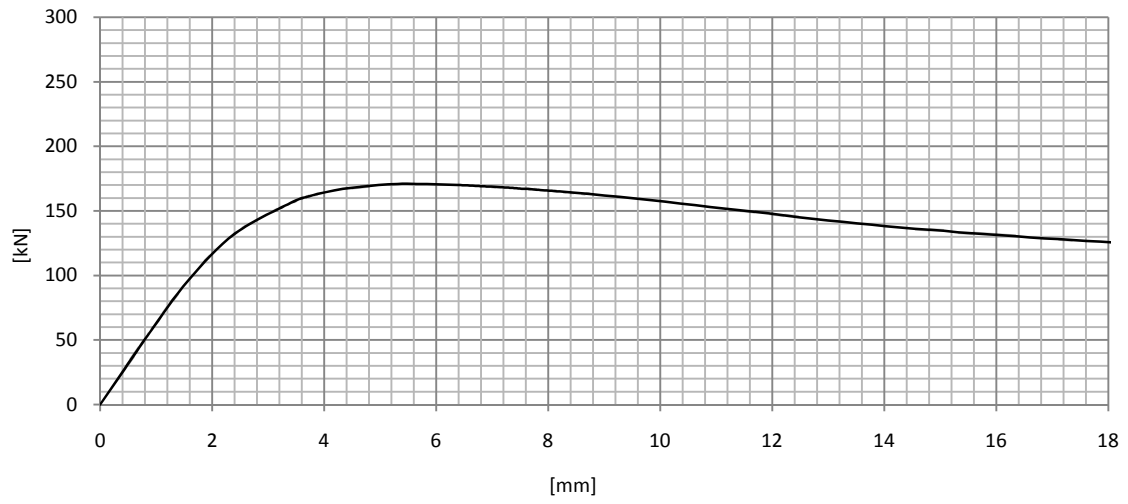
D.2.1.28 Girder 307



D.2.1.29 Girder 308



D.2.1.30 Girder 309



D.2.2 Load/ Vertical-deformation data

D.2.2.1 Girders 100-104

| Increment | Girder 100 | | Girder 101 | | Girder 102 | | Girder 103 | | Girder 104 | |
|-----------|------------|-----------|------------|-----------|------------|-----------|------------|-----------|------------|-----------|
| | Load [kN] | DEF. [mm] | Load [kN] | DEF. [mm] | Load [kN] | DEF. [mm] | Load [kN] | DEF. [mm] | Load [kN] | DEF. [mm] |
| 0 | 0,0 | 0,00 | 0,0 | 0,00 | 0,0 | 0,00 | 0,0 | 0,00 | 0,0 | 0,00 |
| 1 | 28,0 | 0,39 | 28,0 | 0,43 | 28,0 | 0,34 | 28,0 | 0,30 | 28,0 | 0,49 |
| 2 | 55,9 | 0,78 | 56,0 | 0,86 | 56,0 | 0,68 | 56,0 | 0,60 | 56,0 | 0,99 |
| 3 | 97,8 | 1,37 | 97,4 | 1,50 | 98,0 | 1,18 | 98,0 | 1,06 | 97,7 | 1,73 |
| 4 | 159,8 | 2,28 | 156,5 | 2,50 | 160,7 | 1,94 | 160,7 | 1,74 | 107,8 | 1,94 |
| 5 | 174,3 | 2,57 | 168,6 | 2,84 | 220,4 | 2,88 | 251,7 | 2,89 | 117,6 | 2,17 |
| 6 | 188,0 | 2,89 | 177,8 | 3,23 | 233,5 | 3,16 | 271,9 | 3,25 | 123,8 | 2,49 |
| 7 | 200,2 | 3,25 | 182,6 | 3,75 | 245,3 | 3,47 | 276,4 | 3,35 | 123,2 | 2,56 |
| 8 | 208,5 | 3,72 | 183,1 | 3,89 | 247,2 | 3,56 | 280,0 | 3,44 | 121,8 | 2,60 |
| 9 | 209,7 | 3,84 | 183,1 | 4,04 | 248,4 | 3,65 | 282,8 | 3,58 | 120,1 | 2,63 |
| 10 | 210,4 | 3,97 | 183,1 | 4,27 | 247,8 | 3,76 | 278,6 | 3,65 | 118,7 | 2,66 |
| 11 | 209,7 | 4,17 | 182,3 | 4,52 | 243,3 | 3,86 | 274,7 | 3,72 | 116,5 | 2,70 |
| 12 | 207,5 | 4,33 | 180,9 | 4,77 | 238,3 | 3,95 | 271,0 | 3,78 | 113,7 | 2,76 |
| 13 | 204,4 | 4,45 | 178,9 | 5,02 | 233,8 | 4,04 | 268,0 | 3,87 | 109,8 | 2,87 |
| 14 | 200,9 | 4,56 | 176,4 | 5,27 | 229,3 | 4,15 | 265,2 | 3,96 | 105,8 | 3,01 |
| 15 | 197,1 | 4,65 | 173,3 | 5,51 | 225,4 | 4,27 | 262,9 | 4,08 | 102,8 | 3,18 |
| 16 | 191,5 | 4,79 | 170,2 | 5,72 | 221,5 | 4,40 | 260,1 | 4,26 | 100,2 | 3,39 |
| 17 | 185,9 | 4,94 | 167,2 | 5,92 | 218,1 | 4,55 | 257,6 | 4,47 | 98,6 | 3,64 |
| 18 | 180,6 | 5,10 | 164,1 | 6,12 | 214,8 | 4,70 | 255,6 | 4,69 | 97,2 | 3,90 |
| 19 | 175,6 | 5,28 | 160,7 | 6,32 | 211,7 | 4,87 | 254,0 | 4,93 | 96,6 | 4,17 |
| 20 | 170,9 | 5,48 | 157,6 | 6,52 | 209,2 | 5,05 | 252,6 | 5,18 | 96,0 | 4,46 |
| 21 | 166,5 | 5,69 | 154,3 | 6,73 | 206,6 | 5,23 | 250,9 | 5,56 | 95,8 | 4,77 |
| 22 | 162,5 | 5,91 | 151,2 | 6,94 | 204,4 | 5,42 | 249,8 | 5,95 | 95,2 | 5,08 |
| 23 | 158,8 | 6,15 | 147,8 | 7,15 | 202,4 | 5,62 | 248,6 | 6,35 | 94,9 | 5,39 |
| 24 | 155,5 | 6,40 | 144,8 | 7,34 | 200,8 | 5,83 | 247,5 | 6,76 | 94,6 | 5,72 |
| 25 | 152,5 | 6,65 | 142,0 | 7,54 | 199,1 | 6,03 | 246,1 | 7,16 | 94,6 | 6,04 |
| 26 | 149,9 | 6,92 | 138,9 | 7,74 | 197,7 | 6,24 | 244,4 | 7,56 | 94,4 | 6,37 |
| 27 | 147,5 | 7,19 | 136,1 | 7,94 | 196,3 | 6,46 | 242,8 | 7,95 | 94,4 | 6,69 |
| 28 | 145,3 | 7,46 | 133,6 | 8,14 | 195,2 | 6,67 | 240,8 | 8,34 | 94,1 | 7,02 |
| 29 | 143,3 | 7,74 | 131,0 | 8,34 | 193,8 | 6,89 | 238,8 | 8,73 | 94,1 | 7,35 |
| 30 | 141,4 | 8,02 | 128,8 | 8,55 | 192,6 | 7,11 | 236,9 | 9,13 | 93,8 | 7,69 |
| 31 | 139,6 | 8,31 | 126,6 | 8,76 | 191,5 | 7,34 | 234,9 | 9,52 | 93,5 | 8,02 |
| 32 | 138,0 | 8,59 | 124,6 | 8,97 | 190,7 | 7,56 | 233,0 | 9,91 | 93,5 | 8,35 |
| 33 | 136,5 | 8,88 | 122,6 | 9,19 | 189,6 | 7,79 | 231,0 | 10,31 | 93,2 | 8,69 |
| 34 | 135,0 | 9,16 | 121,0 | 9,40 | 188,7 | 8,01 | 229,0 | 10,71 | 93,0 | 9,03 |
| 35 | 133,7 | 9,45 | 119,3 | 9,62 | 187,9 | 8,24 | 227,1 | 11,11 | 92,7 | 9,36 |
| 36 | 132,5 | 9,74 | 117,9 | 9,85 | 187,0 | 8,47 | 225,1 | 11,51 | 92,7 | 9,70 |
| 37 | 131,3 | 10,03 | 116,5 | 10,07 | 186,2 | 8,69 | 223,4 | 11,91 | 92,4 | 10,04 |
| 38 | 130,2 | 10,32 | 115,1 | 10,29 | 185,6 | 8,92 | 221,5 | 12,31 | 92,1 | 10,37 |
| 39 | 129,1 | 10,60 | 113,7 | 10,52 | 184,8 | 9,15 | 220,6 | 12,51 | 91,8 | 10,71 |
| 40 | 128,1 | 10,89 | 112,6 | 10,74 | 184,0 | 9,38 | 220,6 | 12,56 | 91,6 | 11,04 |
| 41 | 127,1 | 11,18 | 111,4 | 10,97 | 183,1 | 9,61 | 220,4 | 12,61 | 91,3 | 11,37 |
| 42 | 126,2 | 11,47 | 110,3 | 11,20 | 182,3 | 9,83 | 220,1 | 12,66 | 91,0 | 11,70 |

| | | | | | | | | | | |
|----|-------|-------|-------|-------|-------|-------|-------|-------|------|-------|
| 43 | 125,3 | 11,76 | 109,5 | 11,42 | 181,4 | 10,06 | 220,1 | 12,71 | 90,7 | 12,02 |
| 44 | 124,5 | 12,05 | 108,4 | 11,65 | 180,6 | 10,29 | 219,8 | 12,77 | 90,4 | 12,35 |
| 45 | 123,7 | 12,33 | 107,5 | 11,88 | 179,8 | 10,52 | 219,5 | 12,82 | 89,9 | 12,67 |
| 46 | 122,9 | 12,62 | 106,7 | 12,10 | 178,6 | 10,74 | 219,2 | 12,87 | 89,6 | 12,98 |
| 47 | 122,1 | 12,91 | 105,8 | 12,33 | 177,8 | 10,97 | 219,2 | 12,92 | 89,3 | 13,29 |
| 48 | 121,3 | 13,19 | 105,0 | 12,56 | 177,0 | 11,20 | 219,0 | 12,97 | 88,8 | 13,60 |
| 49 | 120,6 | 13,48 | 104,2 | 12,78 | 176,1 | 11,42 | 218,7 | 13,02 | 88,5 | 13,90 |
| 50 | 120,3 | 13,62 | 103,6 | 13,01 | 175,3 | 11,65 | 218,7 | 13,07 | 87,9 | 14,19 |

D.2.2.2 Girders 105-109

| Increment | Girder 105 | | Girder 106 | | Girder 107 | | Girder 108 | | Girder 109 | |
|-----------|------------|-----------|------------|-----------|------------|-----------|------------|-----------|------------|-----------|
| | Load [kN] | DEF. [mm] | Load [kN] | DEF. [mm] | Load [kN] | DEF. [mm] | Load [kN] | DEF. [mm] | Load [kN] | DEF. [mm] |
| 0 | 0,0 | 0,00 | 0,0 | 0,00 | 0,0 | 0,00 | 0,0 | 0,00 | 0,0 | 0,00 |
| 1 | 28,0 | 0,34 | 28,0 | 0,39 | 28,0 | 0,39 | 69,8 | 1,02 | 28,0 | 0,40 |
| 2 | 56,0 | 0,67 | 56,0 | 0,78 | 56,0 | 0,78 | 139,0 | 2,05 | 56,0 | 0,80 |
| 3 | 98,0 | 1,18 | 97,7 | 1,37 | 97,7 | 1,37 | 155,2 | 2,38 | 97,7 | 1,40 |
| 4 | 160,2 | 1,94 | 159,9 | 2,28 | 159,9 | 2,28 | 170,3 | 2,75 | 159,3 | 2,34 |
| 5 | 219,5 | 2,76 | 174,4 | 2,57 | 174,2 | 2,57 | 182,3 | 3,21 | 173,3 | 2,65 |
| 6 | 260,1 | 4,02 | 188,2 | 2,89 | 187,9 | 2,89 | 184,7 | 3,34 | 185,4 | 3,03 |
| 7 | 265,7 | 4,38 | 200,5 | 3,25 | 199,9 | 3,27 | 186,8 | 3,47 | 189,8 | 3,53 |
| 8 | 269,4 | 4,78 | 209,7 | 3,68 | 206,1 | 3,77 | 189,2 | 3,69 | 184,8 | 4,04 |
| 9 | 270,2 | 5,21 | 211,4 | 3,80 | 206,6 | 3,90 | 190,3 | 3,91 | 183,7 | 4,15 |
| 10 | 268,5 | 5,70 | 212,8 | 3,92 | 206,1 | 4,02 | 190,0 | 4,13 | 182,3 | 4,27 |
| 11 | 264,9 | 6,22 | 213,6 | 4,12 | 203,8 | 4,19 | 188,2 | 4,33 | 180,9 | 4,39 |
| 12 | 260,1 | 6,77 | 212,5 | 4,31 | 200,8 | 4,33 | 185,7 | 4,51 | 178,4 | 4,56 |
| 13 | 253,7 | 7,33 | 210,0 | 4,47 | 197,4 | 4,45 | 182,9 | 4,67 | 174,7 | 4,80 |
| 14 | 246,1 | 7,89 | 206,9 | 4,60 | 193,8 | 4,56 | 180,2 | 4,83 | 171,1 | 5,04 |
| 15 | 237,7 | 8,41 | 203,6 | 4,71 | 190,4 | 4,67 | 177,5 | 4,99 | 167,4 | 5,28 |
| 16 | 229,3 | 8,92 | 200,2 | 4,80 | 186,8 | 4,78 | 174,9 | 5,15 | 164,1 | 5,53 |
| 17 | 221,5 | 9,43 | 196,3 | 4,89 | 183,4 | 4,89 | 172,5 | 5,32 | 160,7 | 5,78 |
| 18 | 214,2 | 9,95 | 192,6 | 4,97 | 180,0 | 5,01 | 170,2 | 5,50 | 157,9 | 6,05 |
| 19 | 207,5 | 10,48 | 189,0 | 5,06 | 176,7 | 5,14 | 168,1 | 5,67 | 155,1 | 6,33 |
| 20 | 201,3 | 11,02 | 185,4 | 5,15 | 171,9 | 5,33 | 166,0 | 5,86 | 152,6 | 6,61 |
| 21 | 195,4 | 11,56 | 182,0 | 5,26 | 167,7 | 5,54 | 163,1 | 6,14 | 150,4 | 6,90 |
| 22 | 191,5 | 11,96 | 178,6 | 5,37 | 163,5 | 5,77 | 160,5 | 6,43 | 148,4 | 7,19 |
| 23 | 188,7 | 12,26 | 175,3 | 5,49 | 159,9 | 6,00 | 158,0 | 6,73 | 146,4 | 7,48 |
| 24 | 186,8 | 12,48 | 170,5 | 5,68 | 156,5 | 6,25 | 155,7 | 7,03 | 144,8 | 7,78 |
| 25 | 185,4 | 12,65 | 166,3 | 5,88 | 153,4 | 6,51 | 153,6 | 7,35 | 143,1 | 8,08 |
| 26 | 184,2 | 12,78 | 162,4 | 6,10 | 150,6 | 6,78 | 151,6 | 7,66 | 141,7 | 8,38 |
| 27 | 183,1 | 12,90 | 158,8 | 6,33 | 148,4 | 7,05 | 149,7 | 7,98 | 140,3 | 8,68 |
| 28 | 182,6 | 13,00 | 155,4 | 6,57 | 146,2 | 7,33 | 147,9 | 8,31 | 138,9 | 8,98 |
| 29 | 181,7 | 13,09 | 152,3 | 6,82 | 143,9 | 7,61 | 146,1 | 8,63 | 137,5 | 9,28 |
| 30 | 180,9 | 13,19 | 149,5 | 7,08 | 142,2 | 7,90 | 144,5 | 8,96 | 136,4 | 9,58 |
| 31 | 180,3 | 13,26 | 147,0 | 7,34 | 140,6 | 8,18 | 142,9 | 9,28 | 135,2 | 9,88 |
| 32 | 179,8 | 13,33 | 144,8 | 7,61 | 138,9 | 8,47 | 141,4 | 9,61 | 134,1 | 10,18 |
| 33 | 179,2 | 13,40 | 142,8 | 7,88 | 137,5 | 8,76 | 139,9 | 9,94 | 133,3 | 10,48 |
| 34 | 178,9 | 13,45 | 140,8 | 8,15 | 136,1 | 9,05 | 138,4 | 10,26 | 132,2 | 10,78 |

| | | | | | | | | | | |
|----|-------|-------|-------|-------|-------|-------|-------|-------|-------|-------|
| 35 | 178,4 | 13,50 | 139,2 | 8,43 | 134,7 | 9,35 | 136,9 | 10,59 | 131,0 | 11,08 |
| 36 | 178,1 | 13,55 | 137,5 | 8,70 | 133,6 | 9,64 | 135,5 | 10,92 | 130,2 | 11,38 |
| 37 | 177,5 | 13,61 | 135,8 | 8,98 | 132,4 | 9,93 | 134,1 | 11,25 | 129,4 | 11,68 |
| 38 | 177,2 | 13,66 | 134,4 | 9,26 | 131,3 | 10,22 | 132,6 | 11,57 | 128,5 | 11,98 |
| 39 | 177,0 | 13,71 | 133,0 | 9,54 | 130,2 | 10,51 | 131,2 | 11,90 | 127,7 | 12,28 |
| 40 | 176,7 | 13,75 | 131,6 | 9,81 | 129,1 | 10,81 | 129,8 | 12,22 | 126,8 | 12,50 |
| 41 | 176,1 | 13,79 | 130,5 | 10,09 | 128,2 | 11,10 | 128,5 | 12,54 | 126,6 | 12,67 |
| 42 | 175,8 | 13,83 | 129,4 | 10,37 | 127,4 | 11,39 | 127,2 | 12,86 | 126,0 | 12,84 |
| 43 | 175,8 | 13,85 | 128,2 | 10,65 | 126,6 | 11,68 | 125,9 | 13,19 | 125,7 | 12,96 |
| 44 | 175,8 | 13,86 | 127,1 | 10,93 | 125,7 | 11,97 | 124,7 | 13,51 | 125,4 | 13,09 |
| 45 | 175,8 | 13,86 | 126,0 | 11,21 | 124,9 | 12,26 | 123,6 | 13,82 | 125,2 | 13,18 |
| 46 | 175,6 | 13,86 | 125,2 | 11,49 | 124,3 | 12,55 | 122,4 | 14,14 | 124,9 | 13,27 |
| 47 | 175,6 | 13,86 | 124,3 | 11,77 | 123,5 | 12,84 | 121,3 | 14,46 | 124,6 | 13,37 |
| 48 | 175,6 | 13,86 | 123,5 | 12,05 | 122,6 | 13,13 | 120,3 | 14,78 | 124,3 | 13,44 |
| 49 | 175,6 | 13,86 | 122,6 | 12,33 | 122,1 | 13,42 | 119,3 | 15,09 | 124,3 | 13,51 |
| 50 | 175,6 | 13,86 | 121,8 | 12,61 | 121,2 | 13,71 | 118,3 | 15,41 | 124,0 | 13,58 |

D.2.2.3 Girders 200-204

| Increment | Girder 200 | | Girder 201 | | Girder 202 | | Girder 203 | | Girder 204 | |
|-----------|------------|-----------|------------|-----------|------------|-----------|------------|-----------|------------|-----------|
| | Load [kN] | DEF. [mm] | Load [kN] | DEF. [mm] | Load [kN] | DEF. [mm] | Load [kN] | DEF. [mm] | Load [kN] | DEF. [mm] |
| 0 | 0,0 | 0,00 | 0,0 | 0,00 | 0,0 | 0,00 | 0,0 | 0,00 | 0,0 | 0,00 |
| 1 | 28,0 | 0,39 | 27,9 | 0,43 | 28,0 | 0,34 | 28,0 | 0,30 | 28,0 | 0,49 |
| 2 | 55,9 | 0,78 | 55,7 | 0,86 | 56,0 | 0,68 | 56,0 | 0,61 | 55,7 | 0,99 |
| 3 | 97,5 | 1,37 | 96,6 | 1,50 | 97,7 | 1,18 | 98,0 | 1,06 | 97,2 | 1,73 |
| 4 | 158,1 | 2,25 | 118,4 | 1,86 | 160,2 | 1,95 | 160,7 | 1,74 | 107,2 | 1,92 |
| 5 | 172,2 | 2,47 | 137,8 | 2,20 | 220,1 | 2,79 | 222,6 | 2,44 | 117,3 | 2,11 |
| 6 | 185,1 | 2,71 | 153,2 | 2,51 | 233,5 | 3,07 | 237,4 | 2,64 | 126,3 | 2,33 |
| 7 | 196,4 | 3,00 | 164,9 | 2,78 | 236,6 | 3,14 | 252,0 | 2,85 | 127,4 | 2,39 |
| 8 | 200,7 | 3,42 | 173,3 | 3,06 | 239,1 | 3,23 | 265,4 | 3,09 | 127,4 | 2,45 |
| 9 | 198,7 | 3,52 | 173,3 | 3,06 | 241,4 | 3,37 | 275,5 | 3,34 | 126,6 | 2,48 |
| 10 | 196,6 | 3,60 | 173,6 | 3,07 | 240,0 | 3,49 | 277,2 | 3,40 | 125,4 | 2,51 |
| 11 | 194,4 | 3,69 | 173,6 | 3,08 | 238,0 | 3,58 | 278,3 | 3,45 | 124,3 | 2,53 |
| 12 | 192,3 | 3,78 | 173,9 | 3,09 | 236,3 | 3,69 | 279,4 | 3,51 | 122,9 | 2,56 |
| 13 | 190,2 | 3,88 | 174,2 | 3,10 | 234,4 | 3,81 | 280,0 | 3,59 | 121,8 | 2,59 |
| 14 | 188,3 | 3,98 | 174,7 | 3,13 | 233,0 | 3,94 | 282,8 | 3,72 | 120,4 | 2,65 |
| 15 | 186,4 | 4,09 | 175,6 | 3,16 | 231,6 | 4,08 | 282,8 | 3,91 | 118,4 | 2,76 |
| 16 | 184,7 | 4,21 | 176,7 | 3,22 | 229,9 | 4,31 | 279,7 | 4,08 | 116,2 | 2,94 |
| 17 | 183,0 | 4,34 | 178,1 | 3,31 | 228,2 | 4,54 | 275,0 | 4,23 | 112,8 | 3,13 |
| 18 | 180,7 | 4,53 | 179,5 | 3,41 | 225,4 | 4,76 | 270,8 | 4,41 | 109,5 | 3,32 |
| 19 | 178,6 | 4,74 | 180,6 | 3,53 | 221,8 | 4,93 | 267,7 | 4,63 | 106,7 | 3,54 |
| 20 | 176,7 | 4,95 | 181,2 | 3,68 | 218,4 | 5,10 | 265,2 | 4,86 | 104,7 | 3,80 |
| 21 | 174,1 | 5,28 | 175,0 | 3,99 | 215,0 | 5,27 | 263,5 | 5,10 | 103,3 | 4,07 |
| 22 | 171,7 | 5,62 | 171,1 | 4,15 | 211,7 | 5,45 | 262,1 | 5,36 | 102,2 | 4,37 |
| 23 | 169,6 | 5,96 | 166,9 | 4,33 | 208,9 | 5,64 | 260,7 | 5,62 | 101,4 | 4,67 |
| 24 | 167,6 | 6,31 | 163,0 | 4,52 | 206,4 | 5,84 | 259,6 | 5,89 | 100,5 | 4,98 |

| | | | | | | | | | | |
|----|-------|-------|-------|-------|-------|-------|-------|-------|-------|-------|
| 25 | 165,7 | 6,65 | 159,3 | 4,74 | 204,1 | 6,05 | 258,4 | 6,16 | 100,2 | 5,30 |
| 26 | 163,8 | 7,00 | 156,0 | 4,98 | 202,2 | 6,27 | 257,0 | 6,43 | 100,0 | 5,62 |
| 27 | 161,7 | 7,35 | 152,9 | 5,24 | 200,5 | 6,49 | 255,4 | 6,71 | 99,7 | 5,95 |
| 28 | 159,3 | 7,69 | 150,1 | 5,51 | 198,8 | 6,72 | 254,0 | 6,98 | 99,4 | 6,28 |
| 29 | 156,6 | 8,02 | 147,6 | 5,79 | 197,4 | 6,96 | 252,3 | 7,25 | 99,4 | 6,61 |
| 30 | 153,9 | 8,35 | 145,6 | 6,08 | 196,0 | 7,20 | 250,9 | 7,53 | 99,1 | 6,95 |
| 31 | 151,3 | 8,67 | 143,6 | 6,37 | 194,9 | 7,44 | 249,5 | 7,80 | 99,1 | 7,28 |
| 32 | 148,9 | 8,98 | 142,0 | 6,66 | 193,8 | 7,68 | 248,1 | 8,08 | 98,8 | 7,63 |
| 33 | 146,6 | 9,30 | 140,3 | 6,95 | 192,6 | 7,92 | 247,0 | 8,36 | 98,6 | 7,97 |
| 34 | 144,4 | 9,60 | 138,9 | 7,25 | 191,5 | 8,17 | 245,8 | 8,64 | 98,3 | 8,32 |
| 35 | 142,3 | 9,91 | 137,5 | 7,54 | 190,7 | 8,42 | 244,4 | 8,92 | 98,3 | 8,67 |
| 36 | 140,4 | 10,21 | 136,4 | 7,83 | 189,6 | 8,66 | 243,3 | 9,21 | 98,0 | 9,01 |
| 37 | 138,6 | 10,51 | 135,2 | 8,12 | 188,4 | 8,91 | 242,2 | 9,49 | 97,4 | 9,36 |
| 38 | 137,0 | 10,82 | 134,1 | 8,42 | 187,6 | 9,16 | 241,1 | 9,78 | 97,2 | 9,70 |
| 39 | 135,5 | 11,13 | 133,0 | 8,71 | 186,8 | 9,41 | 240,2 | 10,06 | 96,6 | 10,03 |
| 40 | 134,1 | 11,43 | 131,9 | 9,00 | 185,6 | 9,65 | 239,1 | 10,35 | 96,0 | 10,36 |
| 41 | 132,8 | 11,74 | 130,8 | 9,29 | 184,8 | 9,90 | 238,0 | 10,64 | 95,2 | 10,67 |
| 42 | 131,6 | 12,05 | 129,6 | 9,58 | 184,0 | 10,15 | 236,9 | 10,92 | 94,6 | 10,99 |
| 43 | 130,7 | 12,28 | 128,8 | 9,87 | 183,1 | 10,40 | 236,0 | 11,21 | 94,1 | 11,31 |
| 44 | 129,9 | 12,51 | 127,7 | 10,16 | 182,3 | 10,65 | 234,6 | 11,50 | 93,5 | 11,63 |
| 45 | 129,3 | 12,68 | 126,8 | 10,44 | 181,4 | 10,89 | 233,5 | 11,79 | 93,0 | 11,95 |
| 46 | 128,9 | 12,81 | 125,7 | 10,73 | 181,2 | 10,96 | 233,2 | 11,86 | 92,4 | 12,28 |
| 47 | 128,5 | 12,94 | 124,9 | 11,01 | 181,2 | 11,02 | 233,0 | 11,93 | 91,8 | 12,61 |
| 48 | 128,2 | 13,04 | 124,0 | 11,29 | 180,9 | 11,08 | 232,7 | 12,00 | 91,3 | 12,94 |
| 49 | 127,9 | 13,14 | 123,2 | 11,57 | 180,6 | 11,14 | 232,7 | 12,02 | 91,0 | 13,18 |
| 50 | 127,6 | 13,23 | 122,4 | 11,85 | 180,6 | 11,20 | 232,4 | 12,04 | 90,7 | 13,37 |

D.2.2.4 Girders 205-209

| Increment | Girder 205 | | Girder 206 | | Girder 207 | | Girder 208 | | Girder 209 | |
|-----------|------------|-----------|------------|-----------|------------|-----------|------------|-----------|------------|-----------|
| | Load [kN] | DEF. [mm] | Load [kN] | DEF. [mm] | Load [kN] | DEF. [mm] | Load [kN] | DEF. [mm] | Load [kN] | DEF. [mm] |
| 0 | 0,0 | 0,00 | 0,0 | 0,00 | 0,0 | 0,00 | 0,0 | 0,00 | 0,0 | 0,00 |
| 1 | 28,0 | 0,34 | 28,0 | 0,39 | 28,0 | 0,39 | 28,0 | 0,39 | 28,0 | 0,40 |
| 2 | 56,0 | 0,68 | 55,7 | 0,78 | 55,7 | 0,78 | 55,7 | 0,79 | 55,7 | 0,81 |
| 3 | 97,4 | 1,18 | 97,4 | 1,37 | 97,4 | 1,37 | 97,4 | 1,38 | 97,4 | 1,41 |
| 4 | 138,6 | 1,69 | 158,2 | 2,26 | 158,2 | 2,26 | 158,2 | 2,27 | 157,4 | 2,36 |
| 5 | 177,8 | 2,19 | 172,2 | 2,48 | 172,2 | 2,48 | 171,9 | 2,51 | 168,8 | 2,69 |
| 6 | 210,8 | 2,67 | 185,1 | 2,72 | 185,1 | 2,72 | 184,2 | 2,79 | 175,8 | 3,06 |
| 7 | 235,2 | 3,12 | 196,6 | 3,04 | 196,0 | 3,04 | 192,4 | 3,14 | 178,9 | 3,45 |
| 8 | 249,8 | 3,61 | 201,6 | 3,49 | 198,0 | 3,49 | 193,8 | 3,52 | 179,2 | 3,86 |
| 9 | 252,6 | 3,74 | 199,6 | 3,61 | 196,0 | 3,61 | 191,2 | 3,89 | 178,1 | 4,27 |
| 10 | 254,8 | 3,87 | 197,7 | 3,72 | 193,8 | 3,72 | 187,9 | 4,27 | 175,8 | 4,69 |
| 11 | 256,5 | 4,00 | 195,4 | 3,83 | 191,8 | 3,83 | 184,2 | 4,68 | 173,6 | 5,11 |
| 12 | 257,9 | 4,13 | 192,4 | 3,99 | 188,4 | 3,99 | 180,6 | 5,10 | 170,5 | 5,55 |
| 13 | 259,0 | 4,27 | 188,2 | 4,16 | 185,6 | 4,16 | 177,2 | 5,54 | 167,7 | 6,00 |
| 14 | 260,1 | 4,41 | 184,2 | 4,34 | 182,8 | 4,34 | 173,6 | 5,99 | 164,9 | 6,46 |
| 15 | 261,0 | 4,56 | 180,9 | 4,54 | 180,3 | 4,54 | 170,2 | 6,45 | 162,1 | 6,92 |
| 16 | 261,5 | 4,72 | 178,1 | 4,74 | 178,1 | 4,74 | 166,9 | 6,91 | 159,3 | 7,40 |

| | | | | | | | | | | |
|----|-------|------|-------|-------|-------|-------|-------|-------|-------|-------|
| 17 | 261,8 | 4,91 | 175,3 | 4,96 | 176,1 | 4,96 | 163,5 | 7,38 | 157,1 | 7,88 |
| 18 | 261,5 | 5,15 | 173,0 | 5,18 | 174,4 | 5,18 | 160,4 | 7,86 | 154,8 | 8,36 |
| 19 | 259,0 | 5,46 | 170,8 | 5,41 | 172,8 | 5,41 | 157,9 | 8,35 | 152,6 | 8,84 |
| 20 | 254,5 | 5,79 | 168,8 | 5,64 | 171,1 | 5,64 | 155,1 | 8,84 | 150,6 | 9,32 |
| 21 | 249,5 | 6,13 | 166,9 | 5,87 | 169,7 | 5,87 | 152,6 | 9,33 | 148,7 | 9,81 |
| 22 | 243,6 | 6,48 | 164,9 | 6,11 | 168,3 | 6,11 | 150,4 | 9,83 | 146,7 | 10,29 |
| 23 | 242,2 | 6,56 | 162,4 | 6,34 | 167,2 | 6,34 | 147,8 | 10,33 | 144,8 | 10,77 |
| 24 | 240,8 | 6,65 | 159,3 | 6,58 | 165,8 | 6,58 | 145,6 | 10,83 | 142,8 | 11,26 |
| 25 | 239,4 | 6,74 | 156,2 | 6,82 | 164,6 | 6,82 | 143,4 | 11,33 | 141,1 | 11,74 |
| 26 | 238,8 | 6,77 | 153,2 | 7,06 | 163,2 | 7,06 | 141,4 | 11,84 | 139,2 | 12,23 |
| 27 | 238,6 | 6,79 | 150,4 | 7,29 | 162,1 | 7,29 | 139,4 | 12,34 | 137,5 | 12,72 |
| 28 | 238,0 | 6,82 | 147,8 | 7,53 | 160,7 | 7,53 | 137,5 | 12,84 | 135,8 | 13,20 |
| 29 | 237,4 | 6,86 | 145,6 | 7,76 | 159,3 | 7,76 | 135,5 | 13,35 | 134,4 | 13,69 |
| 30 | 236,9 | 6,89 | 143,6 | 7,99 | 157,4 | 7,99 | 133,8 | 13,85 | 132,7 | 14,18 |
| 31 | 236,6 | 6,90 | 141,7 | 8,20 | 155,4 | 8,20 | 132,2 | 14,36 | 131,3 | 14,68 |
| 32 | 236,6 | 6,91 | 140,0 | 8,42 | 153,4 | 8,42 | 130,5 | 14,87 | 129,9 | 15,17 |
| 33 | 236,3 | 6,92 | 138,3 | 8,63 | 151,5 | 8,63 | 128,8 | 15,38 | 128,5 | 15,66 |
| 34 | 236,0 | 6,93 | 136,9 | 8,84 | 149,8 | 8,84 | 127,4 | 15,88 | 127,1 | 16,16 |
| 35 | 235,8 | 6,95 | 135,5 | 9,04 | 148,1 | 9,04 | 126,3 | 16,26 | 125,7 | 16,65 |
| 36 | 235,5 | 6,98 | 134,4 | 9,25 | 146,7 | 9,25 | 125,4 | 16,55 | 124,9 | 17,02 |
| 37 | 234,9 | 7,01 | 133,0 | 9,46 | 145,0 | 9,46 | 124,6 | 16,76 | 124,0 | 17,30 |
| 38 | 234,4 | 7,04 | 131,9 | 9,67 | 143,6 | 9,67 | 124,3 | 16,92 | 124,0 | 17,34 |
| 39 | 234,1 | 7,07 | 130,8 | 9,87 | 142,2 | 9,87 | 123,8 | 17,04 | 123,8 | 17,38 |
| 40 | 233,5 | 7,10 | 129,6 | 10,08 | 140,8 | 10,08 | 123,8 | 17,13 | 123,8 | 17,42 |
| 41 | 233,0 | 7,13 | 128,8 | 10,29 | 139,7 | 10,29 | 123,5 | 17,20 | 123,8 | 17,43 |
| 42 | 232,7 | 7,16 | 127,7 | 10,50 | 138,6 | 10,50 | 123,2 | 17,26 | 123,8 | 17,44 |
| 43 | 232,1 | 7,19 | 126,8 | 10,71 | 137,5 | 10,71 | 122,9 | 17,33 | 123,8 | 17,45 |
| 44 | 231,8 | 7,21 | 126,0 | 10,92 | 136,4 | 10,92 | 122,9 | 17,38 | 123,8 | 17,45 |
| 45 | 231,3 | 7,24 | 125,4 | 11,13 | 135,2 | 11,13 | 122,6 | 17,43 | 123,8 | 17,45 |
| 46 | 230,7 | 7,27 | 124,9 | 11,34 | 134,4 | 11,34 | 122,6 | 17,48 | 123,8 | 17,45 |
| 47 | 230,4 | 7,30 | 124,3 | 11,55 | 133,6 | 11,55 | 122,4 | 17,53 | 123,8 | 17,45 |
| 48 | 229,9 | 7,33 | 124,0 | 11,76 | 132,7 | 11,76 | 122,4 | 17,58 | 123,8 | 17,45 |
| 49 | 229,6 | 7,36 | 123,8 | 11,97 | 131,9 | 11,97 | 122,1 | 17,63 | 123,8 | 17,45 |
| 50 | 229,0 | 7,39 | 123,5 | 12,18 | 131,0 | 12,18 | 122,1 | 17,67 | 123,8 | 17,45 |

D.2.2.5 Girders 300-304

| Increment | Girder 300 | | Girder 301 | | Girder 302 | | Girder 303 | | Girder 304 | |
|-----------|------------|-----------|------------|-----------|------------|-----------|------------|-----------|------------|-----------|
| | Load [kN] | DEF. [mm] | Load [kN] | DEF. [mm] | Load [kN] | DEF. [mm] | Load [kN] | DEF. [mm] | Load [kN] | DEF. [mm] |
| 0 | 0,0 | 0,00 | 0,0 | 0,00 | 0,0 | 0,00 | 0,0 | 0,00 | 0,0 | 0,00 |
| 1 | 27,9 | 0,40 | 27,8 | 0,45 | 28,0 | 0,35 | 28,0 | 0,31 | 27,9 | 0,50 |
| 2 | 55,7 | 0,81 | 55,2 | 0,90 | 56,0 | 0,70 | 56,0 | 0,62 | 55,7 | 1,01 |
| 3 | 96,7 | 1,42 | 94,4 | 1,56 | 97,7 | 1,22 | 97,7 | 1,09 | 70,8 | 1,30 |
| 4 | 150,6 | 2,50 | 123,2 | 2,29 | 159,3 | 2,03 | 160,4 | 1,79 | 91,6 | 1,80 |
| 5 | 151,3 | 2,52 | 127,1 | 2,53 | 174,2 | 2,26 | 221,2 | 2,55 | 95,5 | 1,95 |
| 6 | 151,9 | 2,54 | 129,1 | 2,80 | 188,4 | 2,49 | 235,8 | 2,76 | 99,7 | 2,11 |
| 7 | 152,8 | 2,57 | 130,2 | 3,10 | 208,3 | 2,88 | 250,0 | 2,97 | 103,9 | 2,27 |
| 8 | 154,1 | 2,62 | 131,0 | 3,43 | 224,8 | 3,31 | 269,9 | 3,31 | 110,3 | 2,52 |

| | | | | | | | | | | |
|----|-------|-------|-------|-------|-------|-------|-------|-------|-------|-------|
| 9 | 155,8 | 2,69 | 131,3 | 3,78 | 238,3 | 3,80 | 285,6 | 3,69 | 116,2 | 2,78 |
| 10 | 158,0 | 2,81 | 131,3 | 4,14 | 246,4 | 4,35 | 285,6 | 4,11 | 121,5 | 3,06 |
| 11 | 160,8 | 3,00 | 131,3 | 4,52 | 242,2 | 4,97 | 278,6 | 4,51 | 126,0 | 3,36 |
| 12 | 163,8 | 3,31 | 130,5 | 5,12 | 232,4 | 5,52 | 272,7 | 4,94 | 129,6 | 3,69 |
| 13 | 166,2 | 3,63 | 129,4 | 5,75 | 223,7 | 6,09 | 267,7 | 5,40 | 128,5 | 4,01 |
| 14 | 167,9 | 3,97 | 127,7 | 6,42 | 216,4 | 6,69 | 262,9 | 5,89 | 123,5 | 4,23 |
| 15 | 169,0 | 4,31 | 126,3 | 7,11 | 210,0 | 7,32 | 258,2 | 6,39 | 119,0 | 4,44 |
| 16 | 170,0 | 4,86 | 124,3 | 7,83 | 204,7 | 7,97 | 252,6 | 6,88 | 115,1 | 4,69 |
| 17 | 169,6 | 5,45 | 122,6 | 8,55 | 199,9 | 8,62 | 247,0 | 7,36 | 112,0 | 4,96 |
| 18 | 168,4 | 6,07 | 120,7 | 9,29 | 195,7 | 9,26 | 241,4 | 7,84 | 109,5 | 5,27 |
| 19 | 166,5 | 6,72 | 119,0 | 10,04 | 191,2 | 9,90 | 236,3 | 8,32 | 107,5 | 5,59 |
| 20 | 164,5 | 7,39 | 117,0 | 10,78 | 187,0 | 10,53 | 231,6 | 8,81 | 106,1 | 5,93 |
| 21 | 164,0 | 7,55 | 115,4 | 11,53 | 183,1 | 11,14 | 227,1 | 9,29 | 104,7 | 6,28 |
| 22 | 163,5 | 7,72 | 113,4 | 12,27 | 179,2 | 11,75 | 223,4 | 9,79 | 103,3 | 6,63 |
| 23 | 162,9 | 7,89 | 111,7 | 13,01 | 175,3 | 12,34 | 220,1 | 10,29 | 101,9 | 6,98 |
| 24 | 162,4 | 8,06 | 110,0 | 13,74 | 171,4 | 12,94 | 217,3 | 10,80 | 100,8 | 7,33 |
| 25 | 161,8 | 8,24 | 108,6 | 14,46 | 168,0 | 13,53 | 214,5 | 11,31 | 99,4 | 7,68 |
| 26 | 161,2 | 8,41 | 108,1 | 14,64 | 165,5 | 13,98 | 212,2 | 11,82 | 98,3 | 8,03 |
| 27 | 160,6 | 8,58 | 107,8 | 14,81 | 164,6 | 14,10 | 210,0 | 12,34 | 97,2 | 8,38 |
| 28 | 160,1 | 8,76 | 107,8 | 14,82 | 164,1 | 14,23 | 207,8 | 12,86 | 95,8 | 8,72 |
| 29 | 159,5 | 8,93 | 107,8 | 14,82 | 163,5 | 14,32 | 206,1 | 13,38 | 94,6 | 9,05 |
| 30 | 158,9 | 9,11 | 107,8 | 14,82 | 163,2 | 14,42 | 204,7 | 13,77 | 93,5 | 9,38 |
| 31 | 158,3 | 9,28 | 107,8 | 14,83 | 162,7 | 14,49 | 203,6 | 14,07 | 92,1 | 9,71 |
| 32 | 157,6 | 9,46 | 107,8 | 14,83 | 162,7 | 14,53 | 202,7 | 14,29 | 91,0 | 10,03 |
| 33 | 157,0 | 9,64 | 107,8 | 14,84 | 162,4 | 14,56 | 202,2 | 14,46 | 89,9 | 10,36 |
| 34 | 156,4 | 9,81 | 107,8 | 14,85 | 162,4 | 14,60 | 201,9 | 14,58 | 88,8 | 10,68 |
| 35 | 155,8 | 9,99 | 107,8 | 14,85 | 162,1 | 14,63 | 201,6 | 14,68 | 87,6 | 11,00 |
| 36 | 155,2 | 10,17 | 107,8 | 14,86 | 161,8 | 14,67 | 201,3 | 14,75 | 86,8 | 11,33 |
| 37 | 154,6 | 10,35 | 107,8 | 14,87 | 161,8 | 14,71 | 201,3 | 14,80 | 85,7 | 11,66 |
| 38 | 154,0 | 10,52 | 107,8 | 14,87 | 161,6 | 14,74 | 201,0 | 14,84 | 84,8 | 11,99 |
| 39 | 153,4 | 10,70 | 107,8 | 14,88 | 161,3 | 14,78 | 201,0 | 14,88 | 84,0 | 12,32 |
| 40 | 152,8 | 10,88 | 107,8 | 14,89 | 161,3 | 14,81 | 200,8 | 14,92 | 83,2 | 12,65 |
| 41 | 152,2 | 11,06 | 107,5 | 14,89 | 161,0 | 14,85 | 200,8 | 14,96 | 82,3 | 12,99 |
| 42 | 151,5 | 11,24 | 107,5 | 14,90 | 161,0 | 14,89 | 200,5 | 15,00 | 81,8 | 13,33 |
| 43 | 150,9 | 11,42 | 107,5 | 14,91 | 160,7 | 14,90 | 200,5 | 15,03 | 80,9 | 13,67 |
| 44 | 150,3 | 11,60 | 107,5 | 14,91 | 160,7 | 14,92 | 200,5 | 15,06 | 80,4 | 14,01 |
| 45 | 149,7 | 11,77 | 107,5 | 14,92 | 160,7 | 14,94 | 200,5 | 15,09 | 79,5 | 14,35 |
| 46 | 149,0 | 11,95 | 107,5 | 14,93 | 160,7 | 14,96 | 200,2 | 15,12 | 79,2 | 14,61 |
| 47 | 148,4 | 12,13 | 107,5 | 14,93 | 160,4 | 14,98 | 200,2 | 15,15 | 79,0 | 14,81 |
| 48 | 147,8 | 12,31 | 107,5 | 14,94 | 160,4 | 14,99 | 200,2 | 15,18 | 78,7 | 14,95 |
| 49 | 147,1 | 12,49 | 107,5 | 14,95 | 160,4 | 15,01 | 199,9 | 15,21 | 78,4 | 15,06 |
| 50 | 146,4 | 12,67 | 107,5 | 14,95 | 160,2 | 15,03 | 199,9 | 15,23 | 78,4 | 15,15 |

D.2.2.6 Girders 305-309

| Increment | Girder 305 | | Girder 306 | | Girder 307 | | Girder 308 | | Girder 309 | |
|-----------|------------|-----------|------------|-----------|------------|-----------|------------|-----------|------------|-----------|
| | Load [kN] | DEF. [mm] | Load [kN] | DEF. [mm] | Load [kN] | DEF. [mm] | Load [kN] | DEF. [mm] | Load [kN] | DEF. [mm] |
| 0 | 0,0 | 0,00 | 0,0 | 0,00 | 0,0 | 0,00 | 0,0 | 0,00 | 0,0 | 0,00 |
| 1 | 27,9 | 0,35 | 27,9 | 0,41 | 27,9 | 0,41 | 27,9 | 0,43 | 27,9 | 0,44 |
| 2 | 55,7 | 0,71 | 55,7 | 0,81 | 55,7 | 0,81 | 55,7 | 0,86 | 55,7 | 0,88 |
| 3 | 96,9 | 1,24 | 96,6 | 1,42 | 96,6 | 1,42 | 96,6 | 1,52 | 96,3 | 1,58 |
| 4 | 154,0 | 2,04 | 119,0 | 1,77 | 134,7 | 2,10 | 133,8 | 2,27 | 132,4 | 2,41 |
| 5 | 165,8 | 2,26 | 147,6 | 2,42 | 142,8 | 2,30 | 141,7 | 2,49 | 157,1 | 3,45 |
| 6 | 176,1 | 2,48 | 152,3 | 2,62 | 149,8 | 2,51 | 148,4 | 2,73 | 161,3 | 3,74 |
| 7 | 184,5 | 2,70 | 156,2 | 2,84 | 158,2 | 2,85 | 156,8 | 3,11 | 164,4 | 4,03 |
| 8 | 191,2 | 2,92 | 159,9 | 3,06 | 164,6 | 3,23 | 163,5 | 3,51 | 166,9 | 4,33 |
| 9 | 196,6 | 3,15 | 162,7 | 3,30 | 169,1 | 3,64 | 168,0 | 3,94 | 168,6 | 4,65 |
| 10 | 200,2 | 3,40 | 166,0 | 3,68 | 171,9 | 4,06 | 170,8 | 4,40 | 170,0 | 4,97 |
| 11 | 202,4 | 3,86 | 169,1 | 4,28 | 173,9 | 4,52 | 172,8 | 4,88 | 170,8 | 5,31 |
| 12 | 201,9 | 4,40 | 170,5 | 4,91 | 174,7 | 4,99 | 173,3 | 5,38 | 170,8 | 5,66 |
| 13 | 199,9 | 5,00 | 170,2 | 5,60 | 174,4 | 5,50 | 173,0 | 5,91 | 170,5 | 6,01 |
| 14 | 197,4 | 5,67 | 168,8 | 6,33 | 174,2 | 5,63 | 172,8 | 6,05 | 170,0 | 6,38 |
| 15 | 194,6 | 6,38 | 166,9 | 7,09 | 173,9 | 5,76 | 172,5 | 6,18 | 169,1 | 6,76 |
| 16 | 191,5 | 7,14 | 164,4 | 7,89 | 173,6 | 5,89 | 172,2 | 6,32 | 167,7 | 7,34 |
| 17 | 188,2 | 7,92 | 161,8 | 8,70 | 173,0 | 6,09 | 171,6 | 6,53 | 167,2 | 7,49 |
| 18 | 184,8 | 8,73 | 159,0 | 9,53 | 172,2 | 6,40 | 170,8 | 6,85 | 166,9 | 7,64 |
| 19 | 181,2 | 9,55 | 156,2 | 10,36 | 170,8 | 6,88 | 169,4 | 7,34 | 166,0 | 7,87 |
| 20 | 177,8 | 10,38 | 155,4 | 10,57 | 169,1 | 7,37 | 169,4 | 7,35 | 164,9 | 8,21 |
| 21 | 174,7 | 11,22 | 154,8 | 10,78 | 167,4 | 7,88 | 169,4 | 7,36 | 163,0 | 8,74 |
| 22 | 171,6 | 12,05 | 154,0 | 10,99 | 165,2 | 8,40 | 169,4 | 7,37 | 160,7 | 9,27 |
| 23 | 168,6 | 12,88 | 153,4 | 11,19 | 163,0 | 8,94 | 169,1 | 7,38 | 158,2 | 9,82 |
| 24 | 165,8 | 13,70 | 152,6 | 11,40 | 160,4 | 9,50 | 169,1 | 7,40 | 155,7 | 10,36 |
| 25 | 163,2 | 14,52 | 151,8 | 11,61 | 157,4 | 10,07 | 169,1 | 7,41 | 152,9 | 10,89 |
| 26 | 160,4 | 15,33 | 151,2 | 11,82 | 154,3 | 10,64 | 169,1 | 7,42 | 150,4 | 11,43 |
| 27 | 157,9 | 16,14 | 150,4 | 12,03 | 151,2 | 11,20 | 169,1 | 7,44 | 147,8 | 11,96 |
| 28 | 155,7 | 16,93 | 149,5 | 12,24 | 148,1 | 11,75 | 169,1 | 7,47 | 145,0 | 12,48 |
| 29 | 153,4 | 17,72 | 149,0 | 12,45 | 145,0 | 12,29 | 168,8 | 7,49 | 142,5 | 13,00 |
| 30 | 151,2 | 18,50 | 148,1 | 12,67 | 142,2 | 12,83 | 168,8 | 7,52 | 140,3 | 13,52 |
| 31 | 149,2 | 19,27 | 147,3 | 12,88 | 139,7 | 13,37 | 168,8 | 7,54 | 138,0 | 14,03 |
| 32 | 147,6 | 20,04 | 146,4 | 13,09 | 137,5 | 13,90 | 168,6 | 7,58 | 136,1 | 14,55 |
| 33 | 145,6 | 20,79 | 145,6 | 13,30 | 135,2 | 14,44 | 168,6 | 7,62 | 134,4 | 15,07 |
| 34 | 144,2 | 21,53 | 144,8 | 13,51 | 133,3 | 14,97 | 168,6 | 7,63 | 132,4 | 15,58 |
| 35 | 142,5 | 22,26 | 143,9 | 13,72 | 131,6 | 15,50 | 168,3 | 7,65 | 131,0 | 16,09 |
| 36 | 141,4 | 22,98 | 143,1 | 13,93 | 129,9 | 16,03 | 168,3 | 7,67 | 129,4 | 16,60 |
| 37 | 140,0 | 23,68 | 142,2 | 14,14 | 128,5 | 16,55 | 168,3 | 7,68 | 128,0 | 17,11 |
| 38 | 138,9 | 24,38 | 141,4 | 14,35 | 127,1 | 17,08 | 168,3 | 7,70 | 126,6 | 17,62 |
| 39 | 138,0 | 25,08 | 140,6 | 14,56 | 125,7 | 17,60 | 168,0 | 7,74 | 125,4 | 18,12 |
| 40 | 137,2 | 25,76 | 139,7 | 14,77 | 124,6 | 18,11 | 168,0 | 7,79 | 124,3 | 18,62 |
| 41 | 136,4 | 26,43 | 138,9 | 14,98 | 124,0 | 18,24 | 167,7 | 7,86 | 123,2 | 19,12 |
| 42 | 135,5 | 27,10 | 138,0 | 15,19 | 123,8 | 18,37 | 167,4 | 7,98 | 122,1 | 19,62 |
| 43 | 135,0 | 27,76 | 137,2 | 15,40 | 123,8 | 18,40 | 166,6 | 8,15 | 121,0 | 20,12 |
| 44 | 135,0 | 27,80 | 136,4 | 15,60 | 123,8 | 18,43 | 165,8 | 8,42 | 120,1 | 20,61 |

| | | | | | | | | | | |
|----|-------|-------|-------|-------|-------|-------|-------|-------|-------|-------|
| 45 | 135,0 | 27,85 | 135,5 | 15,81 | 123,8 | 18,47 | 164,1 | 8,82 | 119,0 | 21,10 |
| 46 | 134,7 | 27,89 | 134,7 | 16,02 | 123,8 | 18,47 | 162,4 | 9,23 | 118,2 | 21,60 |
| 47 | 134,7 | 27,93 | 134,1 | 16,22 | 123,8 | 18,48 | 160,7 | 9,65 | 117,3 | 22,09 |
| 48 | 134,7 | 27,97 | 133,3 | 16,43 | 123,8 | 18,48 | 158,5 | 10,07 | 116,5 | 22,58 |
| 49 | 134,7 | 28,01 | 132,4 | 16,64 | 123,8 | 18,48 | 156,5 | 10,49 | 115,6 | 23,06 |
| 50 | 134,7 | 28,05 | 131,9 | 16,84 | 123,8 | 18,48 | 154,3 | 10,91 | 114,8 | 23,55 |

D.2.3 Load/ out-of-plane deformation diagrams

D.2.3.1 Girder 100

| Girder ₁₀₀ | | | | | |
|-----------------------|-----------|-----------------|-----------|-----------------|-----------|
| W _{P1} | | W _{P2} | | W _{P3} | |
| Load [kN] | DEF. [mm] | Load [kN] | DEF. [mm] | Load [kN] | DEF. [mm] |
| 0,0 | 0,00 | 0,0 | 0,00 | 0,0 | 0,00 |
| 28,0 | 0,00 | 28,0 | 0,09 | 28,0 | 0,00 |
| 55,9 | -0,01 | 55,9 | 0,19 | 55,9 | 0,00 |
| 97,8 | -0,02 | 97,8 | 0,33 | 97,8 | 0,00 |
| 159,8 | -0,02 | 159,8 | 0,54 | 159,8 | 0,01 |
| 174,3 | 0,00 | 174,3 | 0,61 | 174,3 | 0,01 |
| 188,0 | 0,05 | 188,0 | 0,72 | 188,0 | 0,02 |
| 200,2 | 0,15 | 200,2 | 0,99 | 200,2 | 0,05 |
| 208,5 | 0,50 | 208,5 | 1,80 | 208,5 | 0,18 |
| 209,7 | 0,65 | 209,7 | 2,06 | 209,7 | 0,25 |
| 210,4 | 0,85 | 210,4 | 2,37 | 210,4 | 0,34 |
| 209,7 | 1,32 | 209,7 | 2,89 | 209,7 | 0,57 |
| 207,5 | 1,87 | 207,5 | 3,39 | 207,5 | 0,92 |
| 204,4 | 2,38 | 204,4 | 3,81 | 204,4 | 1,35 |
| 200,9 | 2,82 | 200,9 | 4,17 | 200,9 | 1,82 |
| 197,1 | 3,20 | 197,1 | 4,49 | 197,1 | 2,28 |
| 191,5 | 3,73 | 191,5 | 4,93 | 191,5 | 2,94 |
| 185,9 | 4,23 | 185,9 | 5,35 | 185,9 | 3,55 |
| 180,6 | 4,69 | 180,6 | 5,75 | 180,6 | 4,13 |
| 175,6 | 5,14 | 175,6 | 6,14 | 175,6 | 4,69 |
| 170,9 | 5,57 | 170,9 | 6,51 | 170,9 | 5,22 |
| 166,5 | 5,98 | 166,5 | 6,87 | 166,5 | 5,72 |
| 162,5 | 6,38 | 162,5 | 7,22 | 162,5 | 6,20 |
| 158,8 | 6,77 | 158,8 | 7,55 | 158,8 | 6,65 |
| 155,5 | 7,14 | 155,5 | 7,87 | 155,5 | 7,08 |
| 152,5 | 7,49 | 152,5 | 8,18 | 152,5 | 7,49 |
| 149,9 | 7,83 | 149,9 | 8,47 | 149,9 | 7,88 |
| 147,5 | 8,16 | 147,5 | 8,74 | 147,5 | 8,25 |
| 145,3 | 8,47 | 145,3 | 9,01 | 145,3 | 8,60 |

| | | | | | |
|-------|-------|-------|-------|-------|-------|
| 143,3 | 8,77 | 143,3 | 9,26 | 143,3 | 8,94 |
| 141,4 | 9,06 | 141,4 | 9,49 | 141,4 | 9,27 |
| 139,6 | 9,34 | 139,6 | 9,72 | 139,6 | 9,58 |
| 138,0 | 9,61 | 138,0 | 9,93 | 138,0 | 9,88 |
| 136,5 | 9,87 | 136,5 | 10,13 | 136,5 | 10,17 |
| 135,0 | 10,13 | 135,0 | 10,33 | 135,0 | 10,45 |
| 133,7 | 10,37 | 133,7 | 10,51 | 133,7 | 10,72 |
| 132,5 | 10,61 | 132,5 | 10,69 | 132,5 | 10,98 |
| 131,3 | 10,84 | 131,3 | 10,85 | 131,3 | 11,23 |
| 130,2 | 11,06 | 130,2 | 11,01 | 130,2 | 11,48 |
| 129,1 | 11,28 | 129,1 | 11,17 | 129,1 | 11,72 |
| 128,1 | 11,49 | 128,1 | 11,31 | 128,1 | 11,95 |
| 127,1 | 11,70 | 127,1 | 11,45 | 127,1 | 12,18 |
| 126,2 | 11,90 | 126,2 | 11,58 | 126,2 | 12,41 |
| 125,3 | 12,09 | 125,3 | 11,71 | 125,3 | 12,62 |
| 124,5 | 12,28 | 124,5 | 11,83 | 124,5 | 12,84 |
| 123,7 | 12,47 | 123,7 | 11,95 | 123,7 | 13,04 |
| 122,9 | 12,65 | 122,9 | 12,06 | 122,9 | 13,25 |
| 122,1 | 12,83 | 122,1 | 12,16 | 122,1 | 13,44 |
| 121,3 | 13,00 | 121,3 | 12,26 | 121,3 | 13,64 |
| 120,6 | 13,17 | 120,6 | 12,36 | 120,6 | 13,83 |
| 120,3 | 13,25 | 120,3 | 12,41 | 120,3 | 13,92 |

D.2.3.2 Girder 200

| Girder ₂₀₀ | | | | | |
|-----------------------|-----------|-----------------|-----------|-----------------|-----------|
| W _{P1} | | W _{P2} | | W _{P3} | |
| Load [kN] | DEF. [mm] | Load [kN] | DEF. [mm] | Load [kN] | DEF. [mm] |
| 0,0 | 0,00 | 0,0 | 0,00 | 0,0 | 0,00 |
| 28,0 | 0,00 | 28,0 | 0,03 | 28,0 | 0,00 |
| 55,9 | 0,00 | 55,9 | 0,06 | 55,9 | -0,01 |
| 97,5 | 0,00 | 97,5 | 0,11 | 97,5 | -0,02 |
| 158,1 | 0,01 | 158,1 | 0,17 | 158,1 | -0,02 |
| 172,2 | 0,02 | 172,2 | 0,17 | 172,2 | -0,02 |
| 185,1 | 0,05 | 185,1 | 0,17 | 185,1 | 0,00 |
| 196,4 | 0,18 | 196,4 | 0,15 | 196,4 | 0,02 |
| 200,7 | 1,31 | 200,7 | 0,59 | 200,7 | 0,04 |
| 198,7 | 1,80 | 198,7 | 0,84 | 198,7 | 0,04 |
| 196,6 | 2,24 | 196,6 | 1,09 | 196,6 | 0,04 |
| 194,4 | 2,64 | 194,4 | 1,35 | 194,4 | 0,04 |
| 192,3 | 3,02 | 192,3 | 1,64 | 192,3 | 0,05 |

| | | | | | |
|-------|-------|-------|-------|-------|------|
| 190,2 | 3,38 | 190,2 | 1,93 | 190,2 | 0,05 |
| 188,3 | 3,72 | 188,3 | 2,25 | 188,3 | 0,06 |
| 186,4 | 4,05 | 186,4 | 2,57 | 186,4 | 0,06 |
| 184,7 | 4,36 | 184,7 | 2,91 | 184,7 | 0,07 |
| 183,0 | 4,66 | 183,0 | 3,24 | 183,0 | 0,08 |
| 180,7 | 5,08 | 180,7 | 3,74 | 180,7 | 0,09 |
| 178,6 | 5,48 | 178,6 | 4,22 | 178,6 | 0,11 |
| 176,7 | 5,85 | 176,7 | 4,68 | 176,7 | 0,13 |
| 174,1 | 6,36 | 174,1 | 5,35 | 174,1 | 0,17 |
| 171,7 | 6,82 | 171,7 | 5,96 | 171,7 | 0,23 |
| 169,6 | 7,25 | 169,6 | 6,53 | 169,6 | 0,31 |
| 167,6 | 7,64 | 167,6 | 7,07 | 167,6 | 0,41 |
| 165,7 | 8,01 | 165,7 | 7,57 | 165,7 | 0,55 |
| 163,8 | 8,35 | 163,8 | 8,04 | 163,8 | 0,75 |
| 161,7 | 8,67 | 161,7 | 8,48 | 161,7 | 1,06 |
| 159,3 | 8,98 | 159,3 | 8,90 | 159,3 | 1,52 |
| 156,6 | 9,27 | 156,6 | 9,30 | 156,6 | 2,05 |
| 153,9 | 9,55 | 153,9 | 9,67 | 153,9 | 2,56 |
| 151,3 | 9,81 | 151,3 | 10,01 | 151,3 | 3,03 |
| 148,9 | 10,06 | 148,9 | 10,34 | 148,9 | 3,46 |
| 146,6 | 10,29 | 146,6 | 10,64 | 146,6 | 3,86 |
| 144,4 | 10,52 | 144,4 | 10,93 | 144,4 | 4,23 |
| 142,3 | 10,74 | 142,3 | 11,20 | 142,3 | 4,57 |
| 140,4 | 10,95 | 140,4 | 11,46 | 140,4 | 4,88 |
| 138,6 | 11,16 | 138,6 | 11,70 | 138,6 | 5,16 |
| 137,0 | 11,36 | 137,0 | 11,94 | 137,0 | 5,42 |
| 135,5 | 11,55 | 135,5 | 12,17 | 135,5 | 5,66 |
| 134,1 | 11,74 | 134,1 | 12,39 | 134,1 | 5,88 |
| 132,8 | 11,92 | 132,8 | 12,61 | 132,8 | 6,09 |
| 131,6 | 12,10 | 131,6 | 12,82 | 131,6 | 6,28 |
| 130,7 | 12,23 | 130,7 | 12,97 | 130,7 | 6,42 |
| 129,9 | 12,36 | 129,9 | 13,11 | 129,9 | 6,55 |
| 129,3 | 12,45 | 129,3 | 13,22 | 129,3 | 6,64 |
| 128,9 | 12,52 | 128,9 | 13,30 | 128,9 | 6,71 |
| 128,5 | 12,59 | 128,5 | 13,38 | 128,5 | 6,78 |
| 128,2 | 12,64 | 128,2 | 13,44 | 128,2 | 6,83 |
| 127,9 | 12,69 | 127,9 | 13,50 | 127,9 | 6,88 |
| 127,6 | 12,74 | 127,6 | 13,55 | 127,6 | 6,93 |

D.2.3.3 Girder 300

| Girder ₃₀₀ | |
|-----------------------|--------------|
| W _{P3} | |
| Load [kN] | DEF. [mm] |
| 0,0 | 0,00 |
| 27,9 | 0,03 |
| 55,7 | 0,06 |
| 96,7 | 0,09 |
| 150,6 | 0,81 |
| 151,3 | 0,84 |
| 151,9 | 0,87 |
| 152,8 | 0,92 |
| 154,1 | 1,02 |
| 155,8 | 1,20 |
| 158,0 | 1,52 |
| 160,8 | 2,02 |
| 163,8 | 2,75 |
| 166,2 | 3,38 |
| 167,9 | 3,96 |
| 169,0 | 4,49 |
| 170,0 | 5,24 |
| 169,6 | 5,95 |
| 168,4 | 6,64 |
| 166,5 | 7,29 |
| 164,5 | 7,92 |
| 164,0 | 8,06 |
| 163,5 | 8,21 |
| 162,9 | 8,35 |
| 162,4 | 8,50 |
| 161,8 | 8,64 |
| 161,2 | 8,77 |
| 160,6 | 8,91 |
| 160,1 | 9,04 |
| 159,5 | 9,17 |
| 158,9 | 9,30 |
| 158,3 | 9,43 |
| 157,6 | 9,56 |
| 157,0 | 9,68 |
| 156,4 | 9,80 |
| 155,8 | 9,92 |
| 155,2 | 10,04 |

| | |
|-------|-------|
| 154,6 | 10,15 |
| 154,0 | 10,27 |
| 153,4 | 10,38 |
| 152,8 | 10,49 |
| 152,2 | 10,60 |
| 151,5 | 10,71 |
| 150,9 | 10,81 |
| 150,3 | 10,91 |
| 149,7 | 11,02 |
| 149,0 | 11,12 |
| 148,4 | 11,22 |
| 147,8 | 11,31 |
| 147,1 | 11,41 |
| 146,4 | 11,50 |